Asymptotic Analysis of Extreme Electrochemical Transport

by

Kevin Taylor Chu

B.S. Chemistry, Stanford University, 1998
M.S. Sci. Comp. & Comp. Math., Stanford University, 1999

Submitted to the Department of Mathematics
in partial fulfillment of the requirements for the degree of

Doctor of Philosophy

at the

MASSACHUSETTS INSTITUTE OF TECHNOLOGY

September 2005

Author .....
Department of Mathematics
June 6, 2005

Certified by .....
Martin Z. Bazant
Associate Professor of Applied Mathematics
Thesis Supervisor

Accepted by .....
Rodolfo Ruben Rosales
Chairman, Applied Mathematics Committee

Accepted by .....
Pavel I. Etingof
Chairperson, Department Committee on Graduate Students

Asymptotic Analysis of Extreme Electrochemical Transport

by

Kevin Taylor Chu

Submitted to the Department of Mathematics
on June 6, 2005, in partial fulfillment of the
requirements for the degree of
Doctor of Philosophy

Abstract

In the study of electrochemical transport processes, experimental exploration currently outpaces theoretical understanding of new phenomena. Classical electrochemical transport theory is not equipped to explain the behavior of electrochemical systems in the extreme operating conditions required by modern devices. In this thesis, we extend the classical theory to examine the response of two electrochemical systems that form the basis for novel electrochemical devices.

We first examine the DC response of an electrochemical thin film, such as the separator in a micro-battery, driven by current applied through reactive electrodes. The model system consists of a binary electrolyte between parallel-plate electrodes, each possessing a compact Stern layer which mediates Faradaic reactions with Butler-Volmer kinetics. Our analysis differs from previous studies in two significant ways. First, we impose the full nonlinear, reactive boundary conditions appropriate for electrolytic/galvanic cells. Since surface effects become important for physically small systems, the use of reactive boundary conditions is critical in order to gain insight into the behavior of actual electrochemical thin films that are sandwiched between reactive electrodes, especially at high current densities. For instance, our analysis shows that reaction rate constants and the Stern-layer capacitance have a strong influence on the response of the thin film. Second, we analyze the system at high current densities (far beyond the classical diffusion-limited current) which may be important for high power-density applications. At high currents, we obtain previously unknown characterizations of two interesting features at the cathode end of the cell: (i) a nested boundary layer structure and (ii) an extended space charge region.

Next, we study the response of a metal (*i.e.,* polarizable) colloid sphere in an electrolyte solution over a range of applied electric fields. This problem, which underlies novel electrokinetically driven microfluidic devices, has traditionally been analyzed using circuit models which neglect bulk concentration variations that arise due to double layer charging. Our analysis, in contrast, is based on the Nernst-Planck equations which explicitly allow for bulk concentration gradients. A key feature of our analysis is the use of *surface conservation laws* to provide effective boundary conditions that couple the double layer charging dynamics, surface transport processes, and bulk transport processes. The formulation and derivation of these surface conservation laws via boundary layer analysis is one of the main contributions of this thesis. For steady applied fields, our analysis shows that bulk concentrations gradients become significant at high applied fields and affect both bulk and double layer transport processes. We also find that surface transport becomes important for strong applied fields as a result of enhanced absorption of ions by the double layer. Unlike existing theoretical studies which focus on weak applied fields (so that both

of these effects remain weak), we explore the response of the system to strong applied fields where both bulk concentration gradients and surface transport contribute at leading order. For the unsteady problem at applied fields that are not too strong, we find that diffusion processes, which are necessary for the system to relax to steady-state, are suppressed at leading-order but appear as higher-order corrections. This result is derived in a novel way using time-dependent matched asymptotic analysis. Unfortunately, the dynamic response of the system to large applied fields seems to introduce several complications that make the analysis (both mathematical and numerical) quite challenging; the resolution of these challenges is left for future work.

Both of these problems require the use of novel techniques of asymptotic analysis (*e.g.,* multiple parameter asymptotic expansions, surface conservation laws, and time-dependent asymptotic matching) and advanced numerical methods (*e.g.,* pseudospectral methods, Newton-Kantorovich method, and direct matrix calculation of Jacobians) which may be applicable elsewhere.

Thesis Supervisor: Martin Z. Bazant
Title: Associate Professor of Applied Mathematics

Dedicated with love to my parents,

Wengenn and Bihju Chu,

and my fiancée,

Anna Chiu

Acknowledgments

Throughout my graduate studies, I have had the good fortune to be surrounded by many wonderful friends and colleagues. Without their generous support and guidance, I would not have been able to complete graduate school and this thesis.

First, and foremost, I would like to thank my advisor, Martin Z. Bazant, for introducing me to challenging problems at the intersection of science/engineering and mathematics and giving me the freedom to explore these (and other) problems independently. During those times when it seemed like all roads to progress were blocked, his boundless energy and enthusiasm were a refreshing source of inspiration and motivation.

I have had the pleasure of working with many excellent scientists during my graduate career. Armand Ajdari from École Supérieure de Physique et de Chimie Industrielles (ESPCI) provided invaluable physical insight for the work on the charging of a metal colloid sphere and electrochemical transport. Rodolfo Ruben Rosales kindly offered advice and perspective on mathematics, science, career development, and life in general. Yuxing Ben and Jeremy Levitan taught me about many practical and theoretical aspects of microfluidic devices. Jaehyuk Choi and Boguk Kim have been wonderful office-mates; much of my understanding of numerical methods have been a direct result of our many white-board discussions. Finally, my experience and understanding of the world (both academic and beyond) has been greatly enhanced by many conversations I have had with fellow students (listed in no particular order): David Vener, David Hu, Fumei Lam, Brian Sutton, Brian Taylor, Jaydeep Bardhan, Bree Aldridge, Nava Ariel, Pak-wing Fok, Chris Rycroft, Alice Chan, Lisa Treat, Per-Olof Persson, and many others.

Completion of my degree and thesis could not have happened without the strong support of my friends and family. My fiancée, Anna Chiu, and our cat, Audrey, kept my life balanced by constantly reminding me that there is life outside of work. I especially appreciate Anna's tireless efforts to keep me well-fed and to shield me from the "little distractions" in life, so I could focus on my work. Our house-mate, Emy Chen, always kept stress at bay (even while she was writing her own thesis) with her laid-back and relaxed view on life. My cousin, David Wu, and his wife, Grace Hsiao, were great neighbors and made home a warm and welcoming place to be. My good friend, Bob Petersen, has always been there to help me see things from other (especially non-academic) perspectives. He and his wife, Gina

Liao, were gracious enough to let me stay with them during my practicum at Lawrence Livermore National Laboratory. Another good friend, Edison Ng, has always helped me to stay connected to the practical side of science and engineering by keeping me abreast of new and exciting developments in technology. He kindly allowed me to "hide-out" at his home for a short period of time while I was writing my thesis but did not allow me to become so absorbed that I forgot to take breaks to have fun. Finally, I cannot thank my parents, Wengenn and Bihju Chu, and my siblings, Alina, Melissa, and Henry, enough for just being good family.

I would also like to express my appreciation to the department's support staff. In particular, Shirley Entzminger, the Physical Applied Math Group's beloved administrator, played a crucial role in the success of the Simple Person's Applied Math Seminar (among many other department and institute activities), and Tivon Luker, Matt Walburn, and Dave Backeberg, the department system administrators, provided invaluable advice and experience for setting up and maintaining the Applied Mathematics Computational Laboratory's Beowulf cluster.

Financial support for my graduate studies was generously provided by the Department of Energy through the Computational Science Graduate Fellowship (CSGF) and a summer research assistantship through the Center for Material Science Research at MIT. The CSGF is truly a fellowship of computational scientists; I feel privileged to have been given the opportunity to be a part of and interact with this extraordinary group of people.

Citations to Previously Published Work

Parts of this thesis have appeared (or will soon appear) in the following published articles:

Chapters 2 and 5

M. Z. Bazant, K. T. Chu and B. J. Bayly. Current-voltage relations for electrochemical thin films. To appear in *SIAM J. Appl. Math.*

Chapters 2 and 5

K. T. Chu and M. Z. Bazant. Electrochemical thin films at and above the classical limiting current, To appear in *SIAM J. Appl. Math.*

Contents

List of Figures

List of Tables

Chapter 1

Introduction

> In spite of its respectable age and obvious practical relevance, electro-diffusion is still remarkably poorly understood.
>
> – Isaak Rubinstein [95]

1.1 Electrochemical Transport

The transport of charge from one location to another is a fundamental process underlying many physical phenomena in industry and nature. Industrial examples abound in a wide range of applications: energy storage and conversion (*e.g.,* batteries and fuel-cells), water treatment and purification (*e.g.,* electrodialysis), microfluidics (*e.g.,* electrokinetically driven pumping and mixing), metallurgy (*e.g.,* electroplating and large-scale production of metals/alloys), and semiconductors devices. Similarly, electrochemical transport appears in many natural processes, such as corrosion and ion transport through ion channels in biological cells.

What makes electrochemical transport phenomena so fascinating (and complicated to understand) is the coupling between multiple physical and chemical processes. In many electrochemical systems, bulk and surface processes occur simultaneously. In the bulk, the driving force for ion motion comes from two fundamentally different sources: diffusion and electromigration. At electrode surfaces, double layer charging, electrochemical reactions, and surface conduction may all be in action. Together, these processes and their interactions

lead to the rich and varied behavior of electrochemical systems seen in nature and and used by industry.

1.1.1 Bulk Transport

For dilute electrolytes, there are two main driving forces for ion motion. At the molecular level, each individual ion simultaneously undergoes Brownian motion as a result of constant bombardment (or collisions) with other species in the electrolyte and feels a force as its charge interacts with the local electric field. The resulting motion is a random walk that is biased in the direction of the electric field. In the continuum limit, this molecular motion becomes a flux of ion concentration containing two terms [5, 86, 95]:

$$\mathbf{J} = -D\nabla C - zC\nabla\Phi, \tag{1.1}$$

where C is the local ion concentration, Φ is the electric potential, and D and z are the diffusivity and charge, respectively, of the ion. The first term in this expression describes diffusion which drives ions from regions of higher concentration to regions of lower concentration. The second term describes electromigration which drags the ion in the direction (or opposite) of the electric field.

At first glance, (1.1) seems relatively straightforward. However, a major complication lies hidden within the electric potential. From basic electricity and magnetism, we know that the source of electric fields is charge [58]. Therefore, the ions themselves contribute to the local electric potential. As a result, ion transport is inherently a *nonlinear* process that tightly couples ion concentrations and the electric potential. This nonlinearity greatly complicates the mathematical analysis of the ion transport equations. Fortunately, nature disfavors the build up of large regions of non-zero charge density, so it is often possible to treat the bulk as locally electroneutral [86, 95]. In this approximation, the only nontrivial charge density resides in very thin regions near interfaces – the electrical double layers.

1.1.2 Surface Processes

The double layer is a region of high activity for many electrochemical systems. Perhaps the most important process that occurs in the double layer is the accumulation of charge density, which is present to some extent in *all* electrochemical systems. For example, it plays a critical role in *all* electrokinetic phenomena [56, 68], which are a result of coupling between ion motion and fluid flow. Double layer charge is also important in the context of electrochemistry where it can affect the expected rate of an electrochemical reaction by adjusting the effective electrode potential via the Frumkin correction [5, 39, 86].

Electrode reactions themselves are another important process that occurs at surfaces. With the aid of electrons donated (or accepted) by an electrode, electrode reactions convert one (or more) species in the solution into another (perhaps several) species via oxidation-reduction reactions. The net result is the passage of charge through the electrode into the electrolyte and a change in concentration of reactive species in the region immediately adjacent to the electrode surface.

One final type of surface process worth mentioning is surface transport which moves charge and ions along surfaces completely within the double layer. Under ordinary circumstances, surface transport is negligible because the double layer possesses only a very small amount of excess ion concentration (relative to the bulk solution). However, it becomes significant at high applied fields for polarizable surfaces due to strong absorption of electrolyte by the double layer. At weaker applied fields, surface conduction is still important (though much weaker) because it plays a role in bulk diffusion, which only occurs as a correction to a uniform background concentration.

1.2 Electrochemical Transport Theory

The theoretical study of electrochemical transport has a very long and distinguished tradition dating back over a century to the work of Helmholtz [53], Nernst [81, 82, 83], Planck [90], and Warburg [113, 114]. Over the years, their original ideas have been successfully developed and applied in many different fields. In all cases, theoretical understanding was made possible through the judicious use of physically appropriate simplifications to the compli-

cated physics. Some typical approximations include: assumption of local electroneutrality, bulk transport purely by diffusion or electromigration, and modeling the bulk as a linear resistor. Fortunately, common experimental procedures, such as the addition of supporting electrolyte [5, 86] and the use of three-electrode cells [5, 10], justify the use of these approximations in many situations.

In modern times, novel electrochemical devices that push the bounds of classical theory are actively being developed [2, 30, 84, 101, 109, 112]. Attempts to understand the operation of these devices have forced the theoretical community to reexamine electrochemical transport theory in exotic new regimes (*e.g.,* high applied voltages and fields [8, 97, 98], very small length scales [6, 25], *etc.*). In addition to being intellectually interesting, the theoretical understanding gained from these investigations (even if qualitative) enhances our ability to engineer and optimize these devices.

1.3 Scope and Outline of Thesis

The work presented in this thesis contributes to the effort of studying the behavior of electrochemical systems in extreme operating conditions. We focus specifically on two problems: (i) the steady response of electrochemical thin-films, which has applications in the design of thin-film batteries [2, 30, 84, 101, 109, 112], and (ii) double layer charging of metal colloid spheres, which has applications to modern induced-charge electro-osmosis driven pumps and mixers [1, 7, 15, 41, 61, 65, 104, 105, 108]. To address these problems, our general approach is to use a combination of asymptotic analysis (in an appropriately chosen parameter) and numerical modeling to obtain solutions to the governing equations, and then explore the behavior of the solutions as a function of the physical (dimensionless) parameters for the system.

We begin in Chapter 2 by formulating a mathematical description of the physical processes involved in electrochemical transport. Here, we devote a considerable amount of time discussing appropriate electrode boundary conditions for Faradaic reactions because they are central to our analysis of electrochemical thin-films. In Chapter 3, we provide a firm mathematical foundation for many common notions from classical electrochemistry

through the use of asymptotic analysis. The main contribution of Chapters 2 and 3 is a unified presentation of the mathematical framework for studying electrochemical systems with an emphasis on systems with reactive electrodes. In Chapter 4, we present a novel formulation and derivation of surface conservation laws in the thin double-layer limit when the transport process within the boundary layer are the same as those in the bulk. These surface conservation laws are important because they make it possible to "integrate" out the spatial structure of the double layer and analyze bulk transport using effective boundary conditions. In Chapter 5, we analyze the DC response of an electrochemical thin-film. Unlike previous studies of 1D electrochemical systems, we pay special attention to the impact of surface phenomena, specifically Faradaic electrode reactions and Stern layer capacitance, and analyze the system far above the classical diffusion-limited current. In our analysis, we examine both current-voltage relationships (*i.e.,* polarographic curves) as well as the concentration and potential profiles through the electrochemical cell. In Chapter 6, we explore the steady and transient response of a metal colloid sphere to an applied electric field. Here, we use the Nernst-Planck equations to model ion transport in the bulk, which allows us to go beyond the standard circuit model approach traditionally used by the electrokinetics community. We also investigate the response of this system over a wide range of applied electric fields (in contrast to many studies which focus solely on weak applied fields). Through numerical simulations, we find that strong applied fields lead to large bulk concentration gradients and significant surface transport within the double layer. For weaker fields, we show, using time-dependent asymptotic analysis, that diffusion processes are still active but only as a first-order correction. Finally, in Chapter 7, we present concluding remarks on extreme electrochemical transport theory and some directions for future research.

Chapter 2

Mathematical Model

> A scientific theory should be as simple as possible, but no simpler.
>
> – Albert Einstein

2.1 Introduction

In order to embark on our theoretical explorations of extreme electrochemical transport processes, we need a firm mathematical description of the system. However, because many of the assumptions underlying common electrochemical models are questionable in extreme operating conditions, we must build our model from basic physical principles. In this chapter, we develop a general mathematical model for electrochemical transport processes. We begin by deriving the governing equations for the bulk region starting from a general form for the ionic flux. Next, we give a detailed discussion of boundary conditions for these equations. We specifically focus on the mathematical description of Faradaic reactions and double layer capacitance because they involve many subtleties and are modeled in multiple different ways throughout the literature. Finally, to facilitate our analysis, we put the governing equations and boundary conditions in dimensionless form. In the process, we identify several important dimensionless parameters that define a parameter space of operating regimes for electrochemical systems.

2.2 Ion Transport Equations

Ion transport processes are mathematically described by conservation laws for the chemical species present in the system:

$$\frac{\partial C_i}{\partial t} = -\nabla \cdot \mathbf{F}_i \tag{2.1}$$

where C_i and $\mathbf{F}_i$ are the concentration and flux of species i. For a general electrolyte solution, the flux of species i is a function of the electrochemical potential gradient of *all* of the species:

$$\mathbf{F}_i = -C_i \left(\sum_j L_{ij} \nabla \mu_j \right) \tag{2.2}$$

where the μ_j are *electrochemical* potentials and the L_{ij} are generalized mobilities that account for the possibility of interactions between the different species [86]. This general form for the flux is necessary when there are strong chemical interactions between the ionic species and forms the basis of *concentrated* solution theory [86].

While it is important to use (2.2) when describing concentrated solutions, it is common to study electrochemical systems in the *dilute-solution* limit for which it is acceptable to neglect the interactions between individual species [5, 86, 95]. In this limit, the flux for species i reduces to

$$\mathbf{F}_i = -u_i C_i \nabla \mu_i \tag{2.3}$$

where u_i is the single species the mobility of the i-th species. Furthermore, in the dilute solution limit, the electrochemical potential can be decomposed into separate diffusion and migration terms:

$$\mu_i = RT \ln C_i + z_i F \Phi \tag{2.4}$$

where T is the absolute temperature, R is the universal gas constant, F is Faraday's constant (a mole of charge), z_i is the charge number of species i, and Φ is the electrostatic potential. It should be noted that the electrostatic potential is a well-defined quantity independent of any choice of a reference ionic species *only* in the dilute solution limit [86].

Equations (2.1), (2.3), and (2.4) form the basis for the well-known Nernst-Planck equa-

tions [5, 86, 95]. Substituting (2.4) into (2.3), we find that the ionic fluxes are given by

$$\mathbf{F}_i = -\left(D_i \nabla C_i + u_i z_i F C_i \nabla \Phi\right) \tag{2.5}$$

where we have made use of the Nernst-Einstein relation $D_i = u_i RT$ to relate the mobility to the diffusion coefficient D_i. Thus, by using (2.5) in (2.1), we arrive at the Nernst-Planck equations for ion transport:

$$\frac{\partial C_i}{\partial t} = \nabla \cdot \left(D_i \nabla C_i + u_i z_i F C_i \nabla \Phi\right) \tag{2.6}$$

This system of equations form the standard starting point for mathematical models of electrochemical transport (in the absence of convection) [5, 86, 95].

2.2.1 Poisson's Equation

Due to the presence of the electric potential in the Nernst-Planck equations, (2.6) do not form a closed system of equations. Closure is provided by Poisson's equation which relates the the electrostatic potential to local ionic concentrations:

$$-\epsilon_s \nabla^2 \Phi = \rho = \sum_i z_i F C_i. \tag{2.7}$$

Here ϵ_s is the permittivity of the solvent, which we have taken to be constant[1]. Taken together, (2.6) and (2.7) are known as the Poisson-Nernst-Planck (PNP) equations and form the basis for many mathematical analyses of electrochemical systems [3, 4, 87].

An important alternative to Poisson's equation for many practical electrochemical systems is the *local electroneutrality* condition:

$$\sum_i z_i F C_i = 0. \tag{2.8}$$

Local electroneutrality plays an important role in many classical (and modern) mathemati-

[1] At large electric fields, such as those that may arise in interfacial double layers, this classical approximation could break down as the polarization of solvent molecules in large electric fields can lower the solvent dielectric permittivity by an order of magnitude [5, 28, 86].

cal models of electrochemical transport [86, 95]. However, it is important to recognize that it is only an approximation to Poisson's equation. Because of its importance in classical electrochemical analysis, we shall discuss local electroneutrality and its connection to to Poisson's equation in more detail in Chapter 3.

In this thesis, we will focus solely on the dilute solution limit of electrochemical transport. While concentrated solution theory is applicable to a wider range of electrochemical systems, dilute solution theory is a good approximation in many practical systems (*e.g.,* "macroscopic" electrochemical cells and electrokinetically driven flows). From the perspective of mathematical analysis, the tight coupling between the different ionic species in concentrated solution theory makes it difficult to make analytical progress. Moreover, the large number of physical parameters present in concentrated solution theory (compared with dilute solution theory) complicates the identification of the dominant physics. For these reasons, we shall follow the tradition within the applied mathematics community of using the PNP equations as the starting point for studying electrochemical transport [3, 4, 87].

2.2.2 A note about the physical domain

There is a subtle, but important, dependency of the spatial domain on the choice of closure relationship for the transport equations (2.6). When closure is provided by Poisson's equation, the physical domain is the entire electrochemical cell *including* the diffuse part of the charged double layer. However, when the local electroneutrality condition is used, the charged double layer *must* be excluded from the physical domain to maintain consistency of the mathematical description.

2.3 Electrode Surface Boundary Conditions

Although the PNP equations constitute a well-understood and widely accepted approximation for electrochemical transport, appropriate boundary conditions for them are not so clear, and drastic approximations, such as constant concentration, potential or surface charge (or zeta potential), are usually made, largely out of mathematical convenience [3, 4, 87, 95, 96, 97]. On the other hand, in the context of electric circuit models

for electrochemical cells [8, 40, 72], much effort has been made to describe the nonlinear response of the electrode-electrolyte interface, while describing the bulk solution as a simple circuit element, such as a linear resistor. For systems driven far from equilibrium, an appropriate choice of boundary conditions is critical because the response of the electrochemical cell can be significantly affected by interfacial physics. In this thesis, we formulate general boundary conditions based on classical models of the double layer [5, 14, 28] and fairly standard models for electrode reactions [5, 86]. The hope is that these boundary conditions at least qualitatively capture the physics at electrode surfaces.

Mathematically, for electrochemical systems composed of N chemical species, the PNP equations form a system of $N + 1$ equations for the concentrations of the N species and the electric potential. Thus, because the governing equations (2.6) and (2.7) are parabolic- and elliptic-like, respectively, we require $N + 1$ boundary conditions to be specified on the domain boundaries. In this section, we discuss the physical origin of boundary conditions for electrochemical cells containing reactive electrode surfaces. First, we shall find that, for the transport equations, consideration of electrode reactions (or lack thereof) naturally leads to Neumann-like boundary conditions on the normal flux of chemical species. Next, we derive the boundary condition for the electric potential by examining the effect of surface capacitance. Finally, we mention other common boundary conditions for the PNP equations that arise in other physical contexts.

Before delving into a discussion of electrode boundary conditions, it is worth mentioning boundary conditions at infinity for unbounded systems. Far from the region of interest[2], it is commonly assumed that the system has a simple response to the applied fields. For example, for a system subjected to an externally applied electric field, we usually assume that concentrations approach the background concentration and that the electric field approaches the applied electric field. While the boundary conditions at infinity are necessary for a complete mathematical description of the system, the boundary conditions at electrode surfaces are much more interesting and lead to much of the rich behavior observed in electrochemical systems.

[2]Distances are typically considered large if they greatly exceed diffusion length scales.

2.3.1 Faradaic electrode reactions

At electrode surfaces, chemical reactions act as sources (or sinks) for electrochemically active species. These electrode reactions are directly related to the current density and ion fluxes at electrode surfaces. In this section, we will discuss the kinetics of electrode reactions and the boundary conditions that they imply for the transport equations. To facilitate the discussion, we will assume that the electrochemical reaction which occurs at the electrode surface is the reduction of species O to form species R:

$$O + e \underset{k_a}{\overset{k_c}{\rightleftharpoons}} R, \tag{2.9}$$

where O and R are the oxidized and reduced species, respectively, and k_c and k_a are the cathodic (forward) and anodic (backward) reaction rate constants.

Mathematically, electrode reactions are the source of ion flux into the system at the electrode surfaces:

$$\mathbf{F}_O \cdot \hat{n} = r\left(C_O, C_R, \Delta\Phi_s\right) \tag{2.10}$$

$$\mathbf{F}_R \cdot \hat{n} = -r\left(C_O, C_R, \Delta\Phi_s\right), \tag{2.11}$$

where $\hat{n}$ is a normal vector pointing out of the system and $r\left(C_O, C_R, \Delta\Phi_s\right)$ is the net reaction rate density for conversion of species O into species R. Note that the net reaction rate density depends only on C_O and C_R, the concentrations of the reactive species at the electrode surface, and on $\Delta\Phi_s$, the potential of the electrode surface measured relative to the neighboring solution (*i.e.,* electric potential drop across the compact part of the electrical double layer).

For the one-step, single electron transfer processes (2.9), it is typical to assume that the reaction rate density is the difference between the forward and backward reaction rates:

$$r\left(C_O, C_R, \Delta\Phi_s\right) = k_c C_O \exp\left(-\frac{\alpha_c z F \Delta\Phi_s}{RT}\right) - k_a C_R \exp\left(\frac{\alpha_a z F \Delta\Phi_s}{RT}\right) \tag{2.12}$$

where α_c and α_a are transfer coefficients for the cathodic and anodic reactions, respectively [5, 10, 86]. The transfer coefficients for a general single electron reaction are free

to vary as long as $\alpha_c + \alpha_a = 1$. For simplicity, however, we will restrict our attention to the symmetric charge transfer case, $\alpha_c \approx \alpha_a \approx \frac{1}{2}$, which is a good approximation in many situations [5, 10, 86]. Notice that the expressions for the forward and backward reactions are biased by the Stern voltage with an Arrhenius temperature dependence; the Stern layer voltage contributes $-zF\Delta\Phi_s$ to the activation energy multiplied by the appropriate transfer coefficient.

The current density at the electrode surface is closely related to the ionic fluxes (and therefore the reaction rate densities). Observing that one unit of positive charge flows out of the electrochemical cell for every molecule of O that is converted to R, the current density J flowing from the electrolyte *into* the electrode is given by

$$J = F\left[k_c C_O \exp\left(-\frac{\alpha_c zF\Delta\Phi_s}{RT}\right) - k_a C_R \exp\left(\frac{\alpha_a zF\Delta\Phi_s}{RT}\right)\right], \tag{2.13}$$

which is the well-known *Butler-Volmer* equation that characterizes the relationship between the current density and reaction rates [5, 14, 86]. It should be noted that (2.13) differs somewhat from the standard forms of the Butler-Volmer equation [5, 86] because it involves $\Delta\Phi_s$ rather than the *surface overpotential* η_s (see Appendix A for a discussion of overpotentials). Fortunately, it is possible to relate the two formulations by expressing the surface overpotential as

$$\eta_s = \Delta\Phi_s - \Delta\Phi_s^{eq}, \tag{2.14}$$

where $\Delta\Phi_s^{eq}$ is the Stern-layer voltage at equilibrium (*i.e.,* in the absence of current). Setting J to zero in (2.13), it is straightforward to derive an explicit formula for $\Delta\Phi_s^{eq}$:

$$\exp\left(\frac{zF\Delta\Phi_s^{eq}}{RT}\right) = \frac{k_c C_O^*}{k_a C_R^*}, \tag{2.15}$$

where C_O^* and C_R^* are the equilibrium concentrations of the reactive species. Combining these last two results, we obtain the overpotential form of the Butler-Volmer equation:

$$J = J_o\left[\frac{C_O}{C_O^*}\exp\left(-\frac{\alpha_c zF\eta_s}{RT}\right) - \frac{C_R}{C_R^*}\exp\left(\frac{\alpha_a zF\eta_s}{RT}\right)\right], \tag{2.16}$$

where the exchange current density, J_o, is given by

$$J_o = F\left(k_c C_O^*\right)^{\alpha_a}\left(k_a C_R^*\right)^{\alpha_c}. \tag{2.17}$$

Physically, the exchange current is the rate of either the forward or backward reactions when the cell is at equilibrium. The magnitude of the exchange current is a measure of the intrinsic rate of the electrode reaction. Before moving on, it is worth commenting on two variations of (2.16) that occur in the literature. Both of these variations make (2.16) more useful for the analysis of experimental data.

Because the total overpotential, $\eta = E - E^{eq}$, which is the difference between the total cell voltage during operation and at equilibrium, for an electrochemical cell is the only experimentally accessible overpotential, (2.16) is sometimes written with the surface overpotential replaced by the total overpotential [5]. The validity of this approximation rests on the assumption that the potential drop across the bulk solution (*i.e.,* concentration overpotential) can be safely neglected. For standard electrochemical analysis, this assumption is experimentally addressed by adding sufficient quantities of *supporting electrolyte* to the solution, which raises the conductivity of the solution (a mathematical justification of this procedure will be described in the next chapter).

A second variant of (2.16) assumes that the concentrations of reactive species at the electrode surface during operation do not change from their equilibrium values [5, 86]: $C_O = C_O^*$ and $C_R = C_R^*$. With this assumption, (2.16) becomes

$$J = J_o\left[\exp\left(-\frac{\alpha_c z F \eta_s}{RT}\right) - \exp\left(\frac{\alpha_a z F \eta_s}{RT}\right)\right]. \tag{2.18}$$

This formulation of the Butler-Volmer equation makes it possible to sidestep the problem of experimentally determining the concentrations of the reactive species at the electrode surface. However, it requires that steps are taken to ensure that mass-transfer effects (*i.e.,* concentration gradients) are negligible. Stirring the solution and running the experiment at low currents are common ways to address this issue [5].

A significant distinction between (2.13) and the traditional overpotential formulations of the Butler-Volmer equation is the physical location where the boundary condition is

applied. The precise position of the physical boundary is important because it implicitly determines how the the driving forces for electrode reactions depend on the local electric potential and concentrations. When using (2.16) or its variants, the local electroneutrality condition is typically used to close the transport equations, so the boundary condition must be applied completely outside of the electrically charged double layer. As a result, the traditional formulations of the Butler-Volmer equation provide only empirical relationships between the current density and the state of the electrically neutral bulk solution; the differences in electric potential and concentrations of reactive species across the *entire* double layer (including the diffuse part) are the driving forces for electrochemical reactions. In contrast, the outer edge of the Stern layer is the physical boundary for the PNP equations, so the driving force for electrochemical reactions depend on differences in the state variables across only the compact part of the double layer. Physically, the driving forces in the PNP equations makes more sense because electrochemical reactions occur at the outer edge of the Stern layer, not across the entire double layer. The application of boundary conditions at the outer edge of the Stern layer was first proposed by Frumkin [39] and forms the basis for the so-called Frumkin correction to the traditional Butler-Volmer current-overpotential relationships [5, 86]. While the the Frumkin correction provides a procedure for incorporating the structure of the diffuse part of the double layer into traditional formulations of the Butler-Volmer, it essentially requires augmenting the locally electroneutral bulk equations with the PNP equations as a "microscopic" model for the double layer [5]. This procedure amounts to studying the PNP equations in the *thin-double layer* limit (further discussed in Chapter 3).

The Butler-Volmer model for electrode reactions is the simplest model that includes charge transfer at the electrode surface because it only involves the transfer of a single electron that occurs in a single step. It is widely accepted that the rate-limiting step in multi-step electron transfer reactions is a single electron transfer reaction [5]. However, there may be other elementary reactions involved in a complete description of the electron transfer mechanism (*e.g.,* adsorption, desorption, etc.). While these additional reaction steps can in principle be included in the description electrode reactions [5], consideration of these multi-step mechanisms is beyond the scope of this thesis.

While the Butler-Volmer equations provide a precise description of the charge transfer process at the electrode surface for general electrochemical systems, they are difficult to analyze due to the strongly nonlinear relationship between the field variables. As a result, many simplifications are commonly used in the electrochemistry literature. While some of these simplifications are inappropriate for the systems we examine in this thesis, they provide a framework for gaining physical insight from electrochemical systems and so are worth mentioning.

Linear response at small overpotentials

At low currents, it is common to use linear circuit models to model electrochemical cells and interpret the response of the system in terms of charge- and mass-transfer "resistances." In this limit, it is most convenient to work with (2.16) because it is the overpotential (not the potential drop across the Stern layer) that is small near equilibrium.

For small currents, we expect the overpotential to be small, so we can linearize (2.16) about $\eta_s = 0$ to obtain

$$J \approx -J_o \frac{\eta_s F}{RT}. \tag{2.19}$$

This linear relationship between the current and overpotential (and therefore the potential drop across the Stern layer) has been used in many studies to make analytical progress while incorporating electrode reactions in the mathematical model [20, 57, 59]. Our work goes beyond these earlier studies by examining the response of electrochemical cells at high currents where (2.19) no longer holds.

Nernstian behavior for fast reactions

Another approximation commonly used to simplify the reaction boundary condition is to assume that electrode reactions are fast so that the electrochemical reactions are essentially at equilibrium at any moderate current. Mathematically, reactions are considered fast when $J \ll J_o$. A slight rearrangement of (2.16) yields

$$\frac{J}{J_o} = \frac{C_O}{C_O^*} \exp\left(-\frac{\alpha_c z F \eta}{RT}\right) - \frac{C_R}{C_R^*} \exp\left(\frac{\alpha_a z F \eta}{RT}\right), \tag{2.20}$$

which shows that for fast reactions, the forward and backward reaction rates must balance each other regardless of the current J. Thus, in the fast reaction limit, the Butler-Volmer reaction rate equation is effectively replaced by an algebraic relationship between the concentrations at the electrode surface and the overpotential:

$$\frac{C_O}{C_R} = \frac{C_O^*}{C_R^*} \exp\left(\frac{zF\eta}{RT}\right). \tag{2.21}$$

Or, in terms of the Stern layer voltage, the boundary condition becomes

$$\frac{C_O}{C_R} \exp\left(-\frac{zF\Delta\Phi_s}{RT}\right) = \left(\frac{k_a}{k_c}\right) \tag{2.22}$$

While the boundary conditions are still nonlinear, the boundary conditions are somewhat simpler because they are Dirichlet-like involving only the concentrations and potential, not their gradients. While the fully nonlinear form of these boundary conditions has been used extensively in the electrochemistry community in the context of locally electroneutral models [5], they do not seem to have received as much attention in the mathematical modeling community studying the PNP equations.

2.3.2 Inert species and Integral Constraints

Faradaic boundary conditions are only appropriate for the electroactive species in an electrochemical system. In contrast, inert species have no means to enter or exit the system, so they satisfy "no-flux" boundary conditions,

$$\mathbf{F}_i \cdot \hat{n} = 0, \tag{2.23}$$

These boundary conditions are valid assuming that the inert species do not specifically adsorb onto the surfaces, which holds for many anions at typical metal surfaces (*e.g.,* SO_4^{-2}, OH^-, F^-).

For time-dependent problems, (2.23) implies that the total amount of each inert species remains fixed for all time:

$$\int_V C_i dV = C_i^{avg} V, \tag{2.24}$$

where V is the total volume of the system; that is, the concentration of each inert species satisfies an integral constraint. This result is easily obtained by integrating (2.1) over the entire system and applying the divergence theorem. For steady problems, the integral constraints (2.24) are an essential part of the mathematical formulation of the problem. Without them, the solution of the PNP equations would not be uniquely specified. The no-flux boundary conditions, by themselves, are insufficient because they are degenerate, leaving one degree of freedom for each inert species.

It is important to realize that the integral constraints do *not* hold for reactive species. While we are accustomed to assuming that we know the total cation concentration at all times based on the original molarity of the solution, this "macroscopic" thinking does not apply when the physics at the microscopic level are explicitly being studied (*e.g.,* diffuse charge layers or micro-electrochemical systems). What distinguishes reactive species from inert species is that electrode reactions can cause reactive species to be injected into or removed from the system. As a result, the total number of ions for a reactive species may change relative to the total number present initially. For steady problems, the total amount of reactive species is completely determined by the Faradaic boundary conditions discussed in the previous section.

Blocking Electrodes

For problems where we are interested in studying ion transport in the absence of electrode reactions, electrodes are treated as *blocking* or *ideal polarized* electrodes [5]. In these situations, (2.23) and (2.24) hold for *all* ionic species. These types of electrodes commonly appear in the context of mercury electrodes [5], electrokinetically driven microfluidic devices [7, 104], and have been studied as a model system for understanding the dynamics of diffuse layer charging [8].

2.3.3 Double layer capacitance

In addition to acting as a driving force for electrode reactions, the potential drop across the Stern layer $\Delta\Phi_s$ provides the boundary condition for the electric potential through the

relation

$$\Phi_{electrode} = \Phi + \Delta\Phi_s, \tag{2.25}$$

where $\Phi_{electrode}$ is the potential applied directly at the electrode surface. The Stern layer potential drop is exactly the quantity required to relate the electrode potential to the potential at the boundary of the electrolyte. To derive a closed form for the electric potential boundary condition, we will need an explicit formula for $\Delta\Phi_s$. This formula can be obtained via a model for the electrical double layer, which we now consider.

As discussed in Chapter 1, local charge neutrality *always* breaks down in the double layers that form at electrode-electrolyte interfaces (see Figure 2-1). Helmholtz first proposed

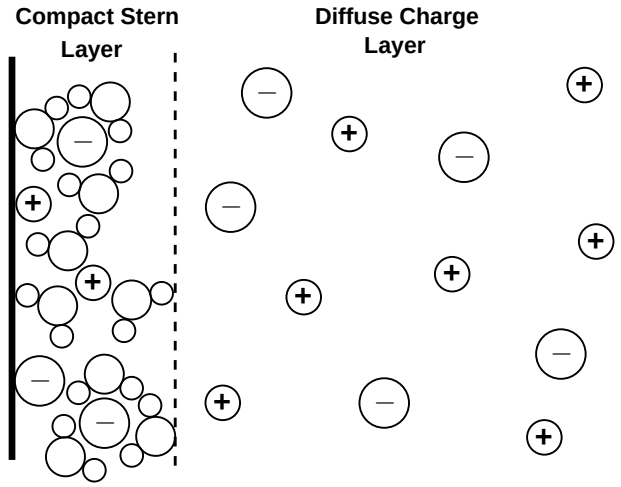

Figure 2-1: Schematic diagram of the structure of the double layer. Immediately adjacent to the electrode is the compact Stern layer which is composed of specifically adsorbed ions (possibly with their solvation structure) or surface contaminants. The ions in this layer are mainly restricted to motion within the compact layer. Further away from the electrode is the diffuse charge layer where ions move freely through the solution.

a very simple model for the double layer treating it as a linear capacitor [53]. While this crude model fails to account for several key features of the double layer, it plays an important role within the Gouy-Chapman-Stern (GCS) model that is commonly used within the electrochemical community [5]. Later Gouy [42] and Chapman [21] developed a theory, confirmed experimentally by Grahame [44, 45], that provides a description of the diffuse part of the double layer (*i.e.,* the region of the double layer composed charged ions free to

move around). A full theoretical understanding of the Stern layer (*i.e.,* compact part of the double layer) is much more challenging and is still an area of active research [50, 51].

To make progress, we use a simple model of the Stern layer based on realistic properties of the interface. Neglecting the specific adsorption of anions, the Stern layer acts as a nonlinear capacitor in series with the diffuse layer. Grahame's celebrated electrocapillary measurements [44, 45] suggest that (*i*) the Stern layer capacitance, C_S, is roughly independent of concentration, depending mainly on the (variable) total charge, σ,

$$\frac{d(\Delta\Phi_s)}{d\sigma} = \frac{1}{C_S(\sigma)}, \tag{2.26}$$

and (*ii*) dilute solution theory accurately describes the capacitance, $C_D(\sigma, C_O, C_R)$, of the diffuse layer, at least when the charge and current are small enough to be well-described by Poisson-Boltzmann theory (discussed in Section 5.3.1). Using Gauss' law, the surface charge density can be expressed in terms of the normal electric field at the outer edge of the Stern layer, $\sigma = -\epsilon_S \partial\Phi/\partial n$, where ϵ_S is an effective permittivity of the compact layer. Therefore, integrating (2.26), Grahame's model corresponds to the assumption,

$$\Delta\Phi_s = -\int_0^{-\epsilon_S \partial\Phi/\partial n} \frac{d\sigma}{C_S(\sigma)}, \tag{2.27}$$

which determines how the voltage across the compact layer (relative to the point of zero charge for which $\Delta\Phi_s = 0$) varies as the two capacitors become charged. The function, $C_S(\sigma)$, should be fit to experimental or theoretical electrocapillary curves at large concentrations (since $1/C_{total} = 1/C_D + 1/C_S \approx 1/C_S$ in that case).

The simplest model that captures this interplay between the compact and diffuse layers is the Gouy-Chapman-Stern (GCS) model [5, 14], which assumes the capacitance of the compact layer, C_S, to be constant [106]. While more complicated models for the compact layer have been proposed [28, 69, 70], the Stern model makes it easy to describe surface capacitance easily in the context of our model of Faradaic reactions. Following Itskovich *et al.* [57], Bonnefont *et al.* [12] and Bazant *et al.* [8], let us introduce an effective width, λ_S, for the compact layer, $\lambda_S = \epsilon_S/C_S$, so that (2.27) reduces to a linear extrapolation of the

potential across the compact layer,

$$\Delta\Phi_s = \lambda_S \frac{\partial \Phi}{\partial n} \tag{2.28}$$

Physically, the Stern layer, as an effective solvation shell for the electrode, is only a few molecules wide, so it is best to think of λ_S as simply a measure of the capacitance of the Stern layer. More generally, the same boundary condition could also describe a thin dielectric layer on the electrode [1, 7, 104] (*e.g.,* arising from surface contamination or a passivating monolayer). It is worth mentioning that because the GCS model neglects the dependence of the Stern layer capacitance on the surface charge density, it is most accurate at low concentrations and near the point of zero charge when the capacitance of the double layer is dominated by the effects of the diffuse layer.

In this thesis, we shall model the double layer using the GCS model. Because our goal is a model that describes surface capacitance and Faradaic reactions in a simple manner, the GCS model is perfect for our purposes. To complete the derivation of the boundary conditions for the electric potential, we substitute (2.28) into (2.25) to obtain a mixed Dirichlet-Neumann boundary condition

$$\Phi_{electrode} = \Phi + \lambda_S \frac{\partial \Phi}{\partial n}. \tag{2.29}$$

2.3.4 Simple Boundary Conditions

The PNP equations have been studied in many contexts with simpler boundary conditions substituted for the reaction (2.10)–(2.11) and Stern boundary conditions (2.29). For example, it is not uncommon to neglect the Stern layer capacitance so that the Stern boundary condition (2.29) reduces to a Dirichlet boundary condition on the electric potential [86]. Similarly, in the field of colloid science, the reaction boundary conditions are replaced by a constant surface charge (or zeta potential) which leads to a simple boundary condition on the electric field. Other important examples include transport in ion channels [3, 4, 87] and electrodialysis [95, 97, 98] where simple Dirichlet boundary conditions on both the concentration and the electric potential are adequate to describe physics at the boundaries. In

these cases, the concentration and electric potential at the boundary are set by externally occurring physical processes.

2.4 Dimensionless Formulation

The analysis of electrochemical systems is greatly simplified by first nondimensionalizing the equations and boundary conditions. This process both facilitates the analysis of equations and helps provide physical insight into the various operating regimes for electrochemical systems. Scaling the basic variables as follows,

$$\tau \equiv \frac{t}{\tau_D}, \quad x \equiv \frac{X}{L}, \quad c_i(x) \equiv \frac{C_i(xL)}{C_{ref}}, \quad \phi(x) \equiv \frac{\Phi(xL)}{RT/F}, \tag{2.30}$$

the PNP equations become

$$\frac{\partial c_i}{\partial \tau} = \nabla \cdot d_i \left(\nabla c_i + z_i c_i \nabla \phi \right) \tag{2.31}$$

$$-\epsilon^2 \nabla^2 \phi = \sum_i z_i c_i. \tag{2.32}$$

where $\tau_D = L^2/D^*$ is a characteristic diffusion time, C_{ref} is a characteristic concentration scale (typically the average concentration or the concentration at "infinity"), and $\epsilon \equiv \lambda_D/Ł$ is the ratio of the Debye screening length $\lambda_D \equiv \sqrt{\frac{\epsilon_s RT}{F^2 C_{ref}}}$ to the characteristic length scale L. Here, the thermal voltage, $V_T = RT/F$, has been used as the scale for the electric potential because bulk diffusion and chemical reactions are both thermally activated processes. Also, the characteristic time scale τ_D is based on an effective diffusivity that is a function of the diffusivities of the species present in solution.

It is worth mentioning that for macroscopic electrochemical systems, ϵ is always extremely small because the Debye length is typically on the order of nanometers and the natural choice for L is the size of the electrochemical cell (for finite systems) or the electrode size (for infinite systems). However, as L or C_{ref} is decreased, ϵ becomes larger, and in the case of electrochemical thin-films, ϵ could be as large as 10.

To nondimensionalize the boundary conditions, we need to introduce a few more characteristic scales. For the flux boundary conditions, we introduce the diffusion-limited flux,

F_D, and current, J_D, densities (see Section 5.3.1):

$$F_D \equiv \frac{C_{ref} D^*}{L} \tag{2.33}$$

$$J_D \equiv zFF_D = \frac{zFC_{ref} D^*}{L}. \tag{2.34}$$

Using these definitions, the reaction boundary conditions (2.10)–(2.11) and the Butler-Volmer equation (2.13) become

$$f_O = -d_O \left(\frac{\partial c_O}{\partial n} + z_O c_O \frac{\partial \phi}{\partial n} \right) = \tilde{k_c} c_O e^{-\alpha_c z \Delta\phi_s} - \tilde{k_a} c_R e^{\alpha_a z \Delta\phi_s}, \tag{2.35}$$

$$f_R = -d_R \left(\frac{\partial c_R}{\partial n} + z_R c_R \frac{\partial \phi}{\partial n} \right) = -\tilde{k_c} c_O e^{-\alpha_c z \Delta\phi_s} + \tilde{k_a} c_R e^{\alpha_a z \Delta\phi_s}, \tag{2.36}$$

$$j = \tilde{k_c} c_O e^{-\alpha_c z \Delta\phi_s} - \tilde{k_a} c_R e^{\alpha_a z \Delta\phi_s}. \tag{2.37}$$

where

$$\tilde{k_c} \equiv \frac{k_c L}{D^*}, \text{ and } \tilde{k_a} \equiv \frac{k_a L}{D^*} \tag{2.38}$$

are dimensionless reaction rate constants. Similarly, the flux boundary conditions (2.23) for the inert species takes the form

$$d_i \left(\frac{\partial c_i}{\partial n} + z_i c_i \frac{\partial \phi}{\partial n} \right) = 0, \tag{2.39}$$

and the integral constraint (2.24) becomes

$$\int_v c_i dv = c_i^{avg} v. \tag{2.40}$$

The final boundary condition to nondimensionalize is the Stern boundary condition (2.29) which becomes

$$\phi_{electrode} = \phi + \delta\epsilon \frac{\partial \phi}{\partial n}, \tag{2.41}$$

where

$$\phi_{electrode} \equiv \frac{F\Phi_{electrode}}{RT} \quad \text{and } \delta \equiv \frac{\lambda_S}{\lambda_D}. \tag{2.42}$$

It is important to note that we have scaled the effective Stern layer width, λ_S, with the

Debye screening length, λ_D, rather than the electrode separation L, thus introducing the factor $\epsilon = \lambda_D/L$ in (2.41). This choice is important for our asymptotic analysis of the limit $\epsilon \to 0$ at fixed δ, which is intended to describe situations in which L is much larger than *both* λ_S and λ_D. Without it, our analysis would assume that as $\epsilon \to 0$ the Stern layer becomes infinitely wide compared to the diffuse layer, even though it is mainly the macroscopic electrode separation which varies. The limit of very small Stern layer capacitance, which amounts to the Helmholtz model of the double layer [53], is best studied by letting $\delta \to \infty$ *after* $\epsilon \to 0$. In contrast, because ϵ and δ would both be small, the limit of very large Stern layer capacitance can be studied by simply letting $\delta = 0$, yielding the Dirichlet boundary condition,

$$\phi = \phi_{electrode} \tag{2.43}$$

of the Gouy-Chapman model of the double layer [21, 42]. In our discussion of electrochemical thin films (Chapter 5), we shall consider both limits, starting with the assumption that $\delta = O(1)$, which corresponds to the GCS model of the double layer.

2.5 Conclusion

In this chapter, we have developed a detailed mathematical model of electrochemical transport processes by collecting together several well-known (but scattered) models from the literature. Our model consists of the Nernst-Planck transport equations with Poisson's equation (or the local electroneutrality condition) as the closure relation. Because surface phenomena greatly affect the behavior of electrochemical cells at extreme conditions, we have paid close attention to the boundary conditions. Specifically, our model includes a detailed description of both the full, nonlinear electrode reactions and surface capacitance effects. Our discussion of the relationship between alternative formulations of the Butler-Volmer equation is particularly significant and novel. Finally, to facilitate the exploration of our mathematical model, we have made it dimensionless. For the remainder of this thesis, we shall take the dimensionless form of the governing equations and boundary conditions as the starting point for our discussions and analysis.

Chapter 3

Aspects of Classical Electrochemical Analysis

> Round up the usual suspects . . .
>
> – Captain Renault in *Casablanca*

3.1 Introduction

Classical analysis of electrochemical systems is based on simplifications of the full, nonlinear Nernst-Planck (2.31) and Poisson (2.32) equations. The simplified equations provide an adequate description for a wide range of experimental situations and form the basis for many standard electrochemical techniques [5]. In this chapter, we discuss the classical analysis of electrochemical systems focusing on the physical and mathematical foundations for the standard approximations.

We begin by reviewing the notion of local electroneutrality and a few of its main implications. Next, we study the impact of supporting electrolyte on electrochemical transport processes using an asymptotic analysis originally approach proposed by Levich [63]. One of the new conclusions from our analysis is that transport at steady-state cannot be unambiguously attributed to either diffusion or electromigration; the two driving forces become directly and linearly related. Using an analogous asymptotic analysis, we next consider

the steady response of locally electroneutral systems at low applied voltages and find that the response is very similar to the situation with sufficient supporting electrolyte. Finally, we close the chapter with a few comments on the use of potential theory in the study of macroscopic electrochemical systems at steady-state.

3.2 Local Electroneutrality

Perhaps the most common approximation made in the analysis of electrochemical systems is that of *local electroneutrality*:

$$\sum_i z_i c_i = 0. \tag{3.1}$$

Physically, this approximation originates from the intuition that creating extended spatial regions of charge density has a high energetic cost. Mathematically, local electroneutrality is a consequence of the fact that ϵ, the ratio of the Debye length to the system size, is very small for "macroscopic" systems (*e.g.,* $\epsilon \approx 1e-5$ for a 1 cm cell). As a result, Poisson's equation

$$-\epsilon^2 \nabla^2 \phi = \sum_i z_i c_i \tag{3.2}$$

reduces to (3.1) at leading order assuming that the Laplacian of the potential remains an order one quantity (which is true at macroscopic length scales). Another way to interpret (3.1) is that charge density only exists in $O(\epsilon)$ boundary layers near interfaces of the electrolyte with other phases. Rescaling the spatial variables using $x - x_o = \epsilon \tilde{x}$ where x_o is an arbitrary position on the interface, we find that (3.1) becomes

$$-\tilde{\nabla}^2 \phi = \sum_i z_i c_i. \tag{3.3}$$

From this equation, it is clear that charge density cannot be neglected within an $O(\epsilon)$ boundary layers near interfaces. This result is also physically obvious since ϵ is the nondimensional Debye length, which is the width of the region near interfaces where we expect to have a nontrivial charge density.

As pointed out by Newman [86] and others, a very common mistake made in studying

electrochemical systems is to use local electroneutrality to imply that the electric potential satisfies Laplace's equation. As our derivation clearly indicates, local electroneutrality is a direct result of ϵ (or equivalently the Debye screening length λ_D) being small, which is *independent* of the electric potential satisfying Laplace's equation. The correct way to interpret local electroneutrality is that it *replaces* Poisson's equation. From the perspective of asymptotic analysis, this procedure is mathematically justified since local electroneutrality is just the leading order approximation to Poisson's equation. The confusion surrounding local electroneutrality and Laplace's equation for the potential is a case which underscores our need to carefully check our physical intuition with rigorous mathematical analysis; simply following physical intuition leads us to the the incorrect conclusion.

Even in the local electroneutral limit, electrochemical systems exhibit interesting and complex behavior. When local electroneutrality is assumed, the Nernst-Planck transport equations can be reformulated in terms of simpler equations that govern electric potential and the total ionic concentration. Both of these quantities play an important role in the response of electrochemical systems, so we take a few moments in this section to consider them. However, a complete discussion of general locally electroneutral systems is outside the scope of this thesis. The interested reader is referred to the book by Rubinstein [95] which gives a detailed analysis of locally electroneutral systems.

3.2.1 Electric Potential

Using (3.1), we can combine the Nernst-Planck equations (2.31) to obtain the following equation for the electric potential:

$$\begin{aligned} 0 &= \nabla \cdot \left[\left(\sum_i z_i^2 d_i c_i \right) \nabla \phi \right] + \sum_i z_i \nabla \cdot (d_i \nabla c_i) \\ &= \nabla \cdot (\kappa(x) \nabla \phi) + \sum_i z_i \nabla \cdot (d_i \nabla c_i) \,, \end{aligned} \tag{3.4}$$

where $\kappa(x) \equiv \sum_i z_i^2 d_i c_i$ is a spatially-varying, dimensionless conductivity. From this equation, it is clear the potential only satisfies Laplace's equation in the special case of uniform concentrations (which implies a uniform conductivity).

Another way of viewing (3.4) is that the divergence of the current density, j, is zero

since j is given by

$$j = -\kappa(x)\nabla\phi - \sum_i z_i \left(d_i \nabla c_i\right). \tag{3.5}$$

In this form, it is clear that for an electrochemical system with concentration gradients, the current density is not simply given by Ohm's law. The concentration gradients can have a significant effect on the current density and even cause the current to flow counter to the direction of the electric field [86]. An interesting consequence of (3.5) is that a gradient in the electric potential can exist even in the absence of current flow. This electric potential, known as the diffusion potential [86], arises to ensure that ions with differing diffusivities move at the same speed. Without the diffusion potential, ions with higher diffusivities would outrun the ions with lower diffusivities leading to charge separation which violates the assumption of local electroneutrality.

In Chapters 5 and 6, we shall consider the case where all of the ions have the same diffusivity. In this case, (3.4) reduces to

$$0 = \nabla \cdot \left(\kappa(x)\nabla\phi\right). \tag{3.6}$$

In this situation, the effect of concentration gradients on the current density appears only implicitly by causing spatial variation in the conductivity.

3.2.2 Pure diffusion of ion concentrations

For locally electroneutral systems, the time evolution of the ion concentrations reduces to the simple diffusion equation in the special cases of (1) binary electrolyte systems and (2) systems where the diffusivities of all ionic species are equal. While these cases impose strict requirements on the electrochemical system, they are useful as model problems to gain physical insight into more complex systems.

Binary electrolyte systems

For binary electrolyte systems, the electroneutrality condition implies that the concentrations of the ionic species are multiples of each other. To facilitate our discussion, we shall use $+$ and $-$ subscripts to denote cation and anion properties, respectively. We start with

the Nernst-Planck equations for the cation and anion concentrations:

$$\begin{aligned} \frac{\partial c_+}{\partial t} &= d_+ \nabla \cdot (\nabla c_+ + z_+ c_+ \nabla \phi) \\ \frac{\partial c_-}{\partial t} &= d_- \nabla \cdot (\nabla c_- + z_- c_- \nabla \phi) \end{aligned} \tag{3.7}$$

Summing these two equation weighted by $1/d_+$ and $1/d_-$, respectively, we can eliminate the electric potential from these equations (using local electroneutrality) to obtain

$$\frac{1}{d_+}\frac{\partial c_+}{\partial t} + \frac{1}{d_-}\frac{\partial c_-}{\partial t} = \nabla^2 (c_+ + c_-) . \tag{3.8}$$

Note that by rearranging (3.1), we can write the anion concentration in terms of the cation concentration:

$$c_- = -\left(\frac{z_+}{z_-}\right) c_+. \tag{3.9}$$

By substituting this equation into (3.8) and carrying out a little algebra, we find that c_+ (and therefore c_-) satisfy the diffusion equation

$$\frac{\partial c_+}{\partial t} = d \nabla^2 c_+, \tag{3.10}$$

where the effective diffusivity is given by

$$d = \frac{(z_+ - z_-)\, d_+ d_-}{z_+ d_+ - z_- d_-}. \tag{3.11}$$

For a symmetric, binary electrolyte, $c_+ = c_-$ and the effective diffusivity is the harmonic mean of the individual diffusivities.

As noted by Newman [86], an interesting feature of binary electrolyte systems is that the concentration distribution of the individual ions is governed by diffusion of the neutral salt (which does not truly exist as an independent chemical species within the electrolyte) with an effective diffusivity that depends only on transport properties of the individual ions. The ease with which the simplified equations are solved depends on the nature of the boundary conditions. As discussed by Newman [86] simple cases where the boundary conditions on the concentration are independent of the electric potential, the diffusion could be solved

first to determine the concentration distribution. (3.4) could then be solved to determine the potential distribution. Finally, the current distribution within the electrochemical cell could be calculated using (3.5). Note that while it is possible, in principle, that (3.5) could be used to solve for the potential, this approach is not practical because the current density within a system (especially in 2D and 3D) is not usually an experimentally controllable quantity. On the other hand, it is easy to control the potential applied at the electrodes.

Equal diffusivity systems

When all ionic species have the same diffusivity $\bar{d}$, the Nernst-Planck equations (2.31) can be summed to derive a diffusion equation for the total ion concentration $\bar{c}$ with diffusion constant equal to $\bar{d}$:

$$\frac{\partial \bar{c}}{\partial t} = \bar{d}\nabla^2 \bar{c}. \tag{3.12}$$

For systems with simple boundary conditions, this result may make it possible to explore some aspects of ion transport without needing to analyze the complete system of Nernst-Planck equations.

3.2.3 Boundary conditions

The replacement of Poisson's equation (a differential equation) with local electroneutrality (an algebraic equation) has the important mathematical consequence that one of the boundary conditions imposed on the PNP equations *must* be dropped; otherwise, the problem would be over specified. For classical electrochemical systems, it is commonly the surface capacitance boundary condition (Section 2.3.3) that is neglected. Part of the reason that the surface boundary condition may be neglected is the focus on overpotentials rather than the electric potential itself. Fortunately, surface capacitance effects can be somewhat accounted for by slightly modifying reaction rate constants using a microscopic model for the charged boundary layer [5].

Recognizing that there must be one less boundary condition for ion transport under locally electroneutral conditions, the transport problem is completely specified by providing one set of boundary conditions for each chemical species present in the system. For systems

that are reaction-limited, Faradaic boundary conditions for reactive species are used with no-flux boundary conditions (and the associated integral constraints) for inert species. For mass-transfer limited systems, Nernstian (Section 2.3.1) or simple boundary conditions (Section 2.3.4) are typically imposed. In addition, either the total voltage drop across the cell (or overpotential) or the total current flowing through the cell is given to close the boundary condition equations (which all depend on the overpotential or the electric potential drop across the Stern layer).

An important complication arises for dealing with electrochemical systems in 2D and 3D. The overpotential is no longer an adequate description of the deviation of the electrode from equilibrium. In these cases, we *must* use a model of the double layer to relate the potential drop across the compact Stern layer to the concentrations within the solution. As mentioned earlier, this relationship is necessary to close the boundary condition equations for the individual chemical species. Since there is really no *a priori* way to specify the current density distribution on the electrode surface, it only makes sense to apply a voltage across the entire cell. The boundary condition for the electric potential takes the form:

$$\phi_{app} - \phi = \Delta\phi_s, \tag{3.13}$$

where ϕ_{app} is the potential applied on the electrode and ϕ is the potential of the electrolyte immediately adjacent to the charged double layer.

3.3 Supporting Electrolyte

The addition of *supporting electrolyte* (*i.e.,* an excess of nonelectroactive ions) to electrochemical solutions is a common experimental technique that greatly simplifies the analysis of electrochemical systems. From a theoretical perspective, the primary advantages of high supporting electrolyte concentrations are (1) a reduction of migration contributions on the transport of electroactive species and (2) a decrease in the bulk resistance of the solution thereby minimizing the "Ohmic losses" between the reference and working electrodes [5]. Supporting electrolyte also provides several experimental and chemical advantages [5], but these are not relevant for understanding the theoretical developments in this thesis.

The experimentally observed advantages of maintaining a high supporting electrolyte concentration can be justified mathematically through an asymptotic analysis. The original analysis of these systems was carried out by Levich [63] in the 1940s. The basis for his analysis is the assumption that the concentrations of the electroactive species are much less than the concentrations of the ions contributed by the supporting electrolyte. Due to its fundamental value in theoretical electrochemistry, we give a variation of his analysis here.

To facilitate our discussion, let us suppose that there are N ionic species in the electrolyte solution and that only the species 1 is electrochemically active. Furthermore, we suppose that $c_1 = O(\alpha)$ with $\alpha \ll 1$ and $c_i = O(1)$ for $i > 1$. For boundary conditions, we have that $\mathbf{F}_i \cdot \hat{n} = 0$ for $i > 1$ since they do not participate in electrode reactions. We begin by expanding the concentrations and electric potential as asymptotic series in the small parameter α:

$$\begin{aligned} c_1 &= \alpha c_1^{(1)} + \alpha^2 c_1^{(2)} + \dots \\ c_i &= c_i^{(0)} + \alpha c_1^{(1)} + \alpha^2 c_1^{(2)} + \dots \\ \phi_i &= \phi_i^{(0)} + \alpha \phi_1^{(1)} + \alpha^2 \phi_1^{(2)} + \dots \end{aligned} \tag{3.14}$$

Plugging these into the transport equations, we find that the leading order equations are

$$\frac{\partial c_i^{(0)}}{\partial t} = d_i \nabla \cdot \left(\nabla c_i^{(0)} + z_i c_i^{(0)} \nabla \phi^{(0)} \right) , \quad i > 1 \tag{3.15}$$

$$\sum_{i>1} z_i c_i^{(0)} = 0. \tag{3.16}$$

By inspection, it is clear that constant $\phi^{(0)}$ and $c_i^{(0)} = c_i^{avg}$ for $i > 1$ satisfy the (3.15) and the no-flux boundary conditions for the inert species. Recalling that we must initially have local electroneutrality at leading order, we see that (3.16) is also satisfied. Assuming that we can prove uniqueness of solutions[1] of (3.15) and (3.16), we conclude that there is no dynamical response at leading order. This conclusion is a direct consequence of the fact that the electroactive species plays absolutely no role in the leading order equations. Any

[1] Uniqueness of the solutions of the locally electroneutral ion transport equations is still not completely understood [95].

nontrivial response of the electrochemical system can only show up at higher order. Using the solution of the leading order equations, we can derive the $O(\alpha)$ equations:

$$\frac{\partial c_1^{(1)}}{\partial t} = d_1 \nabla^2 c_i^{(1)} \tag{3.17}$$

$$\frac{\partial c_i^{(1)}}{\partial t} = d_i \left(\nabla^2 c_i^{(1)} + z_i c_i^{(0)} \nabla^2 \phi^{(1)} \right) , \quad i > 1 \tag{3.18}$$

$$\sum_i z_i c_i^{(1)} = 0. \tag{3.19}$$

The advantages of using supporting electrolyte are a direct consequence of the above analysis. As we can see in (3.17), electromigration plays no role in the transport of the electroactive species. Furthermore, the total potential drop across the electrochemical cell is at most an $O(\alpha)$ quantity because the gradient of the electric potential has no $O(1)$ contribution. Unfortunately, making analytical progress for (3.17) - (3.19) is not straightforward.

For steady state problems, however, further analytical progress can be made because the differences in the diffusivities of different species becomes unimportant. Setting the unsteady term to zero and dividing out the factor of d_i from (3.17) and (3.18), we find that

$$0 = \nabla^2 c_1^{(1)} \tag{3.20}$$

$$0 = \left(\nabla^2 c_i^{(1)} + z_i c_i^{(0)} \nabla^2 \phi^{(1)} \right) , \quad i > 1 \tag{3.21}$$

Note that (3.21) can be rewritten as Laplace's equation for $\psi_i = c_i^{(1)} + z_i c_i^{(0)} \phi^{(1)}$ and that the boundary conditions at $O(\alpha)$ for the inert species are given by

$$\frac{\partial \psi_i}{\partial n} = \frac{\partial}{\partial n} \left(c_i^{(1)} + z_i c_i^{(0)} \phi^{(1)} \right) = 0. \tag{3.22}$$

Thus, we can concluded that ψ_i must be constant for all inert species. Taking the gradient of ψ_i to compute the $O(\alpha)$ flux of species i, we find that

$$\mathbf{F}_i^{(1)} = -d_i \left(\nabla c_i^{(1)} + z_i c_i^{(0)} \nabla \phi^{(1)} \right) = 0 \tag{3.23}$$

for inert species; in other words, there is no net transport of inert species anywhere in the

electrochemical cell. As a result, all of the current density is carried by electroactive species:

$$\mathbf{j} = -z_1 \mathbf{F}_1^{(1)} = -z_1 d_1 \nabla c_1^{(1)}. \tag{3.24}$$

This result is consistent with the common notion that electromigration plays no role in the transport of the electroactive species. However, at steady-state the distinction between diffusion and electromigration becomes ambiguous. The reason for this is that, at steady state, the gradient in the electric potential is proportional to the gradient in the concentration of the electroactive species. This proportionality becomes apparent if we consider the somewhat unusual combination of the ionic fluxes:

$$\sum_i \frac{z_i}{d_i} \mathbf{F}_i^{(1)}. \tag{3.25}$$

We can expand (3.25) in two ways. First, since $\mathbf{F}_i^{(1)} = 0$ for $i \neq 1$, the sum is equal to $-z_1 \nabla c_1^{(1)}$. However, if we directly substitute the expression for $\mathbf{F}_i^{(1)}$ into (3.25), we find that

$$\begin{aligned} \sum_i \frac{z_i}{d_i} \mathbf{F}_i^{(1)} &= -\nabla \left(\sum_i z_i c_i^{(1)} \right) - \left(\sum_{i \neq 1} z_i^2 c_i^{(0)} \right) \nabla \phi^{(1)} \\ &= -\left(\sum_{i \neq 1} z_i^2 c_i^{(0)} \right) \nabla \phi^{(1)}, \end{aligned} \tag{3.26}$$

where we have made use of local electroneutrality at $O(\alpha)$ to arrive at (3.26). Combining these results, we conclude that the concentration gradient for the electroactive species is directly related to the gradient in the electric potential:

$$\nabla c_1^{(1)} = \frac{1}{z_1} \left(\sum_{i \neq 1} z_i^2 c_i^{(0)} \right) \nabla \phi^{(1)}. \tag{3.27}$$

Thus, it is equally correct to consider the gradient in the electric potential as the driving

force for transport of the electroactive species:

$$\mathbf{j} = -d_1 \left(\sum_{i \neq 1} z_i^2 c_i^{(0)} \right) \nabla \phi^{(1)}. \tag{3.28}$$

In other words, the current density is given by an "Ohm's Law"-like relationship. Interestingly, the bulk conductivity is replaced by the bulk ionic strength times the diffusivity of the electroactive species. This modified version of Ohm's law has also been noticed by Rubinstein [95].

Mathematically, the relationship between $\nabla c_1^{(1)}$ and $\nabla \phi^{(1)}$ is a result of the fact that presence of the electroactive species is just a small perturbation to the background concentration of supporting electrolyte. As a result, the response of the electrochemical system can be analyzed by linearizing about the steady-state solution for the supporting electrolyte in the absence of the electrochemically species. In this linearization process, the relationship between the deviations from the steady-state solution naturally turn out to be linear.

Physically, the reason for the ambiguity in the driving force for charge transport is that local electroneutrality and the presence of a gradient in the concentration of the electroactive species requires concentration gradients for the inert species even though they do not contribute to the current density flowing through the cell. Therefore, an electric potential gradient must be induced to to prevent net transport of the inert species.

Another interesting feature of the steady-state system is that the potential *does* satisfy Laplace's equation, which is not generally true during the evolution of the system towards steady state. Summing (3.20) and (3.21) over all species (including the electroactive species) weighted by the charge number z_i, we find that

$$\begin{aligned} 0 &= \nabla^2 \left(\sum_i z_i c_i^{(1)} \right) + \left(\sum_i z_i^2 c_i^{(0)} \right) \nabla^2 \phi^{(1)} \\ &= \left(\sum_i z_i^2 c_i^{(0)} \right) \nabla^2 \phi^{(1)}, \end{aligned} \tag{3.29}$$

where we have made use of local electroneutrality at $O(\alpha)$ to eliminate the diffusive term. Thus, when there is sufficient supporting electrolyte present, the leading order (nontrivial)

potential satisfies Laplace's equation for electroneutral systems at steady-state even in the presence of concentration gradients.

3.4 Low applied voltages

At low applied voltages, we find a similar relationship between the concentration gradients of electroactive species and the gradient in the electric potential. Again, the source of this relationship is that the low applied voltage allows us to perform a linearization about a steady-state solution with uniform concentration profiles. However, there is no need for supporting electrolyte to derive these results.

As in the previous section, let us suppose that there are N ionic species in the electrolyte solution and that only the species 1 is electrochemically active. However, for this discussion, we make no restrictions on the relative concentrations of the chemical species. Also as before, we assume no-flux boundary conditions for the inert species. An important assumption in this analysis is that the current density flowing into and out of the cell are $O(v)$; in other words, for small applied voltages, the cell response is small.

We begin by expanding the concentrations and electric potential as asymptotic series in the applied voltage v (taken to be small parameter):

$$\begin{aligned} c_1 &= c_1^{(0)} + v c_1^{(1)} + \dots \\ c_i &= c_i^{(0)} + v c_1^{(1)} + \dots \\ \phi_i &= \phi_i^{(0)} + v \phi_1^{(1)} + \dots \end{aligned} \tag{3.30}$$

Plugging these into the transport equations, we find the same leading order equations for the supporting electrolyte case. The only difference is that (3.15) also holds for the electroactive species. At leading order, *all* species satisfy no-flux boundary conditions (reactions of the electroactive species lead only to $O(v)$ fluxes), so we arrive at the conclusion that there are no $O(1)$ disturbances from uniform potential and concentrations.

At $O(v)$, we can use the same reasoning as in the supporting electrolyte case to show that $\psi_i = c_i^{(1)} + z_i c_i^{(0)} \phi^{(1)}$ is constant for inert species. Thus, we again find that all of the

current density is carried by the electroactive species:

$$\mathbf{j} = -z_1\mathbf{F}_1^{(1)} = -z_1 d_1\left(\nabla c_1^{(1)} + z_1 c_1^{(0)}\nabla\phi^{(1)}\right) \tag{3.31}$$

Note that in this case, electromigration plays an explicit role in the transport of the electroactive species. However, decomposing the driving force for the flux into diffusion and electromigration contributions is somewhat tenuous because, as in the supporting electrolyte case, $\nabla c_1^{(1)}$ and $\nabla\phi^{(1)}$ are proportional to each other. Expanding (3.25) in two ways as before, we find that

$$\frac{z_1}{d_1}\mathbf{F}_1^{(1)} = -\left(\sum_i z_i^2 c_i^{(0)}\right)\nabla\phi^{(1)}. \tag{3.32}$$

Note that this equation differs from (3.32) because $\mathbf{F}_1^{(1)}$ includes an electromigration term and the sum includes the contribution from the electroactive species. These two terms are equal and cancel out from both sides of (3.32) yielding (3.27) as the relationship between the electric potential gradient and the concentration gradient for the electroactive species.

While the relationship between $\nabla c_1^{(1)}$ and $\nabla\phi^{(1)}$ is the same as in the supporting electrolyte case, the proportionality constant that appears in Ohm's law is slightly modified as a result of the electromigration term. Substituting (3.27) into (3.31), we find that

$$\mathbf{j} = -d_1\left(\sum_i z_i^2 c_i^{(0)}\right)\nabla\phi^{(1)}. \tag{3.33}$$

Note that the sum is over *all* ionic species. Thus, as before, we find that the leading order ionic strength plays the role of the bulk conductivity in Ohm's law. We can also think of the flux of the electroactive species as being driven solely by diffusion:

$$\begin{aligned}\mathbf{j} &= -z_1 d_1\left(\frac{\sum_i z_i^2 c_i^{(0)}}{\sum_{i\neq 1} z_i^2 c_i^{(0)}}\right)\nabla c_1^{(1)} \\ &= -z_1 d_1\left(\frac{1}{1-t_1}\right)\nabla c_1^{(1)},\end{aligned} \tag{3.34}$$

where t_1 is a transference-like number defined by

$$t_1 \equiv \frac{z_1^2 c_1^{(0)}}{\sum z_i^2 c_i^{(0)}}. \tag{3.35}$$

3.5 Potential Theory

One of the important conclusions of the earlier sections of this chapter is that there are many situations where the electric potential or concentration distributions satisfies Laplace's equation. In these situations, it is possible to leverage the extensive body of work surrounding the solution of this famous partial differential equation.

In the context of electrochemistry, the traditional use of potential theory has been to compute the electric potential for systems where concentration gradients can be ignored [86]. Our discussion in the previous sections has indicated the applicability of potential theory in the context of steady-state systems with supporting electrolyte or for weakly driven systems. While these circumstances are uncommon in traditional electrochemical systems, they may play a more significant role for small scale devices where steady-state is more readily achieved. One important distinction between the traditional and steady-state applications of potential theory is the relationship between the gradient in the electric potential and the current density. When concentration gradients are absent, the normal Ohm's law holds and the proportionality constant is the bulk conductivity $\kappa = \sum_i z_i^2 d_i c_i$. However, for steady-state systems, the appropriate proportionality constant is twice the ionic strength $I = \sum_i z_i^2 c_i$ of the electrolyte.

A complete review of the techniques used to solve problems in potential theory is beyond the scope of this thesis. For a more in depth discussion of applications of potential theory to problems in electrochemistry, the reader is referred to the reviews by Newman and West [86, 116].

3.6 Conclusion

In this chapter, we have examined aspects of classical electrochemical transport theory based on the approximation of local electroneutrality. First, we discussed several well-known

implications of the Nernst-Planck equations and local electroneutrality. Next, we used asymptotic analysis to study systems with large concentrations of supporting electrolyte and systems at low applied voltages. In both of these cases, we arrive at the surprising conclusion that transport at steady-state can be described in two seemingly contradictory ways: (i) driven purely diffusion or (ii) driven pure migration. The resolution to this conundrum is that when there is sufficient supporting electrolyte or at low applied voltages, gradients in ionic concentrations and gradients in the electric potential are linearly related. We end the chapter by observing that potential theory is applicable to the steady-state systems discussed earlier in the chapter.

Chapter 4

Surface Conservation Laws

> . . . the interface is a region of small but *finite* thickness . . .
>
> – John L. Anderson

4.1 Introduction

For many physical problems involving interfaces, the concentration of chemical species in the vicinity of the interface plays an important role in the dynamics of the interface (both its motion and evolution of its chemical composition). Examples include the effect of surfactants on surface tension [36, 77, 78], the charging dynamics of electrochemical double layers [8, 33, 54, 55, 100, 102], and soap film dynamics [24, 26].

When studying chemically active interfaces that can be considered macroscopically sharp, the state of the interface is described by specifying the *excess* surface concentrations of all chemical species relative to their bulk concentrations. The focus on excess concentrations is usually based on equilibrium thermodynamic considerations [56, 67]. In many theoretical analyses, the interface is assumed to be in thermal equilibrium so that the excess surface concentrations can be related to other thermodynamic variables (including each other) via adsorption isotherms [5, 36, 56, 67, 86]. However, when the dynamics of surface species is important (*e.g.,* fast adsorption-desorption kinetics, non-negligible surface-diffusion), the isotherm model is replaced by "surface conservation laws" for the surface

excess concentrations:

$$\frac{\partial \Gamma}{\partial t} = -\nabla_s \cdot \mathbf{J}_s + J_n, \tag{4.1}$$

where Γ, $\mathbf{J}_s$ and J_n are the surface excess concentration, the surface flux and the normal flux, ∇_s denotes a surface derivative, and the sign on the normal flux is chosen to be positive when the flux is *into* the boundary layer (see Figure 4-1).

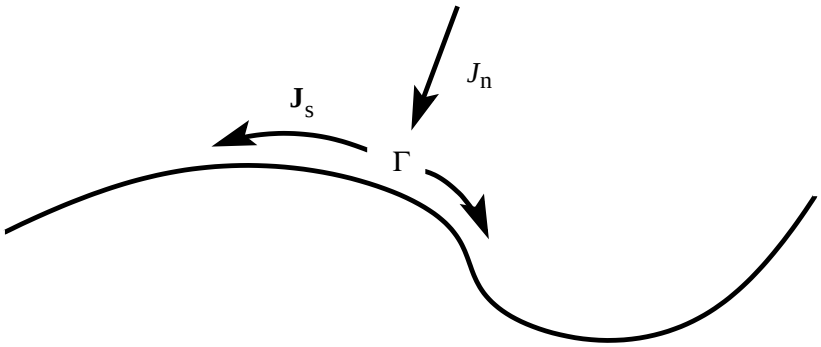

Figure 4-1: Schematic diagram of fluxes at a sharp interface. Note that the surface excess concentration Γ and the surface fluxes J_s are defined *only* on the interface itself.

This equation is physically intuitive: the time rate of change in the surface concentration results from a combination of surface diffusion and flux from the bulk. Note that we have neglected motion and deformation of the interface which would contribute extra terms involving convection in the normal direction and surface dilation [100, 107, 117]. Since our analysis sheds no new insight for these terms, we shall ignore them to keep the discussion simple.

It is tempting to think of equation (4.1) as a conservation law for the chemical species adsorbed to the interface. However, it is important to remember that the equation describes the evolution of *excess* concentrations. It is not physically obvious that tangential fluxes of excess concentration and normal fluxes of bulk concentration contribute solely to changes in the excess concentration (*i.e.,* they do not contribute to changes in the base level of chemical species at the surface).

For microscopically sharp interfaces, such as the monolayer interfaces that arise in prob-

lems involving surfactants at liquid-gas interfaces [36, 77, 78] or the compact layer in electrochemical systems [5, 67], surface conservation laws of the form (4.1) are not surprising. What is interesting is that (4.1) holds even when the interface is *not* a microscopically sharp (see Figure 4-2). For instance, in their studies of the evolution of surface excess concentra-

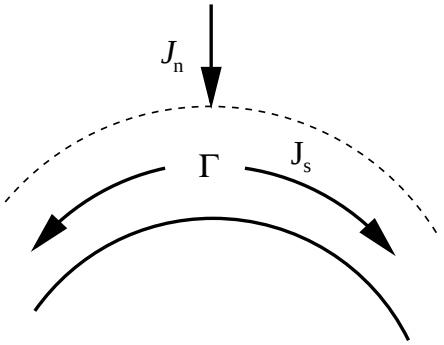

Figure 4-2: Schematic diagram of a microscopically diffuse interface. The dashed line represents the outer "edge" of the boundary layer, which is *not* at a mathematically well-defined location. Note that in addition to the fluxes within the boundary layer, it is possible for the interface to possess fluxes that physically reside on the microscopic interface itself. For some systems, these "microscopic" surface fluxes may provide a significant contribution to the total surface flux in the boundary layer.

tions of electrolyte around colloid particles [29, 33, 102], Dukhin and his colleagues made use of surface conservation laws. that are linearized versions of (4.1). A key point observation about microscopically diffuse interfaces is that surface transport within the boundary layer near the interface is driven by the *same* transport processes that occur in the bulk. Surface transport within microscopically sharp interfaces is fundamentally different because it is driven by physical processes related to the specific nature of the interface (although it may be affected by bulk transport processes).

To derive (4.1) for microscopically "sharp" interfaces, the surface can truly be thought of as a distinct phase, so a conservation law argument based on a balance of fluxes into a "control patch" on the interface is mathematically valid. Unfortunately, this derivation is no longer valid for interfaces that are microscopically diffuse because the notion of a "control patch" is not well-defined. The main problem is the lack of a distinct separation between the bulk and the interfacial region. Rather, there is a thin region near the interface over

which the concentrations vary rapidly. Intuitively, we would like to directly integrate over the boundary layer to define surface quantities. However, care must be exercised during this procedure in order to obtain physically meaningful results. The key idea is that all integrations over the boundary layer should involve only *excess* quantities; integration of absolute quantities leads to divergent results.

In this chapter, we use boundary layer theory to derive the surface conservation laws (4.1) that govern the time-evolution of surface excess concentration for a diffuse species in the "sharp interface" limit (*i.e.,* when the distance over which the volume density of the diffuse species varies is small relative to geometric length scales of the interface). Surprisingly, a general derivation of equation (4.1) for the case of a diffuse interface appears to be missing from the literature. While there exists work that derives linearized versions of (4.1) [29, 33, 54, 55, 102], the surface conservation laws derived in these studies are restricted to weakly perturbed bulk concentration profiles. In contrast, our derivation is applicable to a wider range of transport problems; there is no restriction on the bulk concentration profile (as long as it is not mathematically pathological). We require only that the flux is a linear combination of gradients of field variables with coefficients that are allowed to be arbitrary functions of the field variables.

4.2 Derivation of Surface Conservation Laws

We begin our analysis by writing the full (dimensionless) conservation laws that govern the time evolution of a chemical species throughout the physical domain:

$$\frac{\partial c}{\partial t} = -\nabla \cdot \mathbf{F}, \tag{4.2}$$

where c is the concentration and $\mathbf{F}$ is the flux. Note that the flux $\mathbf{F}$ is not exactly the same as (although it is closely related to) the flux $\mathbf{J}$ that appears in (4.1). For our derivation, we assume that there is no flux of material through the interface itself $\partial\mathbf{F}/\partial n = 0$ and require that $\mathbf{F}$ is a linear combination of gradients of field variables with coefficients that could be

arbitrary functions of the all of the field variables in the problem:

$$\mathbf{F} = \sum_i f_i \left(c_1, c_2, \ldots, c_n\right) \nabla c_i. \tag{4.3}$$

Furthermore, we assume that the spatial coordinates in (4.2) have been nondimensionalized using the characteristic geometric length scale. In these units, the thickness of the boundary layer over which the c varies rapidly is $O(\epsilon)$. The "sharp interface" limit $\epsilon \ll 1$ is best studied via asymptotic analysis using (4.2) for the *outer* equations and deriving the *inner* equations by appropriately rescaling the spatial coordinates. In this discussion, we shall distinguish inner and outer variables by using the hat and bar accents, respectively. Also, we shall use (X, Y, Z) (upper case variables) and (x, y, z) (lower case variables) to represent the outer and inner spatial coordinates, respectively. Since the focus will be on the region immediately neighboring the surface, we shall take (x, y) to be Cartesian coordinates tangential to the interface and z to the coordinate normal to the interface. Rescaling (4.2) using the inner coordinates $(x, y, \epsilon z) = (X, Y, Z)$, we find that the governing equations in the boundary layer are

$$\frac{\partial \hat{c}}{\partial t} = -\nabla_s \cdot \hat{\mathbf{F}}_s - \frac{1}{\epsilon^2} \frac{\partial \hat{F}_n}{\partial z}, \tag{4.4}$$

where the subscripts s and n indicate tangential and normal components of the flux and divergence operator, respectively. Note that in changing to the inner coordinates, the normal derivative of the flux $\hat{F}_n$ picks up a factor of $1/\epsilon$ because flux itself involves derivatives of space: $\hat{F}_n(z) = \epsilon \bar{F}_n(Z)$.

In deriving (4.1), the intuitive idea of just integrating (4.4) from $z = 0$ to $z = \infty$ is inadequate because it leads to divergent integrals which are physically and mathematically meaningless. The key idea to keep in mind when asymptotically integrating over boundary layers is that only *excess* concentrations are integrable; absolute concentrations are *not*.

Using this basic principle, we can systematically derive (4.1) by starting with the excess

(volume) concentration of species i in the boundary layer:

$$\begin{aligned}\gamma(x,y,z,t) &= \hat{c}(x,y,z,t) - \bar{c}(x,y,0,t) \\ &= \hat{c}(x,y,z,t) - \lim_{Z\to 0} \bar{c}(X,Y,Z,t). \end{aligned} \tag{4.5}$$

Taking the time derivative of this equation and using inner and outer evolution equations, (4.2) and (4.4), we find that

$$\frac{\partial \gamma}{\partial t} = \left(-\nabla_s \cdot \hat{\mathbf{F}}_s - \frac{1}{\epsilon^2}\frac{\partial \hat{F}_n}{\partial z}\right) - \left(-\nabla_s \cdot \bar{\mathbf{F}}_s - \lim_{Z\to 0}\frac{\partial \bar{F}_n}{\partial Z}\right). \tag{4.6}$$

To obtain an equation for the surface excess concentration Γ, we would like to integrate this equation over the entire boundary layer. Unfortunately, it is not possible to just integrate over the entire range of the inner variable because integral of the last term on the right hand side is divergent:

$$\int_0^\infty \left(\lim_{Z\to 0}\frac{\partial \bar{F}_n}{\partial Z}\right) dz = \left(\lim_{Z\to 0}\frac{\partial \bar{F}_n}{\partial Z}\right)\int_0^\infty dz. \tag{4.7}$$

However, because the boundary layer has an $O(\epsilon)$ width and all of the integrands are $O(1)$, we expect that all of the integrals should be $O(\epsilon)$ quantities.

The problem with the intuitive approach is that it makes the mistake of equating the asymptotic limit $\epsilon \to 0$ with the spatial limit $z \to \infty$. Realizing this subtle distinction (which is safe to neglect for many asymptotic analyses), we can reformulate the integration over the boundary layer as the limit of a sequence of integrals over finite intervals, which tends to the entire half-space $[0,\infty)$ as $\epsilon \to 0$. In choosing the domain of integration, we want to be sure to capture the entire boundary layer so that the notion of the total surface excess concentration is physically meaningful. In addition, we want the region of integration at the geometric length scale to go to zero as $\epsilon \to 0$ so that we are truly integrating over only the boundary layer. We can simultaneously achieve both of these goals by taking the region of integration at the geometric length scale (*i.e.,* where Z is the variable in the normal direction) to be $[0,\alpha]$ where $\alpha = O(\epsilon^p)$ with $0 < p < 1$. Since the width of the boundary layer is $O(\epsilon)$, this choice of α ensures that the integration region completely covers the

boundary layer but tends to 0 in the asymptotic limit.

Even with this choice of integration region, we still must exercise care to make sure that all integrands are of excess quantities so that integrations over the inner coordinate are convergent. This restriction suggests that we rewrite (4.6) as

$$\frac{\partial \gamma}{\partial t} = -\nabla_s \cdot \left(\hat{\mathbf{F}}_s - \bar{\mathbf{F}}_s \right) - \frac{1}{\epsilon^2} \frac{\partial \hat{F}_n}{\partial z} + \lim_{Z \to 0} \frac{\partial \bar{F}_n}{\partial Z}. \tag{4.8}$$

Integrating over this equation over the boundary layer (at the geometric length scale), we obtain

$$\int_0^\alpha \frac{\partial \gamma}{\partial t} dZ = -\int_0^\alpha \nabla_s \cdot \left(\hat{\mathbf{F}}_s - \bar{\mathbf{F}}_s \right) dZ - \frac{1}{\epsilon^2} \int_0^\alpha \frac{\partial \hat{F}_n}{\partial z} dZ + \int_0^\alpha \left(\lim_{Z \to 0} \frac{\partial \bar{F}_n}{\partial Z} \right) dZ. \tag{4.9}$$

Changing from the outer to the inner coordinate for all of the integrals except the last term yields

$$\begin{aligned} \epsilon \int_0^{\alpha/\epsilon} \frac{\partial \gamma}{\partial t} dz &= -\epsilon \int_0^{\alpha/\epsilon} \nabla_s \cdot \left(\hat{\mathbf{F}}_s - \bar{\mathbf{F}}_s \right) dz - \frac{1}{\epsilon} \int_0^{\alpha/\epsilon} \frac{\partial \hat{F}_n}{\partial z} dz + \int_0^\alpha \left(\lim_{Z \to 0} \frac{\partial \bar{F}_n}{\partial Z} \right) dZ \\ &= -\epsilon \int_0^{\alpha/\epsilon} \nabla_s \cdot \left(\hat{\mathbf{F}}_s - \bar{\mathbf{F}}_s \right) dz - \frac{1}{\epsilon} \hat{F}_n(\alpha/\epsilon) + \alpha \left(\lim_{Z \to 0} \frac{\partial \bar{F}_n}{\partial Z} \right) \end{aligned} \tag{4.10}$$

Note that to move from the first to the second line in the above equations, we have explicitly integrated the normal derivative and applied the no flux boundary condition. Expanding the last term in (4.10) using a Taylor series, we find that

$$\begin{aligned} \epsilon \int_0^{\alpha/\epsilon} \frac{\partial \gamma}{\partial t} dz &= -\epsilon \int_0^{\alpha/\epsilon} \nabla_s \cdot \left(\hat{\mathbf{F}}_s - \bar{\mathbf{F}}_s \right) dz - \frac{1}{\epsilon} \hat{F}_n(\alpha/\epsilon) + \bar{F}_n(\alpha) - \bar{F}_n(0) \\ &\quad + O(\alpha^2). \end{aligned} \tag{4.11}$$

Finally, recalling that $\hat{F}_n(\alpha/\epsilon) = \epsilon \bar{F}_n(\alpha)$, the above equation can be simplified to

$$\epsilon \int_0^{\alpha/\epsilon} \frac{\partial \gamma}{\partial t} dz = -\epsilon \int_0^{\alpha/\epsilon} \nabla_s \cdot \left(\hat{\mathbf{F}}_s - \bar{\mathbf{F}}_s \right) dz - \bar{F}_n(0) + O(\alpha^2). \tag{4.12}$$

By choosing $1/2 < p$ in the definition of α, we find that the $O(\alpha^2)$ term becomes negligible compared to the remaining terms in the $\epsilon \to 0$ limit so that the leading order asymptotic

equation describing surface concentration evolution satisfies:

$$\epsilon \int_0^\infty \frac{\partial \gamma}{\partial t} dz \quad = \quad -\epsilon \int_0^\infty \nabla_s \cdot \left(\hat{\mathbf{F}}_s - \bar{\mathbf{F}}_s \right) dz - \bar{F}_n(0) \tag{4.13}$$

Thus, by substituting the definition for the surface excess concentration

$$\Gamma \equiv \epsilon \int_0^\infty \gamma dz \tag{4.14}$$

and making the identifications $\mathbf{J}_s \equiv \epsilon \int_0^\infty \left(\hat{\mathbf{F}}_s - \bar{\mathbf{F}}_s \right) dz$ and $J_n \equiv \bar{\mathbf{F}} \cdot \hat{n} = -\bar{F}_n$, we arrive at (4.1). The sign difference between J_n and $\bar{F}_n$ is merely a byproduct the choice of orientation for the local coordinate system in our analysis. As mentioned earlier, the sign convention for the normal flux is that J_n be positive when the direction of the flux is into the boundary layer.

It is worth mentioning that the presence of the ϵ in the time dependent term and the surface flux term in (4.13) indicates that the relative importance of these terms relative bulk transport (*i.e.,* the normal flux term) may depend on the choice of time-scales and the magnitude of surface transport. This idea is elaborated upon in Chapter 6 in the context of double layer charging for metal colloid spheres.

4.3 Conclusion

In this chapter, we have presented a general formulation and derivation of surface conservation laws at interfaces that are microscopically diffuse. Our derivation is interesting because it uses only boundary layer theory without requiring the bulk concentration profile to remain near uniform. As we shall see in Chapter 6, this freedom afforded the bulk concentration profiles in our formulation is crucial for analyzing electrochemical systems at extreme operating conditions. Since we shall discuss them at length in Chapter 6, we defer further development of surface conservation laws in the context of electrochemical transport until then.

Chapter 5

Electrochemical Thin Films

> There's plenty of room at the bottom.
>
> – Richard P. Feynman (title of a talk about miniaturization)

> Less is more.
>
> – Robert Browning

5.1 Introduction

Micro-electrochemical systems pose interesting problems for applied mathematics because traditional "macroscopic" approximations of electroneutrality and thermal equilibrium [86], which make the classical transport equations more tractable [95], break down at small scales, approaching the Debye screening length. Of course, the relative importance of surface phenomena also increases with miniaturization. Micro-electrochemical systems of current interest include ion channels in biological membranes [3, 4, 87] and thin-film batteries [2, 30, 84, 101, 109, 112], which could revolutionize the design of modern electronics with distributed on-chip power sources.

In the latter context, the high power-density requirements of many applications, such as portable electronics, means that micro-batteries, consisting of a thin-film electrolyte (solid, liquid, or gel) sandwiched between flat electrodes and interfacial layers where Faradaic

electron-transfer reactions occur [14], are likely to be operated at high current density, possibly exceeding diffusion limitation. Furthermore, due to the small electrode separation for thin film structures, very large electric fields are easily produced by applying only small voltages. As a consequence, the traditional assumption of equilibrium double layers breaks down near the classical diffusion-limited current. Finally, the internal resistance of a micro-battery, which is unlikely to be simply constant (as is usually assumed), is related to the nonlinear current-voltage characteristics of the separator.

Motivated by the application to thin-film micro-batteries, we revisit the classical problem of steady conduction between parallel, flat electrodes, studied by Nernst [83] and Brunner [17, 18] a century ago. Our focus will be on electrochemical thin-films (typically solid or gel), which approach the classical limiting current without hydrodynamic instability [97, 98]. As in subsequent studies of liquid [20, 59] and solid [57, 60] electrolytes, we do not make Nernst's assumption of bulk electroneutrality and work instead with the Poisson-Nernst-Planck (PNP) equations, allowing for diffuse charge in solution [86, 95]. Unlike previous work on current-voltage relations (or "polarographic curves"), here we use more realistic nonlinear boundary conditions describing (i) Butler-Volmer reaction kinetics and (ii) the surface capacitance of the compact Stern layer, as in the recent paper of Bonnefont, Argoul, and Bazant [12]. Such boundary conditions, which complicate the mathematical analysis, generally cannot be ignored in micro-electrochemical cells, where interfaces play a crucial role. Diffuse-charge dynamics, which can be important for high-power applications, also complicates analysis [8], but in most cases it is reasonable to assume that electrochemical thin films are in steady state, due to the short distances for electro-diffusion. We stress, however, that steady state does not imply thermal equilibrium when the system sustains a current.

In the first half of this chapter, we focus on applied currents small enough to justify the standard boundary-layer analysis of the PNP equations, which yields charge densities in thermal equilibrium at leading order in the limit of thin double layers [85]. Here, we focus on the response of the the system in various boundary condition parameter regimes and discuss the breakdown of standard asymptotic analysis as the current approaches the classical diffusion-limited current. In the second half, we extend the analysis to larger currents,

at [103] and above [96] Nernst's diffusion-limited current, and show how more realistic boundary conditions affect diffuse charge, far from thermal equilibrium. Here, our analysis is based on a unified approach to the PNP equations which allows us to systematically study the response of the thin-film at currents far above the diffusion-limited current, which is a relatively unexplored regime. At high currents, we shall find that subtle modifications need to be made to the usual mathematical analysis based on matched asymptotic expansions [23, 73, 85]. The high current analysis is especially important at micron or smaller length scales because the space charge layer need not be "thin" compared to the film thickness and currents may exceed the classical limiting current.

In both cases, we derive matched asymptotic expansions for the concentration profiles and potential in the limit of thin double layers. We also obtain novel formulae for polarographic curves in the same asymptotic limit. These analytical results are validated by comparing them against efficiently computed numerical solutions based on pseudospectral methods (see appendix C). To gain physical insight, we examine our analytical formulae and numerical solutions for a variety of dimensionless physical parameters: the reaction-rate constants (scaled to the typical diffusive flux) and the ratios of the Stern length to the Debye length to the electrode separation. At small length scales, all of these dimensionless parameters play a critical role in the response of the electrochemical cell.

5.2 Mathematical Model

Let us consider uniform conduction through a dilute, binary electrolyte between parallel plate electrodes (Figure 5-1). Our goal is to determine the steady-state response of the electrochemical cell to either an applied voltage, v, or an applied current, j. Specifically, we seek the electric potential $\phi(x)$ and the concentrations $c_+(x)$ and $c_-(x)$ of cations and anions in the region $0 \leq x \leq 1$. The Faradaic current is driven purely by electrodeposition and electrodissolution of the cation at the cathode and anode, respectively,

$$M^+ + e \rightleftharpoons M \qquad \text{(cathode reaction)} \tag{5.1}$$

$$M \rightleftharpoons M^+ + e \qquad \text{(anode reaction)}. \tag{5.2}$$

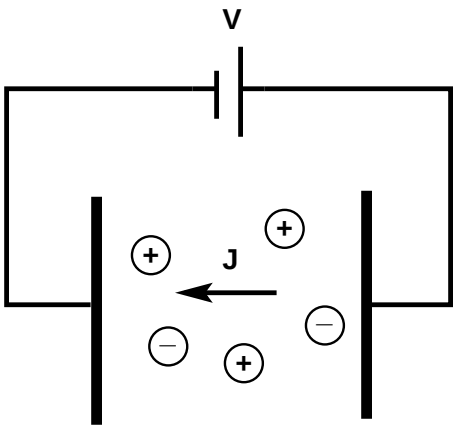

Figure 5-1: Schematic diagram of electrochemical thin-film.

We neglect all other bulk or electrode chemical reactions, such as dissociation/recombination in the bulk solution or hydrogen production. In particular, we assume that the anion does not participate in electrode reactions. Since we do not assume electroneutrality, the region of integration extends to the point where the continuum approximation breaks down near each electrode, roughly a few molecules away. In other words, our integration region includes the "diffuse part" but not the "compact part" of the double layer [5, 14, 28, 86].

5.2.1 Transport Equations

For simplicity we also assume that the electrolyte is symmetric, $z_+ = -z_- \equiv z$, which does not qualitatively affect any of our conclusions as long as $z_+/|z_-|$ is not too different from 1 (which holds for most simple, aqueous electrolytes). In this situation, the transport of cations and anions is described by the steady Nernst-Planck equations

$$\frac{d^2 c_+}{dx^2} + \frac{d}{dx}\left(c_+ \frac{d\phi}{dx}\right) = 0 \tag{5.3}$$

$$\frac{d^2 c_-}{dx^2} - \frac{d}{dx}\left(c_- \frac{d\phi}{dx}\right) = 0, \tag{5.4}$$

and Poisson's equation relates the electric potential to the charge density,

$$-\epsilon^2 \frac{d^2\phi}{dx^2} = \frac{1}{2}(c_+ - c_-). \tag{5.5}$$

Here ϵ is a small dimensionless parameter equal to the ratio of the Debye screening length to the electrode separation (or film thickness). Note that this formulation assumes constant material properties, such as diffusivity, mobility, and dielectric coefficient, and neglects any variations which may occur at large electric fields. The factor of 1/2 multiplying the charge density $c_+ - c_-$ is present merely for convenience.

The two Nernst-Planck equations are easily integrated. Recognizing that the boundaries are impermeable to anions (*i.e.* zero flux of anions at $x = 0$) and taking the nondimensional current density at the electrodes to be $4j$, we find that

$$\frac{dc_+}{dx} + c_+ \frac{d\phi}{dx} = 4j \tag{5.6}$$

$$\frac{dc_-}{dx} - c_- \frac{d\phi}{dx} = 0, \tag{5.7}$$

where we have defined a dimensionless current density, $j \equiv I/I_d$, scaled to the Nernst's diffusion-limited current density (see Section 5.3.1), $I_d \equiv 4zFD_+C_{ref}A/L$. Note that the factor of 4 difference between the definition of I_d here and the definition in Section 2.4 is present solely for analytical convenience. Then by introducing the average ion concentration and (half) the charge density

$$c = \frac{1}{2}(c_+ + c_-) \quad \text{and} \quad \rho = \frac{1}{2}(c_+ - c_-), \tag{5.8}$$

we can derive a more symmetric form for the coupled Poisson-Nernst-Planck equations:

$$\frac{dc}{dx} + \rho \frac{d\phi}{dx} = 2j \tag{5.9}$$

$$\frac{d\rho}{dx} + c \frac{d\phi}{dx} = 2j \tag{5.10}$$

$$-\epsilon^2 \frac{d^2\phi}{dx^2} = \rho. \tag{5.11}$$

5.2.2 Electrode Boundary Conditions

For this system of one second-order and two first-order differential equations, we require four boundary conditions:

$$\phi(0) - \delta\epsilon\frac{d\phi}{dx}(0) = 0, \tag{5.12}$$

$$\phi(1) + \delta\epsilon\frac{d\phi}{dx}(1) = v, \tag{5.13}$$

$$k_c[c(0)+\rho(0)]e^{\alpha_c\phi(0)} - j_r e^{-\alpha_a\phi(0)} = j, \tag{5.14}$$

$$-k_c[c(1)+\rho(1)]e^{\alpha_c(\phi(1)-v)} + j_r e^{-\alpha_a(\phi(1)-v)} = j \tag{5.15}$$

These conditions, which are often simplified or omitted in electrochemical modeling, are central to our analysis. A detailed discussion can be found in Section 2.3, so here we simply give an overview.

The first two boundary conditions, (5.12)–(5.13), account for the intrinsic capacitance of the compact part of the electrode-electrolyte interface, which is taken to be linear (the "Stern model"). The compact-layer charge could contain solvated ions at the point of closest approach to the electrode, as well as adsorbed ions on the surface. The capacitance also accounts for the dielectric polarization of the solvation layer and/or impurities or coatings on the surface. In these boundary conditions, δ is a dimensionless parameter which measures of the strength of the surface capacitance, and v is the total dimensionless voltage drop across the cell.

The next two boundary conditions, (5.14)–(5.15), are Butler-Volmer rate equations which represent the kinetics of Faradaic electron-transfer reactions at each electrode, with an Arrhenius dependence on the compact layer voltage. In these equations, k_c and j_r are dimensionless reaction rate constants and α_c and α_a are transfer coefficients for the electrode reaction. It is important to remember that the dimensionless rate constants decrease with system size, so that "fast reactions" ($k_c, j_r \gg 1$) may become "slow reactions" ($k_c, j_r = O(1)$) as the system is reduced to the micron or sub-micron scale. Also, it is worth noting that α_c and α_a do not vary too much from system to system; typically they have values between 0 and 1 and often both take on values near 1/2.

5.2.3 An Integral Constraint

As formulated above, the boundary value problem is not well-posed. Since the anion flux is constant throughout the cell according to (5.7), the two anion flux boundary conditions are degenerate, leaving one constant of integration undetermined. This is not surprising as we have omitted one crucial parameter – the total number of anions. More precisely, because anions are not allowed to leave the electrolyte by Faradaic processes or specific adsorption, we must specify their total number, which remains constant as the steady state is reached. This constraint is expressed by

$$\int_0^1 [c(x) - \rho(x)]dx = 1 \tag{5.16}$$

As mentioned in Section 2.3, when solving time-dependent problems with the same mathematical model [8, 12], this integral constraint is not needed because the total number of anions is set by the initial condition. Here, we solve for the steady state at different voltages (and currents), assuming the same average concentration of anions to allow a meaningful comparison for the same cell.

5.2.4 Galvanostatic Operating Conditions

It is important to understand that the need for a total of *five* boundary conditions and constraints for the boundary value problem (5.9)–(5.11) reflects the fact that the current-voltage relationship, $j(v)$, or "polarographic curve", is not given *a priori*. As usual in one-dimensional problems [6], it is easier to assume galvanostatic forcing at fixed current, j, rather than the more common experimental situation of potentiostatic forcing at fixed voltage, v. In the former case, j is given, and $v(j)$ is easily obtained from the Stern boundary condition at the anode (5.13). In the latter case, however, v is specified and $j(v)$ must be determined self-consistently to satisfy (5.13). For this reason, we take the former approach in our analysis. For steady-state problems, the two kinds of forcing are equivalent and yield the same (invertible) polarographic curve, $j(v)$ or $v(j)$.

5.2.5 Formulation in terms of the Electric Field

For some of our analysis, it will be convenient to further simplify the problem by introducing the dimensionless electric field, $E \equiv -\frac{d\phi}{dx}$. This transformation is useful because three of the five independent constraints can be expressed in terms of these variables, without explicit dependence on $\phi(x)$, namely the two Butler-Volmer rate equations,

$$k_c(c(0)+\rho(0))e^{-\alpha_c \delta\epsilon E(0)} - j_r e^{\alpha_a \delta\epsilon E(0)} = j, \tag{5.17}$$

$$-k_c(c(1)+\rho(1))e^{\alpha_c \delta\epsilon E(1)} + j_r e^{-\alpha_a \delta\epsilon E(1)} = j, \tag{5.18}$$

and the integral constraint on the total number of anions, (5.16). The potential is recovered by integrating the electric field and applying the Stern boundary conditions (5.12) and (5.13).

5.3 Low Currents ($j \ll 1 - O(\epsilon^{2/3})$)

The steady PNP equations below the classical diffusion-limited current ($j = 1$) have been extensively studied in the literature [4, 23, 73, 85, 87]. However, most of these analyses focus on the thin double-layer limit and impose simple boundary conditions. Moreover, the focus for many of these studies is primarlily the determination of concentration and potential profiles across the cell. The current analysis goes beyond the existing work by (i) imposing boundary conditions appropriate for reactive electrode, (ii) examining the current-voltage relationships implied by the potential profile, and (iii) considering the response of the cell for thick double layers.

5.3.1 Boundary-layer Analysis

In this section, we briefly review the classical asymptotic analysis of the PNP equations, pioneered independently by Chernenko [23], Newman [85], and MacGillivray [73], which involves boundary layers of width, ϵ (corresponding to diffuse-charge layers of dimensional width, λ_D). As discussed below, the classical asymptotics breaks down at large currents approaching diffusion limitation. Unlike most previous authors, who assume either a fixed

potential [21, 42] or fixed interfacial charge [85] at an isolated electrode or fixed concentrations at cell boundaries with ion-permeable membranes [4, 87, 96], we solve for the response of a complete, two-electrode galvanic cell with boundary conditions for Faradaic reactions and Stern-layer capacitance.

Throughout this section, the reader may refer to Figure 5-2, which compares the uniform asymptotic solutions derived below to numerical solutions at several values of ϵ. These figures illustrate the structure of the field variables in the cell as well as give an indication of the quality of the asymptotic solutions. The numerical solutions are obtained by a straightforward iterative spectral method, described in Section 5.5.

Electroneutrality in the Bulk Solution

The most fundamental approximation in electrochemistry is that of bulk electroneutrality [86]. As first emphasized by Newman [85], however, this does not mean that the charge density is vanishing or unimportant, but rather that over macroscopic distances the charge density is small compared to the total concentration, $|C_+ - C_-| \ll C_+ + C_-$, or, in our dimensionless notation, $|\rho| \ll c$. Mathematically, the "macroscopic limit" corresponds to the limit $\epsilon = \lambda_D/L \to 0$. The electroneutral solution is just the leading order solution when asymptotic series of the form $f(x) = f^{(0)}(x) + \epsilon f^{(1)}(x) + \epsilon^2 f^{(2)}(x) + \ldots$, are substituted for the field variables in (5.9)–(5.11).

Carrying out these substitutions and collecting terms with like powers of ϵ, we obtain a hierarchy of differential equations for the expansion functions. At $O(1)$ we have,

$$\frac{d\bar{c}^{(0)}}{dx} = 2j \quad , \quad -\bar{c}^{(0)}\bar{E}^{(0)} = 2j \quad , \quad \bar{\rho}^{(0)} = 0 \tag{5.19}$$

where the bar accent indicates that these expansions are valid in the "bulk region" $\epsilon \ll x \ll 1 - \epsilon$ (or $\lambda_D \ll X \ll L - \lambda_D$). Integrating these equations, we obtain the leading order

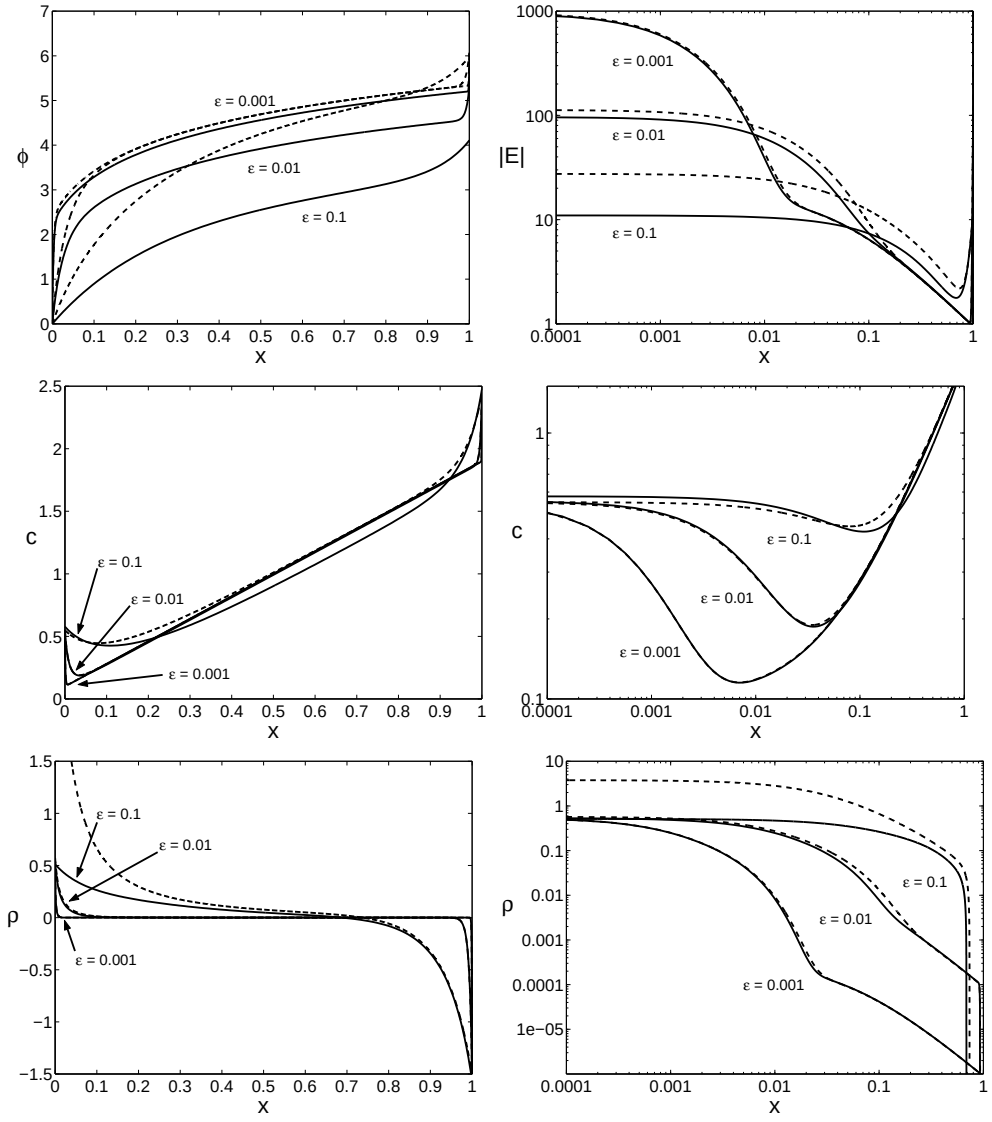

Figure 5-2: Numerical solutions (solid lines) compared with the leading order uniformly-valid approximations (dashed lines) given by (5.43)–(5.46) for the dimensionless potential, $\phi(x)$, electric field, $E(x)$, concentration, $c(x)$, and charge density, $\rho(x)$ for the case $j = 0.9$, $k_c = 10$, $j_r = 10$, $\delta = 0$, and $\epsilon = 0.001, 0.01, 0.1$. Linear scales on the left show the entire cell, while log scales on the left zoom in on the cathodic region. Note that in the concentration and charge density profiles, the numerical and asymptotic solutions are barely distinguishable for $\epsilon \leq 0.01$.

bulk solution:

$$\bar{c}^{(0)}(x) = c_o + 2jx \tag{5.20}$$

$$\bar{E}^{(0)}(x) = \frac{-1}{x + c_o/2j} \tag{5.21}$$

$$\bar{\phi}^{(0)}(x) = \phi_o + \log\left(1 + \frac{2jx}{c_o}\right) \tag{5.22}$$

where the constants of integration c_o and ϕ_o are the values of the bulk concentration and potential extrapolated to the cathode surface at $x = 0$. Note that, despite quasi-electroneutrality, the electrostatic potential does not satisfy Laplace's equation at leading order in the bulk, as emphasized by Levich [64] and Newman [86]. Noting the presence of ϵ^2 in (5.11) for the dimensionless potential, it is clear that a negligible charge density, $\rho = O(\epsilon^2)$, is perfectly consistent with a non-vanishing Laplacian of the potential. More precisely, we have,

$$\bar{\rho}^{(2)}(x) = \frac{d^2\bar{\phi}^{(0)}}{dx^2}(x) = \frac{1}{(x + c_o/2j)^2}, \tag{5.23}$$

at $O(\epsilon^2)$ in (5.11).

The integral constraint, (5.16), can be used to evaluate the constant c_o. If we assume that c_- in the boundary layers does not diverge as $\epsilon \to 0$, then they only contribute $O(\epsilon)$ to the total anion number. Therefore,

$$1 = \int_0^1 c_-(x)dx = \int_0^1 \bar{c}^{(0)}(x)dx + O(\epsilon) = c_o + j + O(\epsilon), \tag{5.24}$$

which implies that $c_o = 1 - j$.

At leading order in the bulk, we have recovered the classical theory dating back a century to Nernst [83, 17, 18]. The solution is electrically neutral with a linear concentration profile whose slope is proportional to the current. This approximation leads to one of the fundamental concepts in electrochemistry, that there exists a "limiting current", $j = 1$, or

$$I = I_d = \frac{4zFD_+C_{ref}A}{L}, \tag{5.25}$$

corresponding to zero concentration at the cathode, $c_o = 1 - j = 0$. The current is limited

by the maximum rate of mass transfer allowed by diffusion, and larger currents would lead to unphysical and mathematically inconsistent negative concentrations (see Appendix B).

Examination of the electric field exposes the same limitation on the current: a singularity exists at $j = 1$ that blocks larger currents from being attained. The leading order bulk approximation to the electric field, $\bar{E}^{(0)} = 1/[x + (1-j)/2j]$, diverges near the cathode like $1/x$ in the limit $j \to 1$. This would imply that the cell voltage v (calculated below) diverges as $j \to 1$, thus providing a satisfactory theory of the limiting current since an infinite voltage would be necessary to exceed (or even attain) it. Unfortunately, this classical picture due to Nernst [83], based on passing to the *singular* limit $\epsilon = 0$, is not valid for any *finite* value of ϵ because the solution is, in general, unable to satisfy all of the boundary conditions.

Diffuse Charge Layers in Thermal Equilibrium

We now derive the leading order description of the boundary layers in the standard way [5, 4, 85, 86], using (5.9)–(5.10). The singular perturbation in (5.11) can be eliminated with the rescaling $y = x/\epsilon$ indicating that the boundary layer at $x = 0$ has a width $O(\epsilon)$. In terms of this inner variable, the governing equations in the cathode boundary layer are

$$\frac{dc}{dy} + \rho\frac{d\phi}{dy} = 2j\epsilon \tag{5.26}$$

$$\frac{d\rho}{dy} + c\frac{d\phi}{dy} = 2j\epsilon \tag{5.27}$$

$$-\frac{d^2\phi}{dy^2} = \rho, \tag{5.28}$$

where ϵ now appears as a regular perturbation since solutions satisfying the cathode boundary conditions and the matching conditions still exist when $\epsilon = 0$. At the anode, the appropriate inner variable is $y = (1-x)/\epsilon$, and the equations are the same as above except that j is replaced with $-j$, since current is leaving the anode layer, while it is entering the cathode boundary layer.

Expanding the cathode boundary layer fields (indicated by the check accent) as asymp-

totic series in powers of ϵ, we obtain at leading order,

$$\frac{d\check{c}^{(0)}}{dy} + \check{\rho}^{(0)}\frac{d\check{\phi}^{(0)}}{dy} = 0 \tag{5.29}$$

$$\frac{d\check{\rho}^{(0)}}{dy} + \check{c}^{(0)}\frac{d\check{\phi}^{(0)}}{dy} = 0. \tag{5.30}$$

Using (5.8) to rewrite these equations in terms of c_+ and c_-, we find that the flux of each ionic species in the boundary layer is zero at leading order:

$$\frac{d\check{c}_{\pm}^{(0)}}{dy} \pm \check{c}_{\pm}^{(0)}\frac{d\check{\phi}^{(0)}}{dy} = 0,. \tag{5.31}$$

While this equation appears to contradict the fact that the current is nonzero, the paradox is resolved in the same way as electroneutrality is reconciled with a non-harmonic potential in the bulk region: tiny fluctuations about the boundary layer equilibrium concentration profiles at $O(\epsilon)$ are amplified by a scaling factor of $1/\epsilon$ to sustain the $O(1)$ current. Thus, the leading order contribution to the current in the boundary layer is

$$\epsilon\left(\frac{d\check{c}_{+}^{(1)}}{dx} + \check{c}_{+}^{(1)}\frac{d\check{\phi}^{(0)}}{dx} + \check{c}_{+}^{(0)}\frac{d\check{\phi}^{(1)}}{dx}\right) = \frac{d\check{c}_{+}^{(1)}}{dy} + \check{c}_{+}^{(1)}\frac{d\check{\phi}^{(0)}}{dy} + \check{c}_{+}^{(0)}\frac{d\check{\phi}^{(1)}}{dy} = 4j. \tag{5.32}$$

Integrating (5.31) and matching with the bulk, we find that the leading order ionic concentrations are Boltzmann equilibrium distributions[1]:

$$\check{c}_{\pm}^{(0)}(y) = c_o e^{\pm[\phi_o - \check{\phi}^{(0)}(y)]} \tag{5.33}$$

where $c_o = 1 - j$ and $\phi_o = \bar{\phi}^{(0)}(0)$ are obtained by matching with the solution in the bulk. Note that the Boltzmann distribution arises not from an assumption of thermal equilibrium in the boundary layer but as the leading order concentration distribution, even in the presence of a non-negligible $O(1)$ current.

The general leading-order solution was first derived by Gouy [42] and Chapman [21] and

[1]The expression for energy in the Boltzmann equilibrium distribution includes only the energy due to electrostatic interactions. "Chemical" contributions to the energy are neglected.

appears in numerous books [5, 56, **?**, 86] and recent papers [4, 12]:

$$\check{c}^{(0)}(y) = c_o \cosh[\phi_o - \check{\phi}^{(0)}(y)] \tag{5.34}$$

$$\check{\rho}^{(0)}(y) = c_o \sinh[\phi_o - \check{\phi}^{(0)}(y)] \tag{5.35}$$

$$\frac{d\check{\phi}^{(0)}}{dy} = 2\sqrt{c_o}\sinh\left(\frac{\phi_o - \check{\phi}^{(0)}(y)}{2}\right) \tag{5.36}$$

$$\check{\phi}^{(0)}(y) = \phi_o + 4\tanh^{-1}\left(\gamma_o e^{-\sqrt{c_o}y}\right), \tag{5.37}$$

where $\gamma_o \equiv \tanh(\zeta_o/4)$ and $\zeta_o \equiv \check{\phi}^{(0)}(0) - \phi_o$ is the leading order "zeta potential" across the cathodic diffuse layer, which plays a central role in electrokinetic phenomena [56, **?**]. Note that the magnitude of the diffuse layer electric field scales as $1/\epsilon$ as illustrated in Figure 5-2.

The value of $\check{\phi}^{(0)}(0)$ hidden in the zeta potential ζ_o is determined by the Stern boundary condition, (5.12). If $\delta = 0$ (Gouy-Chapman model), then $\check{\phi}^{(0)}(0) = 0$, or $\zeta_o = -\phi_o$, which means that the entire voltage drop ϕ_o across the cathodic double layer occurs in the diffuse layer. If $\delta = \infty$ (Helmholtz model), then $\check{\phi}^{(0)}(0) = \phi_o$, or $\zeta_o = 0$, in which case the Stern layer carries all the double layer voltage. For finite $\delta > 0$ (Stern model), ζ_o is obtained in terms of ϕ_o by solving a transcendental algebraic equation,

$$-\zeta_o = 2\delta\sqrt{c_o}\sinh(\zeta_o/2) + \phi_o, \tag{5.38}$$

which can be linearized about the two limiting cases and solved for ζ_o,

$$-\zeta_o \sim \begin{cases} \phi_o - 2\delta\sqrt{c_o}\sinh(\phi_o/2) & \text{if } \delta \ll \phi_o/2\sqrt{c_o}\sinh(\phi_o/2) \\ \phi_o/\delta\sqrt{c_o} & \text{if } \delta \gg \phi_o/2\sqrt{c_o} \end{cases} \tag{5.39}$$

Note that if $\phi_o \ll 1$, then $-\zeta_o \approx \frac{\phi_o}{1+\delta\sqrt{c_o}}$ is a reasonable approximation for any value of $\delta \geq 0$. Finally, we solve for ϕ_o by applying the Butler-Volmer rate equation, (5.14), which yields a transcendental algebraic equation for ϕ_o:

$$k_c c_o e^{-\zeta_o + \alpha_c(\zeta_o + \phi_o)} - j_r e^{-\alpha_a(\zeta_o + \phi_o)} = j. \tag{5.40}$$

Simultaneously solving the pair of equations (5.38) and (5.40) exactly is not possible in

general, but below we will analyze various limiting cases.

In the anodic boundary layer, we find the same set of equations as (5.26)–(5.28) except that j is replaced by $-j$. Therefore, since the fields do not depend on j at leading order, the anodic boundary layer has the same structure but with different constants of integration. Thus, we find that the leading order description of the anodic boundary layer is given by (5.34)–(5.37) with c_o, ϕ_o, γ_o, and ζ_o replaced by different constants c_1, ϕ_1, γ_1, and ζ_1, respectively. Moreover, it is straightforward to show that $c_1 = \bar{c}^{(0)}(1) = 1 + j$ and $\phi_1 = \phi_o + \log\left(\frac{1+j}{1-j}\right)$.

The leading-order anodic zeta potential, ζ_1, and potential drop across the entire anodic double layer, $v - \phi_1$, are found by solving another pair of transcendental algebraic equation resulting from the anode Stern and Butler-Volmer boundary conditions, (5.13) and (5.15),

$$-\zeta_1 = 2\delta\sqrt{c_1}\sinh(\zeta_1/2) + \phi_1 - v \tag{5.41}$$

$$j = -k_c c_1 e^{-\zeta_1 + \alpha_c(\zeta_1 + \phi_1 - v)} + j_r e^{-\alpha_a(\zeta_1 + \phi_1 - v)}. \tag{5.42}$$

As before, the Gouy-Chapman and Helmholtz limits are $\zeta_1 = v - \phi_1$ and $\zeta_1 = 0$, respectively, and for small voltages (or currents) the approximation $\zeta_1 \approx (v - \phi_1)/(1 + \delta\sqrt{c_1})$ is valid for all $\delta \geq 0$.

Leading Order Uniformly-valid Approximations

We obtain asymptotic approximations that are uniformly valid across the cell by adding the bulk and boundary layer approximations and subtracting the overlapping parts:

$$c(x) = [\check{c}^{(0)}(x/\epsilon) - c_o] + \bar{c}^{(0)}(x) + [\hat{c}^{(0)}((1-x)/\epsilon) - c_1] + O(\epsilon), \tag{5.43}$$

$$\rho(x) = \check{\rho}^{(0)}(x/\epsilon) + \epsilon^2\bar{\rho}^{(2)}(x) + \hat{\rho}^{(0)}((1-x)/\epsilon) + O(\epsilon), \tag{5.44}$$

$$E(x) = \frac{1}{\epsilon}\frac{d\check{\phi}^{(0)}}{dy}(x/\epsilon) + \frac{d\bar{\phi}^{(0)}}{dx}(x) - \frac{1}{\epsilon}\frac{d\hat{\phi}^{(0)}}{dy}((1-x)/\epsilon) + O(\epsilon), \tag{5.45}$$

$$\phi(x) = [\check{\phi}^{(0)}(x/\epsilon) - \phi_o] + \bar{\phi}^{(0)}(x) + [\hat{\phi}^{(0)}((1-x)/\epsilon) - \phi_1] + O(\epsilon). \tag{5.46}$$

Note that we have kept the $O(\epsilon^2)$ term in the charge density since it is the leading order contribution in the bulk region and is easily computed from (5.23). As shown in Figure 5-2,

the leading-order uniformly valid solutions are very accurate for $\epsilon \leq 0.01$ (or $L \geq 100\lambda_D$) and reasonably good for $\epsilon = 0.1$. Since higher-order terms are not analytically tractable, it seems numerical solutions must suffice for nanolayers, where $\epsilon \approx 1$, or else other limits of various parameters must be considered, as below.

The discrepancy in electric potential profile at large ϵ in Figure 5-2 is particularly interesting because it arises from a constraint on the total potential drop across the cell. To understand the origin of this voltage constraint, recall that the total cell voltage is determined by the current density flowing through the cell (via the voltage-current relationship). While ϵ is technically a parameter in the voltage-current relationship, a leading-order analysis does not capture the ϵ dependence. Thus, the leading-order cell voltage must be the same for all ϵ which is what we observe in figure 5-2. A close examination of the potential and electric field profiles reveals that most of the error in the asymptotic solution for the potential comes from an over prediction of the electric field strength (and therefore the potential drop) in cathode region.

5.3.2 Polarographic Curves for Thin Double Layers, $\epsilon \to 0$

The relationship between current and cell voltage is of primary importance in the study of any electrochemical system, so we now use the results from the previous section to calculate theoretical polarographic curves in several physically relevant regimes. We focus on the effects of the Stern capacitance and the reaction rate constants through the dimensionless parameters, δ, k_c and j_r, with $\alpha_c = \alpha_a = 1/2$. For a fixed voltage, the mathematical results are valid in the asymptotic limit of thin double layers, $\epsilon \to 0$.

Exact Results at Leading Order

Using the uniformly valid approximation (5.46), we can write the leading order approximation for the cell voltage as

$$v = \phi_o + 2\tanh^{-1}(j) + (v - \phi_1). \tag{5.47}$$

We can interpret this expression as a decomposition of the cell voltage into the potential drop across the cathode, bulk, and anode layers respectively. Note the divergence in the bulk contribution to the cell voltage as $j \to 1$, which we expect from our earlier analysis. In the next section, we explore analytic solutions for several limiting cases and compare them to exact solutions given by (5.47) with the leading-order cathode and anode diffuse layer potential drops determined implicitly by (5.38), (5.40), (5.41). To make plots in our figures, we use Newton iteration to solve for ϕ_o and $v - \phi_1$ in this algebraic system.

Cell Resistance at Low Current

Given the common practice of using linear circuit models to describe electrochemical systems [72, 40, 8], it is important to consider the low-current regime, where the cell acts as a simple resistance, $R = V/I$. First, we compute the potential drop across the double layers. Since the procedure is almost identical for the two boundary layers, we focus on the calculation for the cathode. By writing the boundary conditions (5.14) in the standard Butler-Volmer form involving the exchange current and surface overpotential [5, 86]:

$$j = j_o^c \left(e^{-\alpha_c \eta_s^c} - e^{\alpha_a \eta_s^c} \right) \tag{5.48}$$

where $j_o^c = \left(k_c c_o e^{-\zeta_o} \right)^{\alpha_a} j_r^{\alpha_c}$ and $\eta_s^c = \Delta\phi_S - \Delta\phi_S^{eq}$ are the cathode exchange current and surface overpotential, respectively. Note that the exchange current contains the Frumkin correction through the factor $e^{-\zeta_o}$ [5]. For low current densities, we expect the surface overpotential to be small, so we can linearize this equation to obtain

$$j \sim -j_o^c \eta_s^c \tag{5.49}$$

where we have used the fact that $\alpha_c + \alpha_a = 1$. Rewriting this equation in terms of $\check{\phi}(0)$, we find that

$$\check{\phi}(0) \sim \frac{j}{j_o^c} + \check{\phi}_{eq}(0), \tag{5.50}$$

where $\check{\phi}_{eq}(0)$ is the value of $\check{\phi}(0)$ calculated from the cathode Butler-Volmer rate equation when there is no current flowing through the electrode. The zeta potential ζ_o in the formula

for the exchange current is determined by combining (5.50) with (5.38) to obtain a single equation for ζ_o:

$$-2\delta\sqrt{c_o}\sinh\left(\zeta_o/2\right) \sim \frac{j}{\left(k_c c_o e^{-\zeta_o}\right)^{\alpha_a} j_r^{\alpha_c}} + \log\left(\frac{j_r}{k_c c_o}\right) + \zeta_o. \tag{5.51}$$

Finally, to compute the total double layer potential drop we add the potential drop across the diffuse layer to $\check{\phi}(0)$:

$$\phi_o = \check{\phi}(0) - \zeta_o \sim \frac{j}{j_o^c} + \log\left(\frac{j_r}{k_c c_o}\right). \tag{5.52}$$

A similar calculation at the anode results in

$$v - \phi_1 \sim \frac{j}{j_o^a} + \log\left(\frac{k_c c_1}{j_r}\right), \tag{5.53}$$

where $j_o^a = \left(k_c c_1 e^{-\zeta_1}\right)^{\alpha_a} j_r^{\alpha_c}$ and ζ_1 is determined by the anode equivalent of (5.51).

Combining these results with the potential drop across the bulk solution, we find that the total cell voltage is given by

$$\begin{aligned} v(j) &\sim 4\tanh^{-1}(j) + \frac{j}{j_o^c} + \frac{j}{j_o^a} \\ &\approx j\left(4 + \frac{1}{j_o^c} + \frac{1}{j_o^a}\right). \\ &= j\, r \end{aligned} \tag{5.54}$$

This result gives the dimensionless resistance, r, of the electrochemical thin film as a function of the physical properties of the electrodes and the electrolyte. Note that the Stern-layer capacitance is accounted for implicitly via the calculation of the electrode zeta potentials.

Simple Analytical Formulae

The exact leading-order current-voltage relation simplifies considerably in a variety of physically relevant limits. These approximate formulae provide insight into the basic physics and may be useful in interpreting experimental data.

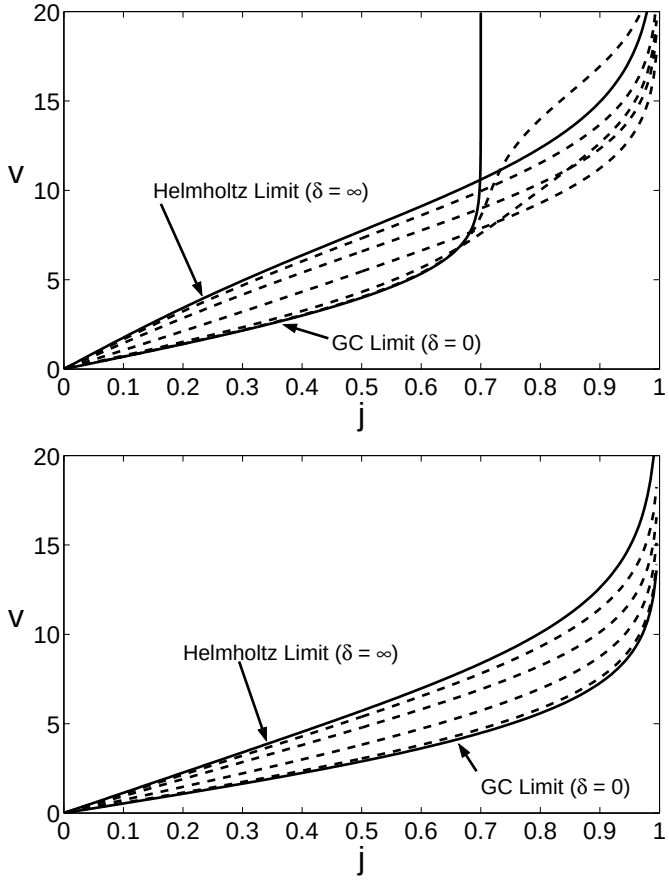

Figure 5-3: Exact polarographic curves (dashed lines) for varying δ values compared to polarographic curves for the Gouy-Chapman ($\delta = 0$) and Helmholtz ($\delta = \infty$) limits (solid lines). Top: a reaction-limited cell ($j_r < 1$) with physical parameters, $k_c = 0.03, j_r = 0.7$. Notice that above the reaction-limited current density, j_r, the highest cell voltages occur for δ values near 0. Bottom: a diffusion-limited cell ($j_r > 1$) with physical parameters: $k_c = 0.05, j_r = 1.5$. In both cases, δ increases as the curves move upwards.

The Gouy-Chapman Limit ($\delta \to 0$) In this limit, the capacitance of the diffuse layer of the charged double layer is negligible compared to the capacitance of the compact layer. As a result, the voltage drop across the diffuse layer accounts for the entire potential drop across the charged double layer. Physically, this limit corresponds to the limits of low ionic concentration or zero ionic volume [5]. Since $\zeta_o = -\phi_o$ and $\zeta_1 = v - \phi_1$ when $\delta = 0$, the Butler-Volmer rate equations, (5.40) and (5.42), reduce to

$$k_c(1-j)e^{-\zeta_o} - j_r = j \quad \text{and} \quad -k_c(1+j)e^{-\zeta_1} + j_r = j. \tag{5.55}$$

Solving for ζ_o and ζ_1, we find that

$$\zeta_o = \ln(1-j) - \ln\left(\frac{j_r + j}{k_c}\right) \quad \text{and} \quad \zeta_1 = \ln(1+j) + \ln\left(\frac{k_c}{j_r - j}\right), \tag{5.56}$$

which can be substituted into (5.47) to obtain

$$v(j) = 4\tanh^{-1}(j) + 2\tanh^{-1}(j/j_r). \tag{5.57}$$

Notice that the boundary layers make a nontrivial contribution to the leading order cell voltage. The $2\tanh^{-1}(j/j_r)$ term is especially interesting because it indicates the existence of a reaction-limited current when $j_r < 1$. In hindsight, it is obvious that reaction limited currents exist in the Gouy-Chapman limit because the reaction kinetics at the anode do not permit a current greater than j_r. We emphasize, however, that the Gouy-Chapman limit is singular because there is no problem achieving current densities above j_r for any $\delta > 0$ (see Figure 5-3). For any finite $\delta > 0$, the shift of the anode double-layer potential drop to the Stern layer helps the dissolution reaction while suppressing the deposition reaction which permits the current density to rise greater than j_r.

Note that the cathodic and anodic boundary layers do not evenly contribute to the cell voltage near the limiting currents. In a diffusion-limited cell, the cathodic layer makes the greater contribution because as $j \to 1$, ζ_o diverges while ζ_1 approaches a finite limit. We expect this behavior because as $j \to 1$, the electric field only diverges at $x = 0$. However, when the cell is reaction-limited, the division of cell voltage between the boundary layers is

reversed as j approaches the limiting current j_r. Even the voltage drop in the bulk becomes negligible compared to ζ_1 in the reaction-limited case. In this situation, the cell voltage diverges as $j \to j_r$ because the only way to achieve a current near j_r is to drastically reduce the deposition reaction at the anode. In other words, the cation concentration at the anode must be made extremely small which requires a huge anodic zeta potential.

The Helmholtz Limit ($\delta \to \infty$) This is the reverse of the Gouy-Chapman limit. Here, the capacitance of the compact layer is negligible, so the potential drop across the double layer resides completely in the compact layer. The Helmholtz limit holds for concentrated solutions or solvents with low dielectric constants and other situations where the Debye screening length becomes negligible [5]. It also describes a thick dielectric or insulating layer on an electrode [1, 8].

In the Helmholtz limit, $\zeta_o = 0 = \zeta_1$, so the Butler-Volmer rate equations take the form

$$k_c(1-j)e^{\alpha_c\phi_o} - j_r e^{-\alpha_a\phi_o} = j \tag{5.58}$$

$$-k_c(1+j)e^{\alpha_c(\phi_1 - v)} + j_r e^{-\alpha_a(\phi_1 - v)} = j. \tag{5.59}$$

Solving these equations for ϕ_o and $v - \phi_1$ under the assumption of a symmetric electron-transfer reaction (*i.e.* $\alpha_c = 1/2 = \alpha_a$) and substituting into the formula for the cell voltage, we find that

$$v(j) = 6\tanh^{-1}(j) + 2\ln\left(\frac{j + \sqrt{j^2 + 4j_r k_c(1-j)}}{-j + \sqrt{j^2 + 4j_r k_c(1+j)}}\right). \tag{5.60}$$

While this expression appears to be more complicated than the one obtained for the Gouy-Chapman model, it is not very different when $j_r > 1$ as can be seen in Figures 5-3 and 5-4. In fact, the wide spread in the polarographic curves observed in Figure 5-3 requires that $k_c \ll j_r$; otherwise, all of the curves would be difficult to distinguish. Moreover, as we shall see in the next section, in limit of fast reactions, both models lead to the same expression for the cell voltage for $j_r > 1$. On the other hand, when $j_r < 1$, the two models are qualitatively very different. While the Gouy-Chapman model gives rise to a reaction-limited current, the Helmholtz model does not.

The Fast-Reaction Limit, $(j_r \gg 1, (j_r)^{\alpha_a}(k_c)^{\alpha_c} \gg j/(1-j)^{\alpha_a})$ The polarographic curves for all δ values collapse onto each other in the limit of fast reaction kinetics (Figure 5-4). Even the assumption of symmetry in the electron-transfer reaction is not required. When reaction rates are much larger than the current, the two reaction-rate terms in the Butler-Volmer equations, (5.40) and (5.42), must balance each other at leading order:

$$k_c(1-j)e^{-\zeta_o+\alpha_c(\zeta_o+\phi_o)} - j_r e^{-\alpha_a(\zeta_o+\phi_o)} \approx 0 \tag{5.61}$$

$$-k_c(1+j)e^{-\zeta_1+\alpha_c(\zeta_1+\phi_1-v)} + j_r e^{-\alpha_a(\zeta_1+\phi_1-v)} \approx 0. \tag{5.62}$$

Since $\alpha_c + \alpha_a = 1$ for theoretical models of single electron-transfer reactions [86, 14, 10], we can solve explicitly for ϕ_o and $v - \phi_1$ to obtain

$$\phi_o = \ln\left(\frac{j_r}{k_c(1-j)}\right) \quad , \quad v - \phi_1 = \ln\left(\frac{k_c(1+j)}{j_r}\right). \tag{5.63}$$

Thus, for fast reaction kinetics, the leading order cell voltage is given by

$$v(j) = 4\tanh^{-1}(j). \tag{5.64}$$

Notice that this is exactly the fast reaction limit of $v(j)$ that we find in both the Gouy-Chapman and Helmholtz limits. It is straightforward to check the validity of the assumptions made in (5.61) and (5.62) by substituting these results into the expressions for the reaction rates and observing that the zeta potentials satisfy the bounds $\zeta_o \leq 0$ and $\zeta_1 \leq \ln\left(\frac{k_c(1+j)}{j_r-j}\right)$ which follow from the monotonicity of ζ_o and ζ_1 as functions of δ.

5.3.3 Thick Double Layers, $\epsilon = O(1)$

Up to this point, we have only examined the current-voltage characteristics in the singular limit $\epsilon \to 0$, where the current density cannot exceed its diffusion-limited value, $j = 1$. The situation changes changes for any finite $\epsilon > 0$.

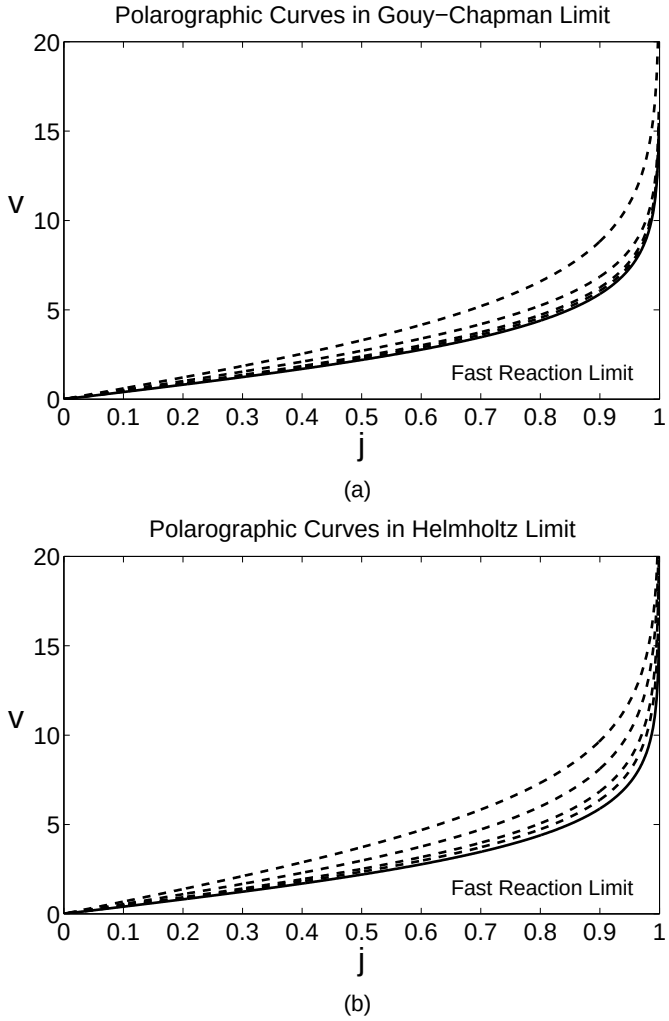

Figure 5-4: Polarographic curves in the (a) Gouy-Chapman limit and (b) Helmholtz limit as the reaction rate constants are increased (dashed lines). For these plots, the reaction rate constants ($j_r = 1, 2, 5,$ and 10) increase as the curves shift towards the lower right and are related by $k_c = j_r/2$. It should be noted that the fast reaction limit is reached very quickly; in both plots, the curve closest to the fast reaction curve has a j_r value of only 10.

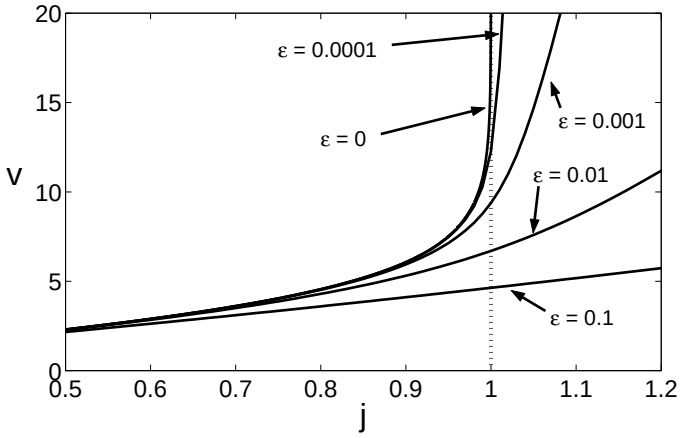

Figure 5-5: Polarographic curves for ϵ values of 0, 0.0001, 0.001, 0.01, and 0.1 (listed in order from uppermost to lowest curves) with the other physical parameters taken to be $\delta = 0$, $k_c = 10$, and $j_r = 10$. Notice that for any $\epsilon > 0$, the cell has no problem achieving current densities higher than the diffusion limited current (dashed vertical line). All of these curves, with the exception of the exact $\epsilon = 0$ curve, were generated by numerically solving (5.9)–(5.11) subject to the boundary conditions (5.12)-(5.16) using the method of Section 5.5.

What Limiting Current?

As is clearly evident in Figure 5-5, the cell has no problem breaking through the classical limiting current for $\epsilon > 0$. Figure 5-5 also shows that the ϵ dependence of the polarographic curves only becomes significant at currents approaching the diffusion-limited current; below $j \approx 0.5$, the curves are nearly indistinguishable. Moreover, as ϵ increases, upper end of the polarographic curves flatten out and shift downwards. This decrease in the cell voltage for large ϵ values arises because the diffuse charge layers overlap and are able to interact with each other. More precisely, the cell has become so small (relative to the Debye screening length) that the electric fields from the two diffuse layers partially cancel each other out throughout the cell resulting in a lower total cell voltage. It should be emphasized that this effect is only observable because we are studying a two electrode system. Single electrode systems (in addition to being not physically achievable) are not capable of showing this behavior because they always implicitly assume an infinite system size which effectively discards any interactions from "far away" electrodes.

Breakdown of the Classical Approximation

For a diffusion-limited cell, the classical nonlinear asymptotic analysis just presented leads to an aesthetically appealing theory that predicts a limiting current at $j = 1$. The existence of this limiting current fits nicely with our physical intuition that the concentration of cations in a solution must always remain nonnegative. In reality, however, the analysis breaks down as the current approaches (and exceeds) its limiting value.

The breakdown of the classical asymptotics is evident upon examining the expansions for the bulk field variables as the current is increased toward its diffusion-limited value. Calculating a few of the higher order terms in the bulk asymptotic expansion, we find that

$$-\bar{E}(x) = \frac{2j}{\bar{c}^{(0)}} + \frac{3}{2}\epsilon^2 \frac{(2j)^3}{\left(\bar{c}^{(0)}\right)^4} + \frac{111}{4}\epsilon^4 \frac{(2j)^5}{\left(\bar{c}^{(0)}\right)^7} + \frac{6045}{4}\epsilon^6 \frac{(2j)^7}{\left(\bar{c}^{(0)}\right)^{10}} + O(\epsilon^8) \quad (5.65)$$

$$\bar{c}(x) = \bar{c}^{(0)} + \frac{1}{2}\epsilon^2 \frac{(2j)^2}{\left(\bar{c}^{(0)}\right)^2} + \frac{3}{2}\epsilon^4 \frac{(2j)^4}{\left(\bar{c}^{(0)}\right)^5} + \frac{231}{8}\epsilon^6 \frac{(2j)^6}{\left(\bar{c}^{(0)}\right)^8} + O(\epsilon^8) \quad (5.66)$$

$$\bar{\rho}(x) = 0 + \epsilon^2 \frac{(2j)^2}{\left(\bar{c}^{(0)}\right)^2} + 6\epsilon^4 \frac{(2j)^4}{\left(\bar{c}^{(0)}\right)^5} + \frac{777}{4}\epsilon^6 \frac{(2j)^6}{\left(\bar{c}^{(0)}\right)^8} + O(\epsilon^8). \quad (5.67)$$

Since $\bar{c}^{(0)} \to 2x$ as $j \to 1$, the higher order terms are clearly more singular than the leading order term at the limiting current. Rubinstein and Shtilman make a similar observation from a potentiostatic perspective; they note that the asymptotic expansions are not uniform in the cell voltage [96].

The inconsistency in the classical approximation was apparently first noticed by Levich who observed that the leading-order solution in the bulk predicts an infinite charge density when the current density reaches 1, which directly contradicts the assumption of bulk charge neutrality [64]. As $j \to 1$, the bulk charge density is given by

$$\bar{\rho} = -\epsilon^2 \frac{d^2\bar{\phi}}{dx^2} = \frac{\epsilon^2}{[x + (1-j)/2j]^2} \approx \frac{\epsilon^2}{x^2}, \quad (5.68)$$

which diverges at the cathode.

Smyrl and Newman first showed that these paradoxical results are related to the breakdown of thermal equilibrium charge profiles near the cathode, leading to a significant expansion of the double layer into the bulk solution [103]. They argue that the assumption

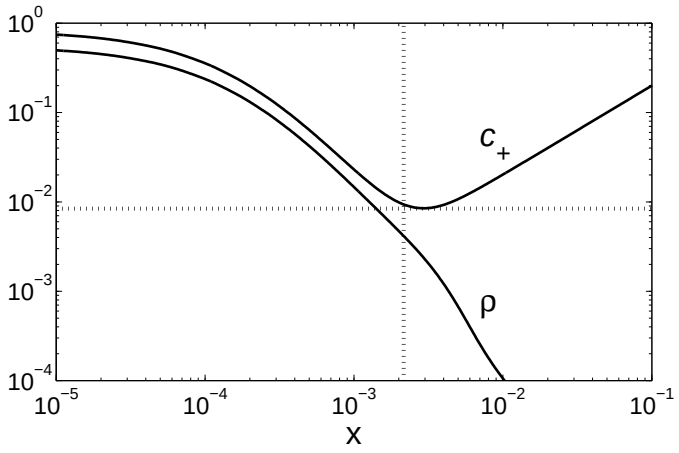

Figure 5-6: Numerical solutions for the dimensionless cation concentration $c_+(x)$ and (full) charge density $2\rho(x)$ at the diffusion-limited current ($j = 1.0$) with physical parameters $k_c = 10$, $j_r = 10$, $\alpha_c = \alpha_a = 0.5$, $\delta = 0.0$ and $\epsilon = 0.0001$. In the cathode region, electroneutrality breaks down as the solution becomes cation rich in order to satisfy the reaction boundary conditions. Note that when $x = O(\epsilon^{2/3})$, c_+ and ρ are both $O(\epsilon^{2/3})$. For reference, the dashed vertical line shows where $x = \epsilon^{2/3}$, and the dashed horizontal line shows where $y = \epsilon^{2/3}\left[(2 + 2^{2/3}) + 4/(2 + 2^{2/3})^2\right] \approx c_+(\epsilon^{2/3})$.

of electroneutrality breaks down when $\bar{\rho} \approx \bar{c}$. Since $\bar{c}$ is proportional to x at the limiting current, the bulk approximation fails to be valid for x smaller than $O(\epsilon^{2/3})$, which leads to a boundary layer that is thicker than the usual Debye length. From an alternative perspective, the problems begin when $\bar{\rho}(0)/\bar{c}(0) \approx 1$ (see Figure 5-6). Using this criterion, we find that the classical asymptotic theory is only appropriate when $c_o \gg (2j\epsilon)^{2/3}$ or, equivalently, $j \ll 1 - (2\epsilon)^{2/3}$. Since the cell voltage is approximately $4\tanh^{-1}(j)$ in many situations, this regime also corresponds to $v = O(|\ln \epsilon|)$. This shows that in thin films, where ϵ is not so small, it is easy to exceed the classical limiting current and achieve rather different charge profiles [25].

5.4 High Currents ($j \geq 1 - O(\epsilon^{2/3})$)

The concept of a "limiting current", due to the maximum, steady-state flux of diffusion across an electrochemical cell, was introduced by Nernst a century ago [83]. Consider the simplest case of a binary electrolyte with cation redox reactions and inert anions, between

parallel plate electrodes. Assuming neutrality, the bulk concentration is a linear function of distance (due to steady diffusion) with a gradient proportional to the current. Since the total number of anions is fixed, the total integral of the bulk concentration must also be fixed, which implies that the concentration at the cathode decreases linearly with current. The "diffusion-limited current" corresponds to a vanishing bulk concentration at the cathode, and, as the name suggests, it can never be reached, except with an infinite voltage.

It was eventually realized that the classical theory is flawed, as illustrated in Figure 5-7 by numerical solutions to our model problem below. The bulk concentration remains linear, but the system is clearly able to achieve and even exceed the classical limiting current (as shown in the lower left panel of the figure). Levich was perhaps the first to notice that the assumption of bulk electroneutrality yields approximate solutions to the Poisson-Nernst-Planck (PNP) equations, which are not self consistent near the limiting current, since the predicted charge density eventually exceeds the salt concentration near the cathode [64]. This paradox was first resolved by Smyrl and Newman, who showed that the double layer expands at the limiting current, as the Poisson-Boltzmann approximation of thermal equilibrium breaks down [103]. Rubinstein and Shtilman later pointed out that mathematical solutions also exist for larger currents, well above the classical limiting value, characterized by a region of non-equilibrium "space charge" extending significantly into the neutral bulk [96]. As shown in Figure 5-7, the space-charge layer exhibits anomalously large electric fields and charge densities, compared to the equilibrium double layers at smaller currents.

The possibility of super-limiting currents has been studied extensively in the different context of bulk liquid electrolytes, where a thin space-charge layer drives nonlinear electro-osmotic slip. This phenomenon of "electro-osmosis of the second kind" was introduced by Dukhin for the nonlinear electrophoresis of ion-selective, conducting colloidal particles [31], and Ben and Chang have recently studied it in microfluidics [9]. The mathematical analysis of second-kind electro-osmosis using matched asymptotic expansions, similar to the approach taken here, was first developed by Rubinstein and Zaltzman for related phenomena at electrodialysis membranes [97, 98]. In earlier studies, the space-charge layer was also invoked by Bruinsma and Alexander [16] to predict hydrodynamic instability during

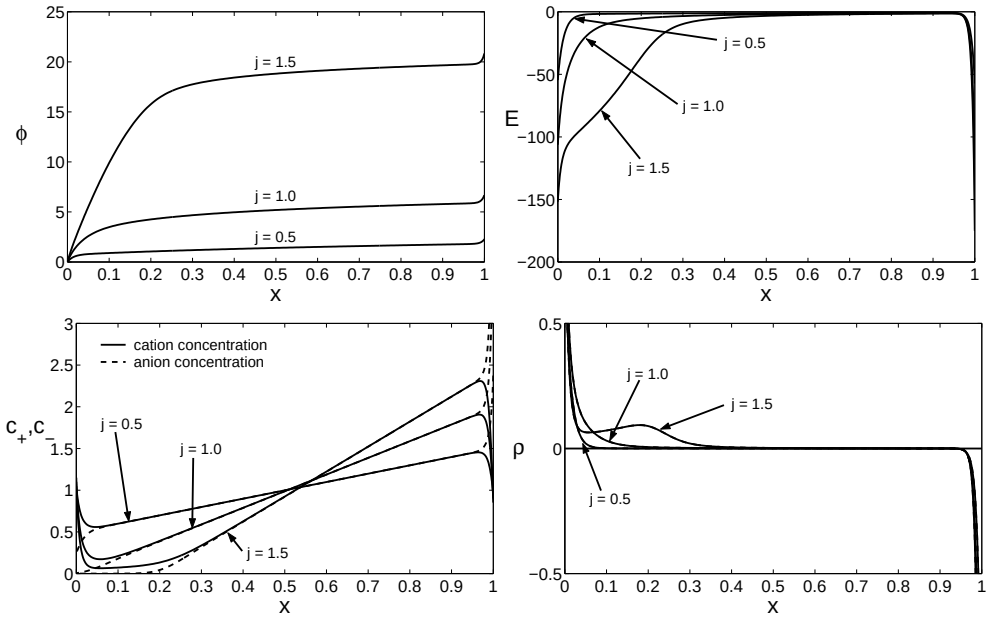

Figure 5-7: Profiles of the dimensionless potential (top left), electric field (top right), total ionic concentration (bottom left), and charge density (bottom right) in three regimes: below the classical diffusion-limited current ($j = 0.5$), at the limiting current ($j = 1$), and above the limiting current ($j = 1.5$). These are numerical solutions to our model problem with the following dimensionless parameters: $\epsilon = 0.01$, $\delta = 0$, $k_c = 10$, $j_r = 10$.

electrodeposition and by Chazalviel [22] in a controversial theory of fractal electrochemical growth.

5.4.1 Unified Analysis at All Currents

Master Equation for the Electrostatic Potential

We begin our analysis by reducing the governing equations, (5.9)–(5.11), to a single master equation for the electrostatic potential. Substituting (5.11) into (5.9) and integrating, we obtain an expression for the average concentration

$$c(x) = \underline{c}_o + 2jx + \frac{\epsilon^2}{2}\left(\frac{d\phi}{dx}\right)^2. \tag{5.69}$$

Then by applying the integral constraint, (5.16), we find that the integration constant, $\underline{c}_o$, is given by

$$\underline{c}_o = (1-j) - \epsilon^2\left[\left(\frac{d\phi}{dx}\right)\Big|_{x=1} - \left(\frac{d\phi}{dx}\right)\Big|_{x=0} + \frac{1}{2}\int_0^1 \left(\frac{d\phi}{dx}\right)^2 dx\right] \tag{5.70}$$

Note that when the electric field is $O(1)$, (5.69) and (5.70) reduce to the leading-order concentration in the bulk when j is sufficiently below the limiting current [6]. We can now eliminate ρ and c from (5.10) to arrive at a single master equation for ϕ

$$\epsilon^2\left[-\frac{d^3\phi}{dx^3} + \frac{1}{2}\left(\frac{d\phi}{dx}\right)^3\right] + (\underline{c}_o + 2jx)\frac{d\phi}{dx} = 2j, \tag{5.71}$$

or equivalently for the electric field E

$$\epsilon^2\left[\frac{d^2E}{dx^2} - \frac{1}{2}E^3\right] - (\underline{c}_o + 2jx)\,E = 2j. \tag{5.72}$$

Once this equation is solved, the concentration, c, and charge density, ρ, are computed using (5.69) and Poisson's equation, (5.11).

The master equation has been derived in various equivalent forms since the 1960s. Grafov and Chernenko [43] first combined (5.6), (5.7) and (5.11) to obtain a single nonlinear differential equation for the anion concentration, c_-, whose general solution they expressed

in terms of Painlevé's transcendents. The master equation for the electric field, (5.72), was first derived Smyrl and Newman [103], in the special case of the classical limiting current, where $j = 1$ and $\underline{c}_o = 0$, where they discovered a non-equilibrium double layer of width, $\epsilon^{2/3}$, which is apparent from the form of the master equation. We shall study the general electric-field and potential equations for an arbitrary current, j, focusing on boundary-layer structure in the limiting and super-limiting regimes.

Recovery of Classical Results Below the Limiting Current, $j \ll 1 - O(\epsilon^{2/3})$

In the low-current regime, the master equation admits the two distinguished limits around $x = 0$ that arise in the classical analysis: $x = O(1)$ and $x = O(\epsilon)$. When $x = O(1)$, we find the usual bulk electric field from (5.71) and the bulk concentration from (5.69). When $x = O(\epsilon)$, the master equation can be rescaled using $x = \epsilon y$ to obtain

$$-\frac{d^3\phi}{dy^3} + \frac{1}{2}\left(\frac{d\phi}{dy}\right)^3 + \underline{c}_o\frac{d\phi}{dy} + 2jy\epsilon\frac{d\phi}{dy} = 2j\epsilon \tag{5.73}$$

which is equivalent to the classical theory at leading order [6]. In particular, the Gouy-Chapman structure of the double-layer can be derived directly from the Smyrl-Newman equation in this limit [12].

The anode boundary layer comes from a similar $O(\epsilon)$ scaling around $x = 1$. Note that in the $j \ll 1 - \epsilon^{2/3}$ regime, the scaling $x = O(\epsilon^{2/3})$ is *not* a distinguished limit because the $\underline{c}_o\left(\frac{d\phi}{dx}\right)$ term would dominate all other terms in (5.71).

5.4.2 Nested Boundary Layers at the Limiting Current, $j = 1 - O(\epsilon^{2/3})$

In this section, we show that a nontrivial nested boundary-layer structure emerges at the classical limiting current when general boundary conditions are considered.

Expansion of the Double Layer Out of Equilibrium

As discussed in Section 5.3.3, the classical analysis breaks down as the current approaches the diffusion-limited current, $j \to 1$. One sign of the problem is that the charge density at

$j = 1$ grows near the cathode ($x \to 0$)

$$\rho = \epsilon^2 \frac{d^2\phi}{dx^2} \sim \frac{\epsilon^2}{x^2}. \tag{5.74}$$

The classical assumption of charged boundary layers of $O(\epsilon)$ width, therefore, fails because the charge density, $\rho = O(1)$, would be much larger than the salt concentration, $c \sim 2x = O(\epsilon)$, at $x = O(\epsilon)$, which violates bulk electroneutrality. This paradox, noted by Levich [64], was resolved by Smyrl and Newman [103], who realized that the structure of the double layer must change near the classical limiting current. In particular, the width of the diffuse part expands to $x = O(\epsilon^{2/3})$, beyond which the bulk charge density remains small, $\rho = O(\epsilon^{2/3})$, as shown in Figure 5-8. Here, we revisit this problem with more general boundary conditions and also consider currents above the classical limiting current.

Mathematically, the classical asymptotics fails because a new distinguished limit for the master equation appears as $j \to 1$. Rescaling the master equation using $x = \epsilon^{2/3} z$ gives us

$$-\frac{d^3\phi}{dz^3} + \frac{1}{2}\left(\frac{d\phi}{dz}\right)^3 + \frac{\underline{c}_o}{\epsilon^{2/3}}\frac{d\phi}{dz} + 2jz\frac{d\phi}{dz} = 2j, \tag{5.75}$$

which implies that we have a meaningful distinguished limit if $\underline{c}_o = O(\epsilon^{2/3})$ or, equivalently, $j = 1 - O(\epsilon^{2/3})$. In this regime, the double layer is no longer in Poisson-Boltzmann equilibrium at leading order, and the potential satisfies the more general equation, (5.75), for $z = O(1)$ or $x = O(\epsilon^{2/3})$.

Unfortunately, at this scale, *all* terms in (5.75) are $O(1)$, so we are forced to solve the full equation. Although general solutions can be expressed in terms of Painlevé's transcendents [95, 9, 43], these are not convenient for applying our nonlinear boundary conditions or obtaining physical insight. Even when $\underline{c}_o = o(\epsilon^{2/3})$, we are left with a complicated differential equation which does not admit a simple analytical solution. However, in the case $\underline{c}_o = o(\epsilon^{2/3})$, it is possible to study the asymptotic behavior of the solution in the limits $z \to 0$ and $z \to \infty$ by considering the behavior of the *neighboring* asymptotic layers.

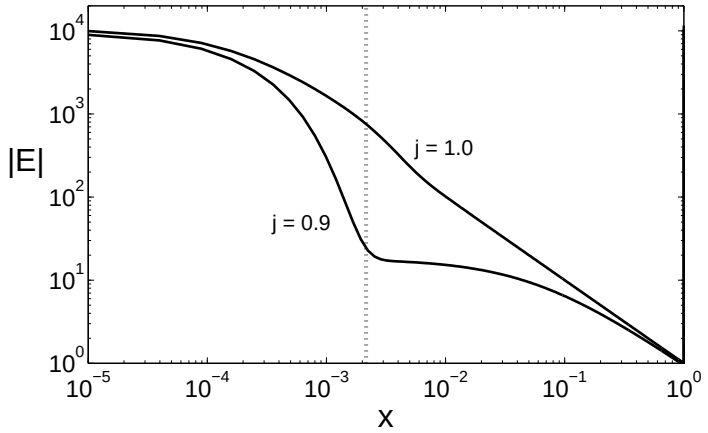

Figure 5-8: Numerical solutions for the dimensionless electric field $E(x)$ at current densities of $j = 0.9$ and $j = 1.0$ demonstrating the expansion of the diffuse layer at the limiting current ($k_c = 1$, $j_r = 2$, $\delta = 0.1$ and $\epsilon = 0.0001$). For reference, the vertical line shows where $x = \epsilon^{2/3}$.

Nested Boundary Layers when $|1 - j| = o(\epsilon^{2/3})$

The appearance of the new distinguished limit for $j = 1 - O(\epsilon^{2/3})$ does not destroy the ones that exist in the classical analysis. In particular, the $O(\epsilon)$ boundary layer at $x = 0$ does *not* vanish. This inner layer was overlooked by Smyrl and Newman because they assumed a fixed surface charge density given by the equilibrium zeta potential [103], rather than more realistic boundary conditions allowing for surface-charge variations and electrochemical reactions.

In the general case, a set of nested boundary layers must exist when the current is near (or above) the classical limiting current. For convenience, we shall refer to the $x = O(\epsilon^{2/3})$ and the $x = O(\epsilon)$ regions as the "Smyrl-Newman" and "inner diffuse" layers, respectively. It is important to realize that, without the inner layer, it would be impossible to satisfy any reasonable boundary conditions describing the electrochemical reactions which support the current. In the Smyrl-Newman layer, the concentration of the active species (here, cations) nearly vanishes at the limiting current, since $\underline{c}_0 = O(\epsilon^{2/3})$, but this would imply a very small reaction rate density. The paradox of the original Smyrl-Newman solution (which ignores reactions) is that there are very few ions available at the cathode, and yet there is a very large reaction rate and current. The resolution involves an inner layer where the

cation concentration increases to $O(1)$.

In the context of our model of electrochemical reactions, we can also understand the nested boundary layers on mathematical grounds. Consider the reaction boundary condition at the cathode, (5.14). To estimate the c and ρ at the electrode surface, we rescale (5.69) and Poisson's equation using $x = \epsilon^{2/3} z$ to obtain

$$c = \underline{c}_o + 2j\epsilon^{2/3} z + \frac{\epsilon^{2/3}}{2}\left(\frac{d\phi}{dz}\right)^2 \tag{5.76}$$

$$\rho = -\epsilon^{2/3}\frac{d^2\phi}{dz^2}, \tag{5.77}$$

which means that the concentration and charge density are both $O(\epsilon^{2/3})$ since $\underline{c}_o = o(\epsilon^{2/3})$ when $|1 - j| = o(\epsilon^{2/3})$. Then, from the Stern boundary condition, we have $\phi(0) = -\delta\epsilon\bar{E} = -\delta\epsilon^{1/3}\grave{E} = O(\delta\epsilon^{1/3})$. Plugging these estimates into the reaction boundary condition, we find

$$k_c O(\epsilon^{2/3}) e^{\alpha_c \delta \epsilon^{1/3}\grave{E}(0)} = j + j_r e^{-\alpha_a \delta\epsilon^{1/3}\grave{E}(0)} = O(1). \tag{5.78}$$

This equation cannot be satisfied in the limit $\epsilon \to 0$ with $\delta \geq 0$ fixed, which implies the existence of the inner diffuse layer. In the Gouy-Chapman model without any compact layer ($\delta = 0$), (5.78) reduces to a contradiction, $O(\epsilon^{2/3}) = j$ =constant, and thus implies the existence of the inner diffuse layer. In the Stern model ($\delta > 0$), it can only be satisfied for very large values, $\delta = O\left(\left|\log \epsilon^{2/3}\right| / \epsilon^{1/3}\right)$, but, since δ is fixed, the nested inner layer must appear as $\epsilon \to 0$. However, this calculation predicts that the magnitude of the concentration at the cathode (within the inner layer) decreases with increasing δ, which is clearly seen in the numerical solutions of Figure 5-9,

To analyze (5.75), it is convenient to focus on the electric field rather than the potential. In terms of the scaled electric field, $\grave{E}(z) \equiv -\frac{d\phi}{dz} = \epsilon^{2/3} E(x)$, (5.75) becomes

$$\frac{d^2\grave{E}}{dz^2} - \frac{1}{2}\grave{E}^3 - 2j\left(z\grave{E} + 1\right) = \frac{\underline{c}_o}{\epsilon^{2/3}}\grave{E} \tag{5.79}$$

which we shall refer to as the "Smyrl-Newman equation". From (5.65), we know that the

first few terms in the expansion for the bulk electric field at the limiting current are

$$\begin{aligned} -\bar{E}(x) &= \frac{1}{x} + \frac{3\epsilon^2}{4x^4} + \frac{111\epsilon^4}{16x^7} + \frac{6045\epsilon^6}{32x^{10}} + \dots \\ &= \frac{1}{\epsilon^{2/3}}\left(\frac{1}{z} + \frac{3}{4z^4} + \frac{111}{16z^7} + \frac{6045}{32z^{10}} + \dots\right). \end{aligned} \tag{5.80}$$

Since the second series is asymptotic for $z \gg 1$, the expansion in the bulk is valid for $x \gg \epsilon^{2/3}$. In order to match the solution in the Smyrl-Newman layer to the bulk, we expect the asymptotic solution to (5.79) as $z \to \infty$ to be given by the expression in parentheses in (5.80). We could also have arrived at this result by directly substituting an asymptotic expansion in $1/z$ and matching coefficients. As we can see in Figure 5-9 the leading order term in (5.80) is a good approximation to the exact solution in the bulk and is matched by the solution in the Smyrl-Newman layer as it extends into the bulk.

We now turn our attention towards the "inner diffuse" layer which gives us the asymptotic behavior of the Smyrl-Newman equation in the limit $z \to 0$. Introducing the scaled variables $y = x/\epsilon = z/\epsilon^{1/3}$ and $\breve{E} = \epsilon\bar{E} = \epsilon^{1/3}\grave{E}$, (5.79) becomes

$$\frac{d^2\breve{E}}{dy^2} - \frac{1}{2}\breve{E}^3 - 2j\epsilon\left(y\breve{E} + 1\right) = \underline{c}_o\breve{E}. \tag{5.81}$$

Near the limiting current (*i.e.* $\underline{c}_o = O(\epsilon^{2/3})$), $\breve{E}$ satisfies $\frac{d^2\breve{E}}{dy^2} = \frac{1}{2}\breve{E}^3$ at leading order with the boundary condition $\breve{E} \to 0$ as $y \to \infty$ from the matching condition that $\grave{E}$ remains bounded as $z \to 0$. Integrating this equation twice with the observation that $\frac{d\breve{E}}{dy} > 0$ gives us

$$\breve{E}(y) \sim -\frac{2}{y+b} \tag{5.82}$$

where b is a constant determined by applying the Butler-Volmer reaction boundary condition at the cathode. We can estimate $\breve{c}(y)$ and $\breve{\rho}(y)$ by substituting (5.82) into (5.69) and Poisson's equation to find

$$\breve{c}(y) = \underline{c}_o + 2jx + \frac{\epsilon^2}{2}\bar{E}(x)^2 = \underline{c}_o + 2j\epsilon y + \frac{1}{2}\breve{E}(y)^2 = \frac{2}{(y+b)^2} + O(\epsilon) \tag{5.83}$$

$$\breve{\rho}(y) = \epsilon^2\frac{d\bar{E}}{dx} = \frac{d\breve{E}}{dy} = \frac{2}{(y+b)^2} + O(\epsilon). \tag{5.84}$$

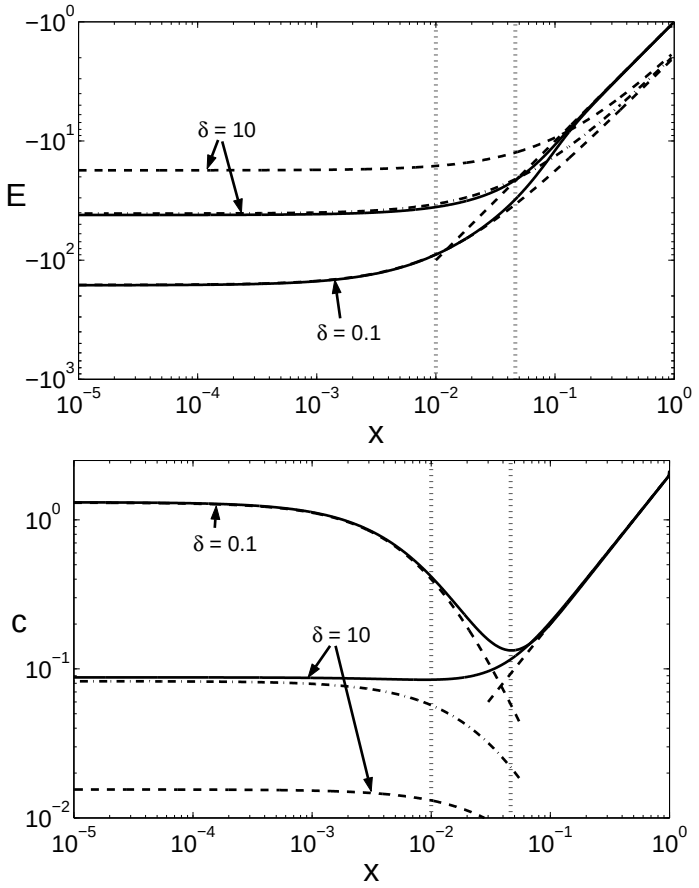

Figure 5-9: Numerical solutions (solid lines) for the dimensionless electric field $E(x)$ and concentration $c(x)$ at the classical diffusion-limited current ($j = 1$) compared with leading order asymptotic approximations (dashed and dot-dashed lines) for $k_c = 1$, $j_r = 2$, $\epsilon = 0.01$ and $\delta = 0.1, 10$. The leading order bulk approximations for $E(x)$ and $c(x)$ are given by (5.80) and $c(x) = 2jx$, respectively. In the diffuse layer, the leading order approximations are given by (5.82) and (5.83). For the $\delta = 10$ curves, the difference between the dashed and dot-dashed curves is that the dashed curve uses an approximate value for b given by (5.88) while the dot-dashed curve uses a b value calculated by numerically solving (5.85). For reference, the vertical lines show where $x = \epsilon$ and $x = \epsilon^{2/3}$. The thin anode diffuse layer field is not shown.

Therefore, b satisfies the following transcendental equation at leading order:

$$k_c \frac{4}{b^2} e^{2\alpha_c \delta/b} = j + j_r e^{-2\alpha_a \delta/b}. \tag{5.85}$$

While this equation does not admit a simple closed form solution, we can compute approximate solutions in the limits of small and large δ values. In the small δ limit, we can linearize (5.85) and expand b in a power series in δ to obtain

$$b \sim 2\sqrt{\frac{k_c}{j + j_r}} + \delta \left(\alpha_c + \frac{\alpha_a j_r}{j + j_r} \right) + O(\delta^2). \tag{5.86}$$

At the other extreme, for $\delta \gg 1$, (5.85) can be approximated by

$$k_c \frac{4}{b^2} e^{2\alpha_c \delta/b} \approx j. \tag{5.87}$$

Then, using fixed-point iteration on the approximate equation, we find that

$$b \sim \frac{2\alpha_c \delta}{\log \kappa - 2 \log \log \kappa + O\left(\log \log \log \delta^2\right)} \tag{5.88}$$

where $\kappa \equiv j\alpha_c^2 \delta^2 / k_c$. Figure 5-9 shows that the leading order approximation (5.82) is very good in the inner diffuse layer as long as an accurate estimate for b is used. While the small δ approximation for b is amazingly good (the asymptotic and numerical solutions are nearly indistinguishable), the large δ estimate for b is not as good but is only off by an $O(1)$ multiplicative factor.

Before moving on, it is worth noting that the asymptotic behavior of the concentration and charge density in the Smyrl-Newman layer as $z \to 0$ and $z \to \infty$ suggest that the charge density is low throughout the entire Smyrl-Newman layer. Figure 5-9 shows how the Smyrl-Newman layer acts as a transition layer allowing the bulk concentration to become small near the cathode while still ensuring a sufficiently high cation concentration at the cathode surface to satisfy the reaction boundary conditions. The transition nature of the Smyrl-Newman layer becomes even more pronounced for smaller values of ϵ.

5.4.3 Bulk Space Charge Above the Limiting Current, $1 + O(\epsilon^{2/3}) \ll j \ll O(1/\epsilon)$

As current exceeds the classical limiting value, the overlap region between the inner diffuse and Smyrl-Newman layers grows to become a layer having $O(1)$ width. Following other authors [96, 22], we shall refer to this new layer as the "*space-charge*" layer because, as we shall see, it has a non-negligible charge density compared to the rest of the bulk. Therefore, in this current regime, the central region of the electrochemical cell is split into two pieces having $O(1)$ width separated by a $o(1)$ transition layer.

In the bulk, the solution remains unchanged except that $\underline{c}_o$ cannot be approximated by $1 - j$; the contribution from the integral term is no longer negligible. The need for this correction arises from the high electric fields required to drive current through the electrically charged space-charge layer. With this minor modification, we find that the bulk solution is

$$\begin{aligned} \bar{c}(x) &= \underline{c}_o + 2jx \\ \bar{E}(x) &= \frac{1}{x_o - x} \end{aligned} \tag{5.89}$$

where $x_o \equiv -\underline{c}_o/2j$ is the point where the bulk concentration vanishes (see Figure 5-10).

In between the two $O(1)$ layers, there is a small transition layer. Rescaling the master equation using the change of variables $z = (x - x_o)/\epsilon^{2/3}$ and $\acute{E}(z) = \epsilon^{2/3}\bar{E}(x)$, we again obtain the Smyrl-Newman equation, (5.79), with right hand side equal to zero. As before, we find that the solution in the transition layer approaches $-1/z$ as $z \to \infty$. In the other direction as $z \to -\infty$, we will find that the appropriate boundary condition is $\acute{E} \to -2\sqrt{j|z|}$ to match the electric field in space-charge layer.

Structure of the Space-Charge Layer

Physically, we could argue that the concentration of ions in the space-charge layer is very small (*i.e.* zero at leading order) because the layer is essentially the result of stretching the ionic content of the overlap between the inner diffuse and Smyrl-Newman layers, which is small to begin with, over an $O(1)$ region. This physical intuition is confirmed by the

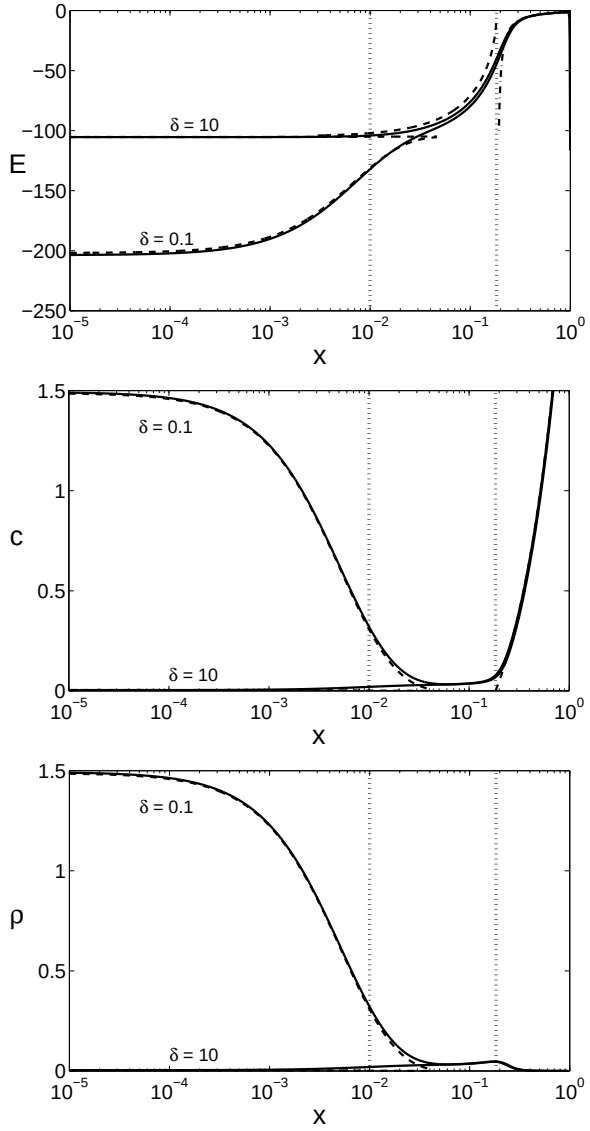

Figure 5-10: Numerical solutions (solid lines) for the dimensionless electric field $E(x)$, average concentration $c(x)$, and charge density $\rho(x)$ above the diffusion-limited current ($j = 1.5$) compared with leading order asymptotic approximations (dashed lines) for $k_c = 1$, $j_r = 2$, $\epsilon = 0.01$, and $\delta = 0.1, 10$. The leading order bulk approximations are given by (5.89). In the space-charge layer, the leading order electric field is given by (5.90), and leading order concentration is 0. Finally, (5.110) and (5.111) are the diffuse layer asymptotic approximations for the electric field and concentration, respectively. For reference, the vertical lines show where $x = \epsilon$ and $x = x_o$.

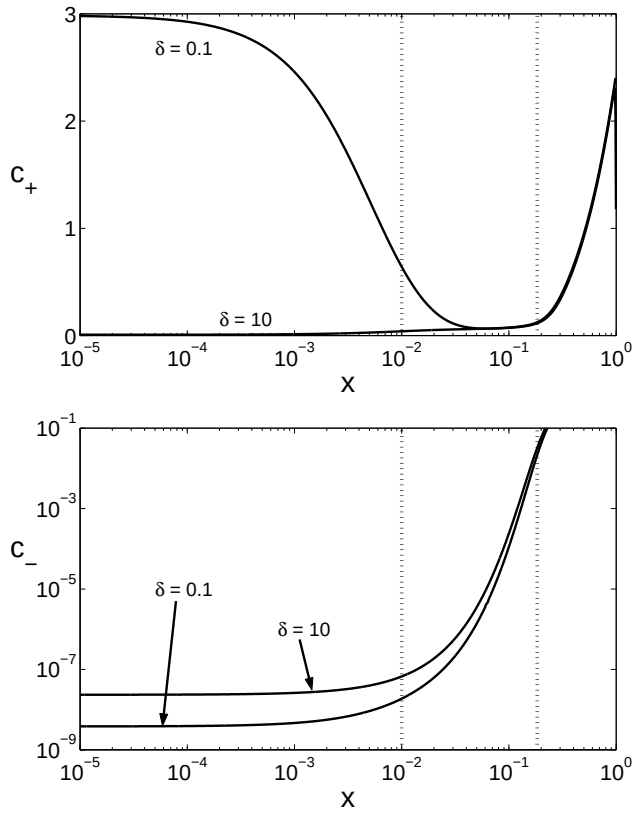

Figure 5-11: Numerical solutions for the dimensionless cation and anion concentrations above the diffusion-limited current ($j = 1.5$) for $k_c = 1$, $j_r = 2$, $\epsilon = 0.01$, and $\delta = 0.1, 10$. For reference, the vertical lines show where $x = \epsilon$ and $x = x_o$.

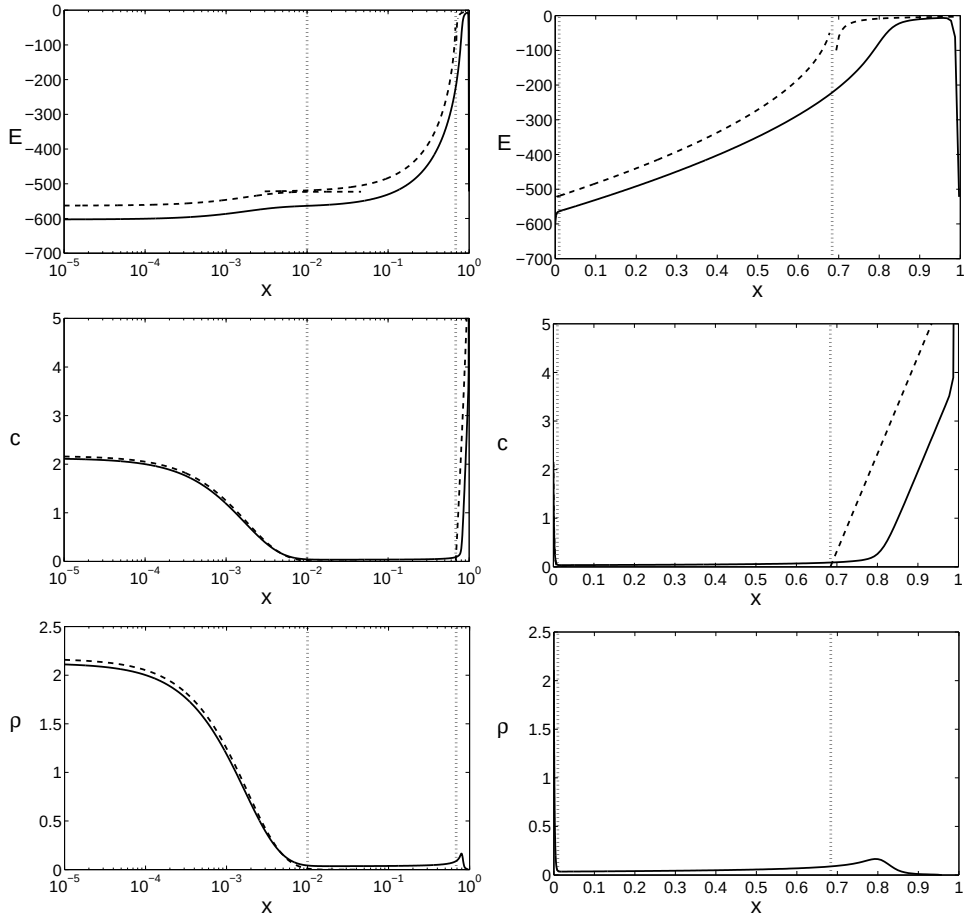

Figure 5-12: Numerical solutions (solid lines) for the dimensionless electric field $E(x)$, average concentration $c(x)$, and charge density $\rho(x)$ far above the diffusion-limited current ($j = 10.0$) compared with leading order asymptotic approximations (dashed lines) for $k_c = 1$, $j_r = 2$, $\epsilon = 0.01$, and $\delta = 0.1$. Each field is shown twice: (1) with x on log scale to focus on the cathode region and (2) with x on a linear scale to emphasize the interior of the cell. Note that $j\epsilon = 0.1$, so the asymptotic approximations are not as good as at lower current densities. For reference, the vertical lines show where $x = \epsilon$ and $x = x_o$.

numerical solutions shown in Figures 5-10, 5-11, and 5-12. Therefore, using (5.69), we obtain the leading order solution for the electric field

$$\tilde{E} \sim \frac{-2\sqrt{j\,(x_o - x)}}{\epsilon}. \tag{5.90}$$

Note that the magnitude of the field is exactly what is required to make the integral term in $\underline{c}_o$ an $O(1)$ contribution. From this formula, it is easy to compute the charge density in the space-charge layer

$$\tilde{\rho} = \epsilon^2 \frac{d\tilde{E}}{dx} \sim \epsilon \sqrt{\frac{j}{x_o - x}}, \tag{5.91}$$

which is an order of magnitude larger than the $O(\epsilon^2)$ charge density in the bulk. The $O(\epsilon)$ charge density also implies that the concentration must be at least $O(\epsilon)$ because the anion concentration, $c - \rho$, is positive.

With the electric field given by (5.90), we can determine the values of x_o and $\underline{c}_o$ by solving the system of equations given by the definition of x_o and $\underline{c}_o$. Using (5.70) to calculate $\underline{c}_o$ and noticing that the leading order contribution to the integral comes from the space-charge layer, we obtain

$$\underline{c}_o \sim 1 - j(1 + x_o^2). \tag{5.92}$$

Combining this result with $x_o = -\underline{c}_o/2j$, we find that

$$x_o \sim 1 - j^{-1/2} \quad , \quad \underline{c}_o \sim 2\left(j^{1/2} - j\right), \tag{5.93}$$

which can be substituted into (5.89) and (5.90) to yield the leading order solutions in the bulk and space-charge layers. It should be noted that the expression for x_o is consistent with the estimate for the width found by Bruinsma and Alexander [16] and Chazalviel [22] in the limits $j - 1 \ll 1$ and small space-charge layer ($x_o \ll 1$), although our analysis also applies to much larger voltages.

The results obtained via physical arguments in the previous few paragraphs motivate an asymptotic series expansion for E whose leading order term is $O(1/\epsilon)$. Moreover, because we want to be able to balance the current density at second-order, we choose the second-order

term to be $O(j)$. Thus, we have

$$\tilde{E} = \frac{1}{\epsilon} E_{-1} + E_0 j + \dots . \tag{5.94}$$

Note that in this asymptotic series, the first term only dominates the second term as long as $j \ll 1/\epsilon$, so the following analysis only holds for current densities far below $O(1/\epsilon)$. Figure 5-12 illustrates the breakdown of the leading-order asymptotic solutions at very high current densities. While the qualitative features of the asymptotic approximation are correct (*e.g.* shape of $E(x)$ in the diffuse layer and slope of $c(x)$ in the bulk), the quality of the approximation is clearly less than at lower values of j.

The key advantage of a more systematic asymptotic analysis is that we are able to calculate the leading-order behavior of the space-charge layer concentration $\tilde{c}$, which is not possible with only knowledge of the leading order behavior for the electric field. Substituting (5.94) into the master equation (5.72), it is straightforward to obtain

$$\tilde{E} \sim -\frac{2}{\epsilon}\sqrt{j\,(x_o - x)} - \frac{1}{2(x_o - x)} + \dots . \tag{5.95}$$

Using this expression in (5.69), we find the dominant contribution to $\tilde{c}$ is exactly the same as $\tilde{\rho}$:

$$\tilde{c} \sim \epsilon\sqrt{\frac{j}{x_o - x}}. \tag{5.96}$$

Since $c_- = c - \rho$, this result leads to an important physical conclusion — *The space-charge layer is essentially depleted of anions*, $c_- = o(\epsilon)$, as is clearly seen in Figures 5-10 and 5-11. This contradicts our macroscopic intuition about electrolytes, but, in very thin films, complete anion depletion might occur. For example, in a micro-battery developed for on-chip power sources using the $Li/SiO_2/Si$ system, lithium ion conduction has recently been demonstrated in nano-scale films of silicon oxide, where there should not be any counter ions or excess electrons [2].

At leading order as $\epsilon \to 0$, the anion concentration, c_-, can be set to zero in the space-

charge layer, leaving the following two governing equations:

$$\frac{dc_+}{dx} + c_+ \frac{d\phi}{dx} = 4j \tag{5.97}$$

$$-\epsilon^2 \frac{d^2\phi}{dx^2} = \frac{1}{2} c_+. \tag{5.98}$$

As with binary electrolyte case, these equations can be reduced to a single equation for the electric potential:

$$\frac{d^3\phi}{dx^3} + \frac{d^2\phi}{dx^2}\frac{d\phi}{dx} = -\frac{2j}{\epsilon^2}. \tag{5.99}$$

Integrating this equation once, we obtain a Riccati equation for $\frac{d\phi}{dx}$

$$\frac{d^2\phi}{dx^2} + \frac{1}{2}\left(\frac{d\phi}{dx}\right)^2 = -\frac{2j}{\epsilon^2}(x - x_o) + h, \tag{5.100}$$

where h is an integration constant. Using the transformations

$$u \equiv e^{\phi/2} \quad , \quad z \equiv -\frac{j^{1/3}}{\epsilon^{2/3}}(x - x_o) + \frac{\epsilon^{4/3} h}{2j^{2/3}}, \tag{5.101}$$

we find that u satisfies Airy's equation

$$\frac{d^2u}{dz^2} - zu = 0. \tag{5.102}$$

Thus, the general solution for $\phi(x)$ is

$$\phi(x) = 2\log\left[a_1 Ai\left(\frac{j^{1/3}}{\epsilon^{2/3}}(x_o - x) + \beta h\right) + a_2 Bi\left(\frac{j^{1/3}}{\epsilon^{2/3}}(x_o - x) + \beta h\right)\right], \tag{5.103}$$

where a_1 and a_2 are constants determined by boundary conditions and $\beta = \frac{\epsilon^{4/3}}{2j^{2/3}}$.

To simplify this expression, note that in the limit $\epsilon \to 0$, the potential drop between $x = x_o$ and $x = 0$ is approximately

$$\phi(x_o) - \phi(0) \sim 2\log\left[\frac{a_1 Ai(0) + a_2 Bi(0)}{a_1 Ai\left(\frac{x_o j^{1/3}}{\epsilon^{2/3}}\right) + a_2 Bi\left(\frac{x_o j^{1/3}}{\epsilon^{2/3}}\right)}\right]. \tag{5.104}$$

Now, using the large argument behavior of the Airy functions, we see that as $\epsilon \to 0$, the argument of the logarithm approaches zero. Thus, we are lead to the conclusion that the electric potential at $x = x_o$ is less than at $x = 0$. But, this is completely inconsistent with our physical intuition and the numerical results, which show that $\phi(x_o) - \phi(0) > 0$. Therefore, it must be the case that $a_2 \approx 0$ so that

$$\phi(x) = 2\log\left[a_1 Ai\left(\frac{j^{1/3}}{\epsilon^{2/3}}(x_o - x) + \beta h\right)\right] \tag{5.105}$$

and

$$E(x) = \frac{2j^{1/3}}{\epsilon^{2/3}} \frac{Ai'\left(\frac{j^{1/3}}{\epsilon^{2/3}}(x_o - x) + \beta h\right)}{Ai\left(\frac{j^{1/3}}{\epsilon^{2/3}}(x_o - x) + \beta h\right)}. \tag{5.106}$$

In principle, the integration constants h and a_1 can be determined by matching to the inner diffuse layer, $x = O(\epsilon)$ (described below), and the bulk transition layer, $|x_0 - x| = O(\epsilon^{2/3})$ (described above). Here, the main point is that the leading order approximation for the electric field when the region is depleted of anions is exactly (5.90), which follows from the asymptotic form of $Ai(z)$ and $Ai'(z)$ as $z \to \infty$ in (5.106). The equivalence of the single-ion equations and the full governing equations at leading-order mathematically confirms the physical interpretation of the space-charge layer as a region of anion depletion.

Boundary Layers Above the Limiting Current

To complete our analysis of the high-current regime, $1 + O(\epsilon^{2/3}) \ll j \ll O(1/\epsilon)$, we must consider the boundary layers. At the anode, all fields are $O(1)$, so we recover the usual Gouy-Chapman solution with the minor modification that $c_1 = 2\sqrt{j}$ which is the value $\bar{c}$ takes as $x \to 1$. The cathode structure, however, is much more interesting because it is depleted of anions (see Figure 5-11). To our knowledge, this non-equilibrium inner boundary layer on the space-charge region, related to the reaction boundary condition at the cathode, has not been analyzed before.

As in the space-charge layer, the leading-order governing equations in this layer are those of a single ionic species with no counterions (5.97) and (5.98). Rescaling those equations

using $x = \epsilon y$, we obtain

$$\frac{d\check{c}_+}{dy} + \check{c}_+ \frac{d\check{\phi}}{dy} = 4j\epsilon \approx 0 \tag{5.107}$$

$$-\frac{d^2\check{\phi}}{dy^2} = \frac{1}{2}\check{c}_+. \tag{5.108}$$

From these equations, it is immediately clear that the cations have a Boltzmann equilibrium profile at leading order: $c_+ \propto e^{-\phi(y)}$. As in the analysis for the space-charge layer, it is possible to find a general solution to (5.107) and (5.108). By combining these equations and integrating, we find that the potential in the cathode boundary layer has the form

$$\check{\phi} \sim \log\left[\sinh^2(py+q)\right] + r, \tag{5.109}$$

where p, q, and r are integration constants. Therefore, the electric field and concentration are

$$\check{E}(y) \sim -2p\coth(py+q) \tag{5.110}$$

$$\check{c}(y) = \frac{1}{2}\check{c}_+(y) \sim \frac{2p^2}{\sinh^2(py+q)} \tag{5.111}$$

Matching the electric fields in the diffuse and space-charge layers, we find that $p \sim \sqrt{jx_o}$. Note that because $p = O(\sqrt{j})$, the electric field in the diffuse charge layer is $O(\sqrt{j}/\epsilon)$ which is same order of magnitude as in the space-charge layer. To solve for q, we use the expression for p in the cathode Stern and Butler-Volmer boundary conditions, which leads to the following nonlinear equation:

$$\frac{4k_c j x_o}{\sinh^2 q}\exp\left(2\alpha_c\delta\sqrt{jx_o}\coth q\right) - j_r\exp\left(-2\alpha_a\delta\sqrt{jx_o}\coth q\right) = j. \tag{5.112}$$

In the limit of small δ, we can use fixed-point iteration to obtain an approximate solution

$$q \sim \sinh^{-1}\left(2\sqrt{\frac{k_c j x_o \exp\left(2\alpha_c\delta\sqrt{jx_o}\coth q_o\right)}{j + j_r\exp\left(-2\alpha_a\delta\sqrt{jx_o}\coth q_o\right)}}\right) \tag{5.113}$$

where q_o has the same form as q with $(\coth q_o)$ set equal to 1. For $\delta \gg 1$, the leading order

$j = 1.0$				$j = 1.5$			
ϵ	δ	v_{exact}	v_{asym}	ϵ	δ	v_{exact}	v_{asym}
1e-4	0.01	13.125	12.101	1e-4	0.01	1297.799	1289.621
1e-4	1.00	13.222	12.374	1e-4	1.00	1297.048	1291.101
1e-4	10.0	14.290	13.571	1e-4	10.0	1305.318	1300.129
1e-3	0.01	10.165	9.146	1e-3	0.01	140.207	132.790
1e-3	1.00	10.277	9.475	1e-3	1.00	139.450	134.270
1e-3	10.0	11.552	10.890	1e-3	10.0	147.717	143.299
1e-2	0.01	7.339	6.303	1e-2	0.01	22.434	15.725
1e-2	1.00	7.479	6.729	1e-2	1.00	21.624	17.206
1e-2	10.0	9.228	8.465	1e-2	10.0	29.886	26.234
1e-1	0.01	4.922	3.649	1e-1	0.01	9.479	2.637
1e-1	1.00	5.005	4.219	1e-1	1.00	7.790	4.118
1e-1	10.0	7.995	6.327	1e-1	10.0	16.088	13.146

Table 5.1: Comparison of the asymptotic approximations (5.117) and (5.118) with numerically calculated values for the cell voltage at various ϵ and δ values. These cell voltages were computed with $k_c = 1$ and $j_r = 2$.

equation is

$$\frac{4k_c j x_o}{\sinh^2 q} \exp\left(2\alpha_c \delta \sqrt{j x_o} \coth q\right) \sim j, \tag{5.114}$$

which implies that $q \gg 1$ so that the left-hand side can be small enough to balance the current. Thus, by using $\coth q \approx 1$ and $\sinh q \approx \exp(q)/2$, we find that $q \sim \alpha_c \delta \sqrt{j x_o} + \frac{1}{2}\log(16 k_c x_o)$. The agreement of these asymptotic approximations with the numerical solutions in the diffuse charge layer is illustrated in Figure 5-10.

5.4.4 Polarographic Curves

We are now in a position to compute the leading-order behavior of the polarographic curve at and above the classical limiting current. Recall that the formula for the cell voltage is given by

$$v = -\delta\epsilon E(0) + \int_0^1 -E(x)dx - \delta\epsilon E(1). \tag{5.115}$$

The integral is the voltage drop through the interior of the cell and the first and last terms account for the potential drop across the Stern layers.

At the limiting current, $j = 1$, we can estimate the voltage drop across the cell by using the bulk and diffuse layer electric field to approximate the field in the Smyrl-Newman transition layer to obtain

$$v \sim -\delta\epsilon E(0) + \int_0^{\epsilon^{2/3}} -E(x)dx + \int_{\epsilon^{2/3}}^1 -E(x)dx - \delta\epsilon E(1) \tag{5.116}$$

$$\sim 2\frac{\delta}{b} + 2\log\left(\frac{\epsilon^{-1/3}+b}{b}\right) - \frac{2}{3}\log\epsilon. \tag{5.117}$$

Notice that in the small δ limit, this expression reduces to $v \sim -\frac{4}{3}\ln\epsilon$ as $\epsilon \to 0$. The dependence, $v(j=0) \propto \ln\epsilon$, is clear in the numerical polarographic curves shown below in Figure 5-13 (See also Figure 5-5). Table 5.1 compares this approximation with the exact cell voltage for a few ϵ and δ values. For small ϵ values ($\epsilon \leq 0.01$), the asymptotic approximations are fairly good (within 5% to 10%).

Above the limiting current, the space-charge layer makes the dominant contribution to the cell voltage. Using (5.89) and (5.90) in the formula for the cell voltage, we find that

$$v \sim \frac{4\sqrt{j}}{3\epsilon}\left(1 - j^{-1/2}\right)^{3/2} + 2\delta\left(j - \sqrt{j}\right)^{1/2}\coth q - \frac{1}{2}\log j - 2/3\log\epsilon. \tag{5.118}$$

The first two terms in this expression estimate the voltage drop across the space-charge and the cathode Stern layers, respectively. The last two terms are the sub-dominant contribution from the bulk where we have somewhat arbitrarily taken $x = x_o + \epsilon^{2/3}$ as the boundary between the bulk layer and the Smyrl-Newman transition layer. Notice that we ignore the contribution from the cathode diffuse and Smyrl-Newman layers. It is safe to neglect the diffuse layer because it is an $O(1)$ contribution. However, the Smyrl-Newman layer has a non-negligible potential drop that we have to accept as error since we do not have an analytic form for the solution in that region.

Figure 5-13 shows that the asymptotic polarographic curves are quite accurate for sufficiently small ϵ values. In Table 5.1, we compare the results predicted by the asymptotic formula with numerical results for a few specific values of ϵ and δ. It is interesting that the approximation is also better for large δ values (we explain this observation in the next section). Also, while the $\log\epsilon$ term is sub-dominant, it makes a significant contribution to

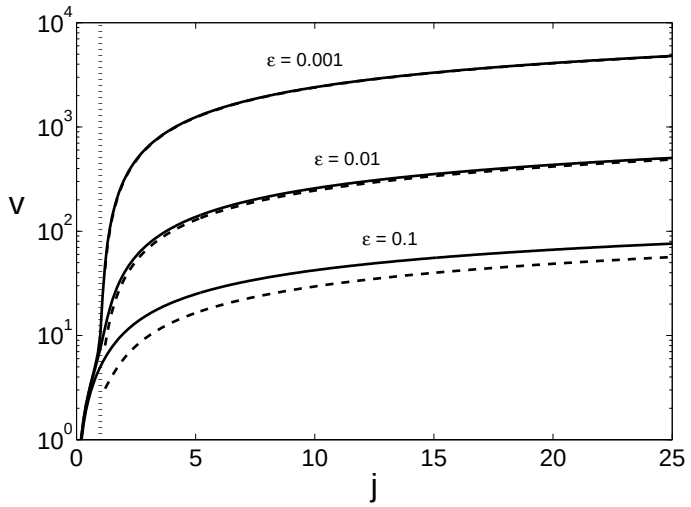

Figure 5-13: Comparison of numerical polarographic curves (dashed lines) with leading-order asymptotic approximations (solid lines) given in (5.118) for several values of ϵ with $\delta = 1.0$, $k_c = 1$ and $j_r = 2$. For $\epsilon = 0.001$, the numerical and asymptotic polarographic curves are indistinguishable on this graph. For reference, the vertical, dashed line shows the classical diffusion-limited current $j = 1$.

the cell voltage for ϵ values as small as 0.01.

As with the width of the space-charge layer, x_o, our expression for the cell voltage, (5.118), is consistent with the results of Bruinsma and Alexander [16] and Chazalviel [22], near the limiting current, $j \to 1^+$, while remaining valid at much larger currents, $j = O(1/\epsilon)$

5.4.5 Effects of the Stern-Layer Capacitance

The inclusion of the Stern layer in the boundary conditions allows us to explore the effects of the intrinsic surface capacitance on the structure of the cell. From Figures 5-9 through 5-11, we can see that smaller Stern-layer capacitances (*i.e.* larger δ values) decrease the concentration and electric field strength in the cathode diffuse layer. This behavior arises primarily from the influence of the electric field on the chemical kinetics at the electrode surfaces. When the capacitance of the Stern layer is low, small electric fields at the cathode surface translate into large potential drops across the Stern layer, (5.12), which help drive the deposition reaction, (5.14). As a result, neither the electric field nor the cation concentration need to be very large at the cathode to support high current densities. These results confirm

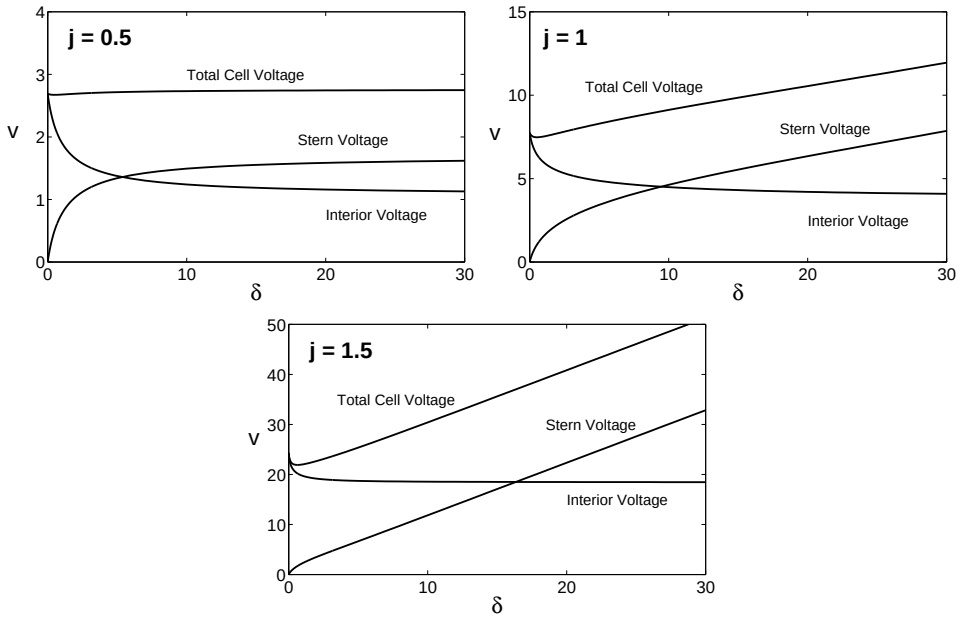

Figure 5-14: These graphs break the total cell voltage into contributions from the cell interior and the Stern layer as a function of δ for $\epsilon = 0.01$, $k_c = 2$, and $j_r = 2$. Note that at and above the classical limiting current, the Stern layer voltage dominates the total cell voltage for large values of δ.

our physical intuition that it is only important to pay attention to the diffuse layer when the Stern layer potential drop is negligible (*i.e* $\delta \ll 1$).

At high currents, another important effect of the Stern layer capacitance is that the total cell voltage becomes dominated by the potential drop across the Stern layer at large δ values (*i.e.* small capacitances). This behavior is clearly illustrated in Figure 5-14. Notice for currents below the classical diffusion-limited current, the total cell voltage does not show a strong dependence on δ. However, for $j > 1$, the total cell voltage increases with δ – the increase being driven by the strong δ dependence of the Stern voltage.

5.5 Numerical Model

To solve the master equation for the electric field with the boundary conditions and integral constraint, we use the Newton-Kantorovich method [13]. Specifically, we use a Chebyshev pseudospectral discretization to solve the linearized boundary-value problem at each itera-

tion [13, 111]. Our decision to use this method is motivated by its natural ability to resolve boundary layers and its efficient use of grid points. We are able to get accurate results for many parameter regimes very quickly (typically less than a few minutes on a workstation) with only a few hundred grid points, which would not be possible at large currents and/or thin double layers using a naive finite-difference scheme. It is important to stress that the boundary conditions and the integral constraint are explicitly included as part of the Newton-Kantorovich iteration. Therefore, the linear BVP solved in each iteration is actually an *integro-differential equation* with boundary conditions that are integro-algebraic equations.

To ensure convergence at high currents, we use continuation in the current density parameter, j, and start with a sufficiently low initial j that the bulk electroneutral solution is a reasonable initial guess; often, initial j values relatively high compared to the diffusion-limited current are acceptable. After a small increase in current, we check that the iteration converges to a correspondingly small perturbation of the previous solution. Analogous continuation in the δ parameter is also sometimes necessary to compute solutions at high δ values.

5.6 Conclusions

In this chapter, we have revisited the classical PNP equations, analyzing for the first time the effect of physically realistic boundary conditions for thin-film galvanic cells and other micro-electrochemical systems. In particular, we have examined the effect of Stern-layer capacitance and Faradaic reactions with Butler-Volmer kinetics. Such boundary conditions contain new physics, such as the possibility of a reaction-limited current due to the slow injection of ions at the anode. We also find that the Stern layer generally allows the cell to exceed limiting currents by carrying diverging portions of the cell voltage, which would otherwise end up in the diffuse part of the double layer.

A key contribution of this work is the derivation of analytical formulae for current-voltage relations below and far beyond the limiting current. These formulae, which are derived using the asymptotic approximations for the fields, compare well with numerical

results and could prove useful in characterizing the differential resistance or interpreting experimental data of thin films, such as those used in on-chip micro-batteries.

Our work also contributes new insight into the exotic regime of super-limiting current densities. Our analysis of the leading-order fields at and above the classical, diffusion-limited current demonstrate the need for a nested boundary layer structure at the cathode in order to satisfy the reaction boundary conditions. In addition, we have shown that the key feature of the bulk space-charge layer is the depletion of anions. Our exact solution of the leading-order problem in the space-charge region, (5.103), could thus also have relevance for Faradaic conduction through very thin insulating films which are likely to be deficient in counter-ions.

A general conclusion of this study is that boundary conditions strongly affect the solution. For example, the Stern-layer capacitance, often ignored in theoretical analysis, plays an important role in determining the qualitative structure of the cell near the cathode, as well as the total cell voltage. The nonlinear boundary conditions for Butler-Volmer reaction kinetics also profoundly affect charge distribution and current-voltage relation, compared to the ubiquitous case of Dirichlet boundary conditions. The latter rely on the assumption of surface equilibrium, which is of questionable validity at very large currents.

We leave the reader with a word of caution. The results presented here are valid mathematical solutions of standard model equations, but their physical relevance should be met with some skepticism under extreme conditions, such as super-limiting current. For example, the PNP equations are meant to describe infinitely dilute solutions in relatively small electric fields [5, 28, 86]. Even for quasi-equilibrium double layers, their validity is not so clear when the zeta potential greatly exceeds the thermal voltage, because co-ion concentrations may exceed the physical limit required by discreteness (accounting also for solvation shells) and counter-ion concentrations may become small enough to violate the continuum assumption. Large electric fields can cause the permittivity to vary, by some estimates up to a factor ten, as solvent dipoles become aligned. Including such effects, however, introduces further *ad hoc* parameters into the model, which may be difficult to infer from experimental data. Instead, we suggest using our analytical results (especially current-voltage relations) to test the validity of the basic model equations in thin-film experiments.

5.7 Future Research

We close this chapter by mentioning a few possible directions for future research on electrochemical thin films. Based on the assumption that the steady-state is quickly reached in thin-films, we have focused on the the steady response of these systems. A natural next step would be to consider the transient response of the system. Bazant, Thornton, and Ajdari [8] have taken a first step in this direction with their analysis of the transient response of a 1D cell to a suddenly applied voltage. However, their analysis focuses on the charging of the double layers and do not include Faradaic reactions at the electrodes. For applications in systems that require a sustained current density, these electrode reactions cannot be neglected.

Another important question that could be addressed is the stability of the steady solutions obtained in this chapter. In our analysis, we have assumed that the concentration and potential profiles are uniform in the directions transverse to the electrode surfaces. However, for many physical systems, interesting instabilities arise in the transverse direction. It would be valuable to know if such instabilities are important to in the context of electrochemical transport.

Chapter 6

Double Layer Charging of Metal Colloid Spheres

> Three important branches of colloid science – the theory of the electric double layer, electrokinetic phenomena, and electric surface forces – have always been developed in close connection with each other and traditionally on the basis of the concept of complete equilibrium of the double layer (DL). However, the DL transforms from its equilibrium state into a non-equilibrium state under any effect causing internal ion flow, e.g. under the influence of an external electric field.
>
> – Stanislav S. Dukhin [32]

6.1 Introduction

Double layer charging plays an important role in many micro-electrochemical and biological systems subject to applied voltages or electric fields. For example, AC electric fields can be used to pump liquid electrolytes [1, 15, 41, 46, 47, 76, 80, 91, 92, 93, 108], to separate or self-assemble colloidal particles [35, 48, 74, 79, 94, 110, 118], and to manipulate biological cells and vesicles [52, 75, 89]. The motivation for our present work on double layer charging comes from recent advances in induced charge electro-osmotic pumping and mixing strategies for

microfluidic devices [1, 7, 15, 41, 61, 65, 104, 105, 108]. In this context, the double layer charging process is critical because it is the sole source of surface charge that generates electrokinetically driven fluid flow [1, 15, 41, 46, 47, 76, 80, 91, 92, 93, 108].

While the problem of double layer charging has been extensively studied in electrochemistry [5, 86] and colloidal science [56, 68, 99], many theoretical results assume that the electrochemical system is adequately described by a circuit model [8, 40]. In circuit models, the bulk concentration is presumed to remain uniform throughout the charging process so that the bulk region may be modeled as a simple linear resistor. As a result, the analysis is greatly simplified because the nonlinear coupling between ionic concentrations and the electric field may be neglected. While convenient, these models neglect the possibility of bulk concentration gradients which become important at high applied fields [8] or when the double layer becomes highly charged [33, 54, 55, 102]. The work of Dukhin and Shilov [33, 102] and Hinch, Sherwood, Chew, and Sen [54, 55] made significant progress beyond the circuit model by including bulk diffusion in their studies of double layer polarization around highly charged, spherical particles in weak applied fields. Their analysis showed that bulk concentration gradients appear as a small correction to a uniform background for small applied electric fields. The present analysis makes further progress in the study of double layer polarization by considering strong applied fields where bulk concentration gradients become so large that they appear at leading order.

Recently, Bazant, Thornton, and Ajdari further examined the effects of nonlinear bulk transport processes by studying the response of a 1D electrochemical cell subjected to a suddenly applied voltage drop [8]. For applied voltages in the *weakly nonlinear* regime, which is analogous to the situation of weak applied fields for higher dimensional systems, they found that while the leading order concentration profile remains uniform, relaxation of the cell to the steady state requires bulk diffusion processes as a first-order correction[1]. They also considered the response of the cell in the *strongly nonlinear* regime (*i.e.,* very high applied voltages) where $O(1)$ bulk concentration variations appear. Here, progress is

[1]It should be noted that in [8], the small parameter that controls the size of the correction is ϵ, the ratio of the Debye length to the system size. In [33, 54, 55, 102], on the other hand, the controlling parameters appear to be both ϵ *and* the strength of the applied electric field (although the small parameters are not explicitly defined).

made primarily through numerical simulation because the leading order equations involve nonlinearities that hinder mathematical analysis. Analytical progress in the strongly nonlinear regime is also made difficult because standard techniques based on asymptotic series break down due to the inadequacy of ordering the terms by ϵ alone. In both regimes, an important conclusion to draw is that absorption of neutral salt by the double layer (and therefore build up of surface charge density) is the key driving force for bulk diffusion.

An important feature that differs between circuit models and models that allow for bulk diffusion is the characteristic dynamic time scale. For circuit models, the characteristic time scale is the so-called RC charging time, $\tau_c = \lambda_D L/D$, where λ_D is the Debye length, L is the system size, and D is the characteristic diffusivity of the ions[2]. For diffusive systems, the dynamics of the system occur on the diffusion time scale, $\tau_L = L^2/D$. Most theoretical analyses of electrochemical systems only consider the dynamics at one of the two dominant time scales – effectively decoupling the dynamics at the two time scales. This decoupling of the dynamics is natural when one considers the wide separation in the time scales that govern the evolution of the system: $\tau_L \gg \tau_c$. One of the interesting contributions of [8] is a discussion of how the two time scales are coupled using ideas related to time-dependent asymptotic matching.

In this chapter, we extend the 1D analysis carried out in [8] to higher dimensions. Specifically, we study double layer charging around an isolated, polarizable sphere. In our analysis, we consider bulk diffusion processes and the coupling between the RC and diffusion time scales. Motivated by the 1D analysis of Bazant, Thornton, and Ajdari, we focus on the thin-double layer limit, which allows us to separate the descriptions of the bulk and the double layer. In effect, we derive a pseudo-circuit model for the electrochemical system where the double layer is treated as a nonlinear capacitor and the bulk is treated as a circuit element that whose dynamics are governed by diffusive processes in the bulk.

One important detail we consider carefully is surface conduction, which only becomes

[2]Note that when charging is driven by an externally applied voltage or field, the relevant relaxation time for double layer charging is *not* the often quoted Debye time, $\tau_D = \lambda_D^2/D$ [56, **?**]. The Debye time is the correct characteristic response time for double layer charging only in the unphysical scenario where charge is instantaneously placed on the particle (as opposed to transported through the electrolyte) [37]. This result has been discovered many times by different scientific communities [8, 32, 34, 60, 71] but only recently seems to be gaining widespread understanding.

important in higher dimensional systems. Using the general theoretical framework developed for the study of surface conservation laws (see Chapter 4), we rigorously derive a set of "effective boundary conditions" that couple the double layer to the bulk. We then use the effective boundary conditions to explore the interplay between bulk neutral salt depletion, surface conduction, and bulk concentration gradients. Our main findings are that (i) strong applied fields can induce $O(1)$ bulk concentration variations and that (ii) at moderate applied fields, surface conduction plays a role in bulk diffusion (which appear at $O(\epsilon)$) even for particles with small equilibrium zeta-potentials. These results complement the extensive work on surface conductance by Russian colloid scientists [29, 33, 102] that examined the charging dynamics of particles with large equilibrium zeta-potentials subjected to weak applied fields.

The outline for this chapter is as follows. We first give a mathematical description for our model problem paying close attention to the derivation of effective boundary conditions. Next, we explore the steady response of the system to high applied electric fields. Even at steady state, the system exhibits rich behavior and displays features that have not previously been fully appreciated. In particular, surface conduction (due to induced surface charge density), $O(1)$ bulk concentration gradients, and $O(1)$ diffusion currents become important at leading order and contribute to ion transport. We then consider the transient response of the system to a suddenly applied, uniform electric field. This analysis is broken into three regimes: (i) weak applied field, (ii) weakly nonlinear dynamics, and (iii) strongly nonlinear dynamics. At weak applied fields, we study the time scales for double layer charging through the use of integral transform methods. In the weakly nonlinear regime, we use boundary layer theory in space *and* time to understand the dynamics of the system at the RC and diffusion time scales. We explicitly discuss coupling of the the dynamics at the two time scales through time-dependent asymptotic matching. Unfortunately, in the strongly nonlinear regime, analysis appears to be very challenging due to non-uniformity in the appropriate effective flux boundary to impose. For this regime, we merely derive the leading order equations and highlight the primary difficulties that arise. Finally, we conclude with a few comments on possible directions for future research.

6.2 Mathematical Model

For our model problem, we consider the response of an isolated, polarizable sphere subjected to a uniform, applied electric field (see Figure 6-1). For simplicity, we shall focus only on

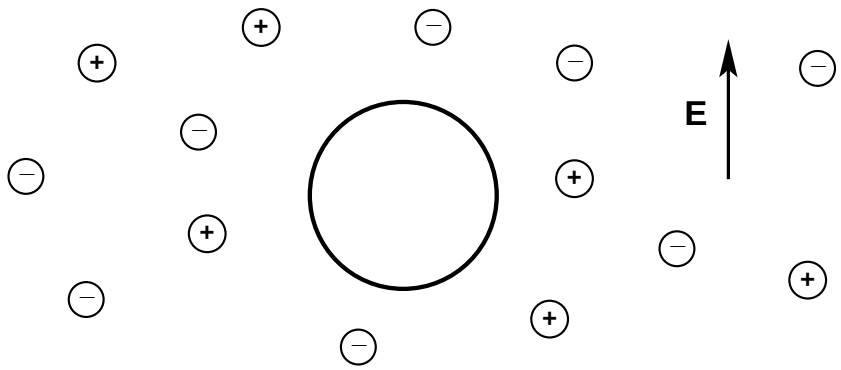

Figure 6-1: Schematic diagram of metal colloid sphere in an electrolyte subjected to an applied electric field.

symmetric, binary electrolytes and assume that all ionic species have identical diffusivities. In order to study nonlinear effects and avoid imposing a time scale, we assume that the uniform electric field is suddenly applied at $t = 0$.

To begin our analysis, we start with the standard mathematical model for electrochemical systems developed in Chapter 2. Ion transport in the electrolyte surrounding the metal sphere is described by the Poisson-Nernst-Planck equations:

$$\frac{\partial c}{\partial t} = \nabla \cdot (\nabla c + \rho \nabla \phi) \tag{6.1}$$

$$\frac{\partial \rho}{\partial t} = \nabla \cdot (\nabla \rho + c \nabla \phi) \tag{6.2}$$

$$-\epsilon^2 \nabla^2 \phi = \rho, \tag{6.3}$$

where we have scaled time to the diffusion time $\tau_D = a^2/D$, and have followed the convention from Chapter 5 of using the average concentration, $c = (c_+ + c_-)/2$, and half the charge density, $\rho = (c_+ - c_-)/2$, to represent the state of the system. Also, note that the electric potential has been nondimensionalized by RT/zF, which is thermal voltage divided by the cation charge number. For the boundary conditions at $r = 1$, we use the Stern boundary condition (2.41) for the electric potential and assume that no Faradaic reactions take place

at the surface of the sphere so that all ionic species satisfy no-flux boundary conditions (2.39):

$$\phi + \delta\epsilon\frac{\partial\phi}{\partial n} = v \tag{6.4}$$

$$\frac{\partial c}{\partial n} + \rho\frac{\partial\phi}{\partial n} = 0 \tag{6.5}$$

$$\frac{\partial\rho}{\partial n} + c\frac{\partial\phi}{\partial n} = 0, \tag{6.6}$$

where the direction of the unit normal is taken to point outwards from the physical domain (*i.e., inwards* towards the center of the sphere). Finally, we impose as initial conditions uniform concentration profiles and an electric potential equal to the applied potential:

$$c(x,0) = 1 \tag{6.7}$$

$$\rho(x,0) = 0 \tag{6.8}$$

$$\phi(x,0) = -E_o x. \tag{6.9}$$

6.2.1 Electroneutral Bulk Equations

In the context of electrokinetics, it is desirable to reduce the complexity of the electrochemical transport problem by replacing the PNP equations with a simpler set of equations that treats the bulk electrolyte and the double layer as separate entities. Circuit models [8, 7, 91, 104] have been used extensively to achieve this goal by reducing the transport problem to an electrostatics problem. However, circuit models make the rather stringent assumption that bulk concentrations remain uniform at all times. Unfortunately, at high applied electric fields, this assumption is no longer valid because concentration gradients become important [8].

In the present analysis, we consider an alternative simplification of the PNP equations that allows for bulk concentration variations. Since we are interested in colloidal systems where particle diameters are on order of microns, ϵ is very small which suggests that we consider the thin double layer limit. In this limit, the bulk remains locally electroneutral, so it is acceptable to replace Poisson's equation with the local electroneutrality condition

(3.1). Thus, the PNP equations are replaced with the approximate equations

$$\frac{\partial c}{\partial t} = \nabla^2 c \tag{6.10}$$

$$0 = \nabla \cdot (c \nabla \phi) \tag{6.11}$$

$$\rho = 0. \tag{6.12}$$

It is important to remember that these equations are only valid in the bulk region of the solution. The structure of the double layer *must* be completely incorporated into the boundary conditions.

6.2.2 Effective Boundary Conditions

As always when using local electroneutrality, we must appropriately modify the boundary conditions imposed at electrode surfaces. In the $\epsilon \to 0$ limit, the double layer remains in quasi-equilibrium, so the GCS model (discussed in Section 2.3.3) can be used to derive effective boundary conditions for the system.

Equilibrium Double Layer Structure

For systems with thin double-layers, the diffuse layer is commonly assumed to have an equilibrium structure. This assumption is mathematically justified through the use of boundary layer theory. Before describing the effective boundary conditions for locally electroneutral systems, we briefly discuss the mathematical origin of the quasi-equilibrium diffuse layer structure.

The set of equations (6.1) – (6.3), form a singular perturbation problem, so we expect boundary layer to exist. To analyze the boundary layer, we introduce a local coordinate system $\{x, y, z\}$ relative to a point $\{X_0, Y_0, Z_0\}$ on the surface of the sphere where x and y are coordinates locally tangent to the surface and z is locally normal to the surface: $\{x, y, z\} = \{(X - X_0), (Y - Y_0), (Z - Z_0)/\epsilon\}$. Since x and y are scaled to the dimensionless radius of the sphere and z is scaled to the dimensionless width of the Debye layer, ϵ, (6.1)-

(6.3) become (using the tilde accent to denote solutions within the boundary layer)

$$\epsilon^2 \frac{\partial \tilde{c}}{\partial t} = \epsilon^2 \nabla_s \cdot \left(\nabla_s \tilde{c} + \tilde{\rho} \nabla_s \tilde{\phi} \right) + \frac{\partial}{\partial z} \left(\frac{\partial \tilde{c}}{\partial z} + \tilde{\rho} \frac{\partial \tilde{\phi}}{\partial z} \right) \tag{6.13}$$

$$\epsilon^2 \frac{\partial \tilde{\rho}}{\partial t} = \epsilon^2 \nabla_s \cdot \left(\nabla_s \tilde{\rho} + \tilde{c} \nabla_s \tilde{\phi} \right) + \frac{\partial}{\partial z} \left(\frac{\partial \tilde{\rho}}{\partial z} + \tilde{c} \frac{\partial \tilde{\phi}}{\partial z} \right) \tag{6.14}$$

$$-\epsilon^2 \nabla_s^2 \tilde{\phi} - \frac{\partial^2 \tilde{\phi}}{\partial z^2} = \tilde{\rho} \tag{6.15}$$

where the subscript s refers to surface derivatives. In terms of the cation and anion concentrations, the first two of these equations are given by

$$\epsilon^2 \frac{\partial \tilde{c}_\pm}{\partial t} = \epsilon^2 \nabla_s \cdot \left(\nabla_s \tilde{c}_\pm \pm \tilde{c}_\pm \nabla_s \tilde{\phi} \right) + \frac{\partial}{\partial z} \left(\frac{\partial \tilde{c}_\pm}{\partial z} \pm \tilde{c}_\pm \frac{\partial \tilde{\phi}}{\partial z} \right) \tag{6.16}$$

Therefore, the leading order solutions in the boundary layer are the classical Gouy-Chapman profiles for an equilibrium diffuse layer. Since the derivation of the equilibrium profiles are greatly discussed in literature [8, 56], we directly quote the results:

$$\tilde{c}_\pm = c(X_0, Y_0, Z_0) e^{\mp \tilde{\psi}} \tag{6.17}$$

$$\tilde{c} = c(X_0, Y_0, Z_0) \cosh \tilde{\psi} \tag{6.18}$$

$$\tilde{\rho} = -c(X_0, Y_0, Z_0) \sinh \tilde{\psi} \tag{6.19}$$

where the $\tilde{\psi}$ is the excess voltage relative to the bulk,

$$\tilde{\psi}(x, y, z, t) = \tilde{\phi}(x, y, z, t) - \phi(X_0, Y_0, Z_0, t). \tag{6.20}$$

The leading order approximation for $\tilde{\psi}$ satisfies the Poisson-Boltzmann equation, which can be directly integrated to obtain

$$\tilde{\psi}_0(x, y, z, t) = -4 \tanh^{-1} \left(e^{-[z\sqrt{c(X_0, Y_0, Z_0)} + K(x, y, t)]} \right), \tag{6.21}$$

where the integration constant

$$K(x,y,t) = \log\coth\left[-\zeta_0(x,y,t)/4\right] \tag{6.22}$$

is determined from ζ_0, the leading order zeta-potential, by the Stern boundary condition at the sphere surface, $z = 0$, and asymptotic matching with the bulk potential. Note that unlike the 1D case, K has spatial dependence along the electrode surface.

At the RC time, the diffuse layer also possesses an equilibrium structure. By rescaling time to the RC time, $\tilde{t} = t/\epsilon$: (6.16) becomes

$$\epsilon\frac{\partial\tilde{c}_\pm}{\partial\tilde{t}} = \epsilon^2\nabla_s\cdot\left(\nabla_s\tilde{c}_\pm \pm \tilde{c}_\pm\nabla_s\tilde{\phi}\right) + \frac{\partial}{\partial z}\left(\frac{\partial\tilde{c}_\pm}{\partial z} \pm \tilde{c}_\pm\frac{\partial\tilde{\phi}}{\partial z}\right). \tag{6.23}$$

The only difference between this equation and (6.16) is that the time derivative loses a factor of ϵ. Thus, the leading order equations do not change, and the diffuse layer also possesses a quasi-equilibrium, Gouy-Chapman profile at the RC time.

Stern Boundary Condition

By rearranging (6.4) and using the GCS model, we can rewrite the Stern boundary condition so that it only explicitly involves the electric potential at the outer edge of the diffuse charge layer:

$$\zeta + 2\delta\sqrt{c}\sinh\left(\zeta/2\right) = v - \phi. \tag{6.24}$$

Here ζ is the potential drop across the diffuse part of the double layer (*i.e.,* zeta-potential) and v is the potential of the metal sphere in the thermal voltage scale. Note that by assuming the GCS model for the double layer, the only dependence of the normal derivative of the electric potential in (6.4) on the double layer structure is through the zeta-potential. A more detailed derivation of this form of the Stern boundary condition can be found in Section 5.3.1.

Ionic Fluxes

The effective boundary conditions for ionic fluxes are a bit more complicated. Because the physical domain no longer contains the diffuse part of the double layer, the no-flux boundary condition no longer applies – it is possible for there to exist ion flux between the bulk region and the double layer. Moreover, there is also the possibility of ion transport within the double layer itself which must be accounted for. In general form, the effective flux boundary conditions for an individual ionic species is

$$\frac{\partial \Gamma_i}{\partial t} = \nabla_s \cdot \left[\nabla_s \Gamma_i + z_i \Gamma_i \nabla_s \phi + \epsilon z_i \int_0^\infty \tilde{c}_i \nabla_s \tilde{\psi} \, dz \right] - \left(\frac{\partial c_i}{\partial n} + z_i c_i \frac{\partial \phi}{\partial n} \right), \tag{6.25}$$

where Γ_i and $\tilde{c}_i$ are the excess surface concentration and diffuse layer concentration of species i, respectively, and $\tilde{\psi} = \tilde{\phi} - \phi$ is the excess electric potential within the diffuse layer. Note that even though our choice of electric potential scale eliminates the need to explicitly refer to the ionic charge numbers, z_i, in the present discussion, we opt to continue using them so that it is clear where the charge number should appear for alternative choices of the electric potential scale[3].

There are a few important features of (6.25) worth mentioning. First, the surface conduction term (first term on the right) does not always contribute to the leading order effective flux boundary condition. Whether the surface conduction term must be retained at leading order depends on the magnitudes of Γ_i (which depends the zeta-potential) and the tangential component of the bulk electric field. Interestingly, when the the surface transport term is significant, the flux boundary condition depends explicitly on the small parameter ϵ. Also, (6.25) allow for two important physical effects that only arise for 2- and 3-D systems: (1) non-uniform double layer charging and (2) surface transport within the double layer itself. The presence of these effects lead to richer behavior for 2- and 3-D systems. Unfortunately, they make it difficult to obtain analytical results. As a result, many of the results in this chapter are based on numerical solutions of the mathematical model.

The derivation of the effective flux boundary conditions (6.25) is based on the general

[3]In our discussion, the z_i are essentially the sign of the "dimensional" ionic charge numbers.

theory of surface conservation laws discussed in Chapter 4. The basic physical idea is to integrate out the spatial variation within the double layer in the direction normal to the electrode-electrolyte interface. The general theory tells us that effective flux boundary conditions have the form

$$\frac{\partial \Gamma_i}{\partial t} = -\nabla_s \cdot \mathbf{J}_i^s + J_i^n, \tag{6.26}$$

where $\mathbf{J}_i^s$ is the tangential flux within and J_i^n is the normal flux into the boundary layer. The effective fluxes $\mathbf{J}_i^s$ and J_i^n are directly related to the flux $\mathbf{F}_i$ for the transport process via

$$\mathbf{J}_i^s = \epsilon \int_0^\infty \left(\tilde{\mathbf{F}}_i^s - \mathbf{F}_i^s \right) \tag{6.27}$$

$$J_i^n = \mathbf{F}_i^n \cdot \hat{n} \tag{6.28}$$

where $\tilde{\mathbf{F}}$ denotes the value of the flux within the boundary layer. For electrochemical transport, the flux is given by the Nernst-Planck equation

$$\mathbf{F}_i = -\left(\nabla c_i + z_i c_i \nabla \phi \right). \tag{6.29}$$

Substituting this expression into (6.27) – (6.28), rearranging a bit, and using the definition

$$\Gamma_i \equiv \epsilon \int_0^\infty \gamma_i dz = \epsilon \int_0^\infty \left(\tilde{c}_i - c_i \right) dz, \tag{6.30}$$

we obtain

$$\mathbf{J}_s^i = -\left(\nabla_s \Gamma_i + z_i \Gamma_i \nabla_s \phi + \epsilon z_i \int_0^\infty \tilde{c}_i \nabla_s \tilde{\psi} dz \right), \tag{6.31}$$

$$J_n^i = -\frac{\partial c_i}{\partial n} - z_i c_i \frac{\partial \phi}{\partial n}. \tag{6.32}$$

The effective flux boundary conditions for electrochemical transport (6.25) follow directly from these results in (6.26).

To put (6.25) into a more useful form, we use the GCS model of the double layer to express the surface flux densities in terms of the zeta-potential and the bulk concentration.

Recalling that the excess concentration of each ionic species is given by

$$\gamma_i = \tilde{c}_i - c_i = c\left(e^{-z_i\tilde{\psi}} - 1\right), \tag{6.33}$$

and that

$$\frac{\partial\tilde{\psi}}{\partial z} = -2\sqrt{c}\sinh\left(\frac{z_+\tilde{\psi}}{2}\right), \tag{6.34}$$

it is straightforward to show that the surface excess concentration is

$$\Gamma_i = \frac{2\epsilon\sqrt{c}}{|z_i|}\left(e^{-z_i\zeta/2} - 1\right). \tag{6.35}$$

Therefore, the first two surface flux density terms in (6.25) can be written:

$$\nabla_s\Gamma_i + z_i\Gamma_i\nabla_s\phi = \epsilon\ \Omega_i(\zeta)\left(\frac{1}{|z_i|}\nabla_s c + 2\ \mathrm{sgn}(z_i)c\ \nabla_s\phi\right) - \epsilon\ \mathrm{sgn}(z_i)\sqrt{c}\ e^{-z_i\zeta/2}\nabla_s\zeta. \tag{6.36}$$

where $\Omega_i(\zeta) = \left[\exp(-z_i\zeta/2) - 1\right]/\sqrt{c}$. To evaluate the last term in the surface flux density, we observe that

$$\nabla_s\tilde{\psi} = -\frac{\nabla_s\zeta}{2\sqrt{c}\ \sinh\left(\zeta/2\right)}\frac{\partial\tilde{\psi}}{\partial z}, \tag{6.37}$$

which follows directly by differentiating (5.37). Using this result, the integral in (6.25) greatly simplifies and yields

$$z_i\int_0^\infty \tilde{c}_i\nabla_s\tilde{\psi}\ dz = \mathrm{sgn}(z_i)e^{-z_i\zeta/2}\sqrt{c}\ \nabla_s\zeta. \tag{6.38}$$

Finally, combining (6.36) and (6.38), the effective flux boundary condition (6.25) becomes

$$\frac{\partial\Gamma_i}{\partial t} = \epsilon\nabla_s\cdot\left[\Omega_i(\zeta)\left(\frac{1}{|z_i|}\nabla_s c + 2\ \mathrm{sgn}(z_i)c\nabla_s\phi\right)\right] - \left(\frac{\partial c_i}{\partial n} + z_i c_i\frac{\partial\phi}{\partial n}\right). \tag{6.39}$$

Notice that the tangential gradients in the zeta-potential have vanished in this equation so that the surface flux density of the individual species is independent of $\nabla_s\zeta$.

Effective boundary conditions similar to (6.39) describing the dynamics of the double layer have been known for some time. In the late 1960s, Dukhin, Shilov and Deryagin used linearized surface conservation laws in their studies of surface conductance and the

polarization of the diffuse charge layer around spherical particles with thin double layers in weak applied fields [29, 33, 102]. Later, Hinch, Sherwood, Chew, and Sen extended this work and explicitly calculated the tangential flux terms for a range of larger surface potentials (but still weak applied fields) and asymmetric electrolytes [54, 55]. Since all of these studies focused on small deviations from bulk equilibrium, the effective boundary conditions they used are basically linearized versions of (6.39). An important distinguishing feature of the our work is that it does not require that the bulk concentration only *weakly* deviates from a uniform profile. Our derivation shows that (6.31) and (6.32) are valid even for large bulk concentration variations.

Surface Charge and Neutral Salt Flux

Since the governing equations (6.10) – (6.12) are formulated in terms of the neutral salt concentration and charge density, it is convenient to derive boundary conditions that are directly related to these quantities. Toward this end, we define ϵq and ϵw to be the surface charge density and surface excess neutral salt concentration, respectively:

$$q = \int_0^\infty \tilde{\rho} dz = \frac{1}{2}\int_0^\infty (\gamma_+ - \gamma_-)\, dz \tag{6.40}$$

$$w = \int_0^\infty (\tilde{c} - c)\, dz = \frac{1}{2}\int_0^\infty (\gamma_+ + \gamma_-)\, dz. \tag{6.41}$$

By integrating (6.18) and (6.19) from Section 6.2.2 and using (6.34), both q and w can be expressed as simple functions of the zeta-potential and the bulk concentration just outside of the double layer:

$$q = -2\sqrt{c}\sinh(\zeta/2) \tag{6.42}$$

$$w = 4\sqrt{c}\sinh^2(\zeta/4). \tag{6.43}$$

Using (6.40) and (6.41), we can combine the effective flux boundary conditions for individual ions (6.25) to obtain

$$\epsilon\frac{\partial q}{\partial t} = \epsilon\nabla_s\cdot\left[\nabla_s q + w\nabla_s\phi + \int_0^\infty \tilde{c}\nabla_s\tilde{\psi}\ dz\right] - c\frac{\partial\phi}{\partial n} \tag{6.44}$$

$$\epsilon\frac{\partial w}{\partial t} = \epsilon\nabla_s\cdot\left[\nabla_s w + q\nabla_s\phi + \int_0^\infty \rho\nabla_s\tilde{\psi}\ dz\right] - \frac{\partial c}{\partial n}. \tag{6.45}$$

Notice that like the PNP equations written in terms of c and ρ, there is a symmetry between q and w in these equations. Finally, as in the previous section, we can use the GCS model to rewrite (6.44) and (6.45) solely in terms of bulk field variables and the zeta-potential:

$$\epsilon\frac{\partial q}{\partial t} = \epsilon\nabla_s\cdot\left(\frac{q}{2c}\nabla_s c + w\nabla_s\phi\right) - c\frac{\partial\phi}{\partial n} \tag{6.46}$$

$$\epsilon\frac{\partial w}{\partial t} = \epsilon\nabla_s\cdot\left(\frac{w}{2c}\nabla_s c + q\nabla_s\phi\right) - \frac{\partial c}{\partial n}, \tag{6.47}$$

which is the form of the effective flux boundary conditions we shall use in our analysis.

Dominant Terms in the Effective Flux Boundary Conditions

In general, the relative importance of the terms in a set of effective flux boundary conditions (written in any form) may depends on the choice of time scales and the magnitude of surface transport. In the context of electrochemical transport, we find that many of the commonly applied boundary conditions are merely the leading order form of the previously discussed effective flux boundary conditions in different asymptotic (and physical) regimes. For instance, in induced charge electro-osmosis problems at weak applied electric fields, ϵq and ϵw remains $O(\epsilon)$ quantities. Thus, compared to the normal flux term, the surface flux term is negligible and the time-dependent term is only important at short times, $t = O(\epsilon)$. In this situation, the double layer charging equation (6.46) becomes [7, 104]:

$$\frac{\partial q}{\partial\hat{t}} = \sigma\frac{\partial\phi}{\partial n}, \tag{6.48}$$

where $\sigma = c$ is the bulk conductivity of the solution and time has been rescaled using $\hat{t} = t/\epsilon$ so that the dynamics are on the RC time scale [7, 8, 104]. At $t = O(1)$ time scales, only the

normal flux remains an $O(1)$ quantity, so we are left with a "no-flux" boundary condition as the effective double layer boundary condition:

$$\sigma \frac{\partial \phi}{\partial n} = 0. \tag{6.49}$$

At higher applied fields or for highly charged particles [33, 54, 55, 102], the surface excess concentration of some ionic species in the double layer becomes an $O(1/\epsilon E)$ quantity so that surface conduction becomes important and evolution of ionic concentrations within the double layer occurs on an $O(1)$ time scale. In this situation, no terms in the effective flux boundary conditions are negligible, so we must retain all terms (6.46) and (6.47).

6.3 Steady response to large applied electric fields

We are now ready to examine the steady response of a metal sphere subjected to a large, uniform applied electric field. At steady-state, the unsteady term is eliminated from the governing equations (6.10) – (6.12) so that

$$0 = \nabla^2 c \tag{6.50}$$

$$0 = \nabla \cdot (c \nabla \phi). \tag{6.51}$$

Similarly, the flux boundary conditions (6.46) – (6.47) become

$$0 = \epsilon \nabla_s \cdot \left(\frac{q}{2c} \nabla_s c + w \nabla_s \phi \right) - c \frac{\partial \phi}{\partial n} \tag{6.52}$$

$$0 = \epsilon \nabla_s \cdot \left(\frac{w}{2c} \nabla_s c + q \nabla_s \phi \right) - \frac{\partial c}{\partial n}, \tag{6.53}$$

Notice that we have retained the surface transport terms in these boundary conditions even though they appear at $O(\epsilon)$. At large applied fields, it is no longer valid to order the terms in an asymptotic expansions by ϵ alone. We also need to consider factors of the form ϵe^{ζ} or $\epsilon \sinh(\zeta)$ since e^{ζ} may be as large as $O(1/\epsilon E)$ for large applied fields. Since both q and w contain factors which grow exponentially with the zeta-potential, we must keep the surface conduction terms in (6.52) and (6.53). Finally, the Stern boundary condition (6.24) remains

unchanged because it does not involve any time derivatives.

As mentioned earlier, the steady problem exhibits interesting features that have not been extensively explored. In this section, we develop a numerical model for the system, which we subsequently use to study the development of $O(1)$ bulk concentration variations and their impact on transport around the metal colloid sphere.

6.3.1 Numerical model

The nonlinearities present in the governing equations and boundary conditions make it difficult to proceed analytically, so we turn towards a numerical model to gain physical insight into the mathematical model. To avoid infinite values of the electric potential, the numerical model is formulated in terms of $\psi \equiv \phi + Er\cos\theta$, the deviation of the electric potential from that of the uniform applied electric field, rather than ϕ itself. Also, we take advantage of the axisymmetry of the problem to reduce the numerical model to two dimensions (as opposed to using a fully 3-D description), which greatly reduces the computational complexity and cost.

Our numerical model is based on a pseudospectral spatial discretization of the exterior of a sphere in spherical polar coordinates. For the computational grid, we use a tensor product grid of a uniformly spaced grid for the polar angle direction and a shifted semi-infinite rational Chebyshev grid for the radial direction (see Appendix C). To obtain discrete differential operators for this grid, we use Kronecker products of the differentiation matrices for the individual one-dimensional grids [111]. The numerical model is then easily constructed by replacing field variables and continuous operators in the mathematical model by grid functions and discrete operators.

To facilitate our discussion of the numerical model, we first fix our notation. Let D_r and D_θ be the radial and angular contributions to the discrete divergence operator, G_r and G_θ be the radial and angular components of the discrete gradient operators, and L be the discrete Laplacian operator. Also, let n and s subscripts denote normal and tangential derivative operators at the surface of the sphere. Finally, let the hat accent ($\hat{}$) indicate discretized field variables.

For the purpose of discussion (and implementation), it is convenient to decompose the

discrete differential operators into pieces that correspond to contributions from finite and infinite grid points. For example, L can be decomposed into L^f and L^∞ which account for the contributions to the Laplacian operator from finite and infinite grid points; that is, $L\hat{c} = L^f\hat{c}_f + L^\infty c_\infty$, where $\hat{c}_f$ and c_∞ are the concentration values at finite and infinite grid points respectively. Similarly, to model the boundary conditions, we shall use derivative operators that act only on surface values. Surface operators and surface field values will be denoted with superscripts s and subscripts s, respectively. Finally, we shall occasionally need to refer to values at interior grid points (*i.e.,* finite grid points that are *not* on the surface of the sphere). In these situations, a subscript i will be used to indicate that a field variable has been restricted to interior grid points.

In this notation, the discretized form of the bulk equations (6.50) and (6.51) are given (in MATLAB notation) by

$$0 = F_1 \equiv L^f\hat{c}_f + L^\infty c_\infty \tag{6.54}$$

$$\begin{aligned} 0 = F_2 \equiv\ & D_r^f\left[\hat{c}_f\ .*\ \left(G_r^f\hat{\psi}_f - E\cos\theta\right)\right] + D_\theta^f\left[\hat{c}_f\ .*\ \left(G_\theta^f\hat{\psi}_f + E\sin\theta\right)\right] \\ & - D_r^\infty\left(c_\infty\ .*\ E\cos\theta\right) + D_\theta^\infty\left(c_\infty\ .*\ E\sin\theta\right). \end{aligned} \tag{6.55}$$

In these equations, the unknowns are the values of the c and ψ at finite grid points; values at infinity are specified by the boundary conditions and so are known quantities (which is why c_∞ does not have a hat accent and $\psi_\infty = 0$ does not show up at all). It should be noted that the above equations are only imposed at interior grid points, leaving an underdetermined system of equations. The remaining degrees of freedom are removed by applying discretized boundary conditions at the grid points on surface of the sphere:

$$\begin{aligned} 0 = H_1 \equiv\ & \epsilon D_s\left[\frac{1}{2}\ \hat{q}./\hat{c}_s\ .*\ \left(G^s\hat{c}_s\right) + \hat{w}\ .*\ \left(G^s\hat{\psi}_s - EG^s\cos\theta\right)\right] \\ & - c_s\ .*\ \left(G_n^f\hat{\psi}_f + E\cos\theta\right) \end{aligned} \tag{6.56}$$

$$\begin{aligned} 0 = H_2 \equiv\ & \epsilon D_s\left[\frac{1}{2}\ \hat{w}./\hat{c}_s\ .*\ \left(G^s\hat{c}_s\right) + \hat{q}\ .*\ \left(G^s\hat{\psi}_s - EG^s\cos\theta\right)\right] \\ & - \left(G_n^f\hat{c}_f + G_n^\infty c_\infty\right). \end{aligned} \tag{6.57}$$

Closure for these equations is given by using (6.42) – (6.43) to relate $\hat{q}$ and $\hat{w}$ to the zeta-

potential and using (6.24) to compute the zeta-potential from ϕ.

Together (6.54) – (6.57), (6.42) – (6.43), and (6.24) form a nonlinear system of equations for $\hat{c}$ and $\hat{\phi}$. To solve these equations, we use Newton's method with continuation [13]. At small values of E (less than 5), an initial iterate of $\hat{c} \equiv 1$ and $\hat{\psi} \equiv 0$ is sufficient to achieve convergence of the Newton iteration. However, for larger values of E, continuation in the magnitude of the electric field is required to obtain a converged solution.

In order to simplify the implementation of Newton's method and improve its computational performance, we analytically compute the Jacobian of of (6.54) – (6.57) using the direct matrix differentiation rules described in Appendix C. The derivatives of F_1 and F_2 with respect to the unknowns $\hat{c}_f$ and $\hat{\psi}_f$ are easily calculated:

$$\frac{DF_1}{D\hat{c}_f} = L^f \tag{6.58}$$

$$\frac{DF_1}{D\hat{\psi}_f} = 0 \tag{6.59}$$

$$\frac{DF_2}{D\hat{c}_f} = D_r^f \mathrm{diag}\left(G_r^f \hat{\psi}_f - E\cos\theta\right) + D_\theta^f \mathrm{diag}\left(G_r^f \hat{\psi}_f + E\sin\theta\right) \tag{6.60}$$

$$\frac{DF_2}{D\hat{\psi}_f} = D_r^f \mathrm{diag}\left(\hat{c}_f\right) G_r^f + D_\theta^f \mathrm{diag}\left(\hat{c}_f\right) G_\theta^f \tag{6.61}$$

The derivatives for the discretized boundary conditions are a little more complicated because $\hat{q}$, $\hat{w}$, and $\hat{c}_s$ implicitly depend on the unknown variables and because surface grid points

must be treated differently than interior grid points:

$$
\begin{aligned}
\frac{DH_1}{D\hat{c}_s} &= -\frac{\epsilon}{4} D_s \mathrm{diag}\left[\ q\ .*\ (G_s c_s)\ ./\ (c_s.\wedge 2)\ \right] \\
&\quad - \frac{\epsilon}{2} D_s \mathrm{diag}\left[\cosh(\zeta/2)\ .*\ \frac{\partial \zeta}{\partial c_s}\ .*\ (G_s c_s)\ ./\ \sqrt{c_s}\ \right] \\
&\quad + \frac{\epsilon}{2} D_s \mathrm{diag}\left[\ q\ ./\ c_s\ \right] * G_s \\
&\quad + \frac{\epsilon}{2} D_s \mathrm{diag}\left[\ w\ ./\ c_s\ .*\ (G_s\psi_s - E G_s \cos\theta)\ \right] \\
&\quad + \epsilon D_s \mathrm{diag}\left[\sqrt{c_s}\ .*\ \sinh(\zeta/2)\ .*\ \frac{\partial \zeta}{\partial c_s}\ .*\ (G_s\psi_s - E G_s\cos\theta)\right] \\
&\quad - \mathrm{diag}\left(G_n^f \psi_f + E\cos\theta \right) \qquad (6.62) \\
\frac{DH_1}{Dc_i} &= 0 \qquad (6.63) \\
\frac{DH_1}{D\psi_s} &= -\frac{\epsilon}{2} D_s \mathrm{diag}\left[\ \cosh(\zeta/2)\ .*\ \frac{\partial \zeta}{\partial \psi_s}\ .*\ (G_s c_s)\ ./\ \sqrt{c_s}\ \right] \\
&\quad + \epsilon D_s \mathrm{diag}(w) G_s \\
&\quad + \epsilon D_s \mathrm{diag}\left[\sqrt{c_s}\ .*\ \sinh\left(\zeta/2\right)\ .*\ \frac{\partial \zeta}{\partial \psi_s}\ .*\ (G_s\psi_s - E G_s\cos\theta)\right] \\
&\quad - \mathrm{diag}\left(c_s\right) G_n^s \qquad (6.64) \\
\frac{DH_1}{D\psi_i} &= -\mathrm{diag}\left(c_s\right) G_n^i \qquad (6.65)
\end{aligned}
$$

$$
\begin{aligned}
\frac{DH_2}{Dc_s} &= -\frac{\epsilon}{4} D_s \mathrm{diag}\left[\ w\ .*\ (G_s c_s)\ ./\ (c_s.\wedge 2)\ \right] \\
&\quad + \frac{\epsilon}{2} D_s \mathrm{diag}\left[\sinh(\zeta/2)\ .*\ \frac{\partial \zeta}{\partial c_s}\ .*\ (G_s c_s)\ ./\ \sqrt{c_s}\ \right] \\
&\quad + \frac{\epsilon}{2} D_s \mathrm{diag}\left[\ w\ ./\ c_s\ \right] * G_s \\
&\quad + \frac{\epsilon}{2} D_s \mathrm{diag}\left[\ q\ ./\ c_s\ .*\ (G_s\psi_s - E G_s \cos\theta)\ \right] \\
&\quad - \epsilon D_s \mathrm{diag}\left[\sqrt{c_s}\ .*\ \cosh(\zeta/2)\ .*\ \frac{\partial \zeta}{\partial c_s}\ .*\ (G_s\psi_s - E G_s\cos\theta)\right] \\
&\quad - G_n^s \qquad (6.66) \\
\frac{DH_2}{Dc_i} &= -G_n^i \qquad (6.67) \\
\frac{DH_2}{D\psi_s} &= \frac{\epsilon}{2} D_s \mathrm{diag}\left[\sinh(\zeta/2)\ .*\ \frac{\partial \zeta}{\partial \psi_s}\ .*\ (G_s c_s)\ ./\ \sqrt{c_s}\ \right] \\
&\quad + \epsilon D_s \mathrm{diag}(q) G_s \\
&\quad - \epsilon D_s \mathrm{diag}\left[\sqrt{c_s}\ .*\ \cosh(\zeta/2)\ .*\ \frac{\partial \zeta}{\partial \psi_s}\ .*\ (G_s\psi_s - E G_s\cos\theta)\ \right] \qquad (6.68) \\
\frac{DH_2}{D\psi_i} &= 0, \qquad (6.69)
\end{aligned}
$$

where

$$
\begin{aligned}
\frac{\partial \zeta}{\partial \psi_s} &= -\frac{1}{1 + \delta\sqrt{c_s}\cosh(\zeta/2)} \qquad (6.70) \\
\frac{\partial \zeta}{\partial c_s} &= -\frac{\delta \sinh(\zeta/2)}{\sqrt{c_s}\left[1 + \delta\sqrt{c_s}\cosh(\zeta/2)\right]}. \qquad (6.71)
\end{aligned}
$$

With these analytical formulae for the Jacobian, the computational performance of Newton's method is greatly improved. While the formulas may look complicated to program, they are actually relatively easy to implement in MATLAB with the appropriate use of restriction (projection) and extension (prolongation) operators. The MATLAB code used in our numerical investigations is provided in Appendix D.

Numerical Solutions For our numerical solutions, we used the numerical model described above with 50 radial and 50 angular grid points. This grid resolution balanced the combined goals of high accuracy and good computational performance. Figure 6-2 shows

typical solutions for the concentration and electric potential (relative to the background applied potential) for large applied electric fields. A comparison of the concentration and electric potential at the surface of the sphere for varying values of E are shown in Figure 6-3.

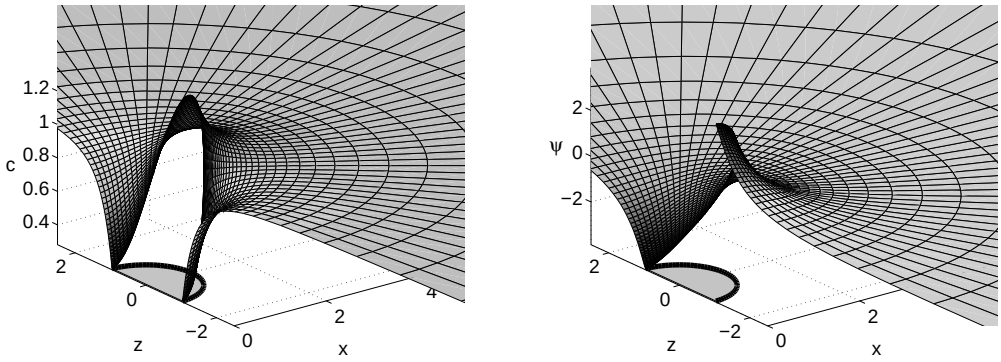

Figure 6-2: Numerical solutions for the concentration (left) and excess electric potential (right) for $E = 10$, $\epsilon = 0.01$, $\delta = 1$. Notice the large gradients in the concentration profile near the surface of the sphere.

6.3.2 Enhanced Surface Excess Concentration and Surface Conduction

Perhaps the most important aspect of the steady response at high applied electric fields is the enhanced surface excess ion concentration within the double layer (see Figure 6-4). As shown in Figures 6-4 and 6-5, the excess surface concentrations become $O(1/E)$, so surface transport within the double layer becomes non-negligible in the leading order effective flux boundary conditions (6.52) – (6.53). Interestingly, the surface conduction (*i.e.,* transport due to electromigration) is the dominant contribution to surface transport (see Figure 6-6). While there are clearly surface gradients in concentration, surface diffusion is smaller than surface migration by a factor on the order of $1/E$. Also, it is worth reiterating that the driving force for surface conduction is solely from surface gradients of the bulk electric potential; the gradients in the zeta-potential do not play a role because they are completely canceled out by the gradients in the surface excess concentrations.

An important feature of the surface fluxes shown in Figure 6-5 is that they are non-uniform. This non-uniformity is strongly influenced by the non-uniformity in the tangential

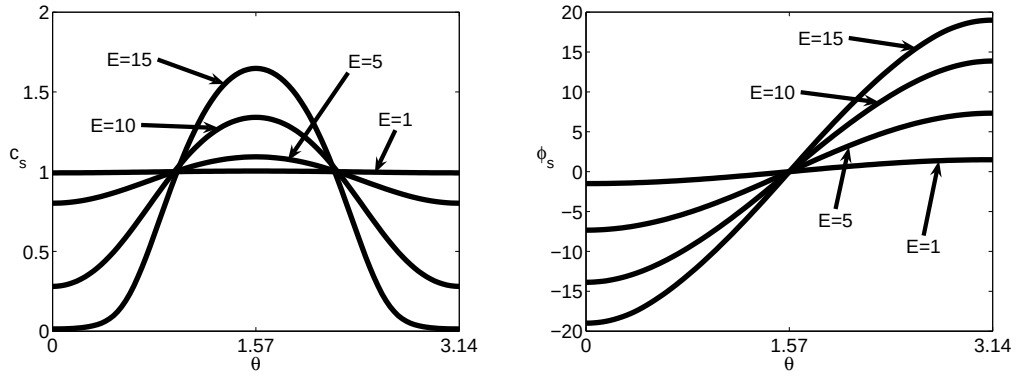

Figure 6-3: Bulk concentration and electric potential at the surface of the sphere for varying values of the applied electric field. In these figures, $\epsilon = 0.01$ and $\delta = 1$. Notice that for $E = 15$, the poles ($\theta = 0$ and $\theta = \pi$) are about to be depleted of ions (*i.e.,* $c \approx 0$).

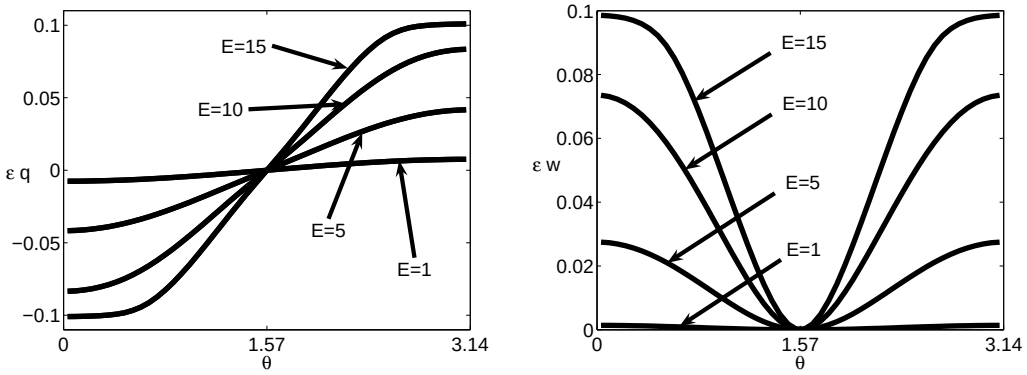

Figure 6-4: Surface charge density (left) and excess surface concentration of neutral salt (right) and for varying values of the applied electric field. In these figures, $\epsilon = 0.01$ and $\delta = 1$. Notice that for large applied fields, $\epsilon w = O(1/E)$ and $\epsilon q = O(1/E)$ so that the surface conduction terms in (6.46) and (6.47) are $O(1)$.

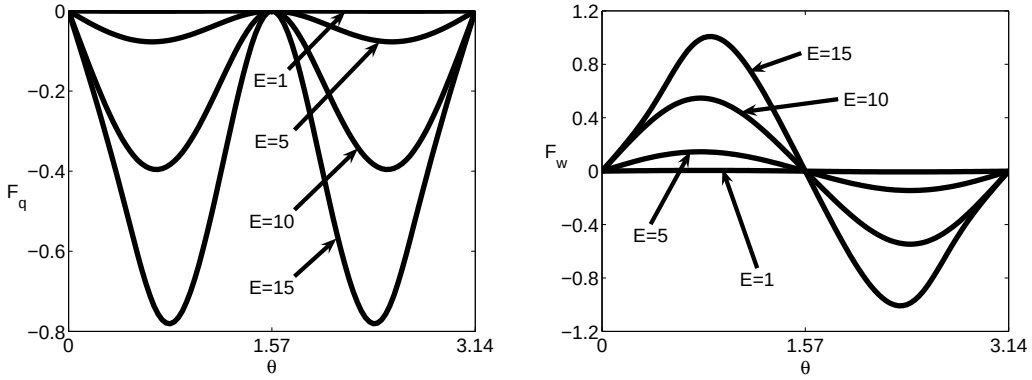

Figure 6-5: Tangential surface fluxes for the surface charge density (left) and excess surface concentration of neutral salt (right) for varying values of the applied electric field. In these figures, $\epsilon = 0.01$ and $\delta = 1$. Notice that for large applied fields, the surface fluxes are $O(1)$ quantities and make a non-negligible leading-order contribution in (6.46) and (6.47).

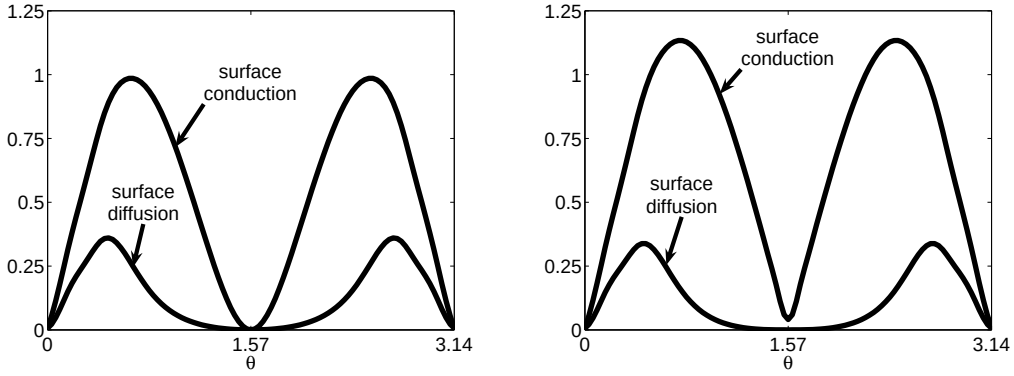

Figure 6-6: Comparison of the magnitudes of surface conduction and surface diffusion for the tangential fluxes of q (left) and w (right) for an applied electric field value of $E = 15$. In these figures, $\epsilon = 0.01$ and $\delta = 1$. Notice that in both cases, the surface diffusion is on the order of $1/E$ times the surface conduction.

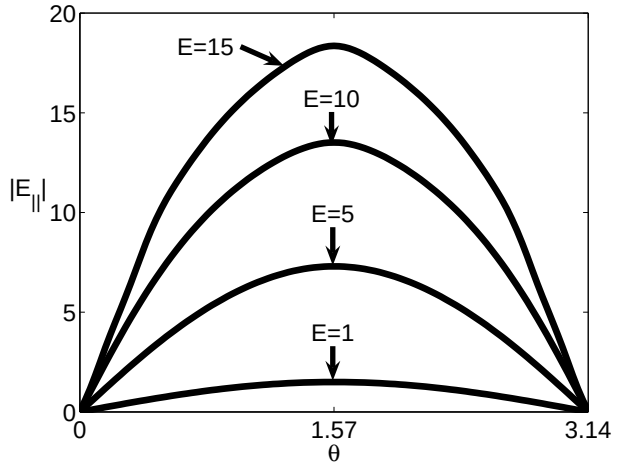

Figure 6-7: Tangential component of bulk electric field at surface of sphere for varying values of the applied electric field. In these figures, $\epsilon = 0.01$ and $\delta = 1$.

electric field (see Figure 6-7). The non-uniformity of the surface excess salt concentration and charge surface density also play a role but to a lesser extent. Since the surface excess concentration of ions remains steady, the non-uniformity in the surface fluxes leads to non-uniform normal fluxes of current and neutral salt from the bulk into the double layer (see Figure 6-8). Notice that the normal flux of neutral salt into the double layer, which is given by $-\partial c/\partial n$, shows an injection of neutral salt at the poles ($-\partial c/\partial n > 0$), where the charging is strongest, and an ejection of neutral salt at the equator ($-\partial c/\partial n < 0$) , where there is essentially no charge build up. This configuration of fluxes leads to the neutral salt depletion at the poles and accumulation at the equator shown in Figures 6-2 and 6-3. Similarly, the normal current density $-c_s \partial\phi/\partial n$, shows an influx of negative (positive) current density at the north (south) pole and a positive (negative) current density closer to the equator. At the equator, there is no normal current density because the normal fluxes of cations and anions exactly balance and there is no normal electric field to drive a migration current.

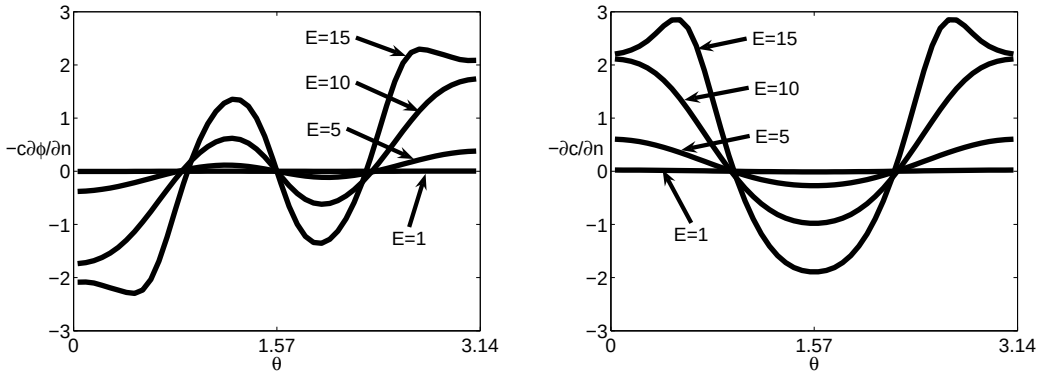

Figure 6-8: Normal flux of current (left) and neutral salt (right) into the double layer for varying values of the applied electric field. In these figures, $\epsilon = 0.01$ and $\delta = 1$.

6.3.3 Bulk Concentration Variation and Diffusion Currents

One major consequence of surface conduction is generation of large fluxes of neutral salt into the double layer. These cause strong concentration gradients to appear near the surface of the sphere (Figures 6-2 and 6-3), indicating that the usual assumption of a uniform concentration profile is invalid at high electric fields. The presence of these large concentration gradients at relatively low electric fields ($E \approx 5$) should not be surprising since it is well-known that large voltage effects often begin with voltages as low as a few times the thermal voltage [8]. The dramatic influence of the voltage arises from the exponential dependence of double layer concentrations on the zeta-potential.

Since the transport of neutral salt is driven by concentration gradients, the presence of these strong variations leads to diffusion currents (see Figure 6-9). An important feature of these diffusion currents is that they are closed; current lines start on the surface of the sphere near the equator where neutral salt is ejected into the bulk (as a result of neutral salt transport within the double layer) and end close to the poles where neutral salt is absorbed by the double layer. These recirculation currents are important because they allow the system to conserve the total number of cation and anions. Without them, the local depletion and accumulation of ions would require global changes to the bulk concentration (*i.e.,* the concentration at infinity would be affected).

While the presence of diffusion currents is interesting, we must be careful in how they

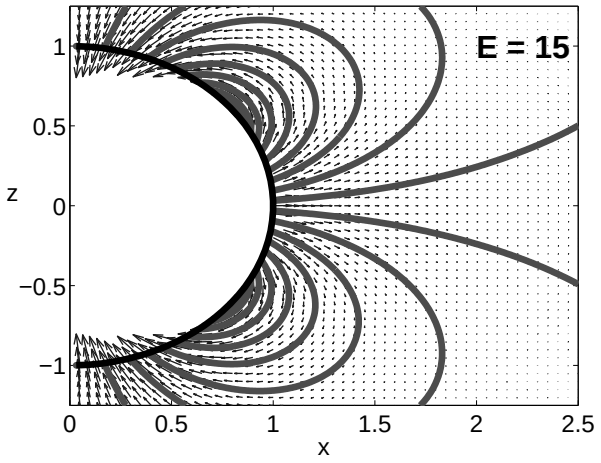

Figure 6-9: Diffusion currents drive transport of neutral salt near the surface of the sphere. In this figure, $E = 10$, $\epsilon = 0.01$ and $\delta = 1$. Notice that streamlines of neutral salt are closed; current lines start on the surface of the sphere near the equator and end closer to the poles.

are interpreted in terms of the motion of individual ion molecules. In actuality, no ions are moving purely under the influence of diffusion. Rather, the cation and anion flux densities are slightly imbalanced due to the presence of a concentration gradient which results in a net flux of neutral salt concentration.

6.3.4 Individual Ion Currents

Since cations and anions are the physical entities that are transported through the electrolyte, it is useful to consider the cation and anion flux densities individually. As shown in Figure 6-10, the contribution of electromigration to transport dominates diffusion. Moreover, within a short distance from the sphere, the electromigration term itself becomes dominated by the contribution from the applied electric field. Thus, the concentration gradient only serves to slightly bias the flux densities so that cation (anion) motion is slightly retarded near the north (south) pole.

Surface transport of the individual ions within the double layer is even more interesting. In the northern hemisphere, the double layer is dominated by anions; similarly, the southern hemisphere is dominated by cations. As a result, transport in each hemisphere is primarily

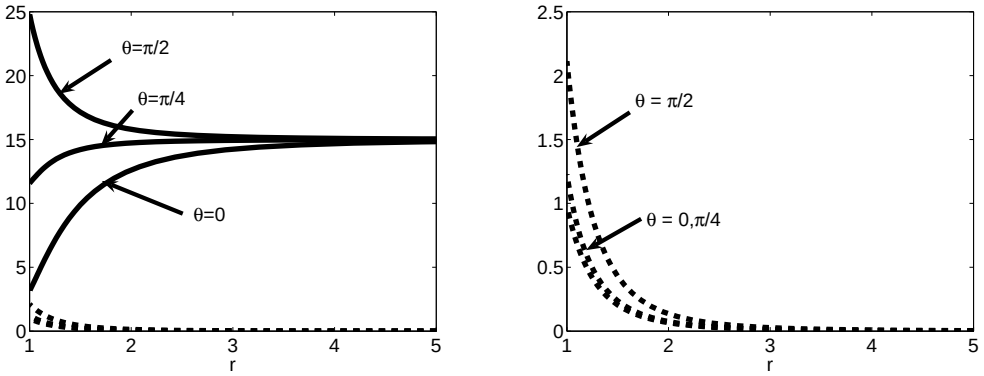

Figure 6-10: Comparison of the magnitudes of bulk electromigration (solid lines) and diffusion (dashed lines) fluxes as a function of distance from the surface of the sphere at $\theta = 0, \pi/4$, and $\pi/2$ (left). The figure on the right zooms in on the diffusion flux. In these figure, $E = 10$, $\epsilon = 0.01$ and $\delta = 1$. Notice that magnitude of the electromigration dominates diffusion and that the electromigration term itself becomes dominated by the contribution from the applied electric field a short distance from the surface of the sphere.

due to only one species (see Figure 6-11).

This observation provides a direct explanation for the depletion and accumulation regions in the concentration profile in terms of the the motion of individual ions. As mentioned earlier, the transport is from the poles to the equator because surface conduction is driven by the tangential component of the bulk electric field (see Figure 6-7). Since the double layer in the norther hemisphere is predominantly anions, the surface ion transport is from the poles towards the equator. A similar argument in the southern hemisphere shows that surface transport of the majority ion is again from the poles towards the equator. Thus, influx of ions into the double layer occurs in the regions near the poles and outflux occurs by the equator.

The dominance of a single species within the double layer for each hemisphere leads to a small conundrum: how does the bulk electrolyte near the surface of the sphere remain locally electroneutral? In the northern hemisphere, it would seem that more anion should be absorbed at the pole and ejected at the equator leading to bulk charge imbalance. Analogous reasoning involving cation leads to the same conclusion in the southern hemisphere. The resolution to the conundrum comes from remembering that both diffusion and electro-

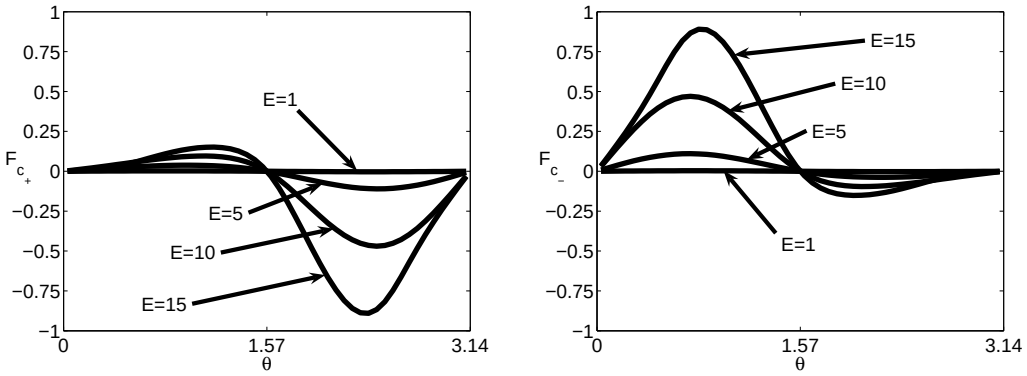

Figure 6-11: Tangential surface fluxes for the cation (left) and anion (right) for varying values of the applied electric field. In these figures, $\epsilon = 0.01$ and $\delta = 1$. Notice that for large applied fields, the surface fluxes are $O(1)$ quantities (in the appropriate hemisphere) which leads to a non-negligible leading-order contribution in (6.39).

migration contribute to transport. The imbalance in the normal flux required to sustain an imbalanced concentration profile in the double layer is achieved by carefully balancing diffusion (which drives both species in the same direction) and electromigration (which drives the two species in opposite directions) so that the normal flux of the appropriate species dominates. For example, at the north pole, an electric field pointing away from the surface of the sphere will suppress the cation flux towards the surface while enhancing the anion flux.

In this situation, the electric field plays a similar role as the diffusion potential transport in an electroneutral solution. Recall that when the cation and anion have different diffusivities, the electric field acts to slow down the species with the higher diffusivity and speed up the species with the lower diffusivity in such a way that both species have equal flux densities. In the current situation, the electric field serves to create the necessary imbalance in the cation and anion flux densities so that the surface excess concentrations within the double layer can be maintained while preserving local electroneutrality in the bulk.

6.4 Linear Response to Weak Applied Fields

When the potential drop across the particle is much smaller than the thermal voltage ($E_o \ll 1$), it is possible to analyze the response of the system *without* assuming that the double layers are thin; that is, we need not assume that ϵ is small and may describe the system using (6.1) – (6.6). Instead, we assume that the response of the system is only a small deviation from the equilibrium solution (*i.e.,* $c \equiv 1$, $\rho \equiv 0$, $\phi = Er\cos\theta$). In this limit, we can linearize the ionic concentrations around a uniform concentration profile so that $c = 1 + \delta c$. Using this expression in (6.2) and making use of Poisson's equation (6.3) to eliminate the electric potential, we find that the charge density, $\rho = (c_+ - c_-)/2 = (\delta c_+ - \delta c_-)/2$, obeys the (dimensionless) Debye-Falkenhagen equation [27]:

$$\frac{\partial \rho}{\partial t} \approx \nabla^2 \rho - \frac{1}{\epsilon^2}\rho. \tag{6.72}$$

Similarly, the flux boundary condition corresponding to this equation reduces to

$$\frac{\partial \rho}{\partial n} + \frac{\partial \phi}{\partial n} = 0. \tag{6.73}$$

Note that (6.72) and Poisson's equation (together with the no-flux and Stern boundary conditions) are a linear system of partial differential equations. Thus, we can take advantage of integral transform techniques.

6.4.1 Transform Solutions for Arbitrary ϵ and δ

Since the model problem is a linear, initial value problem for weak applied fields, it is natural to carry out the analysis using Laplace transforms in time. Transforming the Debye-Falkenhagen and Poisson equations, we obtain

$$\nabla^2 \check{\rho} = \beta^2 \check{\rho} \tag{6.74}$$

$$-\epsilon^2 \nabla^2 \check{\phi} = \check{\rho} \tag{6.75}$$

where

$$\beta(s)^2 = s + \frac{1}{\epsilon^2} \tag{6.76}$$

and the check accent denotes a transformed variable. Similarly, the boundary conditions become

$$\frac{\partial \check{\rho}}{\partial n} + \frac{\partial \check{\phi}}{\partial n} = 0 \tag{6.77}$$

$$\check{\phi} + \delta\epsilon \frac{\partial \check{\phi}}{\partial n} = v s^{-1} \tag{6.78}$$

$$-\nabla \check{\phi} \to E_o s^{-1} \quad \text{as} \quad r \to \infty. \tag{6.79}$$

To solve the resulting boundary value problem, we take advantage of the spherical geometry to write the solution in terms of spherical harmonics. Since $\check{\rho}$ satisfies the modified Helmholtz equation, we can expand it in a series with terms that are products of spherical harmonics, $Y_l^m(\theta, \phi)$, and modified spherical Bessel functions, $k_l(\beta r)$. Moreover, we can reduce the series to a single term

$$\check{\rho}(r, \theta, \phi) = R\ k_1(\beta r)\ Y_1^0(\theta, \phi) = R\ k_1(\beta r)\ \cos\theta \tag{6.80}$$

by taking into account the symmetries of the charge density: (i) axisymmetry, (ii) antisymmetry with respect to $\theta = \pi/2$, and (iii) the "dipolar" nature of the externally applied field. Note that we have only retained the term involving the modified spherical Bessel functions that decays as $r \to 0$ because $\check{\rho}$ vanishes at infinity. Similarly, the general solution for $\check{\phi}$ may be expressed as

$$\check{\phi}(r, \theta, \phi) = -E_o s^{-1} r \cos\theta + A + B\frac{\cos\theta}{r^2} + C\ k_1(\beta r)\ \cos\theta \tag{6.81}$$

where the first term accounts for the boundary condition on the electric field at infinity, the next two terms are the general solution to Laplace's equation possessing the required symmetries, and the last term is the particular solution to Poisson's equation. Note that we have left out the monopolar term in the potential because it is only necessary for charged spheres. Our analysis is not made any less general by neglecting this term; the case of a

charged sphere in an weak applied field is handled by treating it as the superposition of a charged sphere in the absence of an applied field with an uncharged sphere subjected to an applied field.

The coefficients in (6.80) and (6.81) are determined by enforcing Poisson's equation and the boundary conditions (6.77) – (6.78). Plugging (6.80) and (6.81) into Poisson's equation (6.3), we obtain

$$C = -\frac{R}{(\beta\epsilon)^2}. \tag{6.82}$$

To apply the boundary conditions, note that on the sphere $\frac{\partial}{\partial n} = -\frac{\partial}{\partial r}\big|_{r=1}$ so that

$$\frac{\partial \check{\phi}}{\partial n} = E_o s^{-1}\cos\theta + 2B\cos\theta + \frac{1}{(\beta\epsilon)^2}\left.\frac{\partial \check{\rho}}{\partial r}\right|_{r=1}, \tag{6.83}$$

where the last term was obtained by using the relation between C and R. Thus, the no-flux boundary condition (6.77) becomes

$$\begin{aligned} 0 &= E_o s^{-1}\cos\theta + 2B\cos\theta + \left(\frac{1}{(\beta\epsilon)^2} - 1\right)\left.\frac{\partial \check{\rho}}{\partial r}\right|_{r=1} \\ &= \left\{E_o s^{-1} + 2B + R\left(\frac{1}{(\beta\epsilon)^2} - 1\right)\beta k_1'(\beta)\right\}\cos\theta \end{aligned} \tag{6.84}$$

Similarly, the Stern boundary condition (6.78) becomes

$$v s^{-1} = A + \left\{-E_o s^{-1} + 2B - R\left[\frac{1}{(\beta\epsilon)^2}k_1(\beta) - \beta k_1'(\beta)\right]\right\}\cos\theta \tag{6.85}$$

By independently equating the coefficients of the different spherical harmonics in (6.84) and (6.85), we obtain (after a little algebra)

$$A = v s^{-1} \tag{6.86}$$

$$R = \frac{-3E_o s^{-1}(\beta\epsilon)^2}{2k_1(\beta) - \left[(\beta\epsilon)^2(1+2\delta\epsilon) - 1\right]\beta k_1'(\beta)} \tag{6.87}$$

$$B = -\frac{E_o s^{-1}}{2} - \frac{R}{2}\left(\frac{1}{(\beta\epsilon)^2} - 1\right)\beta k_1'(\beta). \tag{6.88}$$

Finally, we can use the fact that [115]

$$k_1(x) = \frac{e^{-x}(x+1)}{x^2} \tag{6.89}$$

to express R as

$$R = \frac{-3E_o s^{-1}}{e^{-\beta}\left[\left(1+\frac{2}{\beta}+\frac{2}{\beta^2}\right)(1+2\delta\epsilon) - \frac{1}{(\beta\epsilon)^2}\right]} \tag{6.90}$$

which is more convenient for analysis.

Following Bazant, Thornton, and Ajdari [8], we focus on times that are long relative to the Debye time ($t = O(\epsilon^2)$ in dimensionless units). In this limit, $s \ll 1/\epsilon^2$ so that the charge density on the surface of the sphere is given by

$$\check{\rho}(r=1,\theta,s) \sim \left(\frac{-K_\rho s^{-1}}{1+\tau_\rho s}\right)\cos\theta \tag{6.91}$$

with

$$K_\rho = \frac{3E_o(1+\epsilon)}{2\gamma} \tag{6.92}$$

$$\tau_\rho = \epsilon\left[\frac{(1+2\delta\epsilon)(1+\epsilon)-\delta\epsilon}{2\gamma(1+\epsilon)}\right] \tag{6.93}$$

$$\gamma = (1+2\delta\epsilon)(1+\epsilon)+\delta \tag{6.94}$$

Inverting the Laplace transform, we see that at long times, the charge at the surface of the sphere has an exponential relaxation with a characteristic time on the order of ϵ:

$$\rho(r=1,\theta,t) \sim -K_\rho\left(1-e^{-t/\tau_\rho}\right)\cos\theta. \tag{6.95}$$

Note that τ_ρ is on the order of the dimensionless RC time, ϵ, which is much larger than ϵ^2, the dimensionless Debye time [4].

[4] In dimensional time, the RC and Debye times are given $\lambda_D a/D$ and λ_D^2/D, respectively.

6.4.2 Response to a Weak, Oscillatory Fields

Due to the close relationship between Fourier and Laplace transforms, the algebra involved in analyzing the response of the sphere to a weak, oscillatory field is almost identical to the response to a suddenly applied field. Thus, for sufficiently low frequencies ($\omega \ll 1/\epsilon^2$), we can immediately write down the response to a weak, oscillatory field of the form $E = E_o \mathrm{Re}\left(e^{i\omega t}\right)$:

$$\rho(r=1,\theta,t) = -K_\rho \mathrm{Re}\left(\frac{e^{i\omega t}}{1+i\omega\tau_\rho}\right)\cos\theta. \tag{6.96}$$

6.4.3 Accumulated Surface Charge Density

Because of its importance in many physical processes, the accumulated surface charge density, $\breve{q}$, is an interesting quantity to consider. It is easily computed from the (volume) charge density ρ by integrating it in the radial direction from $r = 1$ to $r = \infty$. While the identification of this integral with a surface charge density really only makes sense in the thin-double layer limit, the accumulated surface charge density is still interesting to examine. Fortunately, the integral is straightforward because [115]

$$k_1(z) = -k_0'(z) \tag{6.97}$$

and the radial dependence of the charge density is independent of the angle. Using these observations, the surface charge density is given by

$$\begin{aligned} \breve{q}(\theta,s) &= \frac{R\ k_0(\beta)}{\beta}\cos\theta \\ &= \frac{R\ e^{-\beta}}{\beta^2}\cos\theta \end{aligned} \tag{6.98}$$

In the long time limit, we find that the surface charge density has an exponential relaxation $q(\theta,t) = -K_q\left(1-e^{-t/\tau_q}\right)\cos\theta$ with

$$K_q = \frac{3E_o\epsilon}{\gamma} \tag{6.99}$$

$$\tau_q = \epsilon\left[\frac{(1+2\delta\epsilon)(1+\epsilon)}{2\gamma}\right] \tag{6.100}$$

As in with the ρ, we see that the characteristic relaxation time for q is on the order of the dimensionless RC time.

6.4.4 Time Scales for Linear Response

In our analysis, we have seen that at long times both ρ and q relax exponentially with characteristic time scales on the order of the RC time, ϵ. However, as Figure 6-12 shows, the relaxation times for the two quantities are not exactly the same and have a nontrivial dependence on the diffuse layer thickness, ϵ, and Stern capacitance, δ.

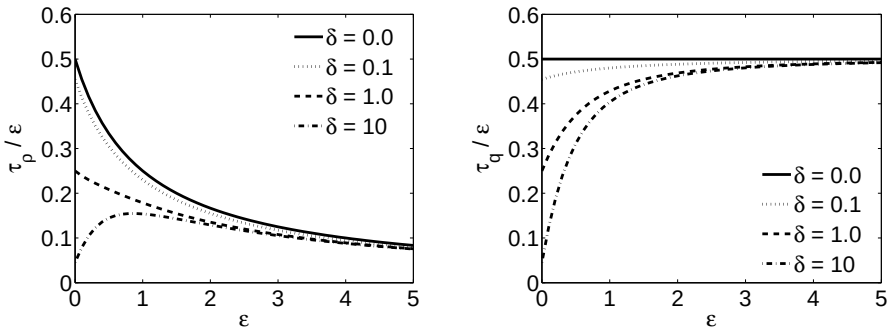

Figure 6-12: Exponential relaxation time constants for the charge density, ρ, and the accumulated surface charge density, q, at weak applied fields as a function of ϵ and δ. The left panel shows the relaxation time constant for the charge density at the surface of the sphere, $\tau_\rho(r = 1, \theta)$. The right panel shows the relaxation time constant for the accumulated surface charge density, τ_q.

Notice that for infinitely thin double layers ($\epsilon = 0$) the relaxation times for the surface charge density and the accumulated charge density are identical. This behavior is expected since for thin double layers, almost all of the charge density in the diffuse layer is located very close to the surface of the particle. In this limit, the relaxation time has a strong dependence on the Stern capacitance. For thick double layers ($\epsilon \gg 1$), this dependence on the Stern capacitance disappears and the relaxation time curves for all δ values converge.

Physically, the difference in the relaxation times for the surface charge and the accumulated charge densities for nonzero ϵ values is an indication of the complex spatio-temporal structure of the double layer charging. For thin double layers, the difference τ_ρ and τ_q is relatively small because the charge in the double layer is restricted to a thin region. For

thick double layers, however, the difference in relaxation times is accentuated because the charge in the double layer is spread out over a larger spatial region, which does not necessarily charge uniformly. In fact, figure 6-12 suggest that regions closer to the surface of the sphere charge faster than regions that are further away.

6.5 Weakly Nonlinear Dynamics

For weak applied fields, the complicated dependence of the Laplace transform solution for small s hints at the presence of multiple time scales in the charging dynamics. In this section, we consider the response of a metal sphere to somewhat higher applied fields for thin double layers ($\epsilon \ll 1$). Using boundary layer theory, we derive a uniformly valid asymptotic solution for the concentrations and electric potential by solving the leading order equations at the two dominant time scales: (1) the RC time and (2) the bulk diffusion relaxation time. We proceed by seeking the leading order term (and in some cases, the first-order correction) to the governing equations (6.1) – (6.6) with both the spatial *and* the time coordinate scaled to focus on the space-time region of interest.

As we discuss in detail in the following sections, the space-time domain is divided into five asymptotically distinct regions (see Figure 6-13). At the RC time, there exist three spatially significant regions: (i) an $O(\epsilon)$ quasi-steady double layer, (ii) an $O(\sqrt{\epsilon})$ dynamically active diffusion layer, and (iii) the quasi-steady, uniform bulk. At this time scale, all of the dynamics is contained within the $O(\sqrt{\epsilon})$ diffusion layer. At the diffusion time, there are only two important spatial regimes: (i) a quasi-steady double layer and (ii) a dynamic bulk that evolves through locally electroneutral, diffusion processes.

6.5.1 Dynamics at the RC Time

In this section, we examine the response of the system at the RC time. We find that the dynamics are driven by double layer charging and diffusion within an $O(\sqrt{\epsilon})$ layer around the sphere. The bulk remains locally electroneutral with a uniform concentration profile. As a result, the only time evolution in the bulk is relaxation of a time-varying harmonic electric potential driven by double layer charging.

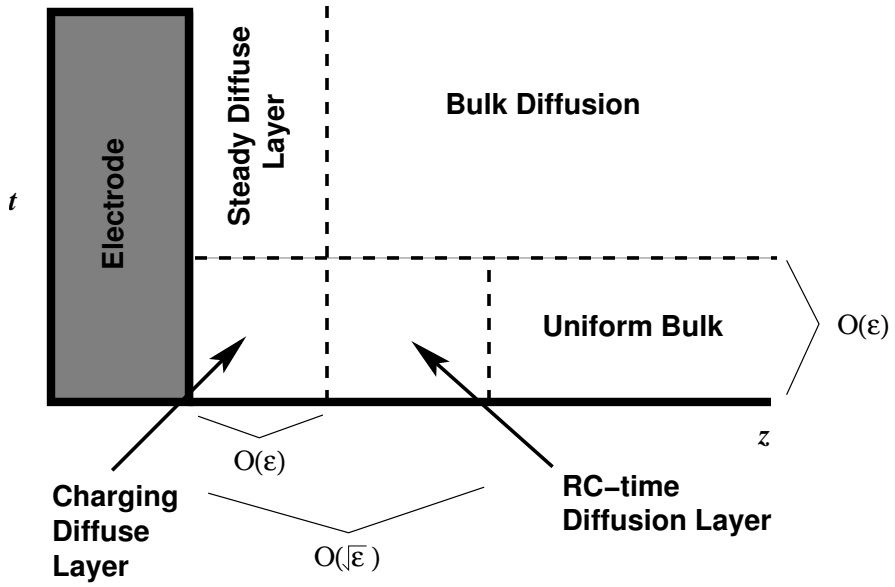

Figure 6-13: Five asymptotically distinct regions of space-time that govern the dynamic response of a metal colloid sphere to an applied electric field. Note the nested spatial boundary layers at the RC time ($t = O(\epsilon)$).

Uniform Bulk and Equilibrium Double Layers

To examine the dynamics at the RC time, we rewrite (6.1) – (6.3) by rescaling time using $\tilde{t} = t/\epsilon$:

$$\frac{\partial c}{\partial \tilde{t}} = \epsilon \nabla \cdot (\nabla c + \rho \nabla \phi) \tag{6.101}$$

$$\frac{\partial \rho}{\partial \tilde{t}} = \epsilon \nabla \cdot (\nabla \rho + c \nabla \phi) \tag{6.102}$$

$$-\epsilon^2 \nabla^2 \phi = \rho, \tag{6.103}$$

Since the spatial coordinate is scaled to the bulk length, the leading order solution of these equations describes the dynamics of the bulk during the double layer charging phase. Substituting a regular asymptotic expansions of the form

$$c(x,t) \sim c_0 + \epsilon c_1 + \epsilon^2 c_2 + \ldots. \tag{6.104}$$

into equations (6.101)-(6.103) yields a hierarchy of partial-differential equations. By sequentially solving the equations using the initial conditions, it is easy to show that the "outer" solutions at the RC charging time scale are

$$c_0\,(x,t) \equiv 1 \tag{6.105}$$

$$c_j(x,t) \equiv 0\,, \quad j=1,2,3,\ldots \tag{6.106}$$

$$\rho_j(x,t) \equiv 0\,, \quad j=0,1,2,\ldots \tag{6.107}$$

with ϕ_j is harmonic at all orders. In other words, the bulk solution can be completely expressed (*without* a series expansion) as a uniform concentration profile, $c\,(x,t) \equiv 1$, and a time-varying harmonic electric potential, ϕ. Note that by taking advantage of spherical geometry and axisymmetry in our problem, we can write the potential as a series in spherical harmonics with zero zonal wavenumber (*i.e.,* Legendre polynomials in $\cos\theta$):

$$\phi(r,\theta,t) = -E_o r\cos\theta + \sum_{l=0}^{\infty} P_l(\cos\theta)\frac{A_l(t)}{r^{l+1}}, \tag{6.108}$$

where the radial dependence of each term has been selected so that ϕ automatically satisfies Laplace's equation at all times.

As discussed in Section 6.2.2, the $O(\epsilon)$ double layer is in quasi-equilibrium at the RC charging time. Therefore, the leading order solution for the concentration and potential are given by (6.18) and (6.21) with the bulk concentration set equal to 1. Notice that at the RC time, bulk concentration gradients have not yet had time to form, so the variation of the diffuse layer concentration and charge density along the surface of the sphere is solely due to a non-uniform zeta-potential.

$O\,(\sqrt{\epsilon})$ Diffusion Layer

The analysis in the previous section leads us to an apparent paradox. The dynamics of the system seem to have been lost since both the bulk and the boundary layers are in quasi-equilibrium at leading order. As discussed in [8], the resolution to this paradox lies in the time-dependent flux matching between the bulk and the boundary layer. Unfortunately, it

is inconsistent to directly match the bulk to the boundary layer; there *must* exist a nested $O\left(\sqrt{\epsilon}\right)$ diffusion layer in order to account for the build up of both surface charge *and* surface excess neutral salt concentration.

Mathematically, the presence of the diffusion layer at the RC time scale appears as a dominant balance in the transport equations by rescaling the spatial coordinate in the normal direction by $\sqrt{\epsilon}$ to obtain:

$$\frac{\partial \bar{c}}{\partial \tilde{\tilde{t}}} = \epsilon^2 \nabla_s \cdot \left(\nabla_s \bar{c} + \bar{\rho} \nabla_s \bar{\phi}\right) + \frac{\partial}{\partial z'}\left(\frac{\partial \bar{c}}{\partial z'} + \bar{\rho}\frac{\partial \bar{\phi}}{\partial z'}\right) \tag{6.109}$$

$$\frac{\partial \bar{\rho}}{\partial \tilde{\tilde{t}}} = \epsilon^2 \nabla_s \cdot \left(\nabla_s \bar{\rho} + \bar{c} \nabla_s \bar{\phi}\right) + \frac{\partial}{\partial z'}\left(\frac{\partial \bar{\rho}}{\partial z'} + \bar{c}\frac{\partial \bar{\phi}}{\partial z'}\right) \tag{6.110}$$

$$-\epsilon^2 \nabla_s^2 \bar{\phi} - \epsilon \frac{\partial^2 \bar{\phi}}{\partial z'^2} = \bar{\rho}. \tag{6.111}$$

Here the bar accent denotes the "diffusion layer" solution at the RC time and $z' = Z/\sqrt{\epsilon}$ is the spatial coordinate in the direction normal to the surface. Notice that at this length scale, the system is *not* in quasi-equilibrium as it is at the bulk and Debye length scales. It is, however, locally electroneutral at leading order as a result of (6.111).

As the double layer charges, it absorbs an $O(\epsilon)$ amount of charge and neutral salt from the $O(\sqrt{\epsilon})$ diffusion layer. Therefore, we expect that concentration changes within the diffusion to be on the order of $\sqrt{\epsilon}$, which motivates the use of an asymptotic expansion of the form

$$\bar{c}(x,t) \sim \bar{c}_0 + \epsilon^{1/2}\, \bar{c}_{1/2} + \epsilon\, \bar{c}_1 + \ldots. \tag{6.112}$$

Using this expansion in (6.109) – (6.111), we find that the leading order equations are:

$$\frac{\partial \bar{c}_0}{\partial \tilde{\tilde{t}}} = \frac{\partial^2 \bar{c}_0}{\partial z'^2} \tag{6.113}$$

$$\frac{\partial}{\partial z'}\left(\bar{c}_0 \frac{\partial \bar{\phi}_0}{\partial z'}\right) = 0 \tag{6.114}$$

$$\bar{\rho}_0 = 0 \tag{6.115}$$

The initial conditions and boundary condition as $z' \to \infty$ for these equations are $\bar{c}_0(t = 0) \equiv 1$ and $\bar{c}_0(z' \to \infty) = 1$, respectively. The boundary condition at $z' = 0$ is given by flux matching with the double layer. Rescaling space and time in (6.46) and

(6.47), we find that the appropriate flux boundary conditions for the diffusion layer are

$$\frac{\partial q}{\partial \tilde{t}} = \epsilon \nabla_s \cdot \left(\frac{q}{2\bar{c}} \nabla_s \bar{c} + w \nabla_s \bar{\phi} \right) + \frac{1}{\sqrt{\epsilon}} \, \bar{c} \frac{\partial \bar{\phi}}{\partial z'} \tag{6.116}$$

$$\frac{\partial w}{\partial \tilde{t}} = \epsilon \nabla_s \cdot \left(\frac{w}{2\bar{c}} \nabla_s \bar{c} + q \nabla_s \bar{\phi} \right) + \frac{1}{\sqrt{\epsilon}} \, \frac{\partial \bar{c}}{\partial z'}. \tag{6.117}$$

Thus, the leading order flux boundary conditions, which appear at $O(1/\sqrt{\epsilon})$, are

$$\bar{c}_0 \frac{\partial \bar{\phi}_0}{\partial z'} = 0 \tag{6.118}$$

$$\frac{\partial \bar{c}_0}{\partial z'} = 0. \tag{6.119}$$

The leading order solutions in the diffusion layer, $\bar{c}_0 \equiv 1$ and $\bar{\phi}_0 = \phi$ $(Z \to 0)$, are easily determined by applying the initial and boundary conditions to (6.113) – (6.115).

To obtain dynamics, we must examine the first-order correction to the solution. At the next higher order, the governing equations are

$$\frac{\partial \bar{c}_{1/2}}{\partial \tilde{t}} = \frac{\partial^2 \bar{c}_{1/2}}{\partial z'^2} \tag{6.120}$$

$$\frac{\partial^2 \bar{\phi}_{1/2}}{\partial z'^2} = 0 \tag{6.121}$$

$$\bar{\rho}_{1/2} = 0, \tag{6.122}$$

where we have made use of the leading order solution to simplify (6.121). Again, the initial conditions and boundary condition at infinity are simple: $\bar{c}_{1/2}(t = 0) \equiv 0$ and $\bar{c}_{1/2}(z' \to \infty) = 0$. The flux boundary conditions at $z' = 0$, however, are more interesting because they involve the charging of the double layer:

$$\frac{\partial q}{\partial \tilde{t}} = \left. \frac{\partial \bar{\phi}_{1/2}}{\partial z'} \right|_{z=0} \tag{6.123}$$

$$\frac{\partial w}{\partial \tilde{t}} = \left. \frac{\partial \bar{c}_{1/2}}{\partial z'} \right|_{z=0}. \tag{6.124}$$

Thus, simple diffusion of neutral salt at $O(\sqrt{\epsilon})$ driven by absorption into the $O(\epsilon)$ double layer dominates the dynamics of the diffusion layer. From (6.121) and (6.123), we see that

the electric potential possesses a linear profile with slope given by rate of surface charge build up in the double layer:

$$\bar{\phi} \sim \phi \ (Z \to 0) + \epsilon^{1/2} \ \left(\frac{\partial q}{\partial \tilde{t}} \right) z' \tag{6.125}$$

Note that constant term at $O(\sqrt{\epsilon})$ is forced to be zero by matching with the bulk electric potential since all higher order corrections to the bulk potential are identically zero.

Effective Boundary Conditions Across Entire Diffusion Layer

It is precisely the fact that the electric potential has the form (6.125) that justifies the common approach of asymptotic matching directly between the bulk and the double layer [7, 8, 104]. For instance, the time-dependent matching used by Bazant, Thornton, and Ajdari [8] rests on the implicit assumption that the leading order electric field in the diffusion layer is a constant and appears at $O(\sqrt{\epsilon})$ so that

$$\left. \frac{\partial \phi}{\partial Z} \right|_{Z=0} = \frac{1}{\sqrt{\epsilon}} \left(\frac{\partial \bar{\phi}}{\partial z'} \right) \Bigg|_{z' \to \infty} \sim \left. \frac{\partial \bar{\phi}_{1/2}}{\partial z'} \right|_{z' \to \infty} = \frac{\partial q}{\partial \tilde{t}}. \tag{6.126}$$

Similarly, the definition of the zeta-potential and the Stern boundary condition (6.24) across the entire diffusion layer require that $\bar{\phi} \sim \phi \ (Z \to 0)$ at leading order.

Leading-order Dynamics

Using the results of our discussion, we now derive the leading order equations that govern the charging dynamics on the surface of the sphere. Since charging is non-uniform over the electrode surface, the equations take the form of partial differential equations on the surface of the sphere. Defining $\Psi(\theta, \phi) \equiv v - \phi(r = 1, \theta, \phi)$, we can write the Stern boundary condition, (6.24), and the double layer charging equation (6.126) as

$$\zeta + 2\delta\sqrt{c} \sinh(\zeta/2) = \Psi \tag{6.127}$$

$$C(\Psi) \frac{\partial \Psi}{\partial \tilde{t}} = \frac{\partial \phi}{\partial n}, \tag{6.128}$$

where we have introduced the leading order differential double layer capacitance $C(\Psi) = -\partial q/\partial\Psi$. Together with (6.42), (6.128) and (6.128) form a complete set of boundary conditions for the leading order electric potential in the bulk region. To compute the double layer capacitance, we can combine (6.42) with (6.128) to obtain

$$C = \frac{1}{\operatorname{sech}(\zeta/2) + \delta}. \tag{6.129}$$

Since C depends on $\tilde{\Psi}$ (via ζ), the charging equation (6.128) is nonlinear which makes the problem analytically intractable.

For small applied fields (where $\zeta \approx E_o$ is a reasonable approximation), analytical progress can be made by linearizing the the double-layer capacitance around $\zeta = 0$ to obtain $C \sim 1/(1+\delta)$. This approximation leads to a linear charging equation, (6.128), making it possible to solve the equations as an expansion in spherical harmonics. Substituting the expansion (6.108) into (6.128) and the definition of Ψ, we obtain a decoupled system of ordinary differential equations for the expansion coefficients:

$$\begin{aligned} \frac{dA_0}{dt} + (1+\delta)A_0 &= \frac{dv}{dt} \\ \frac{dA_1}{dt} + 2(1+\delta)A_1 &= -(1+\delta)E_o + \frac{dE_o}{dt} \\ \frac{dA_l}{dt} + (1+l)(1+\delta)A_l &= 0\ ,\ l > 1. \end{aligned} \tag{6.130}$$

To retain generality, we have allowed for the possibility that the applied electric field and surface potential are time-varying. For the case of a steady surface potential and uniform applied field, we find that the bulk electric potential is

$$\phi = ve^{-(1+\delta)t} - E_o r\cos\theta\left[1 + \frac{1}{2r^3}\left(1 - 3e^{-2(1+\delta)t}\right)\right], \tag{6.131}$$

where we have assumed that both the surface potential and the electric field are suddenly switched on at $t = 0$. The initial condition in this situation is that of a conducting sphere at potential v in a uniform applied electric field E_o: $\phi = v - E_o r\cos\theta\left(1 - 1/r^3\right)$.

Using (6.131), the double layer potential and total diffuse charge are easily determined

to be

$$\Psi = v\left(1-e^{-(1+\delta)t}\right)+\frac{3}{2}E_o\cos\theta\left(1-e^{-2(1+\delta)t}\right) \tag{6.132}$$

$$q \sim \frac{v}{1+\delta}\left(1-e^{-(1+\delta)t}\right)+\frac{3}{2\,(1+\delta)}E_o\cos\theta\left(1-e^{-2(1+\delta)t}\right). \tag{6.133}$$

These results are consistent with the calculations by Bazant and Squires [7, 104], which is expected since the low applied field limit corresponds to the regime where the total diffuse charge is linearly related to the zeta-potential (and therefore the total double layer potential). It is worth mentioning that in the common situation where the surface potential is set well before $t = 0$, then the first term in each of the above expressions is not present.

Numerical Model

For larger applied fields, the nonlinear double layer capacitance forces us to use numerical solutions to gain physical insight. Since the bulk electric potential is a time-varying harmonic function, it is most natural to numerically model the evolution equation for the potential using a multipole expansion with harmonic terms. Truncating (6.108) after a finite number of terms yields a discrete solution of the form:

$$\hat{\phi}(r,\theta,t) = -E_o r\cos\theta+\sum_{l=0}^{N}\frac{A_l(t)}{r^{l+1}}P_l(\cos\theta), \tag{6.134}$$

where the unknowns are the time-dependent coefficients in the expansion. By using (6.134) and enforcing that (6.128) is satisfied at the collocation points $\theta_i = i\pi/N$, we derive a system of ordinary differential equations for the coefficients $A_l(t)$:

$$\mathbf{CP}\frac{d\vec{A}}{dt} = E_o\mathbf{P}(:,2)+\mathbf{Q}\vec{A}, \tag{6.135}$$

where $\vec{A}$ is the vector of expansion coefficients, $\mathbf{P}$ and $\mathbf{Q}$ are collocation matrices that relate the expansion coefficients to ϕ and $\partial\phi/\partial n$, respectively, and $\mathbf{C}$ is a diagonal matrix that represents the double layer capacitance at the collocation points. Note that the second column of $\mathbf{P}$ is the discrete representation of $P_1(\cos\theta) = \cos\theta$, so the term $E_o\mathbf{P}(:,2)$ accounts

for the applied background potential. The explicit forms for the collocation matrices and the discrete double layer capacitance are given by

$$\mathbf{P} = \begin{bmatrix} P_0(\cos\theta_0) & P_1(\cos\theta_0) & \dots & P_N(\cos\theta_0) \\ P_0(\cos\theta_1) & P_1(\cos\theta_1) & \dots & P_N(\cos\theta_1) \\ \vdots & \vdots & \ddots & \vdots \\ P_0(\cos\theta_N) & P_1(\cos\theta_N) & \dots & P_N(\cos\theta_N) \end{bmatrix} \tag{6.136}$$

$$\mathbf{Q} = \begin{bmatrix} P_0(\cos\theta_0) & 2P_1(\cos\theta_0) & \dots & (N+1)P_N(\cos\theta_0) \\ P_0(\cos\theta_1) & 2P_1(\cos\theta_1) & \dots & (N+1)P_N(\cos\theta_1) \\ \vdots & \vdots & \ddots & \vdots \\ P_0(\cos\theta_N) & 2P_1(\cos\theta_N) & \dots & (N+1)P_N(\cos\theta_N) \end{bmatrix} \tag{6.137}$$

$$\mathbf{C} = \text{diag}\left(C(\Psi(\theta_0), C(\Psi(\theta_1), \dots, C(\Psi(\theta_N))\right) \tag{6.138}$$

The system of ODEs for the expansion coefficients is easily solved using MATLAB's built-in ODE solvers by multiplying (6.135) through by $(\mathbf{CP})^{-1}$ and writing a simple function to evaluate the resulting right-hand side function.

Dipole Dominated Charging

From the numerical solution of the charging equation (6.128), we find that the charging is dominated by the dipolar contribution to the response (see Figure 6-14). While the nonlinear capacitance does in fact allow higher harmonics to contribute to the response, the higher harmonics only play a small role even at larger applied fields. As expected, when the sphere is kept at zero voltage, the antisymmetry between the upper and lower hemisphere is not broken and only odd terms contribute to the series solution (6.108). However, as shown in Figure 6-15, if a nonzero potential is applied to the sphere, all harmonics contribute to the solution.

The dipolar nature of double layer charging forms the foundation of much of the work on the charging of colloid particles over the past half century. For instance, the non-equilibrium double layer is often characterized in terms of the induced dipole moment [32]. As shown in (6.131) – (6.133), the monopole and dipole contributions are the *only* contributions in

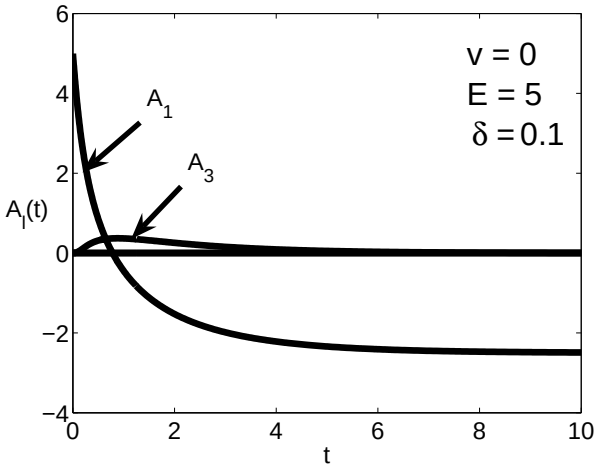

Figure 6-14: Time evolution of the dominant coefficients in the Legendre polynomial expansion of the bulk electric potential in the weakly nonlinear regime at the RC time. In this figure $v = 0$, $E = 5$ and $\delta = 0.1$. Notice that the dipolar term dominates the solution.

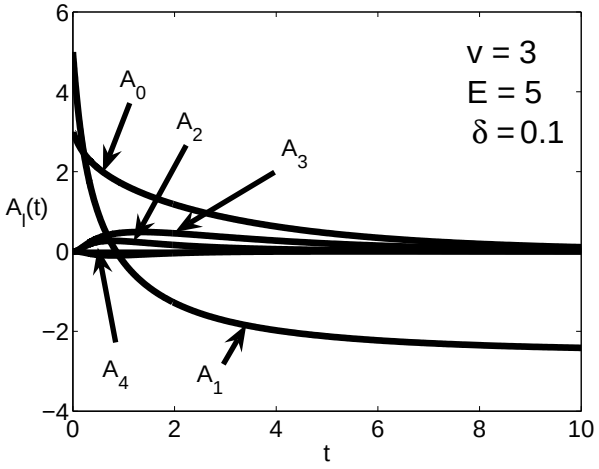

Figure 6-15: Time evolution of the dominant coefficients in the Legendre polynomial expansion of the bulk electric potential in the weakly nonlinear regime at the RC time when the sphere has a nonzero applied voltage. In this figure $v = 3$, $E = 5$ and $\delta = 0.1$. Note that both symmetric and antisymmetric terms make non-negligible contributions.

a linearized theory. Our numerical investigations demonstrate that, even for the nonlinear theory, the dipole response dominates the total response. Our results provides additional theoretical support for the focus on the dipole response when studying colloid particles in applied fields.

Retarded Double Layer Charging

Slowing of double layer charging is one important consequence of nonlinearity in the double layer capacitance (see Figure 6-16). However, as shown in Figure 6-16 retarded charging

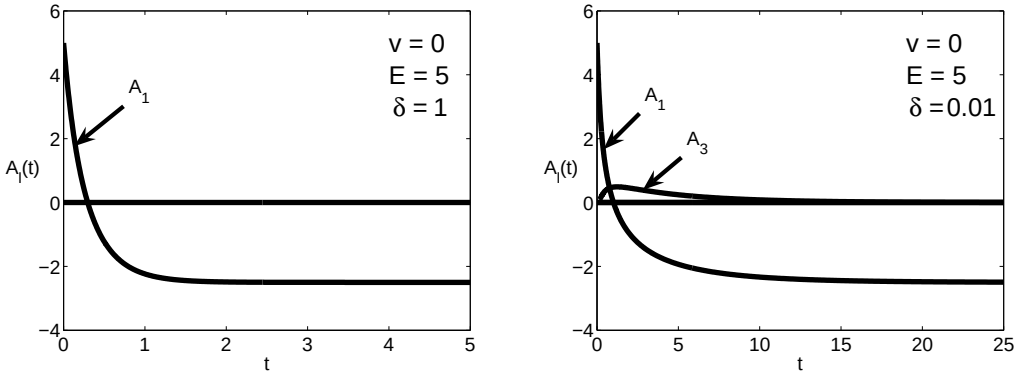

Figure 6-16: Time evolution of the dominant coefficients in the Legendre polynomial expansion of the bulk electric potential in the weakly nonlinear regime at the RC time for low (left) and high (right) Stern capacitance values. In these figures $v = 0$ and $E = 5$. Note that double layer charging is retarded when δ is small but that the slowdown in double layer charging is suppressed for larger δ values.

only occurs for $\delta \ll 1$. Mathematically, we only see slowed charging at small values of δ because the double layer capacitance (6.129) can only become as small as $1/\delta$, which occurs at large zeta-potentials. For sufficiently small δ, charging is slowed at higher applied fields because the $\mathrm{sech}(\zeta/2)$ term in the denominator of the double layer capacitance (6.129) becomes negligible when $\zeta \gg -2\ln(\delta/2)$.

6.5.2 Dynamics at the Diffusion Timescale

In this section, we examine the response of the system at the diffusion time scale. We find that the only dynamic process is diffusion of neutral salt within the bulk in response to

surface adsorption that occurs at the RC time scale. Since the total amount of neutral salt absorbed by the diffuse charge layers during the charging phase is an $O(\epsilon)$ quantity, the bulk concentration only needs to decrease by $O(\epsilon)$ to compensate. Thus, we find that dynamics are not present at leading order; rather, they appear only in higher-order corrections. Also, at the diffusion time, surface transport, which is negligible at the RC time scale, becomes important.

Leading Order Bulk and Double Layer Solutions

Substituting an asymptotic series into (6.1) – (6.3), we obtain the leading order bulk equations:

$$\frac{\partial c_0}{\partial t} = \nabla^2 c_0 \tag{6.139}$$

$$\nabla^2 \phi_0 = 0. \tag{6.140}$$

Applying the initial conditions (obtained by matching to the solution at the RC time) and the leading order boundary conditions (derived from the effective flux boundary conditions (6.46) and (6.47)) yields the simple leading order solutions

$$c_0(\vec{x},t) \equiv 1 \tag{6.141}$$

$$\phi_0(\vec{x},t) = -E_o r\cos\theta\left(1+\frac{1}{2r^3}\right) \tag{6.142}$$

Notice that there is no time dependence for either the concentration or the electric potential. It is worth mentioning that for a general geometry, the initial condition is a uniform concentration profile with the electric potential of an insulator in an applied field and the boundary conditions (which are consistent with the initial conditions) are

$$c_0\frac{\partial \phi_0}{\partial n} = 0 \quad \text{and} \quad \frac{\partial c_0}{\partial n} = 0. \tag{6.143}$$

At the diffusion time scale, the double layer continues to remain in quasi-equilibrium, so its leading order structure is given by (6.18) and (6.21) with the bulk concentration set equal to 1. However, unlike the double layer at the RC time scale, the leading order

zeta-potential is *not* evolving, so the leading order double layer structure is static in time.

Higher-Order Bulk Diffusion

In order to see dynamics, we need to consider the first-order correction to (6.139) and (6.140):

$$\frac{\partial c_1}{\partial t} = \nabla^2 c_1 \tag{6.144}$$

$$\nabla^2 \phi_1 = -\nabla c_1 \cdot \nabla \phi_0. \tag{6.145}$$

The boundary conditions for these equations are a bit more complicated. Using (6.46) – (6.47) and taking into account the leading order solutions, we find that the boundary conditions for the $O(\epsilon)$ equations are

$$q_0\ \delta^+(t) = \nabla_s \cdot (w_0 \nabla_s \phi_0) - \frac{\partial \phi_1}{\partial n} \tag{6.146}$$

$$w_0\ \delta^+(t) = \nabla_s \cdot (q_0 \nabla_s \phi_0) - \frac{\partial c_1}{\partial n}, \tag{6.147}$$

where q_0 and w_0 are the leading order equilibrium surface charge density and surface excess neutral salt concentration. As mentioned earlier, at the diffusion time scale, these quantities are static in time. Also, note the presence of the delta-functions in time, which account for the "instantaneous" adsorption of charge and neutral salt from the bulk during the double layer charging phase [8].

Mathematically, the appearance of the delta-functions is a consequence of the connection between the time derivative of double layer quantities at the two time scales in the asymptotic limit $\epsilon \to 0$. To illustrate this connection, consider the time derivative of the surface charge density, q. Let t and $\tilde{t}$ be scaled to the diffusion and RC times, respectively, so that $t = \epsilon \tilde{t}$. At these two time scales, the surface charge density can be written as $q(t)$ and $\tilde{q}\left(\tilde{t}\right)$ which are simply related by $q(t) = \tilde{q}\left(\tilde{t}\right)$. The time derivatives, however, are related by

$$\frac{\partial q}{\partial t}(t) = \frac{1}{\epsilon}\ \frac{\partial \tilde{q}}{\partial \tilde{t}}\left(t/\epsilon\right). \tag{6.148}$$

Therefore, for nonzero t, $\frac{\partial q}{\partial t} = 0$ in the asymptotic limit because $\frac{\partial \tilde{q}}{\partial \tilde{t}}\left(t/\epsilon\right)$ approaches zero

faster than linearly as $\epsilon \to 0$. In contrast, for $t = 0$, $\frac{\partial q}{\partial t}$ is infinite because $\frac{\partial \tilde{q}}{\partial \tilde{t}}(0)$ has a fixed nonzero value. Next, consider the following integral with $t_2 > 0$:

$$\int_{t_1}^{t_2} \frac{\partial q}{\partial t} dt = \int_{t_1/\epsilon}^{t_2/\epsilon} \frac{\partial \tilde{q}}{\partial \tilde{t}} d\tilde{t} = \tilde{q}\left(t_2/\epsilon\right) - \tilde{q}\left(t_1/\epsilon\right). \tag{6.149}$$

In the asymptotic limit, the integral approaches zero for nonzero t_1 but approaches $\tilde{q}(\infty)$ when t_1 equals zero. Putting the above properties together, we see that $\frac{\partial q}{\partial t}(t)$ is indeed a one-sided delta-function of strength $\tilde{q}(\infty) = q_0$.

In contrast to one-dimensional systems, the boundary layers play a more active role in the evolution of the bulk concentrations because surface conduction continues to play a role well beyond the initial injection of ions at $t = 0$. Note, however, that the surface conduction terms in (6.146) and (6.147) are static, so they essentially impose fixed normal flux boundary conditions on the $O(\epsilon)$ bulk equations.

Comparison with Dukhin's Analysis

It is interesting to compare and contrast our weakly nonlinear analysis with the work of Dukhin and Shilov [33, 102] on the polarization of the double layer for highly charge, spherical particles for weak applied fields. In both cases, bulk concentration variations and diffusion processes appear as a higher-order correction to a uniform background concentration and are driven by surface conduction. However, the significance of the surface conduction term arises for different reasons. As mentioned earlier, the small parameters that controls the size of the correction is different in the two analyses. In Dukhin and Shilov's analysis, the small parameters are ϵ *and* E_o. Because they essentially use asymptotic series in E_o as the basis for their analysis, they require that the double layer be highly charged in order for surface conduction to be of the same order of magnitude as the $O(E_o)$ normal flux of ions from the bulk. More precisely, because the size of the surface conduction is proportional to E_o, the surface charge density *must* be an $O(1)$ quantity: $\epsilon q = 2\epsilon \sinh(\zeta_0/2) = O(1)$. In contrast, we use asymptotic series in ϵ in our analysis and do not restrict E_o to be small, so the surface conduction and normal flux of ions from the bulk have the same order of magnitude for small $O(\epsilon)$ surface charge densities regardless of the strength of the applied

electric field (as long as it is not so large that the asymptotic analysis breaks down). Thus, our weakly nonlinear analysis complements the work of Dukhin and Shilov by extending their analysis to stronger applied electric fields.

6.5.3 Future work

Mathematical analysis of higher-order bulk diffusion is complicated by the presence of nonlinear surface transport terms in the boundary conditions. Numerical analysis is also difficult as a result of the delta-functions present in the boundary conditions. It would certainly be interesting to analytically or computationally explore the leading order dynamics of the bulk at the diffusion time scale. Unfortunately, these topics are beyond the scope of this thesis and are left as possible directions for future work.

6.6 Strongly Nonlinear Dynamics

As discussed in [8], the weakly nonlinear analysis breaks down when the dynamic Dukhin number, $\alpha_d = 4\sqrt{\epsilon}\sinh^2(\zeta_0/4) = \sqrt{\epsilon}\ w$, becomes $O(1)$ because the leading order term in the asymptotic expansion of the bulk concentration no longer dominates the first-order correction. Beyond the weakly nonlinear regime, there are two main effects that occur: (1) transient, local depletion of the leading order bulk concentration and (2) surface conduction at the leading order. As in the case of a steady applied field, perhaps the greatest impact of an $O(1)$ dynamic Dukhin number is that we must pay attention to factors of the form ϵe^{ζ} or $\epsilon\sinh(\zeta)$, in addition to factors of ϵ, when ordering terms in asymptotic expansions.

In the thin double-layer limit, the boundary layers are still in quasi-equilibrium, which suggests that we proceed as in the previous sections and treat the bulk as locally electroneutral with effective boundary conditions. Unfortunately, the analysis of the leading order equations derived in this manner does not appear to be as straightforward as the analysis in the weakly nonlinear limit. The main problem is that it seems difficult to derive a uniformly valid leading order effective boundary conditions along the entire surface of the sphere. For this reason, we merely present the *apparent* leading order equations for the strongly nonlinear regime and leave a thorough analysis for future work.

6.6.1 Leading Order Equation in Strongly Nonlinear Regime

At the leading order in the bulk, we find the usual equations for a neutral binary electrolyte:

$$\frac{\partial c_0}{\partial t} = \nabla^2 c_0 \tag{6.150}$$

$$0 = \nabla \cdot (c_0 \nabla \phi_0) \tag{6.151}$$

with $\rho = O(\epsilon^2)$. The structure of the boundary layers is described by GCS theory with the concentration and charge density profiles given by (6.17) – (6.19). Effective boundary conditions for (6.150) – (6.151) are derived in the same manner as for a steady applied field except that unsteady terms are retained. Recalling that q and w grow exponentially with the zeta-potential, we find that both the surface conduction terms and the time derivatives of the total diffuse charge and excess concentration appear in the leading order boundary conditions:

$$\epsilon \frac{\partial \tilde{q}_0}{\partial t} = \epsilon \nabla_s \cdot (\tilde{w}_0 \nabla_s \phi_0) - c_0 \frac{\partial \phi_0}{\partial n} \tag{6.152}$$

$$\epsilon \frac{\partial \tilde{w}_0}{\partial t} = \epsilon \nabla_s \cdot (\tilde{q}_0 \nabla_s \phi_0) - \frac{\partial c_0}{\partial n}. \tag{6.153}$$

6.6.2 Challenges with Strongly Nonlinear Analysis

It is important to realize that these equations are mathematically much more complicated than the analogous equations in the weakly nonlinear regime. First, the nonlinearity due to the electromigration term explicitly appears in the bulk equations at leading order; the nonlinearity is *not* removed by the asymptotic analysis. Furthermore, the diffuse layer concentrations depends on time explicitly through the bulk concentration at the surface in addition to the zeta potential:

$$\tilde{c}_{\pm}(t) = c_{\pm}(t) e^{\mp \tilde{\psi}(t)}. \tag{6.154}$$

Already, these features of the equations greatly increases the challenge in analyzing the response of the system.

However, the greatest complication to the mathematical model in the strongly nonlinear regime is that effective boundary conditions (6.152) and (6.153) are not uniformly valid

over the surface of the sphere. Near the poles, the double layer charges quickly, so the time-dependent and surface transport terms in the effective boundary conditions become $O(1)$ at very short times. In contrast, the amount of surface charge in the double layer near the equator is *always* a small quantity. Thus, it would seem that the only significant terms in the effective boundary conditions are the normal flux terms. Together, these observations suggest that the appropriate set of boundary conditions to impose on the governing equations (6.150) and (6.151) depends on the position on the surface of the sphere. Moreover, the position where the boundary conditions switch from one set to the other depends on time as double layer charging progresses from the pole towards the equator.

The challenging issues discussed in this section need to be addressed in order to gain a deeper understanding of the behavior of metal colloid systems in the strongly nonlinear regime. Because they are beyond the scope of this thesis, we leave a complete analysis as an open area for future research.

6.7 Conclusions

In this chapter, we have examined the response of a metal colloid sphere to applied electric fields. In particular, we have focused on the charging of the double layer and the development of $O(1)$ gradients in the bulk concentration. The primary purposes of this work were to move beyond the traditional circuit models commonly used to study the response of electrochemical systems and to consider the behavior the system at large applied fields.

Our analysis shows that enhanced ion concentration within the double layer is a major feature of the response of our system to large applied electric fields. By interacting with the bulk electric field, the enhanced concentration within the double layer leads to large surface current densities. In addition, because the double layer does not charge uniformly over the surface of the sphere, tangential concentration gradients within the double layer itself lead to surface diffusion. It is these surface transport process, which are coupled to bulk transport via normal fluxes into the double layer, that drive the formation of bulk concentration gradients.

For metal colloid particles subjected to suddenly applied electric fields, bulk concentra-

tion gradients are *always* present and play an important role in allowing the system to relax to the steady-state. For weak applied fields, they are often neglected because they only appear as a first-order correction to a uniform background concentration profile. However, for strong applied fields, the variations in the bulk concentration becomes as large as the background concentration, so they cannot be ignored. These bulk concentration gradients lead to bulk diffusion currents which result in net circulation of neutral salt in the region near the metal sphere.

A key contribution of this work is a general derivation of the effective boundary conditions the bulk transport equations in the thin double layer limit. Using the general theory of surface conservation laws and the observation that the double layers remain in quasi-equilibrium, we derive a set of boundary equations that relate the time evolution of surface concentrations to surface transport processes and normal flux from the bulk. An interesting feature of the effective boundary conditions is that they explicitly involve the small parameter ϵ and may have different leading order forms depending on the characteristic time scale and the magnitude of double layer ion concentrations.

6.8 Future Research

We conclude this chapter by discussing a few general areas for future research related to electrochemical transport in colloid systems. First, as mentioned earlier, dynamics in the strongly nonlinear regime is still poorly understood. More generally, the effective bulk and boundary conditions in the thin double layer limit have yet to be validated against the full PNP equations. The utility of the thin double layer approximation cannot be fully appreciated until this comparison is completed.

Since microfluidics was the original motivation for our analysis, it would be interesting to connect our results back to the fluid dynamics problem. Assuming that the bulk Peclet number is small, we can use the solution to the charging problem to compute the electrokinetically generated slip-velocity at the surface of the sphere. Because tangential concentration gradients may exist within the double layer, calculation of the slip velocity will need to include the effects of both electro-osmosis *and* diffusio-osmosis. Once the

slip-velocity has been computed, it is straightforward to determine the fluid velocity using series expansions derived by Lighthill [66] (corrected by Blake [11] and written in a slightly different form by Leal [62]).

Finally, it is interesting (but more challenging) to consider the effects of the fluid flow on the charging problem which may be important at large bulk Peclet numbers. In this situation, convection contributes to ion transport so the electrochemical transport problem is no longer decoupled from the fluid flow. As a result, the analysis of the problem would require a coupled analysis of both electrochemical transport and fluid flow.

Chapter 7

Conclusions

> Strongly nonlinear systems . . . the final frontier . . .
>
> – paraphrasing of Jean-Luc Picard from *Star Trek*

As we have witnessed in this thesis, the theoretical study of electrochemical systems conditions continues to be an area filled with interesting and challenging problems, especially in light of modern activity in developing devices that operate under extreme conditions. While the results from classical electrochemical theory will always retain their utility for systems near equilibrium or specially prepared experiments, the need for theoretical results far from equilibrium grows more important as devices based on electrochemical processes push into exotic regimes.

There are a few main sources of difficulty in studying electrochemical systems far from equilibrium. First, in bulk regions, the nonlinear coupling between the potential and concentration fields must be dealt with directly. The linearization process that is common to many classical analyses are no longer valid for strongly driven systems. Second, the inherently nonlinear relationships between the potential and concentration fields within the double layer lead to surface processes that significantly affect bulk dynamics. Mathematically, the surface processes introduce additional terms (which are nonlinear) into the boundary conditions for the bulk. Finally, under extreme operating conditions, Faradaic reactions, which introduce highly nonlinear boundary conditions, become much more likely.

From a mathematical perspective, the analysis of modern electrochemical systems pushes

the limits of commonly used mathematical and numerical methods. Linearization techniques are limited to weakly driven systems. Since many systems can be considered to have thin double layer, asymptotic analysis and boundary layer theory are useful for a wider range of systems. However, even these methods break down when a system is driven too strongly. As we have seen for both electrochemical thin films and metal colloid spheres, it was necessary to use non-standard asymptotic analysis series just to allow for incrementally larger applied voltages and electric fields. Clearly, the field of theoretical electrochemical transport would certainly benefit from the application or development of new mathematical techniques.

At large driving forces, the numerical solution of the equations also present a challenge. Due to the presence of thin boundary layers, methods based on standard low-order finite difference schemes on uniform grids turn out to be too computationally expensive (even in 1D). While it is possible to reduce the computational cost by using high-order (pseudospectral) schemes, at high voltages and electric fields, it is still difficult to achieve convergence of the Newton iteration for the nonlinear system of equations without resorting to continuation in the driving field and other physical parameters. Moreover, good computational performance of the Newton iteration is only attainable by analytically computing the Jacobian for the nonlinear differential operators.

In summary, given the growing interest in micro-electrochemical devices, the development of extreme electrochemical transport theory is timely. There are many unanswered or poorly understood questions that deserve to be addressed. In this thesis, we have taken a few steps in towards this goal and hopefully contributed to a foundation that others can build on.

Appendix A

Overpotentials

> An experiment is a question which science poses to Nature, and a measurement is the recording of Nature's answer.
>
> – Max Planck, *Scientific Autobiography and Other Papers*, 1949

> A theory must be tempered with reality.
>
> – Jawaharlal Nehru

For electrochemical studies focused on the chemistry of electrode processes, it is common to focus on the electrode potential, E, (*i.e.,* the total electric potential drop across the entire cell relative to a reference electrode) without worrying about the spatial dependence of the electric potential within the solution itself. Within this context, the driving force for all electrochemical processes (*i.e.,* mass transport and electrochemical reactions) is the difference between the electrode potential during operation and at equilibrium:

$$\eta \equiv E - E_{eq}. \tag{A.1}$$

Because it is accessible experimentally, the overpotential is a very practical quantity for understanding electrochemical systems. Unfortunately, it is theoretically difficult to work with because it combines the effects of many physical processes (*e.g.,* Stern layer potential drop and concentration polarization) into a single quantity, which makes it inconvenient

for trying to understand the effects of individual processes. However, so that theoretical results may be experimentally tested, it is valuable to connect results derived in terms of the electric potential back to overpotentials.

Appendix B

Positivity of Ion Concentrations for Electrochemical Thin Films

Are you positive?

– common colloquial phrase

For 1D steady problems, the positivity of the ion concentrations follows directly from the Nernst-Planck equations (5.6)–(5.6). For the anion concentration, equation (5.7) can be integrated exactly using the integrating factor e^{ϕ} to yield

$$c_-(x) = Ae^{\phi(x)}, \tag{B.1}$$

which implies that the sign of $c_-(x)$ is the same across the entire domain. Since the integral constraint (5.16) requires that $c_-(x)$ is positive somewhere in the domain, $c_-(x)$ must be positive *everywhere* in the domain.

For the cation concentration, we make use of the reaction boundary conditions (5.14) and (5.15). Integrating equation (5.6) with the integrating factor e^{ϕ}, we obtain

$$c_+(x) = c_+(0)e^{\phi(0)-\phi(x)} + 4je^{-\phi(x)} \int_0^x e^{\phi(y)} dy. \tag{B.2}$$

Clearly, the integral term is positive because e^{ϕ} is positive everywhere. Moreover, the reaction boundary condition (5.14) implies that $c_+(0) > 0$ because both j_r and k_c are

positive. Thus, we find that the cation concentration is strictly positive.

Appendix C

Numerical Methods

> A computation is a temptation that should be resisted as long as possible.
>
> – John P. Boyd, paraphrasing T. S. Elliot [13]

> It is all too easy to equate multiple windows with hard work, and multiple contour plots with progress.
>
> – John P. Boyd [13]

C.1 Pseudospectral Spatial Discretizations

The foundation of many numerical methods for the solution of differential equations is the use of discrete approximations to continuous functions. Two common (and sometimes competing) discrete representations of continuous functions are (1) expansion in a finite basis of continuous functions and (2) specifying the value of the function at discrete grid points. Both of these representations have been successfully used in a wide range of situations [13, 49, **?**]. For the numerical models in this thesis, we have made use of both approaches depending on the nature of the differential equations. When there is a natural basis in which to expand the solution, the first approach is useful and can reduce the computational complexity of the numerical solution procedure (*e.g.,* by reducing a problem from 2- to 1-dimensional). However, most problems lack the structure to benefit from an expansion in

a special basis set, so it is easier to take the second approach and use grid functions which are vectors of function values specified at the grid points[1]. Using grid functions to build numerical methods is often convenient because it is somewhat more intuitive to work with function values than with expansion coefficients.

A second important consideration when designing a numerical method for differential equations is how to derive the discretized differential equations. For numerical methods based on grid function representations of the solution, the discretized differential equations are typically derived by requiring that the discrete approximation to the differential equation be satisfied at a set of specified points (known as collocation points) in the computational domain. In general, the collocation points need not be the same as the grid points where values of the solution are given, but it is common to use the same set of points for both grid points and collocation points. Collocation is also a useful way to derive discrete equations when solutions can be represented in terms of a finite expansions of basis functions. In this situation, collocation points are typically chosen to coincide with the collocation points that would be used for a grid based numerical method appropriate for the type of computational domain (discussed below).

For the numerical models used in this thesis, we make extensive use of spectral collocation (also known as pseudospectral) methods [13, 38, 111]. These grid based numerical methods are particularly well-suited to model problems in applied mathematics where the geometry is relatively simple. Furthermore, they are very computationally efficient making it possible make significant progress using high-level scientific programming environments such as MATLAB. The main disadvantages of these methods are: (1) they are difficult to use when the geometry is complicated and (2) they require that the solution is sufficiently smooth throughout the computational domain [13, 38, 111]. While it is possible to extend pseudospectral methods to handle these difficulties [38, 88], a discussion of these advanced methods is beyond the scope of this thesis.

The computational efficiency of pseudospectral methods comes from the fact that they are very high-order (often exponentially accurate) methods. To achieve high accuracy,

[1]Actually, the two approaches can be related through the ideas of interpolation and sampling, so they are not entirely disconnected. In practice, however, it is useful to make the distinction because numerical methods based on the two representations of continuous functions are somewhat different.

pseudospectral methods make use of *all* of the grid points to compute approximations to derivatives; in effect, derivatives are always computed to the highest-order accuracy possible on a given grid. In contrast, standard finite-difference methods which approximate derivatives using a fixed number of local grid points, can only achieve a fixed-order of accuracy regardless of the number of grid points used in the computation.

Implementation of pseudospectral methods is only marginally more difficult than implementing a low-order finite difference method for a differential equation. The key idea is to recognize that both methods essentially represent the solution using grid functions and approximate derivatives via discrete differentiation operators (*i.e.,* differentiation matrices); in other words, both methods represent the solution by a vector $\hat{u}$ of values at the grid points and represent the differentiation operation by multiplication by a differentiation D:

$$\frac{du}{dx} \approx D\hat{u}, \tag{C.1}$$

where u is the continuous solution. The only difference between a pseudospectral and a finite-difference method is the choice of grid points and differentiation matrix. Thus, any finite difference method is a high-order pseudospectral method in disguise [13]. One merely needs to replace the computational grid and differentiation matrix.

It turns out that the choice of computational grid is very important to achieve high accuracy with pseudospectral methods [13, 38, 19]. In the remainder of this section, we highlight the appropriate computational grids and differentiation matrices for several common physical domains.

C.1.1 Pseudospectral Grids for Common 1-D Computational Domains

Periodic Intervals

For periodic intervals, the appropriate grids for spectrally accurate calculations turns out to be the two commonly used equi-spaced, uniform grids: (i) endpoint grids[2] and (ii) interior

[2]Endpoint grids are grids that contain the endpoints of the domain as part of the grid. They also go by many other names, such as mesh-centered, node-centered, or interface-centered grids.

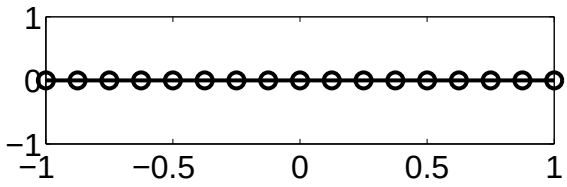

Figure C-1: Equi-spaced endpoint grid for periodic intervals.

grids[3]. As long as the solution and functions involved in the differential equation are not burdened by the presence of very high oscillatory modes, we can expect to obtain very accurate solutions with amazingly few grid points [13, 38, 111].

However, as mentioned earlier, spectral accuracy is only obtained by using all of the grid points when computing derivatives. For a general periodic function (*i.e.,* having both sine and cosine contributions) defined on an endpoint grid, the differentiation matrix for the first and second derivative are given by [13]

$$D_{ij}^{(1)} = \begin{cases} 0 & i = j \\ 0.5(-1)^{i-j} \cot\left[0.5(x_i - x_j)\right] & i \neq j \end{cases} \tag{C.2}$$

and

$$D_{ij}^{(2)} = \begin{cases} -(1 + 2N^2)/6 & i = j \\ 0.5(-1)^{i-j+1} / \sin^2\left[0.5(x_i - x_j)\right] & i \neq j \end{cases} \tag{C.3}$$

where $2N$ is number of grid points and the grid points are

$$x_i = \frac{\pi i}{N} \quad i = 0, \ldots, 2N - 1. \tag{C.4}$$

[3]Interior grids are grids where the grid points lie at the center of grid cells. They are also known as cell-centered grids.

Note that only one endpoint is included as part of the grid since the endpoints are completely equivalent by periodicity. Similar formulas are readily available for interior grids and grids for problems with special symmetry (*e.g.,* even or odd functions) [13].

Spectrally Accurate Numerical Quadrature It is worth mentioning that the simple numerical quadrature rules that are taught in basic calculus classes are spectrally accurate for even-periodic functions when uniform grids are used. For instance, on an endpoint grid, the "trapezoidal rule" is spectrally accurate. Similarly, on an interior grid, the "rectangle rule" is exponentially accurate. For non-periodic functions, these quadrature rules are very crude and low order. For odd-periodic functions, spectrally accuarate quadrature weights are not as trivial, but are still easily computed [13].

Finite, Non-periodic Intervals

To discuss pseudospectral methods for a finite, non-periodic interval, we first map the interval of interest to the canonical domain $[-1, 1]$. On this domain, there are many choices for the appropriate grids for spectral calculations. The most common grids are those based on Chebyshev polynomials. As in the periodic case, there are two variants. The Gauss-Lobatto grid with N points uses the extrema of an $(N-1)$-th order Chebyshev polynomial plus the two endpoints. The alternative, known as the interior or "roots" grid, uses the roots of an N-th degree polynomial, which reside strictly in the interior of $[-1, 1]$. While popular, the Chebyshev grids are not the only choice for finite, non-periodic intervals. It is well-known that any distribution of grid points with an asymptotic density of

$$\mu(x) = 1/\pi\sqrt{1-x^2} \tag{C.5}$$

as $N \to \infty$ yields spectrally accurate results[4] [13, 38, 111]. The key feature of this density is that the grid points cluster *quadratically* near the end points (*i.e.,* grid point spacing $= O(1/N^2)$). Intuitively, this clustering of grid points near the endpoints helps improve the accuracy of the "one-sided" derivatives that are the only available option in those regions of

[4]Fornberg discusses generalizations to this grid point distribution and shows that they may still be quite effective [38].

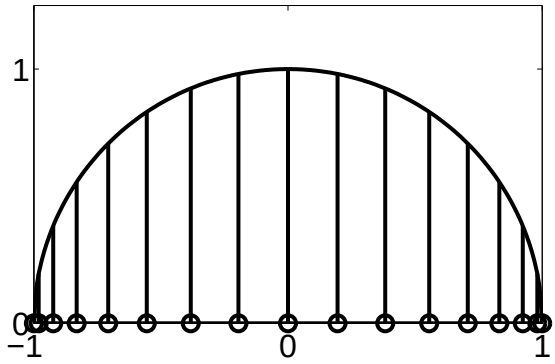

Figure C-2: Chebyshev endpoint grid for finite, non-periodic intervals.

the domain. The clustering also provides exceptional resolution of boundary layers without requiring a fine grid throughout the entire domain.

One reason for the popularity of Chebyshev grids is that both the grid points and the differentiation matrix are analytically computable. Alternative grids having the optimal grid point density[5] often require numerical computation of the grid points and differentiation matrices which complicates their use and introduces an additional source for error in the numerical method. Another important reason that Chebyshev grids are commonly used is that application of the differentiation matrix can be done very efficiently via the fast Fourier transform (FFT) [13, 111]. This feature of of the Chebyshev grid and differentiation matrix comes from the close connection between Chebyshev polynomials and trigonometric functions. The interested reader is referred to [13, 111] for a more detailed discussion of this interesting and powerful connection.

It is worth mentioning an important situation where working with Chebyshev is *not* ideal. Galerkin-type methods (or "weak" formulations) require computing inner products with the basis functions. When using a Chebyshev polynomial basis, the weighting function $w(x) = 1/\sqrt{1-x^2}$ that appears in the inner product is inconvenient (both analytically or numerically). As a result, in these cases, it is more common to use a Legendre polynomial

[5]Grids based on the Jacobi polynomials all have the optimal grid point density (C.5).

basis, which has the simple weighting function $w(x) \equiv 1$.

While the Chebyshev grid points and differentiation matrices are readily available in references on spectral methods [13, 38, 111], we reproduce the formulae here for convenience. For the Gauss-Lobatto grid [13], the grid points are

$$x_i = \cos\left(\frac{\pi i}{N}\right) \quad i = 0, \ldots, N \tag{C.6}$$

and the differentiation matrix for the first derivative is

$$D_{ij} = \begin{cases} (1+2N^2)/6 & i = j = 0 \\ -(1+2N^2)/6 & i = j = N \\ x_j / \left[2(1-x_j^2)\right] & i = j; 0 < j < N \\ (-1)^{i+j} p_i / \left[p_j (x_i - x_j)\right] & i \neq j \end{cases} \tag{C.7}$$

where $p_0 = p_N = 2$ and $p_j = 1$ for $0 < j < N$. A nice feature of the Gauss-Lobatto grid is that higher derivatives are merely powers of the differentiation matrix for the first derivative. For the interior grid [13], the grid points are

$$x_i = \cos\left(\pi \frac{2i-1}{2N}\right) \tag{C.8}$$

and the differentiation matrices for the first and second derivatives are

$$D_{ij}^{(1)} = \begin{cases} 0.5 x_j / (1-x_j^2) & i = j \\ (-1)^{i+j} \frac{\sqrt{(1-x_j^2)(1-x_i^2)}}{x_i - x_j} & i \neq j \end{cases} \tag{C.9}$$

and

$$D_{ij}^{(2)} = \begin{cases} \frac{x_j^2}{(1-x_j^2)^2} - \frac{N^2-1}{3(1-x_j^2)} & i = j \\ D_{ij}^{(1)} \left[\frac{x_i}{1-x_i^2} - \frac{2}{x_i - x_j}\right] & i \neq j \end{cases} \tag{C.10}$$

Infinite Intervals

For infinite and semi-infinite intervals, there are several appropriate choices for the computational grid. Because they are applicable to a wider range of problems, we shall emphasize

the grids based on rational Chebyshev functions. For completeness, we mention that there are three major alternatives for dealing with infinite domains; these are based on expansions in terms of sinc functions, Hermite functions, and Laguerre functions. A weakness common to methods based on these three expansions is that they require the function being approximated to decay exponentially at infinity [13]. The methods based on rational Chebyshev do not share this weakness and are able to approximate functions that only decay algebraically or are constant at infinity.

The rational Chebyshev grids are based on algebraically mapping the finite interval $[-1, 1]$ to the infinite interval. For the domains $(-\infty, \infty)$ and $[0, \infty)$, the respective computational grids are [13]

$$x_i^{(-\infty,\infty)} = \frac{Ly_i}{\sqrt{1-y_i^2}} \tag{C.11}$$

$$x_i^{[0,\infty)} = L\left(\frac{1+y_i}{1-y_i}\right) \tag{C.12}$$

where y_i are the Chebyshev grid points in $[-1, 1]$ and L is a scaling factor that controls how much of the infinite domain is "covered." Alternatively, since the Chebyshev points are just a mapping of the periodic interval $[0, 2\pi)$ to the non-periodic interval $[-1, 1]$, the rational Chebyshev grid points can be also thought of as a mapping from a uniform grid on $[0, 2\pi)$ to infinite and semi-infinite interval via the mappings

$$x_i^{(-\infty,\infty)} = L\cot(\theta_i) \tag{C.13}$$

$$x_i^{[0,\infty)} = L\cot^2\left(\frac{\theta_i}{2}\right) \tag{C.14}$$

where θ_i are a set of uniformly spaced grid points on $[0, 2\pi)$.

The basis function corresponding to these grids are the rational Chebyshev functions. For the domain $(-\infty, \infty)$, the basis functions are

$$TB_n(x) \equiv T_n(y) \tag{C.15}$$

where $y \in [-1, 1]$, T_n is the n-th Chebyshev polynomial and x is related to y via (C.11).

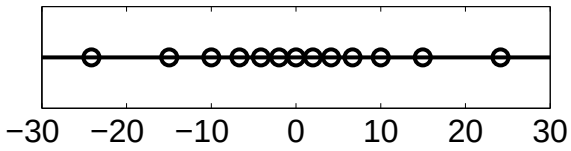

Figure C-3: Rational Chebyshev grid for infinite intervals.

Similarly, the basis functions for the semi-infinite interval $[0, \infty)$ are

$$TL_n(x) \equiv T_n(y). \tag{C.16}$$

where x and y are now related via (C.12).

The differentiation matrices for infinite and semi-infinite intervals are easily computed by using the above mappings and the chain-rule:

$$\frac{d}{dx^{(-\infty,\infty)}} = \frac{(1-y^2)^{3/2}}{L}\frac{d}{dy} \tag{C.17}$$

$$\frac{d}{dx^{[0,\infty)}} = \frac{(1-y)^2}{2L}\frac{d}{dy}. \tag{C.18}$$

Thus, since the multiplication becomes matrix multiplication by a diagonal matrix for the discretized function, we obtain

$$D^{(-\infty,\infty)} = \text{diag}\left[\frac{(1-y_i^2)^{3/2}}{L}\right] * D^{cheb} \tag{C.19}$$

$$D^{[0,\infty)} = \text{diag}\left[\frac{(1-y_i)^2}{2L}\right] * D^{cheb}, \tag{C.20}$$

where D^{cheb} is the differentiation matrix for the Chebyshev grid on a finite, non-periodic

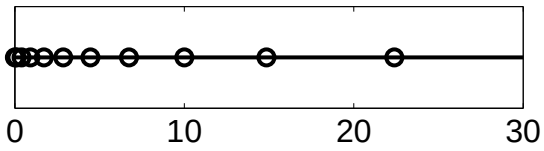

Figure C-4: Rational Chebyshev grid for semi-infinite intervals.

interval. As with the Chebyshev grids for finite, non-periodic domains, the connection between the rational Chebyshev functions and trigonometric functions on periodic domains makes it possible to apply the FFT to quickly compute derivatives when a large number of grid points are required.

C.1.2 Pseudospectral Discretizations in Higher Dimensions

Pseudospectral methods are easily extended to higher dimension (as long as the geometry remains simple). The basic idea is to construct the grid as a Cartesian product of one-dimensional pseudospectral grids. The result is a structured grid (with a potentially non-uniform grid spacing). Therefore, we can treat grid functions as vectors by ordering them in the natural way using "lexicographic" ordering of the grid indices. For example, on the small 3 by 4 Cartesian grid in Figure C-5, we could order the solution vector, $\hat{u}$, one row at a time:

$$\hat{u} = (\hat{u}_{11}, \hat{u}_{12}, \hat{u}_{13}, \hat{u}_{14}, \hat{u}_{21}, \hat{u}_{22}, \hat{u}_{23}, \hat{u}_{24}, \hat{u}_{31}, \hat{u}_{32}, \hat{u}_{33}, \hat{u}_{34})^T \tag{C.21}$$

where $\hat{u}_{ij}$ is the value of u at (x_i, y_j). With this choice of ordering discrete partial derivative operators are simply given as Kronecker product of the differentiation matrices with identity

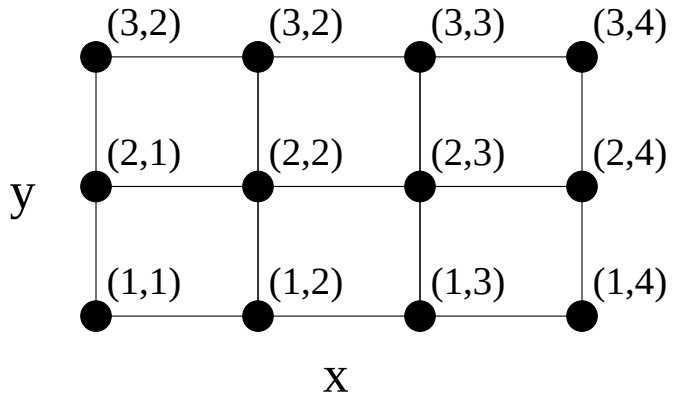

Figure C-5: Example of a 2d grid with four grid points in the x-direction and three grid points in the y-direction.

matrices. For the example in Figure C-5, the partial differentiation matrices are

$$D_x = I_3 \otimes D_4 \tag{C.22}$$

$$D_y = D_3 \otimes I_4 \tag{C.23}$$

where D_n and I_n are the 1d differentiation and identity matrices of size n. Note that care must be take to ensure that order that Kronecker products are taken is consistent with the ordering of the solution vector. Since vector differential operators, such as the divergence and gradient, may be written in terms of partial derivatives once a coordinate system has been chosen, discrete vector differentiation matrices are straightforward to construct in terms of partial differentiation matrices.

C.1.3 References for Spectral Methods

There are many excellent references on spectral and pseudospectral methods. *Spectral Methods in MATLAB* by N. Trefethen [111] is a very good and practical primer on the subject. It comes complete with actual MATLAB code that is a great way to start *playing* with pseudospectral methods. *Chebyshev and Fourier Spectral Methods* by J. P. Boyd [13] gives a more thorough but intuitive treatment of the subject. I highly recommend both of these books for anybody who is looking for a *practical* introduction to pseudospectral methods.

C.2 Computation of Exact Jacobians for Discretized PDEs

Discretized nonlinear boundary value problems (BVP) naturally arise in numerical models of physical systems at steady-state or as intermediate steps of implicit time-integration schemes for nonlinear unsteady partial differential equations. In both of these situations, it is common to use Newton-type iterations to compute the solution to the nonlinear BVP. Therefore, for each Newton iteration, we need a way to compute the Jacobian of the discretized nonlinear operator.

While it is possible to compute a numerical Jacobian, this procedure is very time consuming for systems of equations arising from the discretization of partial differential equations. For a 2-D scalar boundary value problem involving N grid points in each spatial direction, computing the numerical Jacobian requires $O(N^2)$ evaluations of the system of equations or a total of $O(N^4)$ function evaluations. This cost can be considerably reduced by specifying the sparsity pattern in the Jacobian, but it is still high. Therefore, deriving an analytical formula for the Jacobian is an important alternative to consider.

Analytical calculation of the Jacobian for a system of equations is often considered a tedious part and error-prone part of implementing Newton's method for nonlinear partial differential equations. However, it is a relatively straightforward calculation when the discretized equation are written in terms of discrete operators as in (6.54) – (6.57). The main simplifying idea is to carry out the computation directly on the equations and keep the result in matrix form.

Many analytical Jacobian calculations can be carried out by combining a few basic operations and observations.

1. The Jacobian of a matrix vector product (which, in the continuous situation, corresponds to a linear operator acting on a function) is the matrix itself:

$$\frac{\partial}{\partial \hat{u}} \left(A\hat{u} \right) = A. \tag{C.24}$$

   In particular, the Jacobian of a differentiation matrix, D, multiplying $\hat{u}$ is just D.

2. The Jacobian of a pointwise function f of $\hat{u}$ is a diagonal matrix with entries $f'(\hat{u})$:

$$\frac{\partial f(\hat{u})}{\partial \hat{u}} = \text{diag}\left[f'(\hat{u})\right] \tag{C.25}$$

3. The Jacobian of matrix, A, times a function $f(\hat{u})$ is A times the diagonal matrix with entries $f'(\hat{u})$:

$$\frac{\partial}{\partial \hat{u}}\left[A * f(\hat{u})\right] = A * \text{diag}[f'(\hat{u})] \tag{C.26}$$

4. Pointwise multiplication of two grid functions $\hat{u}$ and $\hat{v}$ can be rewritten as the product of a diagonal matrix with entries from one function multiplying the other grid function:

$$\hat{u} \ .* \ \hat{v} = \text{diag}\left(\hat{u}\right) \ .* \ \hat{v} = \text{diag}\left(\hat{v}\right) \ .* \ \hat{u}. \tag{C.27}$$

5. The "product rule" holds when calculating Jacobians of pointwise products of functions:

$$\frac{\partial}{\partial \hat{u}}\left[f(\hat{u}) \ .* \ g(\hat{u})\right] = \text{diag}\left[g(\hat{u})\right] * \frac{\partial f}{\partial \hat{u}} + \text{diag}\left[f\hat{u})\right] * \frac{\partial g}{\partial \hat{u}} \tag{C.28}$$

As an example, let us compute the Jacobian for the discretized form of the simple nonlinear function $f(u) = e^{2u}\frac{du}{dx}$. In discrete form, the function becomes

$$\hat{f}(\hat{u}) = \left[e.\wedge\left(2\hat{u}\right)\right] \ .* \ \left(D\hat{u}\right). \tag{C.29}$$

Using the product rule (C.28), the Jacobian of $\hat{f}$ becomes

$$J_{\hat{f}} = \text{diag}(D\hat{u}) * \frac{\partial}{\partial \hat{u}}\left[e.\wedge\left(2\hat{u}\right)\right] + \text{diag}\left[e.\wedge\left(2\hat{u}\right)\right] * \frac{\partial(D\hat{u})}{\partial \hat{u}}. \tag{C.30}$$

Then applying rules (C.24) and (C.25), we find that

$$J_{\hat{f}} = \text{diag}(D\hat{u}) * \text{diag}\left[(2e.\wedge\left(2\hat{u}\right)\right] + \text{diag}\left[e.\wedge\left(2\hat{u}\right)\right] * D \tag{C.31}$$

Appendix D

MATLAB Code

. . . straight from the source . . .

– common colloquial phrase

This appendix provides the core MATLAB code used to compute numerical solutions of the mathematical models of electrochemical systems explored in this thesis.

D.1 Differentiation Operators

D.1.1 DM_TL.m

```
%
% DM_TL computes the differentiation matrix and grid points
%       for a rational chebyshev function basis expansion of
%       order N with scale factor L
%
% Usage: function [D,x] = DM_TL(N,L)
%
% Input:
%
%   N (req):  highest order basis function to include
%   L (req):  scale factor for transformation between Chebyshev
%             and rational Chebyshev basis
%
% Ouput:
%
%   D:  differentiation matrix
```

```
%   x:  grid points
%
%
% NOTES:
%  (1) the formula for the derivatives is derived by using the
%      coordinate transformation
%
%         x = L(1+y)/(1-y)
%
%      where -1 <= y <= 1 is the domain in the Chebyshev basis.
%
%  (2) The point x = \infty is NOT excluded from the x-grid points.
%
%  (3) this function depends on the CHEB function by Trefethen (2000).
%
% Kevin Chu
% Dept of Mathematics, MIT
% Jan 2005
%

function [D,x] = DM_TL(N,L)

% check inputs
if (nargin < 2)
  error('MATLAB:missingArgs','DM_TL:missing arguments');
  return
end

% compute differentiation matrix in the y-domain
[D_y,y] = cheb(N);
one_minus_y = spdiags(1-y,0,N+1,N+1);

% transform to the x-domain
D = 0.5/L*(one_minus_y^2)*D_y;
warning off MATLAB:divideByZero  % disable warning message when computing x
x = L*(1+y)./(1-y);
warning on MATLAB:divideByZero  % re-enable warning message
```

D.1.2 DM_cosine_interior.m

```
%
% DM_cosine_interior computes the differentiation matrix and grid points
%                    for a cosine cardinal basis expansion of order N
%                    with all grid points in the interior of the domain
%
% Usage: function [D,theta] = DM_cosine_interior(N)
%
% Input:
%
%   N (req):  highest fourier component to include
%
% Ouput:
%
%   D:      differentiation matrix
%   theta:  grid points
%
%
% NOTES:
%  (1) the formula for the derivatives was derived from the formula
%      for the cardinal functions given in Boyd (2000) Appendix F.5
%
%
% Kevin Chu
% Dept of Mathematics, MIT
% Jan 2005
%

function [D,theta] = DM_cosine_interior(N)

% N = 0 case
if N==0, D = 0; theta = 0; return, end

% N > 0
j = 1:N;
theta = (2*j'-1)*pi/2/N;
c = ones(1,N).*(-1).^((1:N)+1);
T = repmat(theta,1,N);

% off-diagonals entries
% NOTES:
%  (1) the eye(N) avoids division by zero on the diagonal, which
%      we don't care about anyways
%  (2) the sin(N*T) term just gives an alternating sequence of
```

```
%      1s and -1s down a column
off_diag_D = repmat(c,N,1).*sin(N*T).*sin(T').*(cos(T')-cos(T)+eye(N));

% diagonal entries
diag_D = -0.5*cot(theta);

% assemble matrix
D = triu(off_diag_D,1) + tril(off_diag_D,-1) + diag(diag_D);
```

D.1.3 div.m

```
%
% div computes the discrete divergence operator in spherical coordinates
%     with azimuthal symmetry
%
% Usage: D_div = div(D_r, D_theta, r, theta)
%
% Input:
%
%   D_r (req):      differentiation matrix in radial direction
%   D_theta (req):  differentiation matrix in polar angle direction
%   r (req):        radial grid points
%   theta (req):    polar angle grid points
%
% Ouput:
%
%   D_div:  discrete divergence operator for solutions stored in
%           radial-major order.  the components of D_div are the
%           operators for the radial and polar angle components of
%           the vector field.
%
%
% Kevin Chu
% Dept of Mathematics, MIT
% Jan 2005
%
% ------------------------------------------------------------------
% CHANGE LOG
% ==========
% 2005/01/26:
%  - Use sparse matrices for identity and diagonal matrices to save
%    memory and improve performance.
%
% 2005/01/25:
%  - Initial version of code.
%  - Used dense matrices for identity and diagonal matrices.
% ------------------------------------------------------------------
%


function D_div = div(D_r, D_theta, r, theta)

num_gridpts_r = length(r);
num_gridpts_theta = length(theta);
```

```
one_over_r = spdiags(1./r,0,num_gridpts_r,num_gridpts_r);
sin_theta_vec = sin(theta);
sin_theta = spdiags(sin_theta_vec,0,num_gridpts_theta,num_gridpts_theta);
one_over_sin_theta = spdiags(1./sin_theta_vec,0, ...
                             num_gridpts_theta,num_gridpts_theta);

D_div = {kron(speye(num_gridpts_theta), 2*one_over_r + D_r), ...
         kron(one_over_sin_theta*D_theta*sin_theta, one_over_r)};
```

D.1.4 grad.m

```
%
% grad computes the discrete gradient operator in spherical coordinates
%      with azimuthal symmetry
%
% Usage: D_grad = grad(D_r, D_theta, r, theta)
%
% Input:
%
%   D_r (req):      differentiation matrix in radial direction
%   D_theta (req):  differentiation matrix in polar angle direction
%   r (req):        radial grid points
%   theta (req):    polar angle grid points
%
% Ouput:
%
%   D_grad:  discrete gradient operator for solutions stored in
%            radial-major order. the components of D_div are the
%            operators for the radial and polar angle components of
%            the vector field.
%
%
% Kevin Chu
% Dept of Mathematics, MIT
% Jan 2005
%
% ------------------------------------------------------------------
% CHANGE LOG
% ==========
% 2005/01/26:
%  - Use sparse matrices for identity and diagonal matrices to save
%    memory and improve performance.
%
% 2005/01/25:
%  - Initial version of code.
%  - Used dense matrices for identity and diagonal matrices.
% ------------------------------------------------------------------
%


function D_grad = grad(D_r, D_theta, r, theta)

num_gridpts_r = length(r);
num_gridpts_theta = length(theta);
```

```
one_over_r = spdiags(1./r,0,num_gridpts_r,num_gridpts_r);
D_grad = {kron(speye(num_gridpts_theta),D_r), ...
          kron(D_theta,one_over_r)};
```

D.1.5 laplacian.m

```
%
% laplacian computes the discrete laplacian operator in spherical
%           coordinates with azimuthal symmetry
%
% Usage: D_laplacian = laplacian(D_r, D_theta, r, theta)
%
% Input:
%
%   D_r (req):      differentiation matrix in radial direction
%   D_theta (req):  differentiation matrix in polar angle direction
%   r (req):        radial grid points
%   theta (req):    polar angle grid points
%
% Ouput:
%
%   D_laplacian:  discrete laplacian operator for solutions stored in
%                 radial-major order.
%
%
% Kevin Chu
% Dept of Mathematics, MIT
% Jan 2005
%
% ------------------------------------------------------------------
% CHANGE LOG
% ==========
% 2005/01/26:
%  - Use sparse matrices for identity and diagonal matrices to save
%    memory and improve performance.
%
% 2005/01/25:
%  - Initial version of code.
%  - Used dense matrices for identity and diagonal matrices.
% ------------------------------------------------------------------
%

function D_laplacian = laplacian(D_r, D_theta, r, theta)

num_gridpts_r = length(r);
num_gridpts_theta = length(theta);
one_over_r = spdiags(1./r,0,num_gridpts_r,num_gridpts_r);
sin_theta_vec = sin(theta);
sin_theta = spdiags(sin_theta_vec,0,num_gridpts_theta,num_gridpts_theta);
```

```
one_over_sin_theta = spdiags(1./sin_theta_vec,0, ...
                             num_gridpts_theta,num_gridpts_theta);

D_laplacian = kron(speye(num_gridpts_theta),2*one_over_r*D_r + D_r^2) ...
  + kron(one_over_sin_theta*D_theta*sin_theta*D_theta, one_over_r^2);
```

D.1.6 div_s.m

```
%
% div_s computes the discrete surface divergence operator in spherical
%       coordinates with azimuthal symmetry
%
% Usage: D_div_s = div_s(D_theta, theta, 4)
%
% Input:
%
%   D_theta (req):  differentiation matrix in polar angle direction
%   theta (req):    polar angle grid points
%   r (req):        radius of sphere
%
% Ouput:
%
%   D_div_s:  discrete surface divergence operator for problems
%             with azimuthal symmetry
%
%
% Kevin Chu
% Dept of Mathematics, MIT
% Jan 2005
%
% ------------------------------------------------------------------
% CHANGE LOG
% ==========
% 2005/01/27:
%  - Initial version of code.
% ------------------------------------------------------------------
%


function D_div_s = div_s(D_theta, theta, r)

num_gridpts_theta = length(theta);
sin_theta_vec = sin(theta);
sin_theta = spdiags(sin_theta_vec,0,num_gridpts_theta,num_gridpts_theta);
one_over_sin_theta = spdiags(1./sin_theta_vec,0, ...
                             num_gridpts_theta,num_gridpts_theta);

D_div_s = one_over_sin_theta*D_theta*sin_theta/r;
```

D.2 Electrochemical Thin-Films

D.2.1 solveSteadyPNP.m

```
%
% function [E, x, residual, delta_E, iter_count] ...
%    = solveSteadyPNP(numPoints, ...
%          j,epsilon,delta,alpha_c,alpha_a,k_c,j_r, ... % physical params
%          res_tol, delta_tol, max_iters, norm_type, ... % Newton params
%          E_initial_guess, ...
%          j_start,dj, ...  % continuation params
%          debugStatFreq,debugPlotFreq)
%
%
% solveSteadyPNP() computes the solution to the steady PNP equations with
% reaction boundary conditions by solving the master equation for the
% electric field using the pseudospectral method.
%
% The master equation for the electric field is
%
%   epsilon^2 (E'' - 0.5*E^3) - (c0(E) + 2*j*x) E = j
%
% where epsilon is the ratio of the Debye screening length to the
% cell size (i.e. = lambda_D/L) and c0(E) is given by
%
%   c0 = 1 - j + epsilon^2 ( E(1) - E(0) - 0.5*int_0^1{E^2 dx} ).
%
% The boundary conditions for this equation are the Butler-Volmer
% rate equations:
%
%  k_c (c(0) + rho(0)) exp(-alpha_c*delta*epsilon*E(0))
%    - j_r exp(alpha_a*delta*epsilon*E(0)) = j
%
%  -k_c (c(1) + rho(1)) exp(alpha_c*delta*epsilon*E(1))
%    + j_r exp(-alpha_a*delta*epsilon*E(1)) = j
%
% where c(x) = c0(E) + 2*j*x + 0.5*epsilon^2*E(x)^2 and
%       rho(x) = epsilon^2*E'(x)
%
%
% Inputs:
%
%   numPoints:  number of grid points/degree of polynomial approximant
%
%   physical parameters:  j, epsilon, delta, alpha_c, alpha_a, k_c, j_r
```

```
%
%   Newton iteration parameters -
%     res_tol:    stopping criterion for the size of residual.
%                 default value is 1e-7.
%     delta_tol:  stopping criterion for the size of the change in E.
%                 default value is 1e-9.
%     max_iters:  maximum number of iterations before stopping
%                 default value is 10000.
%     norm_type:  norm to used to measure size of residual and change in E.
%                 By default, the infinity norm is used.
%
%   E_initial_guess:  initial guess for the electric field
%
%   continuation paramters -
%     j_start:  starting current
%     dj:       step size for current
%
%   debugging parameters -
%     debugStatFreq:  frequency to display iteration statistics.
%                     Set this parameter to 0 (default) to disable
%                     display of statistics.
%     debugPlotFreq:  frequency to plot current solution for E.
%                     Set this parameter to 0 (default) to disable
%                     display of statistics.
%
%
% Outputs:
%
%   E:  electric field
%   x:  grid points (scaled and shifted Chebyshev points) where values of
%       E are computed
%
%   residual:    residual of final solution
%   delta_E:     size of last change in E
%   iter_count:  number of iterations required for the solution
%
%
% NOTES:
%  (1) The code actually solves the master equation after it has been
%      transformed using x = 0.5*(z+1) and E_transformed = 2*E.
%      These transformations are needed to change the domain to [-1,1]
%      for the Chebyshev pseudospectral method.
%  (2) This code depends on cheb.m and clencurt.m written by
%      Nick Trefethen.
%  (3) For delta = 0 (no potential drop across the compact Stern layer),
```

```
%      there is no solution with a current above j_r because such
%      a current is unphysical.
%
% Kevin Chu
% 2004/01/24
%
% ======================================================================
%
% Change Log
% ----------
% * 2004/03/10
%   - fixed a bug that makes it possible to miss the target current
%     if (j-j_start) isn't an integer multiple of dj.
%
% * 2004/04/08
%   - changed the stopping criterion to use the relative residual
%     instead of the absolute residual.
%
% * 2004/08/03
%   - made the final "debug" calculation of the residual a relative
%     residual to be consistent with what is used for the stopping
%     criterion
%   - changed dj to abs(dj) when j_end > j_start and -abs(dj) otherwise
%
% ======================================================================

function [E, x, residual, delta_E, iter_count] ...
         = solveSteadyPNP(numPoints, ...
             j,epsilon,delta,alpha_c,alpha_a,k_c,j_r, ... % physical params
             res_tol, delta_tol, max_iters, norm_type, ... % Newton params
             E_initial_guess, ...
             j_start,dj, ...  % continuation params
             debugStatFreq,debugPlotFreq)


% Read in input parameters
min_args = 8;
max_args = 17;
if (nargin < 8)
  error('MATLAB:missingArgs','solveSteadyPNP:missing arguments');
else
  % set grid size
  N = numPoints;
end
```

```
if (nargin < max_args)
  debugPlot = 0;
else
  if (debugPlotFreq == 0)
    debugPlot = 0;
  else
    debugPlot = 1;
  end
end
if (nargin < max_args-1)
  debugStats = 0;
else
  if (debugStatFreq == 0)
    debugStats = 0;
  else
    debugStats = 1;
  end
end
if (nargin < max_args-3)
  j_continuation = 0;
  dj = 1;
else
  j_continuation = 1;
  if (nargin < max_args-2)
    warning('MATLAB:badopt',...
     'solveSteadyPNP: no step size for j continuation ... using dj=0.1.');
    dj = 0.1;
  else
    if (dj == 0)
      j_continuation = 0;
      dj = 1;
    end
  end
end
if (nargin < max_args-4)
  generateInitialGuess = 1;
else
  if (E_initial_guess == 0)
    generateInitialGuess = 1;
  else
    if (length(E_initial_guess) ~= N)
      warning('MATLAB:badopt', ...
         'solveSteadyPNP: initial guess inconsistent with numPoints ...
          ignoring guess');
      generateInitialGuess = 1;
```

```
    else
      E = 0.5*E_initial_guess;
      generateInitialGuess = 0;
    end
  end
end
if (nargin < max_args-5)
  norm_type = inf;
else
  if (norm_type ~= inf & norm_type ~= 2) norm_type = inf; end
end
if (nargin < max_args-6)
  max_iters = 1e5;
end
if (nargin < max_args-7)
  delta_tol = 1e-9;
end
if (nargin < max_args-8)
  res_tol = 1e-7;
end

% cache some commonly occuring constants
acdeleps = alpha_c*delta*epsilon;
aadeleps = alpha_a*delta*epsilon;

% Generate Clenshaw-Curtis quadrature weights to
% accurately calculate integrals for Chebyshev points.
[z_tmp, W_z] = clencurt(N-1);
clear z_tmp;  % reclaim memory

% Generate Chebyshev differentiation matrix and grid points.
[Dz,z] = cheb(N-1);

% laplacian operator
L = Dz*Dz;

% physical space coordinates
x = 0.5*(z+1);

% initialize iteration variables
RHS = zeros(N,1);
total_count = 0;  % total number of iterations required

% continuation in j
if (j_continuation ~= 0)
```

```
  j_end = j;
  dj = abs(dj);
  if (j < j_start)
    dj = -dj;
  end
else
  j_start = j;
  j_end = j;
end

% check if initial guess already satisfies ODE and BCs
if (generateInitialGuess == 0)
  c0 = 1-j+2*epsilon*epsilon*(E(1)-E(N)-0.5*W_z*(E.*E));
  RHS = epsilon^2*(L*E-0.5*E.*E.*E) - 0.25*j - 0.25*(c0+j*(z+1)).*E;
  RHS(N) = k_c*(c0+epsilon^2*(2*E(N)*E(N)+4*Dz(N,:)*E)) ...
              *exp(-2*acdeleps*E(N)) ...
            -j_r*exp(2*aadeleps*E(N)) - j;
  RHS(1) = -k_c*(c0+2*j+epsilon^2*(2*E(1)*E(1)+4*Dz(1,:)*E)) ...
               *exp(2*acdeleps*E(1)) ...
            +j_r*exp(-2*aadeleps*E(1)) - j;

  if (norm_type == inf)
    res = norm(RHS,inf)/norm(E,inf);
  else
    res = (W_z*(RHS.^2))/(W_z*(E.^2));
  end

  % if residual is sufficiently small, return the original guess
  if (res <= res_tol)
    x = 0.5*(z+1);
    E = E;
    iter_count = 0;
    residual = res;
    delta_E = 0;
  end
end

% generate initial guess if necessary
if (generateInitialGuess == 1)

  % bulk electroneutral solution
  eps23 = epsilon^(2/3);
  j_tmp = j_start;
  if (j_tmp > 1-eps23);
    j_tmp = 1-eps23;
```

```
  end
  c0 = 1-j_tmp;
  c = c0 + 2*j_tmp*x;
  E = -j_tmp./(j_tmp*x+0.5*c0);

  % add Gouy-Chapman layers if j suff. small
  if (j < 1-eps23)
    zetac = log(k_c*(1-j_tmp)/(j_tmp+j_r));
    zetaa = log(k_c*(1+j_tmp)/(j_r-j_tmp));
    gammac = tanh(zetac/4.0);
    gammaa = tanh(zetaa/4.0);

    kappac = sqrt(c0);
    temp = gammac*exp(-kappac*x/epsilon);
    % cathode GC layer
    E = E + 8/epsilon*kappac*temp./(1-temp.*temp);
    kappaa = sqrt(c0+2*j_tmp);
    temp = gammaa*exp(-kappaa*(1-x)/epsilon);
    % anode GC layer
  E = E - 8/epsilon*kappaa*temp./(1-temp.*temp);
  end
end

% set up j_values to use in continuation making sure
% that j_end is the final value
j_values = j_start:dj:j_end;
if (j_values(end) ~= j_end)
  j_values = [j_values j_end];
end

for j = j_values

  % initialize Newton iteration variables for next j value
  c0 = 1-j+2*epsilon*epsilon*(E(1)-E(N)-0.5*W_z*(E.*E));
  RHS = epsilon^2*(L*E-0.5*E.*E.*E) - 0.25*j - 0.25*(c0+j*(z+1)).*E;
  RHS(N) = k_c*(c0+epsilon^2*(2*E(N)*E(N)+4*Dz(N,:)*E)) ...
              *exp(-2*acdeleps*E(N)) ...
           -j_r*exp(2*aadeleps*E(N)) - j;
  RHS(1) = -k_c*(c0+2*j+epsilon^2*(2*E(1)*E(1)+4*Dz(1,:)*E)) ...
               *exp(2*acdeleps*E(1)) ...
           +j_r*exp(-2*aadeleps*E(1)) - j;

  if (norm_type == inf)
    res = norm(RHS,inf)/norm(E,inf);
  else
```

```
  res = (W_z*(RHS.^2))/(W_z*(E.^2));
end

delta_E = 1;    % change in E
count = 0;

% display j for debugging purposes
if (0 ~= debugStats)
  j = j
end

while ( (res > res_tol) & (delta_E > delta_tol) ...
        & (count < max_iters-total_count) )

  RHS = -RHS;  % need to take negative of RHS for
               % Newton-Kantorovich Method

  % construct discrete Frechet derivative operator for the interior
  M = L-1.5*diag(E.*E)+0.5*kron(E,(W_z.*E'));
  M(:,1) = M(:,1) - 0.5*E;
  M(:,N) = M(:,N) + 0.5*E;
  M = epsilon*epsilon*M - 0.25*diag(c0+j*(z+1));

  % construct discrete Frechet derivative operator for the
  % boundary conditions

  % z = -1 (x = 0)
  M(N,:) = -2*(W_z.*E');
  M(N,N) = M(N,N) - 2 + 4*E(N);
  M(N,:) = M(N,:) + 4*Dz(N,:);
  M(N,1) = M(N,1) + 2;
  M(N,:) = epsilon^2*M(N,:);
  M(N,N) = M(N,N) - 2*acdeleps*(c0+epsilon^2*(2*E(N)*E(N)+4*Dz(N,:)*E));
  M(N,:) = k_c*exp(-2*acdeleps*E(N))*M(N,:);
  M(N,N) = M(N,N) - 2*aadeleps*j_r*exp(2*aadeleps*E(N));

  % z = 1 (x = 1)
  M(1,:) = -2*(W_z.*E');
  M(1,1) = M(1,1) + 2 + 4*E(1);
  M(1,:) = M(1,:) + 4*Dz(1,:);
  M(1,N) = M(1,N) - 2;
  M(1,:) = epsilon^2*M(1,:);
  M(1,1) = M(1,1) ...
         + 2*acdeleps*(c0+2*j+epsilon^2*(2*E(1)*E(1)+4*Dz(1,:)*E));
  M(1,:) = -k_c*exp(2*acdeleps*E(N))*M(1,:);
```

```
M(1,1) = M(1,1) - 2*aadeleps*j_r*exp(-2*aadeleps*E(1));

% compute next step
Delta = M\RHS;

% set up for next iteration

% increment E
E = E + Delta;

% compute next RHS
c0 = 1-j+2*epsilon*epsilon*(E(1)-E(N)-0.5*W_z*(E.*E));
RHS = epsilon^2*(L*E-0.5*E.*E.*E) - 0.25*j - 0.25*(c0+j*(z+1)).*E;
RHS(N) = k_c*(c0+epsilon^2*(2*E(N)*E(N)+4*Dz(N,:)*E)) ...
                *exp(-2*acdeleps*E(N)) ...
              -j_r*exp(2*aadeleps*E(N)) - j;
RHS(1) = -k_c*(c0+2*j+epsilon^2*(2*E(1)*E(1)+4*Dz(1,:)*E)) ...
                 *exp(2*acdeleps*E(1)) ...
            +j_r*exp(-2*aadeleps*E(1)) - j;

% update res and delta_E
if (norm_type == inf)
  res = norm(RHS,inf)/norm(E,inf);
  delta_E = norm(Delta,inf);
else
  res = (W_z*(RHS.^2))/(W_z*(E.^2));
  delta_E = W_z*(Delta.^2);
end

% update count
count = count + 1;

% debugging
if ( (0 ~= debugPlot) & (0 == mod(count,debugPlotFreq)) )
  % plot results for debugging purposes
  figure(1), clf;
  %plot(x,2*E);
  semilogx(x,2*E);
  xlabel x, ylabel E;
end

if ( (0 ~= debugStats) & (0 == mod(count,debugStatFreq)) )
  % print stats
  stats = [count res delta_E]
end
```

```
  end  % Newton iteration loop

  % debugging
  if (0 ~= debugPlot)
    % plot results for debugging purposes
    figure(1), clf;
    %plot(x,2*E);
    semilogx(x,2*E);
    xlabel x, ylabel E;
  end

  if (debugStats == 1)
    % print stats
    stats = [count res delta_E]
  end

  % update total_count
  total_count = total_count + count;

end  % j_continuation loop

% calculate residual using pseudospectral formulas
if (0 ~= debugStats)
  disp('Residuals Computed using Pseudospectral formulas');
  c0 = 1-j+2*epsilon*epsilon*(E(1)-E(N)-0.5*W_z*(E.*E));
  Residual = epsilon^2*(L*E-0.5*E.*E.*E) - 0.25*j - 0.25*(c0+j*(z+1)).*E;
  Residual(N) = k_c*(c0+epsilon^2*(2*E(N)*E(N)+4*Dz(N,:)*E)) ...
                  *exp(-2*acdeleps*E(N)) ...
               -j_r*exp(2*aadeleps*E(N)) - j;
  Residual(1) = -k_c*(c0+2*j+epsilon^2*(2*E(1)*E(1)+4*Dz(1,:)*E)) ...
                   *exp(2*acdeleps*E(1)) ...
                +j_r*exp(-2*aadeleps*E(1)) - j;

  Res_L2 = (W_z*(Residual.^2))/(W_z*(E.^2))
  Res_inf = norm(Residual,inf)/norm(E,inf)

  if (0 ~= debugPlot)
    figure(3), clf;
    plot(z,Residual,'b');
  end

end

EE = 0;
```

```
if (debugPlot == 1)
  % plot results
  x_lo = 0;
  x_hi = 1;
  dx = 1e-5;
  xx = x_lo:dx:x_hi;

  figure(2), clf;
  EE = 2*interp1(x,E,xx,'cubic');
  %plot(xx,EE);
  semilogx(xx,-EE);
  xlabel x, ylabel E;
end

% assign output values
x = 0.5*(z+1);
E = 2*E;  % change independent variable back to x
iter_count = total_count;
residual = res;
delta_E = delta_E;
```

D.3 Steady-state, Charging of Metal Colloid Sphere

D.3.1 solveHighFieldSteadyResponse3D.m

```
%
% solveHighFieldSteadyResponse3D solves for the steady response of a
%   spherical particle in the strongly nonlinear limit.  The unknowns
%   are taken to be the concentration, c, and potential relative to the
%   applied potential, psi = phi + E r cos(theta), at finite grid points
%   (r = infinity excluded).
%
% The governing equations for these variables are:
%
%   F1(c,psi) = laplacian(c) = 0
%   F2(c,psi) = div[ c * grad(phi) ] = 0
%
% with boundary conditions given by
%
%   H1 = epsilon * div_s(0.5 q / c_s * (grad_s c_s) + w grad_s phi_s)
%      - [c_s d(phi)/dn ] = 0
%   H2 = epsilon * div_s(0.5 w / c_s* (grad_s c_s) + q grad_s phi_s)
%      - dc/dn = 0
%   -grad(phi) --> E as r --> \infty
%   c --> c_infinity as r --> \infty
%   zeta + 2*sqrt(c_s)*delta*sinh(zeta/2) = v - phi_s
%   q = -2 sinh(zeta/2)
%   w = 4 ( sinh(zeta/4) )^2
%
%  where epsilon is the ratio of the Debye screening length to the
%  particle radius, delta is the ratio of the diffuse layer capacitance
%  to the compact Stern layer capacitance, and zeta is the potential
%  drop across the diffuse layer.
%
%
% Usage:  [c, psi] = solveHighFieldSteadyResponse3D( ...
%                v, E, epsilon, delta, c_infinity, ...
%                N_r, L_r, N_theta, ...
%                c_init, psi_init, ...
%                E_start, dE, ...
%                res_tol, delta_tol, max_iters, ...
%                show_stats, ...
%                zeta_res_tol, zeta_delta_tol, zeta_max_iters)
%
% Inputs:
%
```

```
%   v (req):                potential at electrode surface
%   E (req):                applied electric field
%   epsilon (req):          ratio of Debye length to sphere radius
%   delta (req):            effective surface capacitance
%   c_infinity (req):       boundary condition for conc. at r = infty
%   N_r (req):              order of approximation in radial direction
%   L_r (req):              scale parameter in radial direction
%   N_theta (req):          order of approximation polar angle direction
%   c_init (opt):           initial iterate for c
%   psi_init (opt):         initial iterate for psi
%   E_start (opt):          starting value for E continuation
%   dE (opt):               size of steps for E continuation
%   res_tol (opt):          tolerance for residual in Newton iteration
%   delta_tol (opt):        tolerance for change in Newton iteration
%   max_iters (opt):        max number of iterations for Newton iteration
%   show_stats (opt):       show statistics from psi_i/c_s calculation
%   zeta_res_tol (opt):     tolerance for residual in zeta calculation
%   zeta_delta_tol (opt):   tolerance for change in zeta calculation
%   zeta_max_iters (opt):   max number of iterations for zeta calculation
%
% Outputs:
%   c:    concentration profile
%   psi:  electric potential relative to background applied potential
%
%
% NOTES:
%  (1) The direction of the normal to the surface of the sphere is
%      OUTWARD from the physical domain.  That is, it points INTO
%      the sphere.
%
% Kevin Chu
% Dept of Mathematics, MIT
% March 2005
%
% ------------------------------------------------------------------
% CHANGE LOG
% ==========
% 2005/05/20:
%  - Added the tangential concentration gradient component of the
%    surface transport term in the boundary conditions.
% 2005/03/31:
%  - Fixed a bug in the calculation of the Jacobian that was keeping
%    the Newton iteration from converging for high fields.  The
%    fix also drastically improved the convergence rate of the
%    Newton iteration.
```

```
%  - Changed the status report to show the total number of iterations
%    over all continuation values of the applied field.
% 2005/03/30:
%  - Added continuation in E to be able to reach high fields
%  - Added arguments for setting the initial iterates of c and psi
%  - Removed res_hist from list of return arguments.
% 2005/03/11:
%  - Initial version of code.
% ------------------------------------------------------------------
%

function [c, psi, r, theta] = solveHighFieldSteadyResponse3D( ...
               v, E, epsilon, delta, c_infinity, ...
               N_r, L_r, N_theta, ...
               c_init, psi_init, ...
               E_start, dE, ...
               res_tol, delta_tol, max_iters, ...
               show_stats, ...
               zeta_res_tol, zeta_delta_tol, zeta_max_iters)


%%%%%%%%%%%%%%%%%%%%%%%%%%%%%%%%%%%%%%%%%%%%%%%%%%%%%%%%%%%%
% check argument list and set default values
%%%%%%%%%%%%%%%%%%%%%%%%%%%%%%%%%%%%%%%%%%%%%%%%%%%%%%%%%%%%

max_args = 19;
if (nargin < 8)
  error('MATLAB:missingArgs',...
        'solveHighFieldSteadyResponse3D:missing arguments');
end
if (nargin < max_args)
  zeta_max_iters = 20;
end
if (nargin < max_args-1)
  zeta_delta_tol = 1e-13;
end
if (nargin < max_args-2)
  zeta_res_tol = 1e-9;
end
if (nargin < max_args-3)
  show_stats = 0;
end
if (nargin < max_args-4)
  max_iters = 20;
end
```

```
if (nargin < max_args-5)
  delta_tol = 1e-10;
end
if (nargin < max_args-6)
  res_tol = 1e-6;
end
if (nargin < max_args-8)
  E_continuation = 0;
  dE = 1;
else
  E_continuation = 1;
  if (nargin < max_args-7)
    warning('MATLAB:badopt',...
      'solveHighFieldSteadyResponse3D: no step size for E
       continuation ... using dE = 0.1');
    dE = 0.1;
  else
    if (dE == 0)
      E_continuation = 0;
      dE = 1;
    end
  end
end
if (nargin < max_args-9)
  generate_initial_guess = 1;
else
  if (c_init == 0) | (psi_init == 0)
    generate_initial_guess = 1;
  else
    if (length(c_init) ~= N_r*N_theta) | (length(psi_init) ~= N_r*N_theta)
      warning('MATLAB:badopt', ...
        'solveHighFieldSteadyResponse3D:initial guess inconsistent with
         grid size ... ignoring guess');
      generate_initial_guess = 1;
    else
      c = c_init;
      psi = psi_init;
      generate_initial_guess = 0;
    end
  end
end


% setup E continuation parameters
if (E_continuation ~= 0)
```

```
  E_end = E;
  if (E < E_start)
    dE = -dE;
  end
else
  E_start = E;
  E_end = E;
end

% set up E_values to use in continuation making sure that
% E_end is the final value
E_values = E_start:dE:E_end;
if (E_values(end) ~= E_end)
  E_values = [E_values E_end];
end


%%%%%%%%%%%%%%%%%%%%%%%%%%%%%%%%%%%%%%%%%%%%%%%%%%%%%%%%
% construct computational grid and
% differentiation operators
%%%%%%%%%%%%%%%%%%%%%%%%%%%%%%%%%%%%%%%%%%%%%%%%%%%%%%%%

% construct the differentiation matrices for the polar angle
% and the radial coordinate
[D_r,r] = DM_TL(N_r,L_r);
r = r+1;      % shift 0 to 1
[D_theta,theta] = DM_cosine_interior(N_theta);
num_gridpts_r = length(r);
num_gridpts = (num_gridpts_r-1)*N_theta; % total number of computational
                                         % grid points
num_gridpts_interior = num_gridpts-N_theta;

% construct divergence, gradient, and laplacian operators
D = div(D_r, D_theta, r, theta);
G = grad(D_r, D_theta, r, theta);
L = laplacian(D_r, D_theta, r, theta);

% construct surface derivative operators
D_s = div_s(D_theta, theta, r(end));
G_s = D_theta./r(end);

% construct normal derivative operator
G_n = -kron(speye(N_theta),D_r(end,:));  % d/dn = -d/dr at r = 1
```

```
% construct matrices to extract the rows corresponding to finite
% grid points (everything except for r = infty)
r_finite_pt_extractor = spdiags(ones(num_gridpts_r-1,1), 1, ...
                           num_gridpts_r-1, num_gridpts_r);
finite_pt_extractor = kron(speye(N_theta),r_finite_pt_extractor);

% construct matrix to extract the rows corresponding to interior
% grid points (everything except for r = 1 and r = infty)
r_interior_extractor = spdiags(ones(num_gridpts_r-2,1), 1, ...
                           num_gridpts_r-2, num_gridpts_r);
interior_extractor = kron(speye(N_theta),r_interior_extractor);

% construct matrix to extract the rows corresponding to r = 1 (surface)
% from a vector that already has r = infinity removed
r_surf_extractor = spalloc(1,num_gridpts_r-1,1);
r_surf_extractor(1,num_gridpts_r-1) = 1;
surf_extractor = kron(speye(N_theta),r_surf_extractor);

% construct matrix to extract the rows corresponding to r = infty
r_inf_extractor = spalloc(1,num_gridpts_r,1);
r_inf_extractor(1,1) = 1;
inf_extractor = kron(speye(N_theta),r_inf_extractor);


% split the G operators into two parts:
% (1) contributions from finite points to finite points
% (2) contributions from infinite points to finite points
G_f = { ...
  finite_pt_extractor*G{1}*finite_pt_extractor', ...
  finite_pt_extractor*G{2}*finite_pt_extractor'};
G_inf = { ...
  finite_pt_extractor*G{1}*inf_extractor', ...
  finite_pt_extractor*G{2}*inf_extractor'};

% split the D operators into two parts:
% (1) contributions from finite points to finite points
% (2) contributions from infinity to finite points
D_f = { ...
  interior_extractor*D{1}*finite_pt_extractor', ...
  interior_extractor*D{2}*finite_pt_extractor'};
D_inf = { ...
  interior_extractor*D{1}*inf_extractor', ...
  interior_extractor*D{2}*inf_extractor'};

% split the G_n operators into two parts:
```

```
% (1) contributions from finite points
% (2) contributions from infinity
G_n_f = G_n*finite_pt_extractor';
G_n_inf = G_n*inf_extractor';

% split the Laplacian operators into two parts:
% (1) contributions from finite points to finite points
% (2) contributions from infinity to finite points
L_f = interior_extractor*L*finite_pt_extractor';
L_inf = interior_extractor*L*inf_extractor';

% clear auxilliary operators
clear D G L G_n

%%%%%%%%%%%%%%%%%%%%%%%%%%%%%%%%%%%%%%%%%%%%%%%%%%%%%%%%%%%
% cache common expressions
%%%%%%%%%%%%%%%%%%%%%%%%%%%%%%%%%%%%%%%%%%%%%%%%%%%%%%%%%%%
cos_theta = cos(theta);
sin_theta = sin(theta);
cos_theta_full = kron(cos_theta,ones(num_gridpts_r-1,1));
sin_theta_full = kron(sin_theta,ones(num_gridpts_r-1,1));


%%%%%%%%%%%%%%%%%%%%%%%%%%%%%%%%%%%%%%%%%%%%%%%%%%%%%%%%%%%
% generate initial guess for c and psi if required:
%   c = 1, psi = 0
%%%%%%%%%%%%%%%%%%%%%%%%%%%%%%%%%%%%%%%%%%%%%%%%%%%%%%%%%%%
if (generate_initial_guess)
  c = ones(num_gridpts,1);
  psi = zeros(num_gridpts,1);
end


%%%%%%%%%%%%%%%%%%%%%%%%%%%%%%%%%%%%%%%%%%%%%%%%%%%%%%%%%%%
% Continuation loop for Newton iteration
%%%%%%%%%%%%%%%%%%%%%%%%%%%%%%%%%%%%%%%%%%%%%%%%%%%%%%%%%%%
count_total = 0;
for E = E_values % { begin loop over E_values

  if (show_stats > 1)
    mesg = sprintf('E = %f', E);
    disp(mesg);
  end

  %%%%%%%%%%%%%%%%%%%%%%%%%%%%%%%%%%%%%%%%%%%%%%%%%%%%%%%%%%%
```

```
% compute constant terms in F = (F1,F2,H1,H2)
%%%%%%%%%%%%%%%%%%%%%%%%%%%%%%%%%%%%%%%%%%%%%%%%%%%%
F1_const_term = c_infinity*(L_inf*ones(N_theta,1));
F2_const_term = E*c_infinity*(-D_inf{1}*cos_theta + D_inf{2}*sin_theta);
H2_const_term = - c_infinity*(G_n_inf*ones(N_theta,1));

%%%%%%%%%%%%%%%%%%%%%%%%%%%%%%%%%%%%%%%%%%%%%%%%%%%%
% compute constant parts of Jacobian
%%%%%%%%%%%%%%%%%%%%%%%%%%%%%%%%%%%%%%%%%%%%%%%%%%%%
DF1_Dc_const = L_f;
DF2_Dc_const = ...
  - E*D_f{1}*spdiags(cos_theta_full,0,num_gridpts,num_gridpts) ...
  + E*D_f{2}*spdiags(sin_theta_full,0,num_gridpts,num_gridpts);
DH1_Dc_const = spalloc(N_theta,num_gridpts,N_theta);
DH1_Dc_const(:,num_gridpts_r-1:num_gridpts_r-1:end) = ...
  -E*spdiags(cos_theta,0,N_theta,N_theta);
DH2_Dc_const = -G_n_f;

%%%%%%%%%%%%%%%%%%%%%%%%%%%%%%%%%%%%%%%%%%%%%%%%%%%%
% initialize loop variables using current
% solution for c and psi
%%%%%%%%%%%%%%%%%%%%%%%%%%%%%%%%%%%%%%%%%%%%%%%%%%%%
% extract surface concentration and potential
c_s = c(num_gridpts_r-1:num_gridpts_r-1:end);
phi_s = psi(num_gridpts_r-1:num_gridpts_r-1:end) - E*cos_theta;

% compute zeta potential
zeta = computeZetaPotential( ...
  v-phi_s, c_s, delta, zeta_res_tol, zeta_delta_tol, zeta_max_iters);

% compute surface charge density and excess neutral salt concentration
q = -2*sqrt(c_s).*sinh(zeta/2);
w = 4*sqrt(c_s).*(sinh(zeta/4)).^2;

% compute initial residual
F1 = F1_const_term + DF1_Dc_const*c;
F2 = F2_const_term + DF2_Dc_const*c ...
   + D_f{1}*(c.*(G_f{1}*psi)) + D_f{2}*(c.*(G_f{2}*psi));
H1 = DH1_Dc_const*c ...
   + epsilon*D_s*(0.5*q./c_s.*(G_s*c_s) + w.*(G_s*phi_s)) ...
   - c_s.*(G_n_f*psi);
H2 = H2_const_term + DH2_Dc_const*c ...
   + epsilon*D_s*(0.5*w./c_s.*(G_s*c_s) + q.*(G_s*phi_s));

F = [F1; F2; H1; H2];
```

```
res = norm(F,inf);

%%%%%%%%%%%%%%%%%%%%%%%%%%%%%%%%%%%%%%%%%%%%%%%%%%%%
% Newton iteration loop
%%%%%%%%%%%%%%%%%%%%%%%%%%%%%%%%%%%%%%%%%%%%%%%%%%%%
% initialize delta_soln and count
norm_delta_soln = 1;
count = 0;

% { begin Newton iteration loop
while (res > res_tol && norm_delta_soln > delta_tol && count < max_iters)

  % compute Jacobian
  Dzeta_Dpsi = -1./(1+delta*sqrt(c_s).*cosh(zeta/2));
  Dzeta_Dc_s = -0.5*delta*q./c_s.*Dzeta_Dpsi;
  DH1_Dc_var = ( epsilon * D_s * ( ...
     - spdiags(0.25*q.*(G_s*c_s)./c_s./c_s,0,N_theta,N_theta) ...
     - spdiags(0.5*(G_s*c_s)./sqrt(c_s).*cosh(zeta/2).*Dzeta_Dc_s, ...
              0,N_theta,N_theta) ...
     + spdiags(0.5*q./c_s,0,N_theta,N_theta)*G_s ...
     + spdiags(0.5*(G_s*phi_s).*w./c_s,0,N_theta,N_theta) ...
     + spdiags(-0.5*(G_s*phi_s).*q.*Dzeta_Dc_s,0,N_theta,N_theta) ...
     ) ...
   - spdiags(G_n_f*psi,0,N_theta,N_theta) )*surf_extractor;
  DH1_Dpsi_var = epsilon * D_s * ( ...
      -spdiags(0.5*(G_s*c_s)./sqrt(c_s).*cosh(zeta/2).*Dzeta_Dpsi,...
              0,N_theta,N_theta) ...
     + spdiags(w,0,N_theta,N_theta)*G_s ...
     + spdiags(-0.5*(G_s*phi_s).*q.*Dzeta_Dpsi,0,N_theta,N_theta) ) ...
   * surf_extractor ...
   - spdiags(c_s,0,N_theta,N_theta)*G_n_f;
  DH2_Dc_var = epsilon * D_s * ( ...
   -  spdiags(0.25*w.*(G_s*c_s)./c_s./c_s,0,N_theta,N_theta) ...
   - spdiags(0.25*(G_s*c_s)./c_s.*q.*Dzeta_Dc_s, ...
            0,N_theta,N_theta) ...
   + spdiags(0.5*w./c_s,0,N_theta,N_theta)*G_s ...
   + spdiags(0.5*(G_s*phi_s).*q./c_s,0,N_theta,N_theta) ...
   - spdiags((G_s*phi_s).*sqrt(c_s).*cosh(zeta/2).*Dzeta_Dc_s, ...
               0,N_theta,N_theta) ) * surf_extractor;
  DH2_Dpsi_var = epsilon * D_s * ( ...
      -spdiags(0.25*(G_s*c_s)./c_s.*q.*Dzeta_Dpsi,...
              0,N_theta,N_theta) ...
     + spdiags(q,0,N_theta,N_theta)*G_s ...
     - spdiags((G_s*phi_s).*sqrt(c_s).*cosh(zeta/2).*Dzeta_Dpsi, ...
              0,N_theta,N_theta) ) * surf_extractor;
```

```
J = [DF1_Dc_const, spalloc(num_gridpts_interior,num_gridpts,0); ...
     ( DF2_Dc_const ...
     + D_f{1}*spdiags(G_f{1}*psi,0,num_gridpts,num_gridpts) ...
     + D_f{2}*spdiags(G_f{2}*psi,0,num_gridpts,num_gridpts) ), ...
     ( D_f{1}*spdiags(c,0,num_gridpts,num_gridpts)*G_f{1} ...
     + D_f{2}*spdiags(c,0,num_gridpts,num_gridpts)*G_f{2} ); ...
     ( DH1_Dc_const + DH1_Dc_var ), DH1_Dpsi_var; ...
     ( DH2_Dc_const + DH2_Dc_var ), DH2_Dpsi_var];

% compute delta_soln
delta_soln = -J\F;

% update solution
c = c + delta_soln(1:num_gridpts);
psi = psi + delta_soln(num_gridpts+1:end);

%%%%%%%%%%%%%%%%%%%%%%%%%%%
% update residual
%%%%%%%%%%%%%%%%%%%%%%%%%%%
% extract surface concentration and potential
c_s = c(num_gridpts_r-1:num_gridpts_r-1:end);
phi_s = psi(num_gridpts_r-1:num_gridpts_r-1:end) - E*cos_theta;

% compute zeta potential
zeta = computeZetaPotential( ...
  v-phi_s, c_s, delta, zeta_res_tol, zeta_delta_tol, zeta_max_iters);

% compute surface charge density and excess neutral salt concentration
q = -2*sqrt(c_s).*sinh(zeta/2);
w = 4*sqrt(c_s).*(sinh(zeta/4)).^2;

% compute residual
F1 = F1_const_term + DF1_Dc_const*c;
F2 = F2_const_term + DF2_Dc_const*c ...
   + D_f{1}*(c.*(G_f{1}*psi)) + D_f{2}*(c.*(G_f{2}*psi));
H1 = DH1_Dc_const*c ...
   + epsilon*D_s*(0.5*q./c_s.*(G_s*c_s) + w.*(G_s*phi_s)) ...
   - c_s.*(G_n_f*psi);
H2 = H2_const_term + DH2_Dc_const*c ...
   + epsilon*D_s*(0.5*w./c_s.*(G_s*c_s) + q.*(G_s*phi_s));
F = [F1; F2; H1; H2];
res = norm(F,inf);

% DEBUGGING
% [norm(F1,inf) norm(F2,inf) norm(H1,inf) norm(H2,inf)]
```

```
    % update norm_delta_soln, count, and residual history
    norm_delta_soln = norm(delta_soln,inf);
    count = count + 1;

    % show stats
    if (show_stats > 1)
      status = [res norm_delta_soln count]
    end

  end  % } end Newton iteration loop

  % update count_total
  count_total = count_total + count;

end  % } end loop over E_values

%%%%%%%%%%%%%%%%%%%%%%%%%%%%%%%%%%%%%%%%%%%%%%%%%%%%
% append values at infinity to results
%%%%%%%%%%%%%%%%%%%%%%%%%%%%%%%%%%%%%%%%%%%%%%%%%%%%
c = finite_pt_extractor'*c;
c(1:num_gridpts_r:end) = c_infinity;
psi = finite_pt_extractor'*psi;

%%%%%%%%%%%%%%%%%%%%%%%%%%%%%%%%%%%%%%%%%%%%%%%%%%%%
% error checking
%%%%%%%%%%%%%%%%%%%%%%%%%%%%%%%%%%%%%%%%%%%%%%%%%%%%
% throw a warning if the solution has not converged
if (res > res_tol & norm_delta_soln > delta_tol)
  mesg_id = 'solveHighFieldSteadyResponse3D:solutionNotConverged';
  mesg = sprintf('solveHighFieldSteadyResponse3D:Solution NOT converged!
    res = %0.10f, norm_delta_soln = %0.10f', res, norm_delta_soln);
  warning(mesg_id,mesg);
end

%%%%%%%%%%%%%%%%%%%%%%%%%%%%%%%%%%%%%%%%%%%%%%%%%%%%
% show statistics if requested
%%%%%%%%%%%%%%%%%%%%%%%%%%%%%%%%%%%%%%%%%%%%%%%%%%%%
if (show_stats)
  stats_string = sprintf('\n
    ------------solveHighFieldSteadyResponse3D------------\n
    Residual = %0.5g\n
    Number of Iterations = %d\n
    Last Delta Solution = %0.5g\n
    ----------------------------------------------------\n\n', ...
```

```
  res, count_total, norm_delta_soln);
disp(stats_string);
end
```

D.3.2 computeZetaPotential.m

```
%
% computeZetaPotential computes the zeta potential on the surface of
%   the electrode.  Capable of taking vectorized input.
%
% Input:
%
%   Psi (req):            total potential drop across double layer
%                         (surface potential minus bulk potential)
%   delta (req):          effective surface capacitance
%   res_tol (opt):        tolerance for residual in computation of zeta
%   delta_zeta_tol (opt): tolerance for change in zeta
%   max_iters (opt):      maximum number of Newton iterations
%   show_stats (opt):     show statistics if set to a non-zero value
%
% Output:
%   zeta:  leading order zeta potential
%
%
% Kevin Chu
% Dept of Mathematics, MIT
% Jan 2005
%
% ------------------------------------------------------------------
% CHANGE LOG
% ==========
% 2005/03/11:
%  - Modified code to throw a warning if the solution has not converged.
%  - Modified code to allow user to request computation statistics.
% 2005/02/25:
%  - Modified code to take the bulk concentration at the surface
%    as an input.
% 2005/01/??:
%  - Initial version of code.
% ------------------------------------------------------------------
%


function zeta = computeZetaPotential( ...
           Psi, c_s, delta, ... % physical parameters
           res_tol, delta_zeta_tol, max_iters, ... % iteration parameters
           show_stats ... % show statistics flag
          )
```

```
%%%%%%%%%%%%%%%%%%%%%%%%%%%%%%%%%%%%%%%%%%%%%%%%%%%%%%%%%%%%%%%%%%%%%%%%
% check argument list and set default values
%%%%%%%%%%%%%%%%%%%%%%%%%%%%%%%%%%%%%%%%%%%%%%%%%%%%%%%%%%%%%%%%%%%%%%%%
max_args = 7;
if (nargin < 3)
  error('MATLAB:missingArgs','computeZetaPotential:missing arguments');
end
if (nargin < max_args)
  show_stats = 0;
end
if (nargin < max_args-1)
  max_iters = 20;
end
if (nargin < max_args-2)
  delta_zeta_tol = 1e-13;
end
if (nargin < max_args-3)
  res_tol = 1e-8;
end

%%%%%%%%%%%%%%%%%%%%%%%%%%%%%%%%%%%%%%%%%%%%%%%%%%%%%%%%%%%%%%%%%%%%%%%%
% compute the zeta-potential at the collocation points
%%%%%%%%%%%%%%%%%%%%%%%%%%%%%%%%%%%%%%%%%%%%%%%%%%%%%%%%%%%%%%%%%%%%%%%%

% initialize iteration
zeta = Psi;  % use Psi as an initial guess for zeta
delta_zeta = 1;
res = 1;
norm_res = norm(res,inf);
norm_delta_zeta = norm(delta_zeta,inf);
count = 0;
res = zeta + 2*delta*sqrt(c_s).*sinh(zeta/2) - Psi;

%%%%%%%%%%%%%%%%%%%%%%%%%%%%%%%%%%%%%%%%%%%%%%%%%%%%%%%%%%%%%%%%%%%%%%%%
% Newton iteration
%%%%%%%%%%%%%%%%%%%%%%%%%%%%%%%%%%%%%%%%%%%%%%%%%%%%%%%%%%%%%%%%%%%%%%%%
while (norm_res > res_tol ...
       & norm_delta_zeta > delta_zeta_tol ...
       & count < max_iters)

  J = 1 + delta*sqrt(c_s).*cosh(zeta/2);
  delta_zeta = -res./J;
  zeta = zeta + delta_zeta;
  res = zeta + 2*delta*sqrt(c_s).*sinh(zeta/2) - Psi;
```

```
  % update norm_res, norm_delta_zeta, and count
  norm_res = norm(res,inf);
  norm_delta_zeta= norm(delta_zeta,inf);
  count = count + 1;

end

%%%%%%%%%%%%%%%%%%%%%%%%%%%%%%%%%%%%%%%%%%%%%%%%%%%%%%%%%%%%%%%%%%%%%%%
% error checking
%%%%%%%%%%%%%%%%%%%%%%%%%%%%%%%%%%%%%%%%%%%%%%%%%%%%%%%%%%%%%%%%%%%%%%%
% throw a warning if the solution has not converged
if (norm_res > res_tol & norm_delta_zeta> delta_zeta_tol)
  mesg_id = 'computeZetaPotential:solutionNotConverged';
  mesg = sprintf('computeZetaPotential:Solution NOT converged!
    res = %0.10f, delta_zeta = %0.10f', norm_res, norm_delta_zeta);
  warning(mesg_id,mesg);
end

%%%%%%%%%%%%%%%%%%%%%%%%%%%%%%%%%%%%%%%%%%%%%%%%%%%%%%%%%%%%%%%%%%%%%%%
% show computation statistics if requested
%%%%%%%%%%%%%%%%%%%%%%%%%%%%%%%%%%%%%%%%%%%%%%%%%%%%%%%%%%%%%%%%%%%%%%%
if (show_stats)
  stats_string = sprintf('\n
     -------------computeZetaPotential--------------\n
     Residual = %0.5g\n
     Number of Iterations = %d\n
     Size of Last Change in Solution = %0.5g\n
     ------------------------------------------------\n\n', ...
  norm_res, count, norm_delta_zeta);
  disp(stats_string);
end
```

D.4 Weakly Nonlinear Response of Metal Colloid Sphere

D.4.1 computeBulkChargingDynamicsRC3D.m

```
%
% computeBulkChargingRC3D calculates the time evolution of the bulk region
% at the RC-time for an ideally polarizable sphere.
%
% The governing equation is
%
%   laplacian(phi) = 0
%
% with boundary conditions given by
%
%   -grad(phi) --> E as r --> \infty
%   C(Psi) d/dt(Psi) = d/dn(phi)
%   zeta + 2*delta*sinh(zeta/2) = v - phi = Psi
%   C(Psi) = 1/( delta + sech(zeta/2) )
%
% The solution method takes advantage of the fact that the solution to
% Laplace's equation for in a spherical geometry with azimuthal symmetry
% is simply expressed as an expansion in the Legendre polynomial basis
% (with cosine(theta) as the argument)
%
%  phi = v - E r cos(theta) + sum_{l} A_l(t) P_l(cos(theta))/r^(l+1)
%
% Spatial collocation in angle is used to derive the time evolution
% equations for the coefficients of a truncated series solution.
% The resulting system of ODEs in time are solved using the MATLAB
% ODE solvers.
%
% It should be noted that although the optimal collocation points for
% an N-th degree Legendre polynomial approximation are the roots [or
% extrema plus end points] of the Legendre polynomial of degree (N+1)
% [or degree N], this code takes the collocation points to be
% cos(theta) for evenly spaced theta in the interval [0,pi] because they
% are easier to compute.  Since the optimal Legendre collocation points
% and cos(theta) are distributed on [-1,1] in the same way for large
% N, not too much error is introduced by using uniformly distributed
% angles for the collocation points.
%
% Usage: [T,A,theta,P,Q] = computeBulkChargingRC3D( ...
%          v, E, delta, ...
%          t_init, t_final, ...
%          N, ode_rel_tol, ode_abs_tol, ...
```

```
%          res_tol, delta_zeta_tol, max_iters)
%
% Inputs:
%
%   v (req):              potential of surface of sphere
%   E (req):              applied electric field
%   delta (req):          ratio of diffuse layer capacitance to
%                           to compact layer, surface capacitance
%                           (lambda_S / lambda_D)
%   t_init (req):         initial time
%   t_final (req):        final time
%   N (req):              order of approximation
%   ode_rel_tol (opt):    tolerance for relative residual for ODE solver
%   ode_abs_tol (opt):    tolerance for absolute residual for ODE solver
%   res_tol (opt):        tolerance for residual in computation of zeta
%   delta_zeta_tol (opt): tolerance for change in zeta
%   max_iters (opt):      maximum number of Newton iterations
%
%
% Output:
%   T:      times
%   A:      expansion coefficients ( row k corresponds to time T(k) )
%   theta:  collocation angles
%   P:      collocation matrix for phi at the collocation angles
%   Q:      collocation matrix for d(phi)/dn at the collocation angles
%
%
% Kevin Chu
% Dept of Mathematics, MIT
% Jan 2005
%

function [T,A,theta,P,Q] = computeBulkChargingRC3D( ...
          v, E, delta, ... % physical parameters
          t_init, t_final, ... % time interval to integrate over
          N, ode_rel_tol, ode_abs_tol, ...% numerical parameters
          res_tol, delta_zeta_tol, max_iters ... % zeta Newton parameters
         )

% check argument list and set default values
max_args = 11;
if (nargin < 6)
  error('MATLAB:missingArgs','computeBulkChargingRC3D:missing arguments');
end
if (nargin < max_args)
```

```
  max_iters = 50;
end
if (nargin < max_args-1)
  delta_zeta_tol = 1e-13;
end
if (nargin < max_args-2)
  res_tol = 1e-8;
end
if (nargin < max_args-3)
  ode_abs_tol = 1e-8;
end
if (nargin < max_args-4)
  ode_rel_tol = 1e-8;
end


% collocation points
theta = (0:pi/N:pi)';
X = cos(theta);

% compute the collocation matrix
P = zeros(N+1);
P(:,1) = ones(N+1,1);
P(:,2) = X;
for k=2:N
  % NOTE: In the following recursion formula, the order of
  %       the polynomial is k, but the values are stored in
  %       the (k+1)-th column.
  P(:,k+1) = ( (2*k-1)*X.*P(:,k) - (k-1)*P(:,k-1) )/k;
end

% compute collocation matrix for the normal derivative of phi
Q = P*diag(cumsum(ones(N+1,1)));

% solve the time evolution equations for the coefficients A,
% using the built-in MATLAB ODE solvers
ode_options = odeset('RelTol', ode_rel_tol, 'AbsTol', ode_abs_tol);
A_init = zeros(N+1,1);  % all coefs except A_0 and A_1 are initially zero
A_init(1) = v;  % A_0 initially set to the potential on sphere
A_init(2) = E;  % A_1 initially set so that sphere is isopotential surface
[T,A] = ode15s(@ODE_RHS_BULK_RC, [t_init t_final], A_init, ode_options, ...
               v, E, delta, P, Q);
```

D.4.2 ODE_RHS_BULK_RC.m

```
%
% ODE_RHS_BULK_RC computes the RHS for the system of ODEs obtained
%         for the coefficients of Legendre polynomial expansion of phi.
%         For efficiency, it takes the phi interpolation matrix, P,
%         and the d(phi)/dn interpolation matrix, Q, as arguments.
%
% Usage:  f = ODE_RHS_BULK_RC(t,A, ...
%                             v, E,delta, ...
%                             P,Q,res_tol, ...
%                             delta_zeta_tol,max_iters)
%
% Inputs:
%
%   v (req):              potential at electrode surface
%   E (req):              applied electric field
%   delta (req):          effective surface capacitance
%   P (req):              interpolation matrix for phi
%   Q (req):              interpolation matrix for d(phi)/dn
%   res_tol (opt):        tolerance for residual in computation of zeta
%   delta_zeta_tol (opt): tolerance for change in zeta
%   max_iters (opt):      maximum number of Newton iterations
%
% Kevin Chu
% Dept of Mathematics, MIT
% Jan 2005
%

function f = ODE_RHS_BULK_RC(t, A, ...
           v, E, delta, ... % physical parameters
           P, Q, ... % interpolation matrices
           res_tol, delta_zeta_tol, max_iters ... % iteration parameters
          )

% check argument list and set default values
max_args = 10;
if (nargin < 6)
  error('MATLAB:missingArgs','ODE_RHS_RC:missing arguments');
end
if (nargin < max_args)
  max_iters = 50;
end
if (nargin < max_args-1)
  delta_zeta_tol = 1e-13;
```

```
end
if (nargin < max_args-2)
  res_tol = 1e-8;
end

% compute the zeta-potential at the collocation points

% initialize iteration
Psi = v-P*A+E*P(:,2); % Psi = v - (-E*P_1(cos(theta)) + P*A)
                      % E*P(:,2) term is inhom. term from applied field
zeta = Psi;  % use Psi as an initial guess for zeta
delta_zeta = 1;
res = 1;
count = 0;
res = zeta + 2*delta*sinh(zeta/2) - Psi;

% Newton iteration
while (norm(res,inf) > res_tol ...
       & norm(delta_zeta,inf) > delta_zeta_tol ...
       & count < max_iters)

  J = 1 + delta*cosh(zeta/2);
  delta_zeta = -res./J;
  zeta = zeta + delta_zeta;
  res = zeta + 2*delta*sinh(zeta/2) - Psi;
  count = count + 1;

end

% compute RHS for equation A_dot = f(A,t)
C = sech(zeta/2)+delta;  % C(psi)
P_times_rhs = -diag(C)*(Q*A + E*P(:,2));
f = P\P_times_rhs;

% NOTE: time-dependent electrode potential or applied field can be
%       included by adding the following to P_time_rhs:
%
%       dv_dt + dE_dt*P(:,2)
%
```

Bibliography

[1] A. Ajdari. AC pumping of liquids. *Phys. Rev. E*, 61:R45–R48, 2000.

[2] N. Ariel, G. Ceder, D. R. Sadoway, and E. A. Fitzgerald. Electrochemically-controlled transport of lithium through ultra-thin SiO_2 for novel electronic and optoelectronic devices. Submitted for publication.

[3] V. Barcilon, D.-P Chen, and R. S. Eisenberg. Ion flow through narrow membrane channels: Part II. *SIAM J. Appl. Math*, 52:1405–1425, 1992.

[4] V. Barcilon, D.-P. Chen, R. S. Eisenberg, and J. W. Jerome. Qualitative properties of steady-state poisson-nernst-planck systems: Perturbation and simulation study. *SIAM J. Appl. Math*, 57:631–648, 1997.

[5] A. J. Bard and L. R. Faulkner. *Electrochemical Methods*. John Wiley & Sons, Inc., New York, NY, 2001.

[6] M. Z. Bazant, K. T. Chu, and B. J. Bayly. Current-voltage relations for electrochemical thin films. *SIAM J. Appl. Math.* Accepted for publication.

[7] M. Z. Bazant and T. M. Squires. Induced-charge electro-kinetic phenomena: Theory and microfluidic applications. *Phys. Rev. Lett.*, 92:066101, 2004.

[8] M. Z. Bazant, K. Thornton, and A. Ajdari. Diffuse charge dynamics in electrochemical systems. *Phys. Rev. E*, 70:021506, 2004.

[9] Y. Ben and H.-C. Chang. Nonlinear smoluchowski slip velocity and micro-vortex generation. *J. Fluid. Mech.*, 461:229–238, 2002.

[10] R. S. Berry, S. A. Rice, and J. Ross. *Physical Chemistry*, pages 999–1008. Oxford University Press, New York, NY, 2000. "Kinetics of Electrode Reactions" by C. Chidsey.

[11] J. R. Blake. A spherical envelope approach to ciliary propulsion. *J. Fluid Mech.*, 46:199–208, 1971.

[12] A. Bonnefont, F. Argoul, and M.Z. Bazant. Analysis of diffuse-layer effects on time-dependent interfacial kinetics. *J. Electroanal. Chem.*, 500:52–61, 2001.

[13] J. P. Boyd. *Chebyshev and Fourier Spectral Methods*. Dover Publications, Inc., Mineola, NY, 2nd edition, 2001.

[14] C. M. A. Brett and A. A. O. Brett. *Electrochemistry. Principles, Methods, and Applications*. Oxford Science Publications, Oxford, 1993.

[15] A. B. D. Brown, C. G. Smith, and A. R. Rennie. Pumping of water with ac electric fields applied to asymmetric pairs of microelectrodes. *Phys. Rev. E*, 63:016305, 2001.

[16] R. Bruinsma and S. Alexander. Theory of electrohydrodynamic instabilities in electrolytic cells. *J. Chem. Phys.*, 92:3074–3085, 1990.

[17] E. Brunner. Reaktionsgeschwindigkeit in heterogenen systemen. *Z. Phys. Chem.*, 47:56–102, 1904.

[18] E. Brunner. Die kathodische und anodische stromspannungskurve bei der electrolyse von jod-jodkaliumlösungen. *Z. Phys. Chem.*, 58:1–126, 1907.

[19] Mark H. Carpenter and David Gottlieb. Spectral methods on arbitrary grids. *J. Comput. Phys.*, 129:74–86, 1996.

[20] H.-C. Chang and G. Jaffé. Polarization in electrolytic solutions. part I. theory. *J. Chem. Phys.*, 20:1071–1077, 1952.

[21] D. L. Chapman. A contribution to the theory of electrocapillarity. *Philos. Mag.*, 25:475–481, 1913.

[22] J.-N. Chazalviel. Electrochemical aspects of the generation of ramified metallic electrodeposits. *Phys. Rev. A*, 42:7355–7367, 1990.

[23] A. A. Chernenko. The theory of the passage of direct current through a solution of a binary electrolyte. *Dokl. Akad. Nauk. SSSR*, 153:1129–1131, 1962. English translation, pp. 1110–1113.

[24] J. M. Chomaz. The dynamics of a viscous soap film with soluble surfactant. *J. Fluid Mech.*, 442:387–409, 2001.

[25] K. T. Chu and M. Z. Bazant. Electrochemical thin films at and above the classical limiting current. *SIAM J. Appl. Math.* Accepted for publication.

[26] Y. Couder, J. M. Chomaz, and M. Rabaud. On the hydrodynamics of soap films. *Physica D*, 37:384–405, 1989.

[27] P. Debye and H. Falkenhagen. *Physik. Z.*, 29:121, 1928.

[28] P. Delahay. *Double Layer and Electrode Kinetics*. New York, NY, 1965.

[29] B. V. Deryagin and S. S. Dukhin. The theory of surface conductance. *Colloid. J. USSR.*, 31:277–283, 1969.

[30] N. J. Dudney, J. B. Bates, D. Lubben, and F. X. Hart. Thin-film rechargeable lithium batteries with amorphous $Li_xMn_2O_4$ cathodes. In J. Bates, editor, *Thin Film Solid Ionic Devices and Materials*, pages 201–214. The Electrochemical Society, Pennington, NJ, 1995.

[31] S. S. Dukhin. Electrokinetic phenomena of the second kind and their applications. *Adv. Colloid Interface Sci.*, 35:173–196, 1991.

[32] S. S. Dukhin. Non-equilibrium electric surface phenomena. *Adv. Colloid Interface Sci.*, 44:1–134, 1993.

[33] S. S. Dukhin and V. N. Shilov. Theory of static polarization of the diffuse part of the thin electric double layer of spherical particles. *Colloid. J. USSR.*, 31:564–570, 1969.

[34] S. S. Dukhin and V. N. Shilov. Kinetic aspects of electrochemistry of disperse systems. part II. induced dipole moment and the non-equilibrium double layer of a colloid particle. *Adv. Colloid Interface Sci.*, 13:153–195, 1980.

[35] C. Faure, N. Decoster, and F. Argoul. AC field induced two-dimensional aggregation of multilamellar vesicles. *Eur. Phys. J. B*, 5:87–97, 1998.

[36] J. K. Ferri, K. J. Stebe, and D. Blankschtein. Which surfactants reduce surface tension faster? a scaling argument for diffusion-controlled adsorption. *Adv. Colloid Interface Sci.*, 85:61–97, 2000.

[37] J. D. Ferry. Frequency dependence of the capacity of a diffuse double layer. *J. Chem. Phys.*, 16:737–739, 1948.

[38] B. Fornberg. *A Practical Guide to Pseudospectral Methods*. Cambridge University Press, New York, NY, 1998.

[39] A. Frumkin. Wasserstoffüberspannung und struktur der doppelschict. *Z. Phys. Chem.*, 164A:121–133, 1933.

[40] L. A. Geddes. Historical evolution of circuit models for the electrode-electrolyte interface. *Ann. Biomedical Eng.*, 25:1–14, 1997.

[41] A. González, A. Ramos, N. G. Green, A. Castellanos, and H. Morgan. Fluid flow induced by non-uniform ac electric fields in electrolytes on microelectrodes. ii. a linear double-layer analysis. *Phys. Rev. E*, 61:4019, 2000.

[42] M. Gouy. Sur la constitution de la charge électrique a la surface d'un électrolyte. *J. de Phys.*, 9:457–468, 1910.

[43] B. M. Grafov and A. A. Chernenko. Theory of the passage of a constant current through a solution of a binary electrolyte. *Dokl. Akad. Nauk. SSSR*, 146:135–138, 1962. English translation, pp. 629–632.

[44] D. C. Grahame. The electrical double layer and the theory of electrocapillarity. *Chem. Rev.*, 41:441–501, 1947.

[45] D. C. Grahame. Differential capacity of mercury in aqueous sodium fluoride solutions. i. effect of concentration at 25°. *J. Am. Chem. Soc.*, 76:4819–4823, 1954.

[46] N. G. Green, A. Ramos, A. González, A. Castellanos, and H. Morgan. Fluid flow induced by nonuniform ac electric fields in electrolytes on microelectrodes. III. observation of streamlines and numerical simulation. *Phys. Rev. E*, 66:026305, 2002.

[47] N. G. Green, A. Ramos, A. González, H. Morgan, and A. Castellanos. Fluid flow induced by nonuniform ac electric fields in electrolytes on microelectrodes. I. experimental measurements. *Phys. Rev. E*, 61:4011–4018, 2000.

[48] N. G. Green, A. Ramos, and H. Morgan. Ac electrokinetics: a survey of submicrometre particle dynamics. *J. Phys. D*, 33:632–641, 2000.

[49] B. Gustafsson, H.-O. Kreiss, and J. Oliger. *Time Dependent Problems and Difference Methods*. Wiley Interscience, New York, NY, 1995.

[50] J. E. Guyer, W. J. Boettinger, J. A. Warren, and G. B. McFadden. Phase field modeling of electrochemistry i: Equilibrium. *Phys. Rev. E*, 69:021603, 2004.

[51] J. E. Guyer, W. J. Boettinger, J. A. Warren, and G. B. McFadden. Phase field modeling of electrochemistry ii: Kinetics. *Phys. Rev. E*, 69:021604, 2004.

[52] W. Helfrich. *Z. Naturforsch. C*, 29:182, 1974.

[53] H. Helmholtz. Studien über electrische grenzschichten. *Ann. Phys. Chem.*, 7 (ser. 3):337–382, 1879.

[54] E. J. Hinch and J. D. Sherwood. The primary electroviscous effect in a suspension of spheres with thin double layers. *J. Fluid. Mech.*, 132:337–347, 1983.

[55] E. J. Hinch, J. D. Sherwood, W. C. Chew, and P. N. Sen. Dielectric response of a dilute suspension of spheres with thin double layers in an asymmetric electrolyte. *J. Chem. Soc. Faraday. Trans. II*, 80:535–551, 1984.

[56] R. J. Hunter. *Foundations of Colloid Science*. Oxford University Press, Oxford, 2001.

[57] E. M. Itskovich, A. A. Kornyshev, and M. A. Vorotyntsev. Electric current across the metal-solid electrolyte interface. i. direct current, current-voltage characteristic. *phys. stat. sol. (a)*, 39:229–238, 1977.

[58] J. D. Jackson. *Classical Electrodynamics*. John Wiley & Sons, Inc., 1998.

[59] G. Jaffé and C. Z. LeMay. On polarization in liquid dielectrics. *J. Chem. Phys.*, 21:920–928, 1953.

[60] A. A. Kornyshev and M. A. Vorotyntsev. Conductivity and space charge phenomena in solid electrolytes with one mobile charge carrier species, a review with original material. *Electrochimica Acta*, 26:303–323, 1981.

[61] D. J. Laser and J. G. Santiago. A review of micropumps. *J. Micromech Microeng*, 14:R35–64.

[62] G. Leal. *Laminar flow and convective transport processes : scaling principles and asymptotic analysis*. Butterworth-Heinemann, Boston, 1992.

[63] V. Levich. The theory of concentration polarization. *Acta Physicochimica U.R.S.S*, 17:257–307, 1942.

[64] V. G. Levich. *Physico-chemical Hydrodynamics*. Prentice-Hall, London, 1962.

[65] J. A. Levitan, S. Devasenathipathy, V. Studer, Y. Ben, T. Thorsen, T. M. Squires, and M. Z. Bazant. Experimental observation of induced-charge electro-osmosis around a metal wire in a microchannel. Submitted for publication.

[66] M. J. Lighthill. On the squirming motion of nearly spherical deformable bodies through liquids at very small reynolds numbers. *Comm. Pure Appl. Math.*, 5:109–118, 1952.

[67] J. Lyklema. *Fundamentals of Interface and Colloid Science. Volume I: Fundamentals*. Academic Press Limited, San Diego, CA, 1991.

[68] J. Lyklema. *Fundamentals of Interface and Colloid Science. Volume II: Solid-Liquid Interfaces*. Academic Press Limited, San Diego, CA, 1995.

[69] J. R. Macdonald. Theory of the differential capacitance of the double layer in unadsorbed electrolytes. *J. Chem. Phys.*, 22:1857–1866, 1954.

[70] J. R. Macdonald. Static space charge and capacitance for a single blocking electrode. *J. Chem. Phys.*, 29:1346–1358, 1958.

[71] J. R. Macdonald. *Trans. Faraday Soc.*, 16:934, 1970.

[72] J. R. Macdonald. Impedance spectroscopy: Old problems and new developments. *Electrochim. Acta*, 35:1483–1492, 1990.

[73] A. D. MacGillivray. Nernst-planck equations and the electroneutrality and donnan equilibrium assumptions. *J. Chem. Phys.*, 48:2903–2907, 1968.

[74] C. Marquet, A. Buguin, L. Talini, and P. Silberzan. Rectified motion of colloids in asymmetrically structured channels. *Phys. Rev. Lett.*, 88, 2002.

[75] M. D. Mitov, P. Méleard, M. Winterhalter, M. I. Angelova, and P. Bothorel. Electric-field-dependent thermal fluctuations of giant vesicles. *Phys. Rev. E*, 48:628–631, 1993.

[76] M. Mpholo, C. G. Smith, and A. B. D. Brown. Low voltage plug flow pumping using anisotropic electrode arrays. *Sens. Actuators B*, 92:262–268, 2003.

[77] M. Mulqueen, , S. S. Datwani, K. J. Stebe, and D. Blankschtein. Dynamic surface tensions of aqueous surfactant mixtures: Experimental investigation. *Langmuir*, 17:7494–7500, 2001.

[78] M. Mulqueen, K. J. Stebe, and D. Blankschtein. Dynamic interfacial adsorption in aqueous surfactant mixtures: Theoretical study. *Langmuir*, 17:5196–5207, 2001.

[79] F. Nadal, F. Argoul, P. Hanusse, B. Pouligny, and A. Ajdari. Electrically induced interactions between colloidal particles in the vicinity of a conducting plane. *Phys. Rev. E*, 65, 2002.

[80] F. Nadal, F. Argoul, P. Kestener, B. Pouligny, C. Ybert, and A. Ajdari. Electrically-induced flows in the vicinity of a dielectric stripe on a conducting plane. *Eur. Phys. J. E*, 9:387–399, 2002.

[81] W. Nernst. Zur kintetik der in lösung befindlichen körper. *Z. Phys. Chem*, 2:613–637, 1888.

[82] W. Nernst. Die elektromotorische wirksamkeit der ionen. *Z. Phys. Chem*, 4:129–181, 1889.

[83] W. Nernst. Theorie der reaktionsgeschwindigkeit in heterogenen systemen. *Z. Phys. Chem.*, 47:52–55, 1904.

[84] B. J. Neudecker, N. J. Dudney, and J. B. Bates. "lithium-free" thin-film battery with *in situ* plated Li anode. *J. Electrochem. Soc.*, 147:517–523, 2000.

[85] J. Newman. The polarized diffuse double layer. *Trans. Faraday Soc.*, 61:2229–2237, 1965.

[86] J. Newman. *Electrochemical Systems*. Prentice-Hall, Inc., Englewood Cliffs, NJ, second edition, 1991.

[87] J.-H. Park and J. W. Jerome. Qualitative properties of steady-state poisson-nernst-planck systems: Mathematical study. *SIAM J. Appl. Math*, 57:609–630, 1997.

[88] A. T. Patera. A spectral element method for fluid dynamics - laminar flow in a channel expansion. *J. Comput. Phys.*, 54:468–488, 1984.

[89] R. Pethig. *Crit. Rev. Biotechnol.*, 16:331, 1996.

[90] M. Planck. Ueber die erregung von elektricität und wärme in electrolyten. *Ann. Phys. Chem.*, 39 (ser. 3):161–186, 1890.

[91] A. Ramos, A. González, A. Castellanos, N. G. Green, and H. Morgan. Pumping of liquids with ac voltages applied to asymmetric pairs of microelectrodes. *Phys. Rev. E*, 67:056302, 2003.

[92] A. Ramos, H. Morgan, N. G. Green, and A. Castellanos. Ac electrokinetics: a review of forces in microelectrode structures. *J. Phys. D*, 31:2338–2353, 1998.

[93] A. Ramos, H. Morgan, N. G. Green, and A. Castellanos. AC electric-field-induced fluid flow in microelectrodes. *J. Colloid Interface Sci.*, 217:420–422, 1999.

[94] W. D. Ristenpart, I. A. Aksay, and D. A. Saville. Electrically guided assembly of planar superlattices in binary colloidal suspensions. *Phys. Rev. Lett.*, 90, 2003.

[95] I. Rubinstein. *Electro-Diffusion of Ions*. SIAM Studies in Applied Mathematics, SIAM, Philadelphia, PA, 1990.

[96] I. Rubinstein and L. Shtilman. Voltage against current curves of cation exchange membranes. *J. Chem. Soc. Faraday. Trans. II*, 75:231–246, 1979.

[97] I. Rubinstein and B. Zaltzman. Electro-osmotically induced convection at a permselective membrane. *Phys. Rev. E*, 62:2238–2251, 2000.

[98] I. Rubinstein and B. Zaltzman. Electro-osmotic slip of the second kind and instability in concentration polarization at electrodialysis membranes. *Math. Models Meth. Appl. Sci.*, 2:263–299, 2001.

[99] W. B. Russel, D. Saville, and W. R. Schowalter. *Colloidal Dispersions*. Cambridge University Press, Cambridge, England, 1989.

[100] D. A. Saville. Electrohydrodynamics: The taylor-melcher leaky dielectric model. *Annu. Rev. Fluid Mech.*, 29:27–64, 1997.

[101] Z. Shi, L. Lü, and G. Ceder. Solid state thin film lithium microbatteries. Technical report, Singapore-MIT Alliance Technical Report: Advanced Materials for Micro- and Nano-Systems Collection, January 2003. URI - http://hdl.handle.net/1721.1/3672.

[102] V. N. Shilov and S. S. Dukhin. Theory of polarization of the diffuse part of a thin double layer at a spherical particle in an alternating electric field. *Colloid. J. USSR.*, 32:90–95, 1970.

[103] W. H. Smyrl and J. Newman. Double layer structure at the limiting current. *Trans. Faraday Soc.*, pages 207–216, 1967.

[104] T. M. Squires and M. Z. Bazant. Induced-charge electro-osmosis. *J. Fluid Mech.*, 509:217–252, 2004.

[105] T. M. Squires and S. R. Quake. Microfluidics: fluid physics on the nanoliter scale. *Rev. Mod. Phys.*, 2005. to appear.

[106] O. Stern. Zur theorie der electrolytischen doppelschicht. *Z. Elektrochem.*, 30:508–516, 1924.

[107] H. A. Stone. A simple derivation of the time-dependent convective-diffusion equation for surfactant transport along a deforming interface. *Phys. Fluids A*, 2:111–112, 1990.

[108] V. Studer, A. Pépin, Y. Chen, and A. Ajdari. Fabrication of microfluidic devices for ac electrokinetic fluid pumping. *Microelec. Eng.*, 61:915–920, 2002.

[109] N. Takami, T. Ohsaki, H. Hasabe, and M. Yamamoto. Laminated thin Li-ion batteries using a liquid electrolyte. *J. Electrochem. Soc.*, 149:A9–A12, 2002.

[110] M. Trau, D. A. Saville, and I. A. Aksay. Assembly of colloidal crystals at electrode interfaces. *Langmuir*, 13:6375, 1997.

[111] L. N. Trefethen. *Spectral Methods in MATLAB*. SIAM, Philadelphia, PA, 2000.

[112] B. Wang, J. B. Bates, F. X. Hart, B. C. Sales, R. A. Zuhr, and J. D. Robertson. Characterization of thin-film rechargeable lithium batteries with lithium cobalt oxide cathodes. *J. Electrochem. Soc.*, 143:3204–3213, 1996.

[113] E. Warburg. Ueber das verhalten sogenannter unpolarisirbarer elektroden gegen wechselstrom. *Ann. Phys. Chem*, 67 (ser. 3):493–499, 1899.

[114] E. Warburg. Ueber die polarisationscapacität des platins. *Ann. Phys. Chem*, 6 (ser. 4):125–135, 1901.

[115] E. W. Weisstein. Modified spherical bessel function of the second kind. From MathWorld–A Wolfram Web Resource. http://mathworld.wolfram.com/ModifiedSphericalBesselFunctionoftheSecondKind.html.

[116] A. C. West and J. Newman. Determination of current distributions governed by laplace's equation. *Modern Aspects of Electrochemistry*, 23:104–147, 1992.

[117] H. Wong, D. Rumschitzki, and C. Maldarelli. On the surface mass balance at a deforming fluid interface. *Phys. Fluids*, 8:3203–3204, 1996.

[118] S. Yeh, M. Seul, and B. Shraiman. Assembly of ordered colloidal aggregrates by electric-field-induced fluid flow. *Nature (London)*, 386:57, 1997.